SEPTEMBER 30, 2019

University of Nottingham

UK | CHINA | MALAYSIA

THE ROLE OF MESENCHYMAL CELL-MEDIATED PARACRINE SIGNALLING IN BREAST CANCER PROGRESSION AND METASTASIS

THESIS FOR DOCTOR OF PHILOSOPHY

SUBMITTED

BY

AMARNATH PAL

DEPARTMENT OF CANCER AND STEM CELLS

SCHOOL OF MEDICINE, QUEEN'S MEDICAL CENTRE

UNIVERSITY OF NOTTINGHAM

2015-2019

Abstract

Breast cancer (BC) is the second most common cancer type and a major health issue responsible for death in women. Paracrine signalling actively participates in normal breast development and also play a crucial role in breast cancer cell (BCC) proliferation and invasion. Previous indirect 2D co-culture studies have demonstrated the possibility that mesenchymal stem cells (MSCs) promote BC progression through secretion of paracrine factors including growth factors, cytokines and chemokines. This effect may therefore also occur in the tumor microenvironment (TME) within patient tumors. However, very little is known regarding the influence of MSCs on BCCs in mixed cell populations (direct coculture) in 2D cell culture. Therefore, investigating the paracrine effect of MSCs in switching ductal carcinoma *in situ* (DCIS) into invasive ductal carcinoma (IDC) using 2D co-culture may facilitate identification of targeted therapeutics to treat BC in patients. However, failure of 2D cell culture model in representing the natural TME limits the scope of the discovery of the potential targeted therapeutics to treat advanced BC in patients. Since 3D spheroid models are more representative of a number of aspects of tumour biology, the spheroid model is considered a promising pre-clinical tool for drug discovery. Therefore, in parallel with 2D co-culture, for the first time in this study a BCC spheroid co-culture model incorporating MSCs was used in order to investigate the impact of MSCs on the BC progression. The BCC proliferation capacity of MSCs in 2D and spheroid models was determined by several *in vitro* assays and further confirmed by increased Ki-67 expression in BCC in the spheroid co-culture model. Beyond determining the effect of MSCs on BCC proliferation, the epithelial-

mesenchymal transition (EMT)-inducing property of MSCs in non-invasive BCC in the co-culture models was also investigated in this study. An alteration in the phenotype was observed including cytoskeletal rearrangement and changes in expression of E-cadherin (downregulated) and vimentin (upregulated) in BCCs in the 2D co-culture, together highlighting the induction of EMT in the BCCs in the presence of MSCs. Similarly, the EMT-promoting effect of MSCs in BCC was determined through histology in the spheroid co-culture, which was consistent with an increased migration in the non-invasive BCCs, including in DCIS patient-derived BC xenografts (PDXs) incorporating MSCs.

Since the collective observations in this study demonstrated a likely role of MSCs in the progression of DCISs toward IDCs, further investigation on the MSC-exerted signalling pathways associated with BC progression in the co-culture was performed. Downregulation of SnON in MCF-7 in co-culture models highlighted the probable underlying mechanism behind MSC-induced EMT associated with the BC invasion. In addition, the β-catenin inhibitor, MSAB-mediated arrest of growth and invasion in MCF-7 in the co-culture indicates the MSC-driven paracrine activation of this pathway in MCF-7 cells. Therefore, it appears that targeting β-catenin may be a novel approach to reduce BC invasion and SnON may be a marker of invasion that could be used to indicate the aggressiveness of the disease. However, a broader analysis of SnON is required in PDXs and patient samples to understand its role as a potential bio-marker for BC invasiveness in more detail, and further detailed studies of other potential signalling pathways active in BCC in the co-culture models may

contribute towards identifying other possible targets for therapeutic intervention in IDC patients.

Keywords: Breast cancer (BC), Ductal carcinoma *in situ* (DCIS), Invasive ductal carcinoma (IDC), Spheroid co-culture model, Mesenchymal stem cells (MSCs), Tumor microenvironment (TME), Epithelial-mesenchymal transition (EMT), Paracrine signalling, Sloan Kettering Institute (SnON), β-catenin and Methyl 3-{[(4-methylphenyl) sulfonyl] amino} benzoate (MSAB).

DECLARATION

I declare that the thesis and the work illustrated in it are my own and the findings therein are entirely from the original work performed by me in the laboratory.

Amarnath Pal

ACKNOWLEDGEMENT

I dedicate this work to my parents who devoted their lives to raising their son and daughter. Without their support this work would not have been accomplished. Finally, to my well-wishers and close friend Mr. Aniruddha Halder for keep believing me and inspiring me to achieve my dream.

I am very grateful to Professor Anna. M. Grabowska for her role as my project supervisor and a research group leader. Under her supervision, laboratory experiments became a source of joy and writing up became a challenge to achieve excellence. I also tribute my warm thanks to Dr. Cinzia Allegrucci, my co-supervisor for showing her interest and providing opinions during my study. I believe that their principles will be guidance in my future in academia.

I am also thankful to Dr. Phillip Clarke, Pamela Collier and Catherine Probert for providing precious training, experiences and laboratory resources to accomplish important parts of my work. As well as Sal Jones for her huge contribution in proofreading my thesis.

I am really grateful for the great help from David Onion and Nicola Croxall in the Flow cytometry work. In addition, I pay my tribute to Dr. Andrew Benest for providing training in the confocal microscope and appreciate my colleague Naseeb Malhi for her kind help in accessing the microscope whenever I required.

I would also like to take an opportunity to thank my friend Mr. Abdul Aziz Alfahed for sharing knowledge through scientific

discussions during my PhD. Alongside; it is also an absolutely great honor and joy sharing the laboratory and office with other PhD students and Post doctorates.

At last but not least, I am hugely grateful to the International Vice Chancellor Scholarship for providing me the opportunity to have my PhD in the cancer science and to get in touch with such lovable people across the globe.

ABBREVIATIONS

4HT: 4 Hydroxy tamoxifen

5FU: 5 Fluorouracil

Adip-CM: Adipocyte conditioned medium

AKT/PKB: Protein Kinase B

ALK-2: Activin-like kinase 2

AP-1 : Activator protein 1

AREG: Amphiregulin

ATP: Adenosine triphosphate

BAD: Bcl-2-associated death promoter protein

BC: Breast cancer

BCC: Breast cancer cell

bm-MSCs: Bone-marrow-derived mesenchymal stem cells

BMP-4: Bone morphogenetic protein 4

CAFs: Cancer associated fibroblasts

CAMKII: Calcium/calmodulin-dependent protein kinase II

CBP/p300: CREB-binding protein/E1A binding protein p300

CCL2: Chemokine (C-C motif) ligand 2

CCL5: Chemokine (C-C motif) ligand 5

CREB/ATF-2: cAMP response element binding protein/Activating transcription factor 2

CRK: CT10 Regulator of Kinase

CSF-1: Colony stimulating factor 1

CTSB: Cathepsin B

CXCL12: Chemokine (C-X-C motif) ligand 12

DAG: Diacylglycerol

DCIS: Ductal carcinoma *in situ*

Dvl: Dishevelled

EC: Endothelial cells

ECM: Extracellular matrix

EGF: Epidermal growth factor

EMT: Epithelial-mesenchymal transition

EndMT: Endothelial-mesenchymal transition

EREG: Epiregulin

ERK1/2: Extracellular signal-regulated kinase 1/2

FAK: Focal adhesion kinase

FAP-α: Fibroblast activation protein-alpha

FGF: Fibroblast growth factor

FOXO: Forkhead box O

FRS-2: FGFR substrate-2

FZD: Frizzled

GAB-1: GRB-2-associated binding protein-1

GJIC: Gap junctional intracellular communications

GOI: Gene of interest

GPCR: G-protein couple receptor

GRB-2: Growth factor receptor bound protein 2

GSK-3: Glycogen synthase kinase-3

GSTP1: Glutathione S-transferase

HAT: Histone acetyl transferase

HBMEC: Human brain microvascular endothelial cells

HGF: Hepatocyte growth factor

IBC: Invasive breast cancer

ID2: Inhibitor of DNA binding-2

IDC: Invasive ductal carcinoma

IFN-y: Interferon-y

IL: Interleukin

IMC: Immature myeloid cells

JNK: Janus Kinase

LCIS: Lobular carcinoma *in situ*

MAPK: Mitogen activated protein kinase

MCM: Mesenchymal stem cell conditioned medium

MCP-1: Monocyte chemotactic protein-1

MCs: Mesenchymal cells

MDSCs: Myeloid derived suppressor cells

MET: Mesenchymal-epithelial transformation

MMP: Matrix metalloproteinases

MSAB: Methyl 3-{[(4-methylphenyl) sulfonyl] amino} benzoate

MSCs: Mesenchymal stem cells

NADH: Nicotinamide adenine dinucleotide

NADPH: Nicotinamide adenine dinucleotide phosphate

NFAT: Nuclear factor of activated T cells

NF-κβ: Nuclear factor kappa B

NK: Natural killer cells

NLK : Nemo-Like Kinase

NRG-3: Neuregulin 3

OPN: Osteopontin

P38 MAPK: Mammalian p38 Mitogen activated protein kinase

PARP: Polyadenosinediphosphate ribose polymerase

PDGF-β: Platelet-derived growth factor

PDXs : Patient-derived xenografts

PI-3K: Phosphatidylinositol-4,5-bisphosphate 3-kinase

PLC: Phosphoinositide Phospholipase C

PTHrP: Parathyroid hormone-like peptide

RANKL: Receptor activator of nuclear factor kappa-B ligand

RFU: Relative fluorescence unit

RLU: Relative luminescence unit

RPPA: Reverse phase protein microarray

sFRP-1: Secreted Frizzled-related protein-1

SHC: Src homology 2 domain

SHP-2: Src homology region 2 domain-containing phosphatase-2

Ski/SnON: Ski (Sloan-Kettering Institute)-novel protein

SMAD: Mothers against decapentaplegic homolog

SMC: Smooth muscle cell

SOCS3: Suppressor of cytokine signaling 3

STAT3: Signal transducer and activator of transcription 3

TAMs: Tumor associated macrophages

TBX3: T-Box3

TCF: Transcription factors

TEC: Tumor endothelial cells

TGF-β: Transforming Growth factor beta

TIMP: Tissue inhibitor of metalloproteinase

TME: Tumor microenvironment

TNBC: Tripple negative breast cancer

uPA: Urokinase plasminogen activator

VEGF: Vascular endothelial growth factor

α-SMA: alpha-smooth muscle actin

β-Arrestin : Beta-arrestin

β-catenin: Beta-catenin

TABLE OF CONTENTS

TABLE OF FIGURES:

LIST OF TABLES:

CHAPTER 1: INTRODUCTION

Breast cancer (BC) is the second most common cancer worldwide. The incidence of BC is increasing and will be a leading cause of death in the future in women[1]. In the United states, 1 in 8 women develops invasive ductal carcinoma and 180,000 new cases of invasive BC are diagnosed each year[2]. Hence, in an attempt to understand the disease and treatment, BC is classified into categories depending upon the origin and molecular patterns of cancer cells in the breast. According to the site of origin of cancer, the American Cancer Society classifies BC into two categories: Lobular Carcinoma and Ductal Carcinoma. However, in respect of growth, invasion and the presence of hormone receptors, BC is further classified accordingly based on histological and molecular characteristics.

1.1 Histological classification of BC

Histological Classification is based on the growth of BC as *in situ* carcinoma or invasive carcinoma. In terms of the origin, *in situ* breast carcinoma is subdivided into Lobular carcinoma *in situ* (LCIS) and Ductal carcinoma *in situ* (DCIS). DCIS is more common than LCIS and is a precursor of invasive BC (IBC)[3]. A statistical analysis demonstrated that survival of the patients diagnosed with DCIS is 98%, but it is just 27% in the patients with the IBC[2]. According to distinct architectural patterns DCIS is further classified into comedo, cribriform, papillary, micropapillary and solid[3]. Similarly, IBC is broadly classified into invasive/infiltrating ductal carcinoma (IDC), invasive lobular carcinoma (ILC), ductal/lobular, mucinous (colloid), tubular, medullary and papillary

carcinomas. Among these, IDC encompasses 70%-80% of all IBCs[4]. Therefore, it seems that all the IBCs may not necessarily originate from DCIS as previously mentioned[3] but it appears that in general *in situ* carcinoma in the ducts is a precursor for IBC in BC patients. Therefore, based on the growth, differentiation and invasion, BC is classified into well-differentiated (Grade 1), moderately differentiated (Grade 2) and poorly differentiated (Grade 3)[5].

1.2 Molecular classification of BC

Although the histological classification helps in categorising BC in terms of origin, growth and invasion, the molecular classification facilitates differentiating similar histopathological cancer types and acts as a good predictor for different treatment outcomes[6]. Based upon the presence of hormone receptors, BC is divided into Luminal A, Luminal B, Human epidermal growth factor (Her2) enriched, and basal type or triple negative BC (TNBC)[7,8].

BC subtypes	Hormone receptors
Luminal A	**ER+, PR+, HER2-**
Luminal B	**ER+, PR+, HER2+**
Her2 enriched	**ER-, PR-, HER2+,**
Basal/TNBC	**ER-, PR-, HER2-**

Table 1-1: Molecular classification of BC: Luminal A, B, Her2-enriched and basal are the BC subtypes based upon the presence of hormone receptors: Estrogen receptor (ER), Progesterone receptor (PR), Human epidermal growth factor receptor (Her2). Due to the absence of the ER, PR and Her2, the term triple negative BC or TNBC was coined for basal-like BC[7,8].

In terms of prognosis, among the four BC subtypes luminal B shows poor prognosis comparing to Luminal A while Her2-enriched and TNBCs have worse outcome comparing to the Luminal A and B subtypes in BC patients[9]. In addition to the presence of hormone receptors, the differential expression profile of the proliferation marker, Ki-67 assists pathologists to understand the prognosis of the disease in different BC subtypes. It has been reported that the expression of Ki-67 is high in Her2 compared to the Luminal B subtypes[10] and highest in TNBCs but least in Luminal A[10,11]. Further, the overexpression of Ki-67 correlates with lower Disease free survival (DFS) and overall survival (OS) rates compared with those BC patients with a low Ki-67 index[11]. Thus, the expression of the hormone receptors and Ki-67 altogether provides an useful information regarding the prognosis among different BC subtypes in contrast to the histological classification.

1.3 Current therapeutic intervention in BC

In parallel to contributing in understanding the prognosis, molecular classification helps in selecting therapeutics regimen to treat BC patients.

BC subtypes	Drugs	Prognosis
Luminal A	**Tamoxifen**	**Good**
Luminal B	**Tamoxifen, Herceptin**	**Not good as Luminal A**
Her2-enriched	**Herceptin**	**Unfavorable**
Basal Like/TNBC	**Platinum group chemotherapy and PARP inhibitors**	**Worse**

Table 1-2: Current targeted therapeutics in BC: A list of the drugs and the corresponding prognosis of the treatment in BC. PARP is the acronym of Polyadenosinediphosphate ribose polymerase[8].

For Luminal A and B, inhibition of estrogen signalling by tamoxifen and aromatase inhibitors is effective, while Herceptin or trastuzumab are beneficial in Her2-positive BC in patients. On the other hand, due to the absence of known hormone receptors, TNBCs do not response to the hormone-receptor targeted therapeutics and are therefore associated with a worse prognosis[8]. Platinum-based chemotherapies, PARP inhibitors, taxol derivatives and anthracycline chemotherapy are commonly used therapeutic regimens for TNBCs[8,12]. Since 15% to 20% of IDCs are TNBCs[2] and derive mainly from the DCISs[13], a deeper understanding of the underlying mechanism transforming DCIS into IDC is required in order to identify a druggable target which may replace conventional chemotherapy and improve the prognosis in IDC and TNBC patients.

1.4 Epithelial-mesenchymal transition (EMT)

Previous studies described EMT plays an important role in the transformation of DCIS into IBC and facilitates dissemination of cancer cells to the distant organs in patients[14]. EMT is a process whereby cells lose their epithelial traits and gain mesenchymal characteristics; it is associated with embryo development, but also with wound healing and invasion in several types of cancers including BC[15]. Therefore, according to its functional role, EMT is classified into Type 1, Type 2 and Type 3. While Type 1 and 2 relate to embryogenesis and wound healing, Type 3 involves cancer cell invasion[16]. Disruption of the intercellular integrity, cell-basement membrane attachment, alteration in the cytoskeletal organisation, acquiring spindle-shape, expression of mesenchymal genes including alpha-smooth muscle actin (α-SMA), N-cadherin and vimentin are key characteristics observed in cells that have undergone EMT[15,14]. Along with the phenotypic alteration, expression of EMT-regulatory genes in BCCs was also investigated. E-cadherin plays an important role in cell-cell interaction in epithelial cells and upregulation of Snail 1 and 2 represses its expression in BCCs. Similarly, Zeb 1 and 2 reduce expression of proteins associated with the gap junction, tight junction and desmosomes results in the disruption of the epithelial traits in the BCCs. In addition, the expression of Twist 1 and 2 triggers angiogenesis and promotes metastasis through upregulating vascular endothelial growth factor (VEGF) in the BCCs.

Although the molecular mechanisms responsible for EMT and its role in BC are understood to some extent, the factors responsible for inducing EMT in BCCs are still under investigation. Since the tumor microenvironment (TME) plays a crucial role in cancer

progression[17], this study focuses on the EMT-regulatory role of TME-associated stromal cells in BCCs.

1.5 Tumor microenvironment (TME) in BC

The concept of the association of TME with cancer progression was first described by the English surgeon Steven Paget in the "Seed and Soil" theory in 1889. The TME is the site where cancer grows and consists of fibroblasts/myofibroblasts, endothelial cells, immune cells, pericytes, myeloid derived suppressor cells (MDSCs), fat cells, secreted components from these cells and extracellular matrix (ECM) that support growth, invasion and metastasis of cancer cells[18,19]. In addition to promoting the growth and survival of cancer, the TME promotes EMT and drug resistance in cancer cells[20]. Therefore, the following summarises the TME-residing cell-types and their association with BC progression.

1.5.1 Fat cells or adipocytes

Obesity is a risk factor associated with TNBC in younger women[21]. *In vitro* studies demonstrated adipocyte-conditioned medium (Adip-CM) increased cell motility, increased expression of serine protease urokinase plasminogen activator (uPA), and altered expression of several genes responsible for cell adhesion and invasion in BCCs[22]. Leptin, adiponectin and interleukin-6 (IL-6) are the three adipokines secreted by adipocytes in the TME. Leptin and IL-6 participate in maintaining the population of BC stem cells through upregulation of Notch, Wnt, cell proliferation, survival and EMT regulatory genes in BCCs. On the other hand, adiponectin exerts anti-oncogenic property on BCCs. Therefore, low levels of adiponectin in serum highlights an increased risk of BC[23].

1.5.2 Natural Killer cells (NK cells)

NK cells are components of the innate immune system and have potential to prevent cancer growth through exerting cytotoxic effect in the target cells. Therefore, infiltration of NK cells into the tumor stroma may provide a good clinical outcome in BC patients[24]. However, Prostaglandin E from BCCs impaired the cytotoxic effect of NK cells resulting in BCCs escaping from the NK cell-driven cytotoxicity[25].

1.5.3 Tumor associated macrophages (TAMs)

The presence of TAMs in the TME is associated with a poor prognosis in breast and endometrial cancer. The hypoxic condition of TME, immobilizes TAMs in the stroma of BC and endometrial cancer[26]. TAMs derive from the tissue resident macrophages or from bone marrow. Phenotypically, macrophages are classified into two types: M1 and M2, where M1 macrophages are responsible for the immune response and secretes type 1 cytokines, M2 macrophages secrete type 2 cytokines displaying pro-tumorigenic effect. Although the exact mechanism responsible for M1 to M2 transition is not clear, hypoxic areas in tumors promote M2 accumulation in the TME[27]. Since TAMs share expression of M2 markers, it appears TAMs are closely related to the M2 macrophages in the TME[28] and such accumulation of TAMs results in BC metastasis via promoting angiogenesis[29].

1.5.4 Myeloid derived suppressor cells (MDSCs)

Myeloid derived suppressor cells (MDSCs) are a heterogenous group of immature myeloid cells, which expand in inflammation, infection and cancer, and have the potential to suppress the action

of T-cells. In inflammation or cancer, immature myeloid cells (IMC) cannot differentiate into other mature myeloid cells including granulocytes, macrophages and dendritic cells resulting in an expanded population of MDSCs in the microenvironment[19]. Mouse MDSCs (Grl+CD11b+) or Human MDSCs (CD14-CD11b+CD33+) produce arginase-1 which breaks down L-arginine, an essential amino acid that helps in T-cell proliferation, ζ-Chain expression and IL-2 production[30]. Another subtype of human MDSCs (CD14+HLA-DR-/Low) collected from the peripheral blood of hepatocarcinoma patients induces the expression of T-Regulatory cells (CD24+CD25+Foxp3+) when co-cultured with autologous T-Cells[31]. In BC, increased numbers of MDSCs are found in advanced BC and are associated with poor survival[32]. In addition, MDSC-derived IL-1β induce CD4+T cells to secrete IL-17 which helps in bypassing the effect of 5-Fluorouracil (5FU) and gemcitabine[33] and thus contributes towards drug resistance in cancer.

1.5.5 Endothelial cells (ECs)

Endothelial cells lining the blood vessels, lymphatic vessels and the heart, control the diffusion of nutrients into tissues from blood, maintain the flow of blood and also regulate the migration of leukocytes. Like pericytes wrapped around the capillaries, smooth muscle cells (SMC) support the bed of endothelial cells underneath and provide stability to the vessels[34]. Hypoxia induces VEGF, platelets-derived growth factor-β (PDGF-β) and transforming growth factor-β (TGF-β) mediated angiogenesis to support growth and metastasis of cancer cells[35,36]. Unlike normal endothelial cells, tumor endothelial cells (TECs) are irregular in shape, size and comparatively long, participate in intussusceptive angiogenesis, a process where transvascular extension of the vessel wall in the

lumen splits the vessel into two halves, a more rapid process than sprouting to increase the vessel density in TME[37]. In parallel to angiogenesis, it has been reported that endothelial cells can be a precursor of mesenchymal stem cells. Either mutation in Activin-like kinase-2 (ALK-2) or under the influence of TGF-β and bone morphogenetic protein 4 (BMP-4), ECs transform into mesenchymal phenotype through the process of Endothelial-mesenchymal transition (EndMT)[38].

1.5.6 Pericytes

Pericytes or Rouget cells are the perivascular cells, which wrap around the vascular wall. Pericytes are also known as mural cells, have contractile features and contain long cytoplasmic processes that embrace the wall of blood vessels and directly communicate with endothelial cells via Gap junctions or PDGF-β paracrine signalling[39]. Depletion of pericytes leads to poor prognosis in BC as low coverage of pericytes, increases EMT, upregulates Met receptor (receptor for hepatocyte growth factor or HGF) and increased angiogenesis result in invasion and metastasis of cancer[40,41].

1.5.7 Extracellular matrix (ECM)

ECM is a collection of extracellular molecules, secreted by fibroblasts which provide support to the surrounding cells and plays a vital role in tissue morphogenesis, differentiation and homeostasis. The ECM is composed of water, proteins and carbohydrates[42], and dynamic due to its constant remodeling by matrix metalloproteinases (MMPs)[43]. Some of the MMPs involved include MMP-9, MMP11, MMP2, MMP14 and MMP13. These are involved in BC invasion leading to the progression of DCIS to IDC

by degrading collagen IV, the major protein found in the ECM[44,45]. The ECM also helps in signal transduction by binding growth factors and by direct interaction with the cell surface receptors resulting in the alteration of gene expression in the target cells[42]. For example, binding of cell surface integrins to the RGD (Arginine-Glycine-Asparginine) sequence of fibronectin promotes cell attachment and migration where heparin sulphate chains of proteoglycan binds with FGF (Fibroblast growth factors), helping them to bind with their cell surface receptors[46] and consequently triggering intracellular signalling in BCCs[47]. In addition, uPA in the ECM plays an important role in BC invasion via activation of MMP-9 and can be a good prognostic marker in primary BC[48]. Hence, it can be said that competitive inhibition of growth factor binding within the proteoglycan milieu or inhibition of uPA could be an efficient approach to control BC invasion.

1.5.8 Fibroblasts

Fibroblasts are found in copious amounts in connective tissues and secrete components of ECM to support tissues and function of organs. Fibroblasts also participate in wound healing and fibrosis[49]. During wound healing, fibroblasts differentiate into myofibroblasts and normally then disperse once their role has been completed, but they remain high in the stroma of cancer. This type of myofibroblast is termed a Cancer-associated fibroblast or CAF, which expresses high levels of alpha-smooth muscle actin (α-SMA)[50]. However, CAFs are not only derived from resident fibroblasts but can also differentiate from MSCs under the influence of osteopontin (OPN) secreted by TNBCs[51]. CAFs secrete various growth factors such as HGF, FGF, TGF-β and chemokine CXCL12/SDF-1 (C-X-C motif chemokine ligand 12 or Stromal cell-

derived factor 1), which together promote tumor growth, EMT and invasion in cancer cells[40]. *In vivo* studies reveal that inactivation of fibroblast activation protein alpha (FAP-α)-expressing fibroblasts in tumor stroma leads to interferon-γ (IFN-γ) and tumor necrosis factor-α (TNF-α)-mediated tumor necrosis[52]. Similarly, application of αFAP-PE38, a FAP-targeting immunotoxin, inhibits BC metastasis in mice. In addition, depletion of CAFs alters the expression of various growth factors and cytokines that play an important role in the recruitment of several type of immune cell, that in turn, also support growth and metastasis of cancer cells[53].

Therefore, inhibition of fibroblasts is another potential way to treat cancer growth and metastasis. However, inhibition of fibroblasts could cause adverse effects as they play an important role in normal wound healing and also help in maintaining normal body homeostasis.

1.5.9 Mesenchymal Stem cells or MSCs

In the TME, CAFs originate from the fibroblasts or can be formed from the bone marrow-derived mesenchymal stem cells (bm-MSCs)[54]. In addition to within the bone-marrow, MSCs are found in a broad range of adult tissues including adipose tissue, trabecular bone chips, periosteum, synovial fluid, periodontal ligament, palatine tonsil, parathyroid gland, fallopian tube and traumatized muscle tissue. MSCs are also found in prenatal tissues such as umbilical cord, Wharton's jelly and primary tooth pulp[55]. Being multipotent stem cells MSCs have the ability to differentiate into adult tissues[56] and participate in tissue repair[57]. MSCs retain their self-renewal property under tight regulation of autocrine

action of Wnt signalling[58] and characterised by the presence of cell surface markers including CD73, CD90 and CD105[59]. Although MSCs have the ability to maintain body homeostasis, studies have shown a role for MSCs in promoting BC metastasis[60]. The tumor-promoting properties of MSCs are not restricted to BC but also plays an important role in proliferation and invasion in prostate[61] and gastric cancer[62]. While studies have shown the bm-MSCs cause BCCs to grow, there are instances in which umbilical cord and adipose tissue-derived mesenchymal cells (MSCs) prevent metastasis in BC mouse models[59]. Hence, it appears that not all MSCs are identical in terms of cancer progression and therefore, understanding the underlying mechanisms driven by the bm-MSCs in BC progression has become of interest in the field of cancer research.

1.6 Importance of MSCs in mammary gland development

Breast has a structure consisting of lobules, milk ducts and adipose tissues. Each lobule is consisted of alveoli having lactocytes responsible for the production of breast milk. On the other hand, milk ducts carry milk from lobules to nipple in lactating women[63]. Although the role of female hormones in breast development is well documented[64], involvement of paracrine signalling has been observed during ductal and alveolar development in chimeric mice with both estrogen and progesterone receptor negative (ER^-/PR^-) and wild-type mammary epithelial cells[65]. Further investigation revealed that paracrine signalling between parenchyma and MSCs plays an essential role in normal breast development in embryos[66].

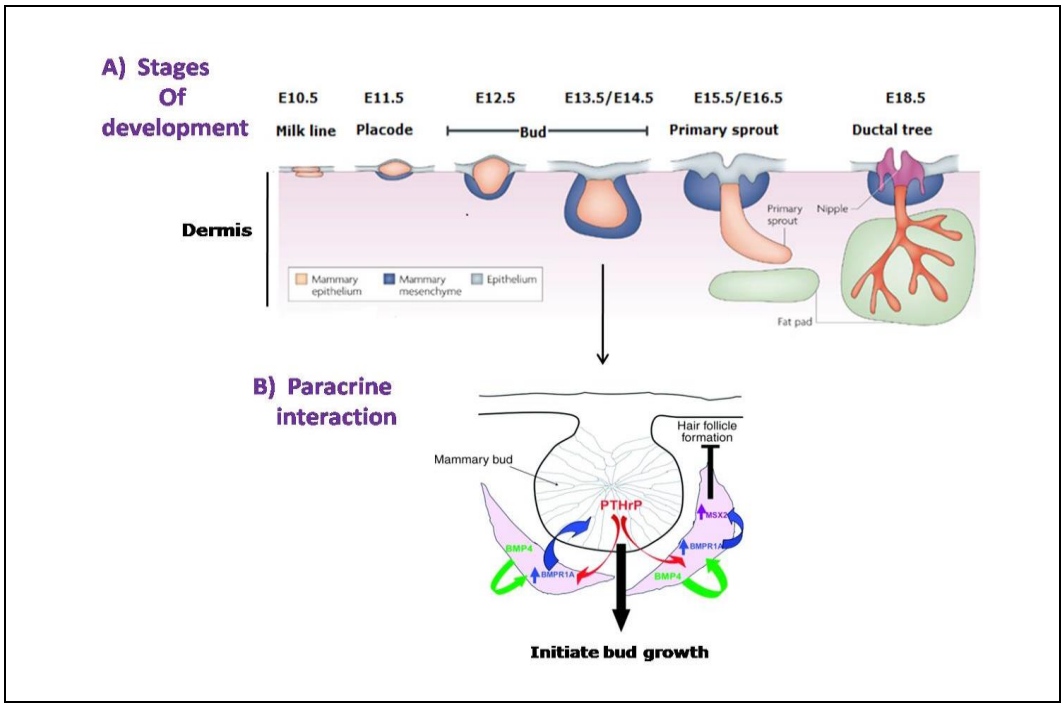

Figure 1-1: Role of MC-driven paracrine signalling in the development of normal breast: A. Concomitant stages of maturation of breast from embryonic stage to adult[67]. Alphabet 'E' followed by numeric demonstrates different time points of embryonic development in mice. **B.** Epithelial cell-secreted parathyroid hormone like peptide (PTHrP) stimulates mesenchymal cells to assist in mammary bud sprouting and thus the paracrine interaction between mesenchymal cells and mammary epithelial cells during breast development[66].

In mouse embryos, it has been observed that somite-secreted Fibroblast growth factor-10A (FGF10A) induces the expression of Wnt10 signalling in the milk line and helps in the formation of placode which signals and transforms somites into specialized mesenchymal cells known as the primary mammary mesenchyme. These primary mesenchymal cells secrete FGF, Wnt, and NRG3 (Neuregulin3) which induces placode to form the mammary bud[67] and helps in sprouting of mammary bud under the influence of mammary epithelial cell-secreted Parathyroid hormones such as PTHrP[68] (Figure 1-1). During this period, mammary bud invades the surrounding mesenchymal region and forms the lactiferous duct and lobules. The epithelial cells lining the lumen of the

lactiferous duct become secretory in nature and the basal layer becomes myoepithelial cells. At this stage, residual mesenchymal cells transform into fibroblasts, smooth muscle cells, endothelial cells and adipocytes[69].

1.7 Homing of MSCs in the TME and the interaction with BCCs

Although MSCs play an important role in the development of breast, the association of MSCs with BC progression was also reported. MSCs are recruited to the TME from the bone marrow under the influence of several inflammatory factors[70]. Upon arrival in the TME under the influence of VEGF, basic fibroblast growth factor (b-FGF), PDGF, TGF-β, and TNF-alpha[71] MSCs support cancer progression either by direct paracrine actions, by differentiating into CAFs, via promoting angiogenesis or as an immunosuppressor to protect cancer cells against the immune system[72].

The differentiation of MSCs into CAFs gives rise to a heterogenous population of cells. Therefore, the term Mesenchymal stem cell (MSC) becomes a topic of debate in research. Stem cells are the undifferentiated form of cells, which are able to differentiate into specialized cell lines and have self-renewal properties for the lifetime of an organism. MSCs may not be an appropriate term for such cells following *in vitro* culture due to phenotypic changes (intended or otherwise) such as decreased telomerase activity, loss of plasticity, limited passage number, and presence of heterogenous population of cells in cell culture[73,74]. However, the term MSC is still frequently used but with different meanings and

therefore careful attention needs to be paid to the definition and source of these cells in individual studies.

In the co-culture, different forms of physical interactions between MSCs and BCCs are observed. Notch signalling, Gap junctional intercellular communication (GJIC), Nanotubes formation, Trogocytosis, and cell fusion are the most notable physical interaction which facilitate acquisition of CD90, mitochondrial enrichment and chemoresistance in BCCs in the 2D co-culture[74]. Along with the physical interaction, MSC-secreted growth factors, cytokines and chemokines influence BC progression in the TME. Direct co-culturing of BCCs with MSCs increases the expression of MMP11, VEGF, Insulin-like growth factor-1 (IGF-1) and BCL2 responsible for invasion, angiogenesis and survival of BCCs. In the same study it was also observed that the presence of MSCs elevates the expression level of EMT markers including N-cadherin, Vimentin, TWIST and Snail, in BCCs[75]. Further, a hypoxia induced MSCs to secrete angiogenic factors VEGF, IL-6, Monocyte chemotactic protein-1 (MCP-1) and growth factors including HGF and TGF-β, responsible for the cancer cell proliferation and metastasis[76].

As tumor can be considered a chronic inflammation[77], either the influence of prolonged exposure to PDGF and TGF-β[78] or BCC-derived OPN drives the formation of CAFs from the MSCs in the TME[79]. Later, the CAF-secreted growth factors and cytokines including EGF, HGF, FGF, TGF-β and CXCL12 promote BCC proliferation, metastasis and angiogenesis via paracrine signalling[80,81]. In parallel with the aforementioned growth factors and cytokines, a high concentration of chemokine (C-C motif) ligand 5 (CCL5) in the MSC-conditioned medium (MCM) is

associated with BC metastasis in co-culture models[82]. In addition, ectopic expression of Wnt3A by human mammary fibroblasts[83] and secretion of leptin from bm-MSCs[84] further provide an evidence of paracrine function of MSCs in BC progression. Paracrine signalling not only linked with BCC proliferation and invasion, but exogenous application of these paracrine factors alters the expression of cell surface receptors and promotes the drug resistance in BCCs. Cell culture studies demonstrate that TGF-β and HGF signalling axes induce expression of G-protein coupled receptor CXCR4 in BCC[85,86] while CXCL12/CXCR4 signalling promotes expression of Her2 (EGF receptor) in BCCs[87]. Therefore, the upregulation of these cell surface receptors may be an important reason underlying increased nuclear expression of proliferation marker Ki-67 in the tissue and aggressiveness of BC in patients. Further, being a G-protein coupled receptor (GPCR), the Gα subunit of G-protein associated with CXCR4 promotes the expression of Glutathione S-transferase protein 1 (GSTP1), responsible for drug resistance in many cancers[88,89]. This highlights the possible role of MC (MSC+CAF)-exerted paracrine role in bypassing the drugs used to treat IBCs. Although studies showed BC-promoting effect of MSCs, the inhibitory role of MSCs in BC invasion has also been demonstrated. The presence of tissue inhibitor metalloproteinases (TIMPs) including TIMP1 and TIMP2 in MCM highlighted the inhibitory role of MSCs in BC metastasis[90]. This contradictory role of MSCs in BCC raised a doubt regarding the tumor-promoting effect of the MCs. Therefore, a direct co-culture study of BCCs with MSCs is required to explore its impact on BC invasion.

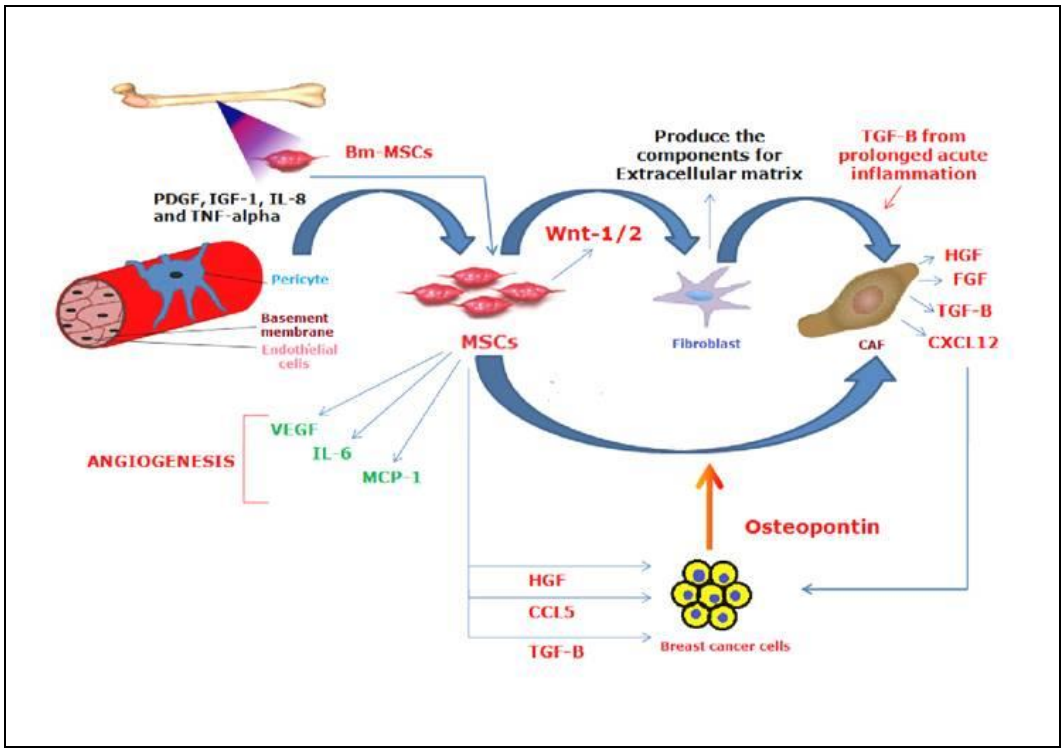

Figure 1-2: Paracrine factors from MCs (MSCs and CAF) in the Tumor microenvironment (TME): Under the influence of several inflammatory cytokines (PDGF, IGF-1, IL-8, and TNF-alpha) bone marrow derived mesenchymal stem cells (bm-MSCs) migrate to the tumour niche where MSC-secreted angiogenic factors (VEGF, IL-6 and MCP-1) and growth factors (HGF CCL5 and TGF-β) altogether promote growth and metastasis of BC[70,71,76,82]. Where, Wnt from MSCs support proliferation of fibroblasts in the TME[91] and osteopontin from BCCs transform MSCs into CAFs[79]. On the other hand, prolonged exposure of TGF-β helps in transformation of residual fibroblasts into CAFs[78] which secrete various growth factors and chemokines including HGF, FGF, TGF-B and CXCL12 which promote growth, proliferation, EMT and cell survival via triggering several intracellular signalling pathways[80,81].

1.8 Paracrine signalling pathways in BC

Since MSCs secrete a broad spectrum of growth factors and cytokines in the TME and impact on BCC proliferation and invasion, a deeper understanding of each signalling axis may be helpful in order to decipher the downstream effect of each signalling molecules and identify potential targets to suppress BC invasion.

1.8.1 Epidermal growth factor (EGF) signalling pathway

EGF signals through binding to the epidermal growth factor receptor (EGFR) which belongs to a family of tyrosine kinases that includes erbB2/Her-2, erbB3/Her-3 and erbB4/Her-4. However, the somatic mutation or overexpression of EGFR in cancer cells results in intracellular signalling in an EGF-independent manner. The potential downstream molecules activated by EGF/EGFR signalling are mitogen-activated protein kinase (MAPK), phosphatidylinositol-3kinase (PI-3K), phospholipase Cy (PLC-γ), signal transducers and activators (STAT) and Src kinase, which play crucial role in cell proliferation, survival and migration[92] and induce EMT in non-invasive BCC line through Smad signalling[93]. Since most of the IBCs and TNBCs overexpress EGF receptor on their surface and inhibition of the signalling axis increases chemosensitivity in TNBCs, EGFR was identified as a potential therapeutic target for invasive BC. Although several drugs targeting EGFR have been developed, the efficacy of drugs in clinical studies has not been promising[94].

1.8.2 Fibroblast growth factor (FGF) signaling pathway

In cells, FGF induces dimerization of the fibroblast growth factor receptor (FGFR), another tyrosine kinase receptor, and triggers downstream intracellular signalling pathway by recruiting several intracellular signalling molecules such as FGFR substrate 2 (FRS-2) and PLC-γ; these further activate the Ras/Diacylglycerol (DAG) signalling pathway that drives proliferation and cell survival. However, mutation in FGFR also leads to dimerization of receptors and thus triggers spontaneous signalling[95]. The FGF signalling axis upregulates the expression of EGFR ligands amphiregulin (AREG)

and epiregulin (EREG) in mouse mammary cells and MCF7 BCC lines[47] and accelerates the development of mammary carcinoma in mouse models[96]. Although FGF signalling is known to induce Ras and MAPK signaling resulting in increased growth and cell survival, the association of FGF with EMT has only recently been demonstrated: inhibition of FGFR1 with PD173074 triggers mesenchymal-epithelial transformation (MET) by suppressing p38-MAPK/AP-1 signalling axis in BC[97] highlighting their role in promoting EMT.

1.8.3 Hepatocyte growth factor (HGF) signalling pathway

HGF is primarily expressed in the stromal cells and overexpression of HGF receptor c-MET in IDC tissues suggests association of HGF signalling pathways with BC metastasis in patients[98]. HGF signalling axis also assists in circumventing the effect of receptor tyrosine kinase inhibitors, resulting in drug resistance in various cancers including Her2-enriched BC[99].

Upon binding of HGF, activated c-MET acts as a docking site for several adaptor proteins including Growth factor receptor bound protein 2 (GRB2), src homology 2 domain containing (SHC), and v-crk sarcoma virus CT10 oncogene homolog (CRK). Upon activation of GRB-2, its downstream signalling molecule GAB-1 or GRB-2-associated binding protein 1 further stimulates MAPK, PLC-y, PI-3K, CRK and src homology region 2 domain-containing phosphatase -2 (SHP-2) signaling responsible for cell survival and proliferation. In addition, docking of Src with the cytoplasmic domain of c-MET results in the activation of Focal adhesion kinase (FAK)-dependent cell motility in cancer cells. Similarly, triggering

STAT3 and CRK-dependent activation of Janus kinase (JNK), induces cellular transformation and invasion in cancer cells[100].

1.8.4 Transforming growth factor-β (TGF-β) signalling pathway

TGF-β is an endogenous growth inhibitory factor but is also associated with the growth of cancer cells[101]. Previous studies demonstrated proteins belonging to the Smad family act as downstream signalling molecules for TGF-β signalling. Normally, TGF-β induces the expression of p15INK4b (inhibitor of Cyclin D-CDK4/6 complex) and p21 (inhibitor of Cyclin E/A-CDK2 complex) via Smad-FOXO/C-EBPβ complex and Smad-FOXO complex respectively and thus inhibits mammary epithelial proliferation[101]. Smurf 1-driven degradation of Smad[102] and Caveolin-mediated internalisation of TGF-β receptor (TGF-βR) rescue cells from the TGF-β-effect. However, the association of syntenin with the cytoplasmic tail of TGF-βR interrupts the receptor internalisation and therefore, resulting hyperphosphorylation of Smad induces EMT[103]. Although the role of syntenin was not well characterised in invasive BCCs, EMT and overexpression of TGF-βR in BC stem cells[104] and downregulation of syntenin may facilitate a TGF-β signalling-driven invasive phenotype in BCCs.

1.8.5 Wnt signalling pathway

Wnt was first discovered as the product of the murine-int1 gene in murine mammary tumors developed as a result of murine mammary tumor virus infection[105]. In flies, the Wnt pathway regulates wing development by controlling the signalling cascade involving glycogen synthase 3 (GSK-3) and armadillo, known as Beta-catenin (β-catenin) in mammals[106]. Based upon the

activation of β-catenin, Wnt signalling cascade is divided into Classical (β-catenin-dependent) and non-classical (β-catenin independent) signalling pathways. In the case of the classical pathway, binding of Wnt to its receptor Frizzled (Fzd) activates Dishevelled (Dvl), which rescues β-catenin through disassembly of the destruction complex. Later, β-catenin facilitates expression of cell proliferation regulatory genes C-MYC, Cyclin D and ID2 (inhibitor of DNA binding 2) through heteromeric association with other transcription factors including TCF, CBP and STAT 3 in the nucleus[107]. Interestingly, as well as involvement in Wnt signalling, β-catenin serves as a downstream signalling molecule of EGF[108] and CCL5[109] and thus may facilitate the convergence of Wnt, EGF and CCL5 signalling axes in BC.

In contrast, the non-canonical Wnt cascade is independent of β-catenin and, based upon the co-receptors; it is sub-classified into Fzd-LRP5/6-mediated but β-catenin-independent, Fzd-ROR2/RYK pathway or only Wnt-Fzd pathways. Interestingly, unlike the classical pathway the non-classical pathway mainly associates with actin remodeling, migration and survival through activation of downstream signalling molecules including Rac1, Rho A, Calcium/calmodulin-dependent protein kinase II (CAMKII), and the calcium-dependent molecules calcineurin and nuclear factor of activated T cells (NFAT)[107,110]. Therefore, downregulation of the Wnt inhibitory molecule, secreted Frizzled-related protein 1 (sFRP1) is associated with a poor prognosis in BC[111]. Accordingly, inhibition of Wnt by pyrvinium pamoate leads to a significant decrease of stemness in MDA-MB-231 and delayed tumor growth in a mouse BC models[112]. In addition, Wnt pathway is involved in rescuing the ER+ BCC line from the effect of anti-proliferative

drugs 4-Hydroxy-tamoxifen (4HT)[113]. Thus, the evidence demonstrates the association of Wnt signalling with growth, stemness and drug resistance in BC.

1.8.6 RANKL or Receptor activator of NFκ-β ligand signalling pathway

RANKL initiates intracellular signalling through binding with the RANK receptor and plays an important role in bone remodeling[114]. However, a role for RANK signalling in mammary gland development has also been demonstrated. RANK knockdown mice fail to develop lobulo-alveolar mammary epithelial cells responsible for milk production in breasts[115]. In addition, the high expression of RANK in the surface of BC cell line[116] and pulmonary metastasis of Her2 BCCs under the influence of regulatory T-cell-secreted RANKL provide a clue regarding the association of RANKL/RANK signalling with BC metastasis[117,118]. Whether MSCs act as a constitutive source for RANKL is unknown, but under the influence of PTHrP (Parathyroid hormone-related protein), bm-MSCs show high expression of RANKL[119]. Since PTHrP is secreted from TNBCs[120] and is involved in bone metastasis in patients[121], it appears that regulation of RANKL in MSCs is influenced by BCCs in advanced disease. In addition, inhibition of nuclear factor-κβ (NF-κβ), the natural downstream signalling molecule of RANKL, increases chemosensitivity in BCCs[122].

1.8.7 CXCL12 signalling pathway

CXCL12 is a chemokine responsible for chemotactic movement of cells. The binding of CXCL12 to CXCR4, its G-protein coupled receptor (GPCR), increases intracellular Ca^{2+} level and triggers PI-3k, Ras/Raf and P38MAPK signalling resulting in increased cell

survival, proliferation and migration[123]. The tumor-promoting effect of CXCL12 was observed in BCCs[124] and administration of CXCR4-antagonist inhibits tumor growth in human xenograft models of different types of cancer[125]. Although it appears that inhibiting CXCL12/CXCR4 signalling suppresses BC progression, the binding capability of CXCL12 with its alternative GPCR receptor, CXCR7 may bypass the effect of CXCR4 antagonist[126]. Therefore, more detailed study of the CXCL12 signalling cascade is required in order to enable targeting of the signalling axis for BC therapy in patients.

1.8.8 JAK/STAT signalling pathway

The JAK/STAT pathway is associated with the signalling triggered by various cytokines and peptide hormones (i.e. Prolactin, Oncostatin, Growth hormone, Leukemia inhibitory Factor). Among the proteins belonging in the Janus kinases (JAKs), JAK1 and JAK2 are expressed in many tissues including mammary tissue. Similarly, depending upon the tissue type and the ligands, JAKs activate the members of the STAT (Signal transducer and activator of transcription) family including STAT1-4, STAT5a, STAT5b and STAT6. Among the STATs, increased phosphorylation of STAT1, STAT2, STAT3 and STAT5 is observed in different solid tumors including head and neck, breast and lung cancers[127]. Since inhibition of STAT3 suppressed tumorigenicity of MCF-7 in mice[128], it seems inhibition of cytokine signalling can be a promising approach in BC therapeutics. The activation of STAT3 in BCCs is mainly governed by IL-6 produced by BCCs and fibroblasts[129]. Therefore, IL-6 may exert its effect through in both an autocrine and paracrine manner in BC. Similarly, although the impact of MSC-secreted IL-6 was investigated on angiogenesis[76], MSCs may

induce BC invasiveness through the IL-6/STAT3 pathway. Along with the IL-6, STAT3 serves as a downstream signalling molecule of the leptin signalling axis[130,23]. It has been observed that Leptin upregulates numerous genes associated with cell proliferation and survival of BCCs[131]. Although MSCs do not secrete leptin autonomously, *in vitro* studies demonstrated proinflammatory cytokine IL-17, induces leptin production in MSCs[132]. Therefore, Leptin production under the influence of T-lymphocyte-secreted IL-17 in the TME[129] may be another aspect of MSC-driven activation of JAK/STAT signalling results in the invasiveness in BCCs.

1.9 Mesenchymal cell-secreted paracrine factors and the possible paracrine signalling crosstalk in BCCs

Although exogenous application of growth factors and cytokines individually in cell culture studies revealed the importance of paracrine signalling in BC progression, the situation in the natural TME may be different. Along with MSCs, CAFs derived from resident fibroblasts and MSCs enrich MC population in the TME where they secrete a broad range of paracrine factors (Table 1-3).

Growth factors secreted from mesenchymal cells (MCs)	
MSCs	**CAFs**
TGF-β, IL-6, HGF[76]	EGF, HGF, FGF, TGF-β, CXCL12[40]
CCL-5[82]	IL-6, EGF[80]
RANKL[119]	
Leptin[132]	
Wnt[58]	

Table 1-3: A comparative list of growth factors, cytokines and chemokines secreted from mesenchymal cells (MSCs and CAFs).

Therefore, because of the presence of abundant numbers of MCs, it is most likely that cancer cells are exposed to many growth factors, cytokines and chemokines simultaneously. Hence, the chance of crosstalk between the signalling pathways might exert synergistic effects on proliferation, EMT, invasion and metastasis of BC in patients.

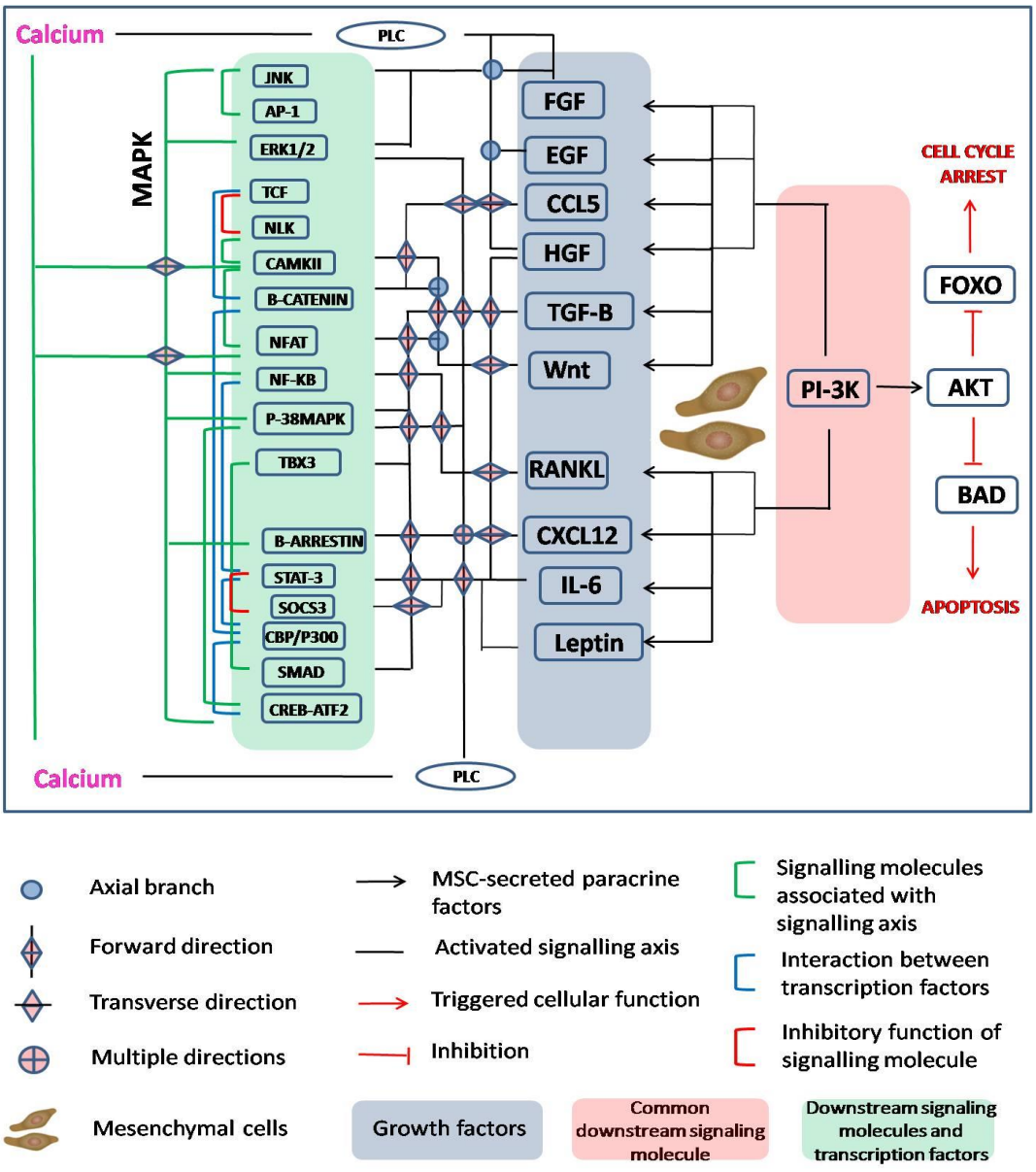

Figure 1-3: MC-secreted growth factors and the associated signalling crosstalk in BC: A. Hypothetical interactive model of paracrine signalling network exerted by the paracrine factors secreted from the MCs in BCCs. **B.**

The interactive model of paracrine signalling was developed following review of the literatures and using different geometrical shapes (boxes, arrows and symbols) in PowerPoint.

An interactive model of signalling network was developed based upon evidence from the literature of the individual signalling pathways investigated using commercially available growth factors and cytokines, known to be secreted by mesenchymal cells, in 2D cell culture. Mapping of individual paracrine signalling demonstrate a complex MSC-exerted paracrine signalling network in the BCCs.

Among the signalling pathways, the MAPK pathway is the multifunctional pathway associated with the proliferation, cell survival, apoptosis and migration in cancer cells. However, a number of upstream and downstream signalling molecules of MAPK signalling axis are shared by cytokines and chemokines signalling axes in several types of cancer including BC. In addition, molecules of MAPK signalling axis support other signalling axes at the transcriptional level[133]. Therefore, developing a consolidated map of various signalling pathways and associated transcription factors with those signalling pathways might be useful in understanding the basis of paracrine signalling-dependent BC progression and also help to identify novel targeted therapeutics to treat IBCs.

Extracellular signal-regulated kinase 1/2 (ERK1/2) is a member of MAPK family and the downstream target of signalling axes induced by EGF, HGF, FGF and CXCL12[134,135]. ERK1/2 promotes the BCC proliferation[136] and associates with the reduction in the expression of ER in BCCs resulting in the insensitivity toward anti-estrogen therapy[137]. The activation of ERK1/2 is not only dependent upon

the aforementioned paracrine factors, but can be driven by Wnt signalling[138]. Although the Wnt-mediated transactivation of ERK1/2 has not been investigated in BCCs, the role of β-catenin in mammary cancer has been demonstrated. The presence of Wnt, activates β-catenin which in turn interacts with TCF and facilitates the upregulation of cyclin D1 responsible for the mammary hyperplasia[139]. Further IHC characterisation determined that an increased level of cytoplasmic and nuclear β-catenin is associated with high Ki-67 expression and poor survival in BC patients[140]. Since the Wnt and MAPK signalling axes are both involved in cell proliferation, inhibition of one signalling pathway may not be sufficient to suppress the proliferation of cancer cells. Although the association of TCF with β-catenin is important for proliferation, the transcriptional efficiency of TCF is dependent upon the acetylation of β-catenin, the presence of co-activator CBP/p300 and the phosphorylation status of TCF.

CBP/p300 has histone acetyl transferase (HAT) activity. The acetylation of β-catenin at lysine 345 by CBP/p300 increases the transcriptional efficiency of the TCF/β-catenin[141]. The recruitment of CBP/p300 in the cell nucleus is enhanced on activation of NF-κβ[142] the molecule responsible for the downregulation of ER and overexpression of EGFR and CXCR4 in BCCs[143,144]. Hence, it seems that the activation of NF-κβ is associated with the phenotypic switch of luminal A BCC into more aggressive BCC phenotype. Although the precise mechanism involved in ER regulation of NF-κβ in BCC is unknown, inhibition of NF-κβ suppresses the proliferation and migration of BCCs[145]. Since NF-κβ is activated by RANKL and CXCL12 signalling axes[146,147], crosstalk with the Wnt/β-catenin signalling axis results in nuclear augmentation of

CBP/p300 in the BCCs. Therefore, it seems that the inhibition of NF-κβ or CBP/p300 may be a promising approach to treat IBCs.

Besides β-catenin, CBP/p300 also interacts with STAT3 in the cell nucleus. CBP/p300 acetylates the lysine residues (lysine 49 and lysine 87) at the N-terminus of STAT3. Acetylation of these lysine residues facilitates transcription of SOCS3 which participates in the negative feedback loop of STAT3 signalling triggered by IL-6[148]. Similarly, expression of SOCS3 opposes leptin/STAT3 signal-driven cell survival n MCF-7[149]. Therefore, inhibition of CBP/p300 facilitates IL-6, growth factors and G-protein-driven constitutive activation of STAT3, which results in overexpression of Cyclin D1, TWIST, vimentin, Oct-4, Sox-2, and CD44, in BCCs[150]. In agreement with that study, low expression of SOCS3 is associated with the lymph node metastasis in BC patients[151]. Hence, SOCS3 is an important component for regulating proinflammatory cytokines-mediated STAT3 signalling axes. Therefore, while inhibition of NF-κβ or CBP/p300 may be a suitable approach for interfering with one signalling pathway it could be problematic with regard to other cytokines and growth factor/STAT3 signalling pathways.

So far, the agonist effect of signalling crosstalk on Wnt/β-catenin has been described, but signalling crosstalk can also be antagonistic to the Wnt/β-catenin signalling axis. The phosphorylation of TCF by nemo-like kinase (NLK), the downstream signalling molecule of CAMKII governed by the Wnt non-canonical pathway, suppresses proliferation by inhibiting the binding of the β-catenin-TCF complex with DNA[152]. Therefore, it seems that the non-canonical Wnt pathway opposes the canonical

Wnt-signalling pathway and may have tumor-suppressing properties.

In the non-canonical pathway, Wnt-driven activation of PLC increases intracellular calcium ions which in turn activates CAMKII and calcineurin/NFAT signalling in the stimulated cells[153,154,155]. Since PLC is activated by FGF, HGF, EGF, RANKL and CXCL12[156,100,157,158,159], it highlights possible crosstalk between the growth factor and Wnt signalling axis. Although, such crosstalk has not been investigated individually in BCCs, the expression of NFAT increases with increasing doses of TGF-β in MDA-MB-231[160]. In the same study, knockdown of NFAT was shown to reduce the expression of N-cadherin, SnON and matrix metalloproteinases (MMP2 and 9) in MDA-MB-231 in the presence of TGF-β. Therefore, it seems that the NFAT and SnON may have EMT-inducing properties in BCCs. In contrast, other studies demonstrate that shRNA-mediated knockdown of Ski/SnON suppresses proliferation but induces EMT and MMP production in breast and lung cancer cells in the presence of TGF-β[161]. Therefore, due to the contradictory results, although it is difficult to be sure about the EMT-regulatory effects of SnON, the relation with histone deacetylases (HDAC) also suggests a role in oncogenesis[162]. Although the downstream effector molecule of SnON is not known, the interaction between SnON and Smad 4 results in the suppression of TGF-β signalling in epithelial cells[163]. The binding of TGF-β with its receptor represses proliferation in breast epithelial cells by activation of the pro-migratory molecule TBX3[164]. Since the activation of TBX3 is dependent upon TGF-β/Smad signalling[165], it seems that downregulation of SnON may increase the migration of BCCs. Although the TGF-β/smad3/4

signalling axis is important for the activation of TBX3, the association of Jun B with Smad3/4 complex has a crucial role in the activation of TBX3 in the breast epithelial cells[165]. Further, and Fos together form a complex, AP-1, which contributes to the EMT in the epithelial cells in the response to TGF-β[166].

AP-1 is a downstream target of MAPK (Jnk and p38)[133]. p38MAPK activates ATF-2 which in turn interacts with AP-1 and induces expression of MMP-2 and MMP-9 in breast epithelial cells[167,168]. Further, in BCCs, activation of Jnk signalling under the influence of IL-6 increases production of Cathepsin B (CTSB)[169], a molecule that facilitates cancer invasion through activation of MMPs and angiogenesis[170]. Transcription efficiency of ATF-2 increases in the presence of CBP/p300[171] which interacts with the β-catenin and STAT3, the downstream signalling molecules of Wnt, CCL5, IL-6, and Leptin in several cancers including colorectal cancer, BC and multiple myeloma[172,109,173,174]. Since CBP/p300-mediated acetylation of various transcription factors is an important downstream step for several signalling pathways, it may be a useful therapeutic target.

Although, a role for Jnk and p38MAPK in BC invasion has been shown, the association of Jnk and p38MAPK signalling axes with apoptosis are also reported[175,176]. Therefore, the activation of Jnk and p38MAPK in response to stress signals (such as UV radiation, growth factors including FGF and EGF, and inflammatory cytokines) may induces apoptosis[175,177,97]. Hence, question of what mechanism maintains cell viability during EMT is an important one. Studies have shown that the PI-3k/AKT axis results in phosphorylation of BAD on Serine 136. This phosphorylated form of BAD is functionally inactive resulting in cell survival[178]. In

addition, transcription factors belonging to the FOXO family, an essential component required for stress-induced cell-cycle arrest and apoptosis in cancer cells, are also deactivated under the influence of activated AKT/PKB[179,180]. Therefore, the activation of PI-3K signalling axis in the presence of HGF, FGF, EGF and CXCL12[181,182,183,184] may rescue cancer cells from the apoptotic effect of Jnk/p38MAPK signalling. In parallel to the effect on cell survival, CXCL12-mediated activation of PI-3K/AKT signalling pathway enables BCCs to migrate through the human brain microvascular endothelial cells (HBMEC) resulting during metastasis of cancer to the brain[185]. Also, EGF/AKT signalling-mediated phosphorylation of β-catenin at Serine 552 induces tumor invasion in the epidermoid carcinoma cell line[186]. Although, EGF/AKT-mediated β-catenin activation in BC has not been previously reported, the presence of EGF in the TME highlights another possibility of β-catenin-mediated invasion of BCCs.

Hence, from the paracrine signalling crosstalk it is now clear that exogenous application of growth factors in cell culture may help in understanding the importance of individual signalling pathways in BC progression, paracrine signalling in the original TME may be more complex. Hence, a drug developed for targeted therapeutics based upon observations on a single signalling axis in cell culture studies may fail in the clinic. Therefore, a more global study of paracrine signalling may contribute toward the development of targeted therapeutics to treat BC patients. In addition, the cell culture model used may play an important role in the drug discovery process. The cellular arrangement in the models and the presence of MSCs with the cancer cells to better resemble the real

physiology are also important for identifying promising drug targets to treat BC.

1.10 Models used for cancer studies

A suitable cell culture model (*in vitro*) is required to test hypotheses relating to the role of MSCs in BC, and to identify the potential paracrine signalling pathways involved, for the development of targeted therapeutics to prevent or treat BC invasion.

1.10.1 2D cell culture model

Exogenous application of growth factors and chemokines in 2D cell culture studies has contributed to progress in understanding the disease. However, drugs developed based upon the knowledge of the activated signalling pathways in cancer often fail or show little therapeutic impact in treating the disease in patients. At present, in the market there are a number of FDA-approved cancer drugs available but some drugs have side-effects in patients; a number of drugs targeting the downstream signalling molecules associated with paracrine signalling are also under investigation[187].

Development of anticancer drug usually involves testing the candidate compounds in cell culture followed by testing in *in vivo* cancer models[188]. 2D monolayer has been used extensively for many years in cancer studies but by definition such 2D models are unsuitable for studying the impact of the microenvironment on cancer cell proliferation and metastasis. In 2D cell culture, cells grow on flat surfaces made of polystyrene plastics which are very hard and unnatural in contrast to the normal architecture of a physiological system. Extracellular matrix (ECM) is made up of

proteins and carbohydrates which support cells through focal adhesion and also participates in cell signalling by helping interaction between growth factors with cell surface receptors[42,46]. Therefore, the absence of ECM is a major drawback of 2D cell culture system. Along with the presence of ECM, the increased expression of gap junction is one of the major characteristics of cancer cells. The Gap junctions facilitates in cell-cell communication through exchanging ions and secondary metabolites including c-AMP, Ca^{2+} and IP3, and helps in clearing waste materials from the cells[189]. However, in 2D cell culture system cells have already lower number of gap junctions indicating high sensitivity towards drugs masking the real effect of drugs in cancer cells[190]. In addition, cells growing in 2D monolayer are exposed uniformly to nutrients and oxygen[191] compared to cells in the real tumors[192]. Hence, in order to grow the cancer cells in a more physiological system for screening the effects of drugs, cancer mouse models have been developed.

1.10.2 Mouse models *(In vivo* models*)*

Mouse models are used as an important tool to understand the pathophysiology of a particular disease and the mechanism behind metastasis of cancer. There are two ways to develop cancer models. Cancer models are developed by tumour transplantation or by gene alterations. As this study is focusing on the involvement of MSCs in the progression of the BC and to characterise the molecule for target therapy to treat invasive BC, mouse models developed by tumor transplantation is the major focus in this study.

1.10.2.1 Tumor Transplantation

To investigate the growth and metastasis of human BC, established cell lines are implanted in immunocompromised mice[193]. Subcutaneous or orthotopic implantation, or injection via the tail vein are commonly used for preparing xenografts[194]. Due to technical ease in terms of cancer cell implantation, recording tumor growth and drug response, subcutaneous models are frequently used for *in vivo* studies[195]. Subcutaneous BC xenografts were used for investigating the ability of MSCs to influence BC progression[82] and for studying stemness in BCCs[196]. However, subcutaneous implantation results in deprivation of the natural TME of a mammary tumor. Therefore, in order to provide a more relevant TME, orthotopic xenografts were introduced. Orthotopic xenografts, developed by implanting cancer cells in mammary fat pad or into the duct, allow the tumour to form at the primary site of BC development; subsequent metastasis to distant organs resembles more accurately the stages of cancer development in patients. However, cross-species interaction between human tumor and murine stromal cells and absence of immune system in the mouse physiology further fails in mimicking the human TME[197]. In addition, drugs tested in mouse xenograft models often fail in clinical trials[198].

In contrast, patient-derived xenografts (PDXs) represent primary tumors more accurately in terms of immunohistochemical characteristics and drug response[199], which make them an important tool for preclinical evaluation of drugs[200] and are increasingly being used as an *in vivo* model in BC research[201]. In addition, transplantation of total peripheral blood or hematopoietic stem cells along with primary cancer cells may facilitate in

understanding the role of immune system in the progression of human cancer[202]. However, engrafting patient tissues is not always successful and use of subcutaneous implantation, the site more frequently used for PDX formation, results in loss of tissue-specificity of primary tumors. Even in the case of successful orthotopic transplantation, the stromal compartment of primary tumor is replaced by host stromal components. Thus, lack of cross-talk between grafts and host stroma may mask the real effect of the tested drug[203].

The use of mouse models in biomedical research is also a topic of debate due to the need to consider ethical aspects of research including the use of living organisms for experimentation for human benefit[204]. Hence, from the perspectives of cost, failure of drugs in clinical trials, lack of a proper TME and ethical issues together restrain use of mice and encourage development of a robust preclinical *in vitro* model for high throughput screening of cancer drugs in bioscience research.

1.10.3 3D cell culture system

Hence, considering all of the above-mentioned limitations of 2D cell culture systems and the need to replace mouse models for anti-cancer drug testing when possible, 3D cell culture models have been introduced. Compared to 2D cell culture, in 3D culture, cancer cells display slower growth rates, increased glycolysis, altered gene expression profiles and increased drug resistance. In addition, the morphology of cancer cells in the 3D more closely resembles that of cells in tissue[205].

In 3D culture, cells grow in aggregates or form spheroids in the presence or absence of scaffolds. Polyethylene glycol (PEG),

Polyvenyl alcohol (PVA), Polylactide-co-glycolide (PLG) and polycarboplactone (PLA) are the main synthetic scaffolds/matrices that have been used to facilitate organization of cells into three dimensional structures. On the other hand, Matrigel™ and Cultrex® basement membrane extracts have been used as more natural scaffolds/matrices for 3D cell culture[206].

Natural hydrogels have some advantages over synthetic hydrogels for cell culture studies. Natural hydrogels are biocompatible and bioactive; in contrast, lack of factors required to support cell growth makes synthetic hydrogels less effective for cell culture[207]. Currently, the most common scaffolds/matrices (hydrogels) used for 3D culture are biologically-derived materials including collagen and Matrigel. Collagen is a major protein in the ECM with which cells are attached via integrins. On the other hand, Matrigel is extracted from Engelbreth-Holm Swarm mouse sarcoma, also known as Cultrex and EHS matrix[208]. The presence of ECM components including collagen, laminin, enactin and growth factors including EGF, bFGF and PDGF in the Matrigel[209] facilitates cell growth in 3D within natural ECM[210]. Although, the cell-cell interaction and cell-Matrigel interaction in the scaffold/matrix-based 3D cell culture mimic the normal microenvironment found in vivo, the risk of inconsistency in the experimental outcome in scaffold/matrix-based 3D culture persists due to the variability in the biologically derived matrices[206].

In contrast, spheroid is a scaffold-free 3D cell culture formed by various approaches including rotatory cell culture system, pellet culture system, hanging drop culture methods, and magnetic levitation method[211]. Spheroids are tightly-packed 3D tumour-like structure and because of low permeability of glucose and oxygen

a hypoxic core can form in the centre of spheroids[206]. Due to the above features, which can influence drug penetration and cancer cell drug response, drug sensitivity in spheroid models is more similar to that in a physiological setting. Therefore, spheroid models can be used as a preclinical tool for drug screening and delivery[212]. Hence, the spheroid model appears to be a potential bridge between the 2D monolayer system and *in vivo* research.

Therefore, incorporation of the MSCs in BCC spheroid model may provide a deeper understanding regarding the role of MSCs in the progression of BC. Further, since the spheroid formation takes place while the cells in the suspension, technically it provides a window to incorporate other stromal cells including endothelial cells and immune cells in order to prepare a replica of natural TME.

1.11 Summary

With the help of acquired knowledge in human physiology and cell biology we have made great progress in BC drug development but, the key factors inducing EMT, metastasis and drug resistance are still under investigation. Although, through development of receptor-based targeted therapy and the combined efforts of surgeons, oncologists and research, treatment regimens for primary BC have improved, acquired drug resistance and failure of drugs in advanced stage of BC are still challenging in clinical practice. Hence, to improve the therapeutic options for treating invasive BC, there is interest in the potential role of tumor-stroma in the development of non-invasive form of cancer into invasive subtypes. Analysis of tumor-stroma interactions reveals the presence of a large set of potential growth factors and cytokines that may influence the progression of the disease. In addition,

homing of bm-MSCs in BC patient tissues highlights the potential role of MSC-driven paracrine signalling in the progression of BC. Although, the exogenous application of individual growth factors or cytokines in 2D cell culture studies demonstrate alteration of BCC proliferation and invasion, more global studies of the paracrine signalling network have not been performed. Hence, an interactive model has been designed to allow us to develop hypotheses about the complex MC-driven paracrine signalling within BC. In parallel to investigating the paracrine signalling in BC, the need to improve cell culture models has been taken into account. Since 3D cell cultures display more similarity to the *in vivo* situation in terms of cellular arrangement and drug response, investigating the BC progression-promoting capacity of MCs in spheroid co-culture may facilitate development of effective targeted-therapeutics to treat patients with invasive BC.

1.12 AIMS OF THE STUDY

The main goal of this study is to develop *in vitro* models of cancer which can be used to carry out a comprehensive study of the role various paracrine signalling pathways in BCCs, and in particular to understand the impact of Mesenchymal cells in BCC (BCC) proliferation, EMT and invasion. Ultimately, this will enable development of novel targeted therapeutics against BC metastasis.

In the light of the pathology and morphology of BCCs the study aims to understand the factors fuel EMT which transform DCIS into IDC in patients taking into account differences between the DCIS-derived IDC and TNBC. Clinical studies suggest IDCs are derived from DCIS in patients and among IDCs; TNBCs are the most invasive BCCs with poor survival rate in patients. Cell culture studies demonstrated TNBCs are mesenchymal in appearance and that EMT induces invasion through suppressing the epithelial features in non-invasive BCCs.

Since Mesenchymal stem cells (MSCs) migrate from the bone-marrow into the TME of BC, it has been hypothesised that may be the MC-derived paracrine factors influence the proliferation and EMT in DCIS BC. Therefore, in order to investigate the impact of mesenchymal cells on BC progression, the following work plan was developed:

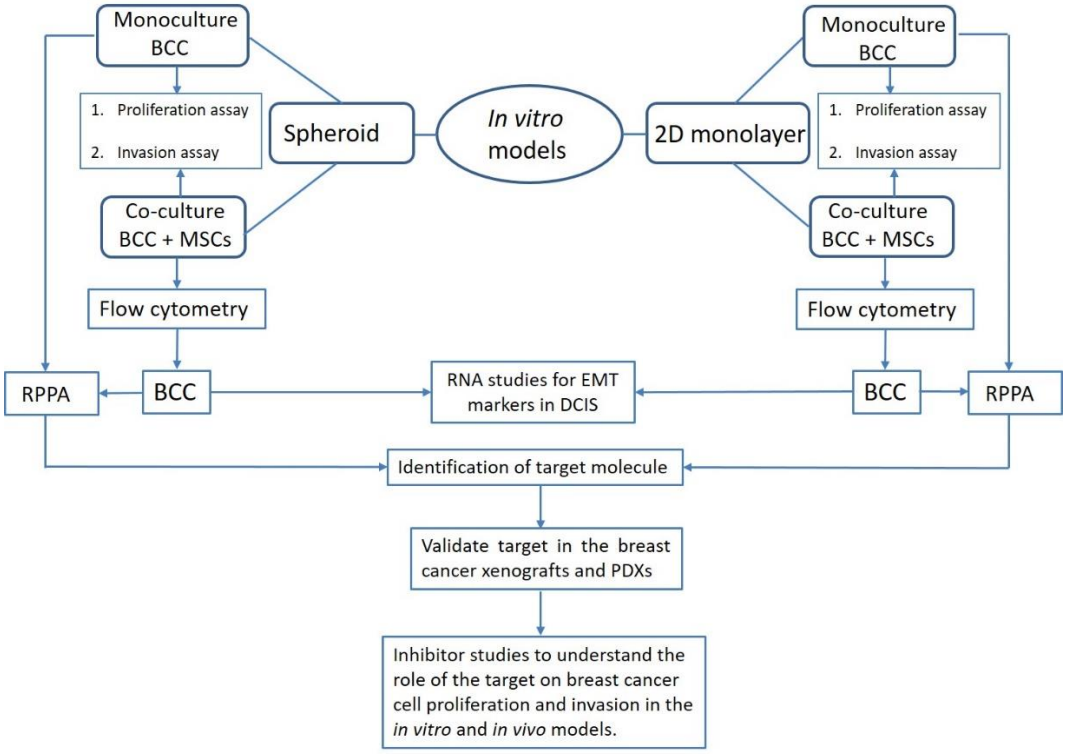

Figure 1-4: Plan of the study: A direct co-culture in 2D monolayer and spheroid model will be established in order to investigate the proliferation and invasion promoting effect of MSCs in BCC. Later, BCC will be FACS-sort from the co-culture models in order to access the expression of EMT markers in the BCC through RNA study. FACS-sorted BCC will be further processed for Reverse phase protein microarray (RPPA) to identify the downstream signaling molecule through investigating the MSC-exerted signalling pathways associated with the BC progression. The expression of the downstream molecule will be further validated in the BC xenografts and PDXs and the effect of the signalling pathways on BCC proliferation, EMT and invasion will be investigated through target inhibition studies. Fonts having different sizes are used in the work plan in order to differentiate between the models and the downstream assays included in the study.

- Indirect co-culture studies demonstrated the migration of MSCs towards MDA-MB-231-derived cell culture media[82], but the effect of MSCs in MDA-MB-231 cells in direct co-culture has not been investigated in large scale. Therefore, in this study a direct 2D co-culture model will be established using MDA-MB-231 in order to investigate the potential proliferation-promoting role of MSCs in TNBCs. In addition, a direct 2D co-culture using MCF-

7 and MSCs is included in this study to explore the role of MSCs in promoting cell proliferation in DCIS BC cell line.

- Since, cells grown in 2D *in vitro* model show less similarity with the actual tumor, the impact of MSCs on BCC proliferation will be further investigated in the 3D spheroid model where cells are allowed to imitate the cancer cell-geometry in a patient tumor more realistically. In addition, unlike cells in 2D models, gradient of oxygen and nutrients in 3D models may compromise the cell viability and perhaps induce necrosis, which may interfere with experimental outcomes. Since the existence of gradient in oxygen and nutrients is dependent upon the spheroid size, Propidium iodide staining will be included in the study in order to detect cell viability in the spheroid monoculture and co-culture model in order to select appropriate seeding densities of BCCs to set up spheroids. In addition, spheroid co-culture will be established using BCCs and MSCs to study the cell arrangement and cell viability therein.

- Once the cell seeding density of BCCs and MSCs for spheroid co-culture is optimised, the impact of MSCs on BCC proliferation will be investigated using MCF-7 and MDA-MB-231. Since clinical studies show that IDCs derive from DCIS in patients, in parallel with investigating the proliferation-promoting effect of MSCs in BCCs, the invasion-inducing effect of MSCs in BCCs will also be studied by incorporating the less innate-invasive DCIS BC cell line MCF-7 in spheroid co-culture. This may allow us to understand the role of MSCs in promoting IDCs from DCIS BC.

- Since EMT is associated with invasion, RNA studies will be performed in the FACS-sorted MCF-7 from the co-culture models in order to investigate the expression of EMT markers including N-cadherin, vimentin, Twist, Snail and Zeb, induced by MSCs in spheroid co-culture. Expression of EMT markers in MCF-7 from 2D co-culture will be further investigated for comparative studies of MSC-driven expression of EMT between 2D and spheroid co-culture. In parallel, studies to investigate the presence of EMT markers in MDA-MB-231 in 2D and spheroid monocultures will be performed in order to determine the expression of EMT markers in MCF-7 resulting from the presence of MSCs in different *in vitro* co-culture models. This may allow us to understand whether MSCs induce TNBC traits in DCIS BCCs in co-culture.

- Based on the observation of proliferation and EMT-promoting effect of MSCs in MCF-7, protein lysates from FACS-sorted MCF-7 from 2D and spheroid co-culture will be subjected to reverse phase protein microarray (RPPA) in order to investigate the MSC-exerted paracrine signalling pathways responsible for proliferation and EMT in the DCIS BC cell line. Lysates from MDA-MB-231 in 2D and spheroid monoculture will be included in the study in order to observe the active signalling pathways responsible for mesenchymal traits in TNBCs. In addition, comparative studies of the active signalling pathways between MCF-7 in the *in vitro* co-culture models and MDA-MB-231 in those models may allow deeper insight regarding the signalling axes associated with EMT and invasion in DCIS BCCs.

- It is also planned to make use of *in vivo* models generated from the established BC cell lines and PDXs in order to observe the pattern of the expression of EMT markers in the TME in a more physiological setting in the presence of MSCs. Studying xenografts could provide a reference in the selection of *in vitro* models that could be used to study the impact of MSCs on the progression of the disease in the TME in terms of growth, EMT and invasion, replacing the use of animals for that purpose. Detailed investigation of the MSC-exerted active paracrine signalling axes in BC *in vivo* models may allow us to select the proper *in vitro* model to develop novel targeted therapeutics to treat BC cases.

CHAPTER 2: MATERIALS AND METHODS

2.1 Cell culture conditions

BCCs (BCCs), MCF-7 and MDA-MB-231 were maintained in phenol red-free RPMI-1640 media supplemented with 10% fetal bovine serum (FBS) and 2mM L-Glutamine. The bone marrow-derived mesenchymal stem cells (bm-MSCs) were maintained in MSCM media supplemented with FBS and MSCGS. MSCM, FBS and MSCGS were purchased from ScienCell. Similar passage numbers (below passage 40) for both BCC lines were maintained throughout the study. MSCs from passage numbers 8 to 10 were used consistently throughout the study. Each cell line was expanded in the presence of 5% CO_2 at $37^{O}C$ in the incubator having humidified atmosphere. Mycoplasma tests were performed intermittently throughout the study to avoid using infected cells. MCF-7 and MDA-MB-231, transduced with Firefly luciferase (Fluc) gene were used for luciferin-dependent growth kinetic assay. MCF-7 was stable-transduced with tdTomato and was used in spheroid invasion assay and for FACS-sorting from the 2D and spheroid co-culture. MSC was stable-transduced with Green fluorescent protein (GFP) and used for optimizing FACS-sorting of BCCs from the mixed cell population in co-culture models. MSC-GFP was also used to investigate the retention of MSCs in spheroid co-culture and for differential identification from invading MCF-7 cells in the spheroid co-culture invasion assay. Lentiviral-mediated stable transductions (including Fluc, tdTomato, GFP) and Mycoplasma tests were performed by our laboratory technicians Pamela Collier and Catherine Probert based on routinely-used standard operating procedures described in Appendix C.

2.1.1 Proliferation assay in the 2D monolayer

MCF-7Fluc and MDA-MB-231Fluc were seeded in monoculture and co-culture with different numbers of MSC-GFP in standard clear-flat bottom 96-well culture plate, purchased from Costar. 200µl of media was used in each well of the culture plate. For each condition, 10% (v/v) of 10X Luciferin was added in each well of the plate and incubated for 15 minutes at 37^{o}C in the cell culture incubator maintaining 5% carbon dioxide. Next, the relative luminescence (RLU) was measured by the plate reader from BMGlabtech. In parallel with the Luciferase assay, the Alamar blue assay was performed by adding 5% (v/v) of the reagent to the wells for the comparative study between the assays. The relative fluorescence unit (RFU) was measured with an emission wavelength of 590nm and excitation of the compound at a wavelength of 540nm.

2.2 Establishing spheroid mono and co-culture

96-well ultra-low attachment round bottom plates (ULA) (#7007) were purchased from Corning, where cells did not attach on the surface of the plate but formed cell aggregates. MCF-7Fluc and MDA-MB-231Fluc were seeded alone for the spheroid monoculture and for spheroid co-culture; BCCs were mixed with MSC-GFP and seeded in a ULA plate. Extracellular matrix (ECM)-rich Cultrex (#3433-05-01) from PathClear was mixed at the final concentration of 100µg/ml in order to form tight and round spheroids of MDA-MB-231 in monoculture. In order to maintain the consistency, Cultrex was supplemented at the same concentration to MCF-7 spheroid monoculture and in the co-culture of both BCC lines. Once the cell suspension was mixed with

Cultrex, 200µl of that mixture was suspended in each well of the ULA plate and centrifuged for 5 minutes at 300 RCF and incubated in the cell culture incubator until the cells form spheroids. The volume of the spheroids was measured by a macro, a plugin application of ImageJ. The macro calculates the area (A) which facilitates in determining the radius ($r = \sqrt{\frac{A}{\pi}}$) and subsequently, the volume ($V = \frac{4}{3}\pi r^3$) of the relevant spheroid. The macro was provided by Deliyan Ivanov, a post-doctorate researcher in our laboratory.

2.3 Propidium Iodide staining in the spheroid model

Propidium Iodide (PI) ready to use solution (#00-6990-50) was purchased from eBioscience. The spheroid monocultures seeded using different numbers of BCCs were incubated with 5% (v/v) PI for 3 hours at day 3, 5 and 7. Since the dead cells appear red in the presence of PI, the formation of a necrotic core in the spheroid monocultures with different cell densities was observed under a fluorescence microscope and images were captured at the different time-points of the study. The concentration of PI was used according to the manufacturer instruction.

2.4 Live/dead cell staining in spheroid cell-culture model

Live/dead cell staining in the spheroid model was performed using Calcein AM and PI staining. Calcein AM (code: 65-0853-39) was purchased from eBioscience. Lyophilised Calcein AM was dissolved in 250µl of DMSO, which gives a stock concentration of 4mM. The final concentration of Calcein AM was 2µM, used for live cell staining in spheroid monoculture and co-culture. 5% PI was used to stain dead cells in spheroid mono and co-culture. A final

concentration of 33μM Hoechst 33342 was used for visualising the cell nuclei in the spheroids. Next, spheroids were incubated for 3 hours in the incubator in the presence of 5% CO_2 at 37°C. Then, spheroids were washed twice with PBS by removing 100μl of the media with great care each time. Washing with PBS is necessary to remove any background noise caused by the stains during imaging. Finally, the fluorescence images of spheroids were captured under the fluorescence microscope. The intensity of each stain in spheroids of each condition from day 3, 5 and 7 was quantified by measuring the optical intensity across the spheroid-diameters. During imaging, the exposure time for fluorescence was kept constant. The concentrations of Calcein AM and Hoechst were borrowed from the previous study performed for characterisation of spheroid model[213].

2.5 BCC proliferation assay in spheroid monoculture and co-culture

2.5.1 Luciferase and Alamar blue assay

Two different sets of experiments were established for the Luciferase and Alamar blue dependent growth kinetic studies for BCC proliferation in the spheroid mono and co-culture models. Once the BCCs formed spheroids in the absence and presence of MSCs, 5% (v/v) Luciferin and Alamar blue were added separately in each well of the ULA plate and incubated for 90 mins at 37°C in the cell culture incubator maintaining 5% carbon dioxide. Relative luminescence (RLU) was measured at day 3, 5 and 7 respectively by using the plate reader from BMGlabtech. For Alamar blue assay, Relative fluorescence (RFU) at day 3, 5 and 7 was measured. Three replicates for each condition were used for measuring the RLU and RFU respectively. Standard error between the replicates

and the significance of the study were analysed in Prism by plotting the values of RLU and RFU from each condition at different time points of the culture.

2.5.2 CellTrace Violet-mediated BCC proliferation assay in spheroid mono and co-culture

MCF-7Fluc and MDA-MB-231Fluc were harvested and cell pellets of both BCCs were prepared by following standard laboratory protocol for cell passaging. Cell pellets of MCF-7 and MDA-MB-231 were suspended separately in 5ml of RPMI-1640 without FBS. Concentration of each cell line was adjusted up to 10^6 cell/ml and volume was adjusted to 1ml with RPMI-1640 without FBS. Then, 1µl of CellTrace violet solution was added to 1 ml of BCCs in suspension, and incubated for 20 minutes at 37^OC with gentle agitation for 5 mins. Next, 4 ml complete culture medium was added to the stained cells and mixed gently with repeated pipetting and incubated for 5 mins at 37^OC in the incubator to quench the unbound dye in the solution. After the incubation, cells were centrifuged and resuspended with fresh pre-warmed complete RPMI-1640 medium. Cells were analysed by flow cytometry to ensure maximum number of cells were stained with CellTrace violet and finally, stained cells were seeded immediately for spheroid mono and co-culture with MSCs. MSCs were used as a negative control for CellTrace violet. The spheroid mono and co-cultures from day 3 and day 5 respectively were dissociated by the Accumax (#A7089 from Sigma) and the progressive decrease in the intensity of CellTrace violet in BCCs were analysed by flow cytometry at the excitation and emission wavelengths of 405nm and 450nm respectively. The relative histograms and statistics for decreased intensity of CellTrace violet in BCCs from the spheroid

mono and co-cultures at different time points were analysed by using the software Weasel.

2.6 3D spheroid invasion assay of BCCs in co-culture

MCF-7 with or without the MSCs were seeded in a round bottom ULA 96-well plates supplemented with 100µg/ml low-gelling Cultrex in 200µl of complete media in each well. MDA-MB-231 cells were seeded as a positive control for invadopodia formation during invasion. Once the spheroid formed at day 3, 185µl of media was discarded from each well and spheroids were embedded in high-gelling Cultrex having the concentrations of 3mg/ml in complete medium made up to 100µl in each well. Next, the plate was kept at 37^{o}C in the incubator for 1 hour until the gel solidified. Finally, 50µl of complete medium was overlaid on the top of the gel and images were captured for next 72 hours of post gel-embedding. Hoechst 33342 was applied to observe the presence of cells in the projections formed on BCC invasion.

2.7 Enzyme-mediated dissociation of spheroids to prepare single cell suspension

2.7.1 Accutase and Accumax-mediated dissociation of the spheroid culture

Enzyme-mediated spheroid dissociation was performed in order to prepare single cell suspension from spheroid. Accutase (#A6964) and Accumax (#A7089) were purchased from Sigma. The spheroid monoculture (MCF-7tdTomato) and co-culture (MCF-7tdTomato and MSC-eGFP) were harvested and collected in 15ml centrifuge tubes separately. Once the spheroids settled down at the bottom of the tube, the media was expelled carefully without disturbing the spheroids and the spheroids were washed twice

with PBS. After washing with PBS, 1ml of enzyme was added to the spheroids and the tube was transferred into the water bath maintaining 37^{O}C with continuous shaking for 3 minutes. Then, repeated pipetting (4 to 5 times) was performed in order to dissociate spheroids into single cell suspension. Thereafter, 2ml of complete medium RPMI-1640 was added in the tube and centrifuged at 300 RCF for 5mins. After centrifugation, supernatant was discarded without disturbing the cell pellet and 200µl of fresh pre-warmed RPMI-1640 media was added to the tube and pipetted repeatedly to make a homogenous single cell suspension. Then the cell suspensions of digested spheroids were transferred into a 96wells culture plate and observed under the microscope to investigate the digestion efficiency of the enzymes.

2.7.2 Accumax-mediated spheroid dissociation

Since the Accumax demonstrated more efficiency in terms of dissociating the spheroid co-culture, further optimisation was performed in order to ensure the formation of single cell suspension and the cell viability in it. Two different methods, direct Accumax-mediated digestion and controlled Accumax-mediated digestion were applied to satisfy the purpose of the experiment. Direct method for digesting the spheroid co-culture was again subdivided into two different approaches based on the incubation time in the incubator and water bath. The cell viability after each following digestion was confirmed by the trypan blue exclusion method and the images of cell suspension was captured under fluorescence microscope at 10X magnification. The TC20 automated cell counter machine from Bio-Rad was used to determine the cell viability and the presence of single cells on the following digestion of spheroids in each method.

2.7.2.1 Method 1: Direct Accumax-mediated digestion with 3 minutes incubation in water bath

The spheroid mono and co-cultures were harvested and transferred into the 15ml conical tubes. Medium was discarded and spheroids were washed twice with PBS carefully. Next, 1 ml of Accumax (at the concentration provided by the manufacturer) was added to the tube containing spheroids and the tube was transferred in the water bath maintaining 37^{O}C with continuous shaking for 3 minutes. After incubation in the water bath, four to five times repeated pipetting was performed to ensure complete dissociation of spheroids in the suspension. Then, 2ml of complete media was added to inactivate the Accumax and the tube was centrifuged for 5 minutes at 300 RCF in room temperature. Finally, supernatant was discarded and the cell pellet was suspended in 200µl of complete media.

2.7.2.2 Method 2: Direct Accumax-mediated digestion with total 5 minutes incubation (2 minutes incubation in the incubator and next 3 minutes in the water bath)

The spheroid mono and co-culture were harvested and transferred into a 15ml sterile falcon tube. Media was discarded and spheroids were washed twice with PBS carefully. Next, 1 ml of Accumax was added to the tube containing the spheroids and the tube was incubated for first 2 minutes in the cell culture incubator at 37^{O}C. Next, the tube was transferred to the water bath at 37^{O}C with continuous shaking for 3 minutes. Following the incubation, four to five times repeated pipetting was performed to ensure complete dissociation of spheroids. Then, 2ml of complete media was added to inactivate the Accumax and the tube was centrifuge for 5 minutes at 300 RCF in room temperature. Finally, supernatant was

discarded and the cell pellet was suspended in 200µl of complete media.

2.7.2.3 Method 3: Controlled Accumax-mediated digestion of the spheroid

Spheroids were incubated with 1ml Accumax for 90 seconds with continuous shaking in the water bath at 37^{o}C. Following settling of undigested spheroids in the tube, supernatant was transferred into the second 15ml falcon tube (Tube 2) containing 2ml of complete media. 1ml of Accumax was added to the remaining undigested spheroids in the first tube (Tube 1) and incubated in the water bath for next 90 seconds with continuous shaking. At the end of the following incubation, the supernatant from the digested spheroids in the Tube 1 was transferred into another 15ml tube (Tube 3) having the 2ml complete media. Then, Tube 2 and Tube 3 were centrifuged at 300 RCF for 5 minutes and the cell pellets in each tube were suspended in 200µl complete media.

2.8 Flow cytometry-based MCF-7-sorting from the 2D and spheroid co-culture

Optimisation for FACS-sorting of pure population of MCF-7 from 2D and spheroid co-culture was performed in two different approaches depending on the fluorescence intensity of MCF-7 and MSC. In the beginning, MCF-7 was mixed with MSC-eGFP and the mixed-cell suspension was analysed using the Astrios cell sorter at the excitation and emission wavelengths of 488-513/26 band pass filter. Since using the MSC-eGFP did not provide a pure population of MCF-7 on FACS-sorting, MCF-7tdTomato was used and mixed with non-labelled MSCs. The excitation and emission wavelengths of tdTomato were 561nm and 579/16 used for the

flow cytometry-based analysis of mixed cell population and pure population of relatively high tdTomato-expressing MCF-7 was recovered from the mixed-cell suspension by using the gate. Sorted MCF-7tdTomato was expanded in complete RPMI-1640 supplemented with 1X Antimycotic/antibacterial (Ab/Am) solution in a controlled laboratory environment to prevent fungal and bacterial infection. The cell culture media was changed every two days interval until the cells became confluent. At least two passages were performed in the controlled environment and finally Mycoplasma test was performed. Once it was ensured that sorted MCF-7tdTomato was healthy and infection free, cells were used to establish 2D and spheroid co-culture with MSCs for the main experiments. The same gate was used in each round of sorting of MCF-7tdTomato from the co-culture containing MSCs. During sorting MCF-7tdTomato was collected in antibiotic/antimycotic (Ab/Am) supplemented complete RPMI-1640 medium to prevent any kind of FACS-derived infection as these sorted cells are used for several downstream experiments relevant for this project.

2.9 Protein extraction

The FACS-sorting yields a low number of MCF-7tdTomato from 2D and spheroid co-culture. Therefore, optimisation for protein extraction from MCF-7 was performed by following three different approaches: Standard method, Sonication and Snap-freezing. The protein extraction buffer used in each method was formulated with the RIPA lysis buffer (#89900) supplemented with the phosphatase and protease inhibitor (PPI) (#78440) at a final concentration of 1% v/v. The RIPA lysis buffer and the PPI were purchased from Thermo Fisher Scientific. The protein-yield from

each method was quantified by bicinchoninic acid assay (BCA assay) using the Pierce™BCA Protein Assay kit (#23225).

2.9.1 Standard protein extraction from mammalian cells

MCF-7 was harvested and the cell pellet was suspended in 100µl protein extraction buffer in a 1ml of centrifuge tube. Next, the tube was allowed to stand for 30 minutes in ice with repeated vortexing at every 10 minutes interval for complete cell lysis. Then, the tube was centrifuged at 4^{o}C for 10 minutes in microcentrifuge machine at 10,000g. Finally, the supernatant was collected in a fresh ice-cold centrifuge tube and stored at -20^{o}C or processed immediately for protein quantification.

2.9.2 Protein extraction by sonication

100µl extraction buffer was added to the cell-pellet and mixed homogenously with repeated pipetting and incubated for 15 minutes on ice. Following incubation with the extraction buffer, the mixture was vortexed occasionally in the interval of 10 minutes. Next, the sample was sonicated for 60 seconds distributed between 10 seconds of sonication and incubation on ice each to ensure complete lysis of the cells. Finally, tubes were centrifuged at 10,000g for 20 minutes at 4^{O}C and the supernatant was collected in fresh ice-cold centrifuge tubes and the freshly prepared lysates were stored at -20^{O}C or processed immediately for the BCA assay.

2.9.3 Protein extraction by snap-freezing

100µl of RIPA lysis buffer was added to the MCF-7 pellet in the centrifuge tube and vortex thoroughly for 10 seconds and kept on ice for 15 minutes. Next, the sample was processed for four cycles

of freezing on dry ice for 10 minutes followed by thawing at 37^{O}C for 20 minutes. Finally, the sample was centrifuged at 216g at room temperature for 1 minute and the supernatant was collected in fresh ice-cold centrifuge tube. The freshly prepared protein lysates were stored at -20^{O}C or processed immediately for BCA assay.

2.10 Western blot analysis

Aliquots containing equal amounts of protein (20µg) extracted from the BCCs were mixed with one part of 4X SDS sample buffer with 3 parts of total volume of the lysates in each tube and mixed with repeated pipetting and the samples were boiled at 95^{O}C for 5 minutes. Next, the samples were placed on ice for 5 minutes and short spin was performed to condense the vapor caused during the heating of the samples. Then, the protein in the samples was separated by Nu-PAGE 4-12% Bis-Tris gel, purchased from Novex Life Technologies (#NPO335BOX) and transferred onto a methanol-activated polyvinylidene difluoride (PVDF) membrane by semidry transfer method. The voltage and time for transferring protein from the gel to membrane were 25V for 30 minutes. Once the protein was transferred, the PVDF membrane was blocked by incubating with 5% (w/v) milk in Tris-buffer saline with 0.1% Tween-20 (v/v) (TBST) for 1 hour at room temperature. Then, the membrane was incubated overnight with the following primary antibodies diluted in the blocking solution: Polyclonal mouse anti-alpha tubulin, monoclonal rabbit anti-E-cadherin, monoclonal rabbit anti-vimentin and monoclonal rabbit anti-SnON. The following day, the membrane was washed three times (5 minutes each) with TBST, and then incubated with horseradish peroxidase-conjugated goat anti-mouse and anti-rabbit IgG for 2h

at room temperature. Following incubation, the membranes were washed two times with TBST and one time with TBS (5 minutes each) and the presence of the targeted proteins was determined using enhanced chemiluminescence (ECL) using a membrane scanner. Each target protein was normalized against alpha-tubulin through dividing the optical density of the target protein by the optical density of the alpha-tubulin. The optical densities of each target were determined by the principal of densitometry in ImageJ.

Antibodies

List of antibodies (Ab) used for the Western blot analysis			
Primary			
Antibodies	**Dilution**	**Sources**	**Cat. no**
Polyclonal mouse anti-alpha tubulin Ab	1:2000	Abcam	Ab7291
Monoclonal rabbit anti-E-cadherin Ab	1:1000	CST	3195S
Monoclonal rabbit anti-Vimentin Ab	1:1000	CST	5741
Monoclonal rabbit anti-SnON Ab	1:1000	CST	4973
Secondary			
Polyclonal Goat anti-rabbit-HRP	1:3000	Sigma	A6154
Polyclonal Goat anti-mouse-HRP	1:3000	Sigma	A4416

Table 2-1: List of antibodies and the corresponding dilutions used for the Western blot analysis. CST stands for Cell Signalling Technology.

2.11 Phalloidin staining in BCCs in the 2D cell culture

MCF-7tdTomato was seeded in 8 well chamber slides (Nunc™ Lab-Tek™ Chamber slide™ System; #154534PK) in the presence or absence of MSCs. 200ul/well of RPMI-1640 cell culture medium was added and cells were allowed to grow in the cell culture incubator. One chamber slide was prepared for MDA-MB-231 monoculture. At day 3 and day 5 of culture, cell culture medium

was discarded and slides were washed twice with PBS carefully without dislodging cells from the surface of the slides and incubated for 10 minutes with 200µl of 4% paraformaldehyde (PFA) in each well of the slide. In the following steps, the cells in each well were washed three times with Dulbecco's Phosphate buffer saline (PBS) and cells were incubated with 200µl of PBS contained 0.1% Triton X-100 (Permeabilising solution) and incubated for 5 minutes at room temperature. Next, the permeabilised cells were washed with PBS 3 times and incubated for 90 minutes with 200µl of 1x Phalloidin-iFluor 488 Reagent (Abcam; #ab176753) in each well. 20µM Hoechst 33342 was added in this stage to stain the cell nucleus in the culture. Following incubation, cells were washed three times with PBS and slides were left for drying at room temperature, protected from the light. Finally, the chambers slides were covered with mounting medium, Fluoroshield and cover slips were placed on top of the slides and sealed with clear nail varnish. Images were captured with the assistance of confocal microscope.

2.12 Immunofluorescence staining for β-catenin in MCF-7 in 2D mono and co-culture

Immunofluorescence staining was performed for β-catenin in MCF-7tdTomato in 2D mono and co-culture. 2000 MCF-7 alone or with 4000 MSCs were seeded in 8 wells chamber plate and allowed to grow in the cell culture incubator. At day 5, media from the wells were discarded, wells were washed once with PBS (200ul/well) and cells were fixed in the presence of 4% PFA. After 10 minutes of incubation, cells were washed twice with PBS and permeabilised with the assistance of permeabilising solution for 5 minutes. Then, the cells were washed once with PBS and blocked

by adding blocking solution formulated with 3% chicken serum in permeabilising solution. After the incubation with blocking solution for 1 hour, cells were kept at $4^{O}C$ overnight in a moist chamber by incubating with monoclonal rabbit anti-β-catenin (#8480S, Cell signalling technology) at 1:100 dilution in the blocking solution. Another slide of MCF-7tdTomato monoculture was probed Rabbit monoclonal IgG1 (#3900 from Cell signalling technology) used as a negative control. The following day, cells were washed with PBS three times and incubated with Alexa Fluor 488 conjugated-chicken anti-rabbit IgG (1:1000 in PBS, #A21441, Thermo Fisher Scientific) for 1 hour at room temperature. For nuclear staining, cells were incubated with Hoechst 33342 for 15 minutes and then cells were washed with PBS three times for 5 minutes each and finally mounted with cover slips in the presence of mounting medium. Confocal images were captured under 40X objective to observe the localisation of β-catenin in MCF-7 in the mono and co-culture.

2.13 Immunohistochemical (IHC) staining of spheroids

2.13.1 Harvesting the spheroids from ULA plate and fixation

In order to perform the IHC in spheroid model, ten spheroids were harvested from the 96 well ULA culture plates and transferred to 0.5 ml eppendorf tube individually aiming for one spheroid in each tube. Once spheroids settled at the bottom of the eppendorf tubes, the culture media was discarded carefully without disturbing the spheroids. Next, each tube was washed 2-3 times to remove the residual culture medium that transferred whilst transferring the spheroid from the culture plate to the eppendorf tube. Then, 200µl of 4% PFA was added to each tube to fix the

spheroid and incubated for 60 minutes at room temperature. Once fixed, spheroids were washed 2-3 times with PBS to remove the PFA and to avoid over fixation. At this stage spheroid can be stored in PBS at $4^{O}C$ or can be processed immediately for preparing the array in agarose block.

2.13.2 Preparing the spheroid array for IHC

A. Preparation of spheroid array in agarose block

An agarose solution (2% w/v) in distilled water was prepared by microwaving to ensure agarose was completely dissolved in the water. Care was taken to avoid spillage in this step as this may alter the concentration of agarose and the solution would not be solidified on cooling. Once the agarose solution was prepared, 2-3 ml of agarose solution was poured into a tissue-processing metal cassette placed on ice and wells were made in the agarose-bed with a plastic mould[214]. Ten spheroids from different conditions were placed one-by-one in each well by using a P200 pipette. Edge-wells in the agarose block were not used in order to avoid loss of spheroid during sectioning. The agarose block with the spheroids was then centrifuged at 200RCF for 20 seconds to ensure the spheroids in the array all settle in the same plane. After that, a layer of 2% agarose (melted but not too hot or else it may melt the agarose bed underneath) was overlaid on top of the array-block in order to keep the embedded-spheroid in their respective positions in the agarose wells and the block was incubated at $-20^{o}C$ for 2 minutes. Next, the agarose block was removed from the cassette and placed in a tissue processor plastic cassette followed by overnight incubation in 1X Neutral buffer formalin (NBF) solution. Overnight incubation in NBF increases the

melting temperature of the agarose block and therefore the chance of losing spheroids during processing in the tissue processor was markedly reduced.

B. Processing and paraffin-embedding of spheroid array

The following day, the NBF-fixed agarose block with the spheroids was transferred into the automated tissue processor. In the tissue processor, the samples were dehydrated in a series of alcohol solutions with increasing concentrations (one bath of 50%, 70%, 90%, and 4 baths of 100% methanol, 1 hour each), cleared in xylene (3 baths, 1 hour each), and permeated with molten paraffin (2 baths, 2 hours each). Next day, the processed block was removed from the tissue processor and embedded directly in the paraffin in the metal cassette.

C. Sectioning of the paraffin-embedded spheroid

Once the paraffin was solidified, the block was trimmed using the microtome. Generally, after trimming approximately 100-200 microns, there was a high possibility of getting the spheroid in the sections. At this stage, Hematoxylin and eosin (H&E) staining was performed on 10 sections, each of 5 microns thickness to ensure the presence of spheroids. Once the presence of spheroids in the sections was determined by Hematoxylin and Eosin staining, subsequent sections were placed on clean poly-L-lysine coated glass slides and stored at room temperature for overnight to dry for immunostaining in spheroids.

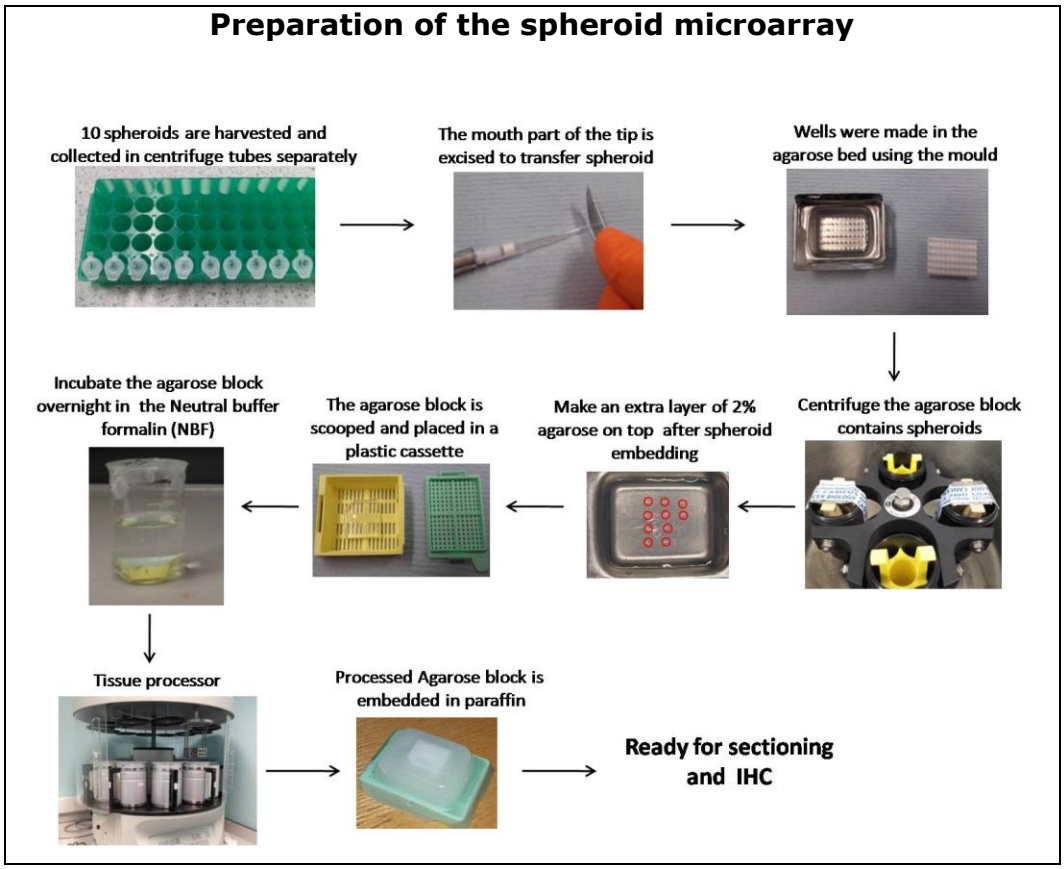

Figure 2-1: Preparing the paraffin-embedded spheroid microarray: The spheroids were harvested and embedded in the wells of agarose block. After processing the agarose block through the intermediate steps, agarose block was paraffin-embedded and trimmed by microtome to prepare the sections of spheroid microarray.

D. IHC staining of the spheroid microarray

Samples were deparaffinised in xylene (2 times for 3 minutes each) followed by rehydrating in 100% methanol (2 times, 1 minute each) and the antigen was retrieved in 10mM sodium-citrate buffer (pH 6.0) using a microwave. The sections were treated with 3% hydrogen peroxide in PBS to exhaust endogenous peroxidase activity. After 10 minutes, samples were washed with PBS twice for 5 minutes each and blocked with 5% (v/v) animal serum, produced from the host for secondary antibody, and incubated for 30 minutes at room temperature. Next, the samples

were incubated overnight with mouse anti-Ki-67 monoclonal antibody, mouse anti-human E-cadherin monoclonal antibody, mouse anti-human vimentin monoclonal antibody, and mouse anti-human SnON monoclonal antibody. One slide of spheroid array probed with Mouse IgG1 was used as a universal negative control for Ki-67, E-cadherin and vimentin, while colon tissue probed with Mouse IgG1 used as a negative control for SnON. The following day, samples were washed with PBS twice (5 minutes each) and incubated with biotinylated-secondary Rabbit anti-mouse IgG (1:300 dilution in PBS) for 30 minutes. Next, samples were again washed with PBS (2 times, 5 minutes each) and incubated with the avidin-biotin peroxidase complex (Vectastain; #PK-4000) for 30 minutes. Next, the samples were rinsed with PBS twice and incubated with the Diaminobenzidine (DAB chromogen) for 10 minutes at room temperature. After incubation, samples were rinsed under running tap water for 1 minute and counter stained with the Hematoxylin for 2-3 minutes. After removing the excess hematoxylin under running water the samples were rehydrated in 100% methanol twice (1 minute each) followed by clearing in xylene bath twice (3 minutes each). Finally, the cover slip was mounted on the slide in the presence of mounting medium, DPX. The DAB positive cells in the samples were quantified by following the algorithm in imageJ Fiji[215].

Antibodies

List of antibodies (Ab) used for IHC			
Primary			
Antibodies	**Dilution**	**Sources**	**Cat. no**
Monoclonal mouse anti-Ki-67 Ab (MIB-1)	1:40	DAKO	M7240
Monoclonal mouse anti-vimentin Ab (clone V9)	1:50	DAKO	M0725
Monoclonal mouse anti-E-cadherin Ab (clone NCH-38)	1:50	DAKO	M3612
Monoclonal mouse anti-SnON Ab (clone 1A6)	1:150	LS Biosciences	C175154
Mouse-IgG1, Negative control	1:50	DAKO	X0931
Secondary			
Polyclonal rabbit anti-mouse IgG-Biotinylated	1:300	DAKO	E0354

Table 2-2: List of antibodies and the corresponding dilutions used for the IHC performed in the sections of paraffin-embedded microarray.

2.14 Inhibitor studies

The β-catenin inhibitor (#SML1726), MSAB (methyl 3-{[(4-methylphenyl) sulfonyl] amino} benzoate) was purchased from Sigma. The 2D and spheroid cultures were treated with different concentrations (0μM, 1μM, 3μM, 5μM, 10μM, 15μM, 20μM, 25μM, 30μM and 40μM) of MSAB. After 48 hours of treatment, proliferation was measured using the Alamar blue assay. The IC_{50} value of MSAB was determined from the non-linear drug response curve developed by plotting the Logarithmic values of the MSAB against the normalised RFU in the Prism. The experiment was repeated twice and the bar graph was developed based upon the IC_{50} values in the independent replicates.

2.15 Patient-derived xenografts (PDXs)

BR15 and BR8 are DCIS and TNBC PDX samples included in the study for investigating the impact of MSCs in the progression of BC in the spheroid model. BR8 and BR15 both obtained with full consent and ethical approval through our biobank agreement. They had been harvested from the patient and implanted in the mammary fat pad of mice with MSCs and Matrigel by experienced *in vivo* technicians under project license PPL 3003444. The strains of the mice used for maintaining the PDXs were eRAG and CD1 nudes depending on the strains supporting the growth of the PDXs. BR8 (at passage 18) was harvested from eRAG mice for incorporation in spheroids, whereas BR15 (at passage 14) was harvested from CD1 nude mice.

2.15.1 Dissociating the PDX tumors

The dissociation of the PDXs was performed by following the standard protocol used in our laboratory[216]. The fresh PDX tumors were finely minced and treated with dispase (2.4 U/ml; Invitrogen) and type II collagenase (100U/ml; Invitrogen) in HBSS (Sigma) and incubated at 37^{O}C at constant rotation. Disaggregated cells were removed at 1 hour intervals and placed in the high glucose DMEM media supplemented with 20% FBS, 2mM L-Glutamine, 1X Antibiotic/Antimycotic, 0.12% hydrocortisone and 0.09% insulin until the tumors were completely digested. Next, the cells were centrifuged at 300 RCF for 5 minutes and suspended in 5 ml of fresh media. Cell number was quantified by the trypan blue exclusion method with the assistance of TC-20 automated cell counter from Bio-Rad.

2.15.2 Establishing spheroid model of PDXs for cell-proliferation and invasion assay

Spheroid mono and co-culture were seeded using BR15 and BR8 in the absence or presence of MSC-eGFP. The cell numbers for PDXs and the MSCs were kept consistent with the numbers of MCF-7 and MDA-MB-231 used for the proliferation and invasion assay in the spheroid model. Alamar blue assay was performed to quantify the proliferation of PDXs in the spheroid model at different time-points of the study. BR15 was used for the invasion assay in the spheroid model. The cell culture media used for PDX spheroid model was high glucose DMEM media instead of RPMI-1640 used for MCF-7 and MDA-MB-231.

2.16 Statistical analysis

The linear and bar graphs represent the standard error of mean in the replicates. The group data was analysed using the Two-way ANOVA, except where otherwise indicated. Data were analysed and where appropriate, the statistical significance of the differences between mean values were determined from the P values at the level of 95% confidence interval using Prism software.

CHAPTER 3: INVESTIGATION OF GROWTH PROMOTION EFFECT IN BCCs IN THE PRESENCE OF MSCs IN 2D CO-CULTURE

The aim of the first part of this study was to understand the impact of mesenchymal cell-mediated paracrine signalling on BCC proliferation. A high proliferation rate is one of the major characteristics of aggressive subtypes of BC in patients[11]. Uncontrolled proliferation in cancer cells results from abnormal signalling pathways triggered by growth factors or hormones or as a result of mutations and epigenetic alterations[217]. Mesenchymal cells (MCs) in the TME secrete a broad range of signalling molecules and show a positive impact on the proliferation of PDX samples of a range of cancers including for example lung cancer[216]. The association of tumor microenvironment (TME) with BC progression is also widely recognised[218] but detailed knowledge of the specific signalling pathways involved is still needed.

Therefore, in order to investigate the paracrine influence of MC-secreted signalling molecules on the proliferation of BCCs, a 2D co-culture model using BCCs with mesenchymal stem cells (MSCs) was initially established. At the beginning of the study, however, certain questions about co-culture needed to be addressed. First, it was crucial to determine the cell seeding density of BCCs for co-culture, as the proliferation of BCCs in co-culture can lead to cell death resulting from the over-confluence. Similarly, too many MSCs in the co-culture may lead to cell death due to over-confluence, and on the other hand, too few MSCs may be insufficient to show a proliferation effect on BCCs. Hence,

determining the cell seeding density for MSCs was equally important to set up the 2D co-culture. Second, it was required to select the cell culture-based assay to determine the MC-driven BCC proliferation in the co-culture. The Alamar blue is a metabolic dye that is reduced by living cells and the resulting fluorescence (relative fluorescence unit or RFU) provides information on cell viability and proliferation in culture[219]. Hence, Alamar blue may be useful for measuring the proliferation of BCCs in monoculture but not in co-culture as it is not specific for BCCs. Therefore, a luciferase assay was introduced as an alternative assay to investigate the BCC proliferation in the co-culture. Luciferin is a substrate for luciferase, an enzyme produced by luciferase-transduced BCCs in culture. Therefore, the relative luminescence (RLU) should be directly proportional to the total number of BCCs in the co-culture at a given time-point of the study.

3.1 Cell density optimisation to choose proper numbers of BCC for studying growth kinetics

Before developing the 2D co-culture system, cell density optimization in the monoculture system using 6-well culture plate was performed to select the appropriate cell plating density to achieve 75% - 80% confluence at specific time-points to avoid cell death during the course of the study. For 24, 48, 72 and 144hr time-points, cells were seeded at densities of 300K, 400K and 500K; 100K, 200K and 300K; 30K, 50K and 100K; or 10K, 30K and 50K cells per well respectively (Figure 3-1 and Figure 3-2). The cell confluency in each well at relevant time-points was assessed by visualizing under a brightfield microscope (Nikon Eclipse Ti). 400K cells/well, 300Kcells/well, 100K cells/well, 30K cells/well were selected for 24hrs, 48hrs, 72hrs and 144hrs

respectively for MCF-7 and MDA-MB-231. These cell densities in the 6-well culture plate were used as the references in developing the growth curve in the 2D co-culture system in a 96-wellplate.

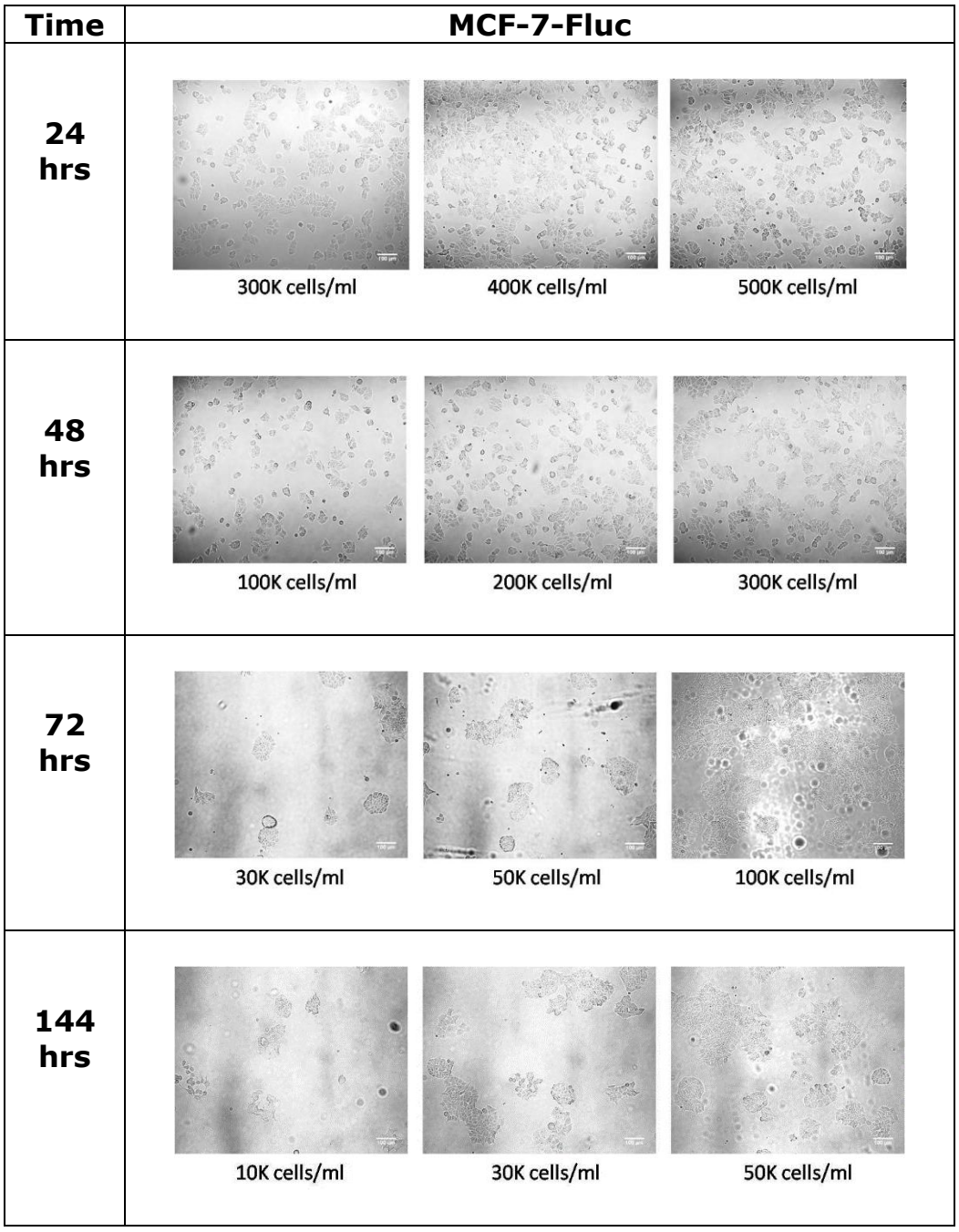

Figure 3-1: Cell density optimization for MCF-7Fluc: Cells were seeded at different densities to identify the relevant time-points at which cells became 75%-80% confluent. Brightfield microscope images are shown for each time point and different cell seeding densities. Images were captured at 10X magnification.

Time	MDA-MB-231-Fluc
24 hrs	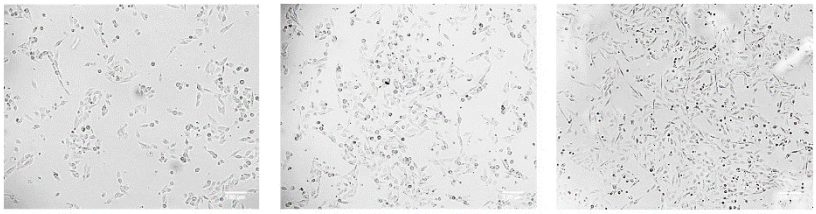 300K cells/ml 400K cells/ml 500K cells/ml
48 hrs	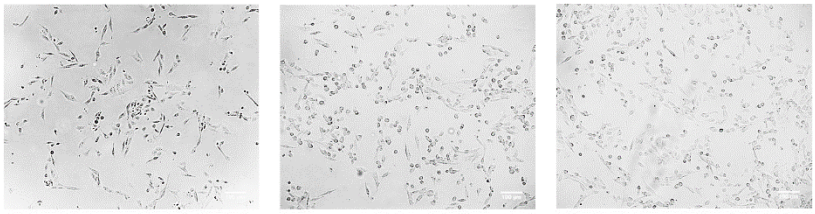 100K cells/ml 200K cells/ml 300K cells/ml
72 hrs	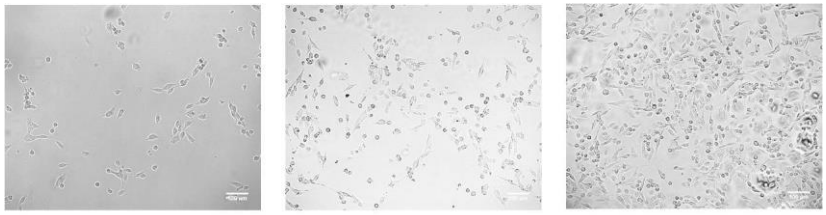 30K cells/ml 50K cells/ml 100K cells/ml
144 hrs	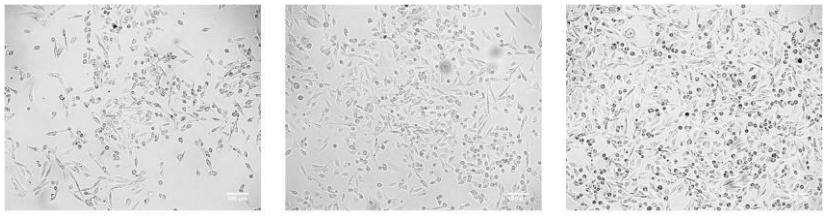 10K cells/ml 30K cells/ml 50K cells/ml

Figure 3-2: Cell density optimization for MDA-MB-231-Fluc: Cells were seeded at different densities to identify the relevant time-points at which cells became 75%-80% confluent. Brightfield microscope images are shown for each time point and different cell seeding densities. Images were captured at 10X magnification.

3.2 Optimisation for the total cell numbers in the 2D co-culture to study the growth promotion effect of the MSCs in BCCs

In order to study the impact of human MSCs on growth of BCCs, Alamar blue and Luciferase assays were performed in 2D co-culture system with different ratios of cancer cells: MSCs (1:1, 1:2 and 2:1) keeping the numbers of BCCs constant. Since there is no reference guideline available for the cell seeding density to set up the co-culture, the cell seeding number of the BCCs in the 96 well cell-culture plate was selected based upon the following strategies:

1. Based on the differences in the cell surface areas of the 6-well used for cell-density optimisation compared with the 96well plates:

No. of BCC/well in the 96 well plates = (30K cells/well) /9.5*0.32. The equation provides the cell seeding number of BCC is 9868 cells/well. 9.5cm^2 and 0.32cm^2 are the corresponding cell surface areas of the 6-well and 96-well cell culture plate. 30K cells/well in the 6-well plate was selected based upon the confluency status up to 144hrs in the cell seeding density optimisation step.

2. Based upon the volume of the cell culture media in each well of the 6 well and the 96-well cell culture plates:

No. of BCC/well in the 96-well plates = (30K cells/well*200ul) /1000ul. The equation provides the cell seeding number of BCC is 6K cells/well. 1000µl and 200µl are the corresponding volumes of the cell culture media used in each well of 6-well and 96-well cell culture plates. 30K cells/well in the 6-well plate was selected based upon the confluency status at 144hrs in the cell seeding

density optimisation step. Since, the BCC from the first strategy was almost 1.7 times higher than the later one, 6K BCC/well was selected for the monoculture.

Alamar blue assay is a metabolic assay which was used for measuring total cells (BCCs and MSCs) in the co-culture at particular time points, and the luciferase assay was used to measure the cancer cell numbers specifically in the co-culture at particular time points. MSCs were labelled with GFP to assess their presence by visualizing under a microscope in the co-culture. Alamar blue and luciferase assay both demonstrated increased proliferation of total cells and BCCs in the co-culture compared to the monoculture of BCCs starting from 48hours of the cell culture (Figure 3-3) and then the proliferation decreased after 96hrs. Co-culture using a BCC:MSC ratio of 1:2 resulted in the highest increase in BCC proliferation, which was consistent with the statistical analysis of growth kinetics (Table 3-1). Therefore, from the growth kinetic analysis (Alamar blue and luciferase assay) and statistical analysis it seems that the MSCs induce proliferation in the BCCs in 2D co-culture and the highest effect ($P<0.05$) was observed at 96 hours of the co-cultures. However, over-confluency of cells in the co-culture after 96 hours may adversely affect the cell viability resulting in the deterioration of RLU and RFU (Figure 3-3A&B). In addition, the decreased GFP signal intensity and distorted structure of MSCs from 96hrs onward highlighted possible cell death resulted from the over-confluency of cell in 2D co-culture (Figure 3-4).

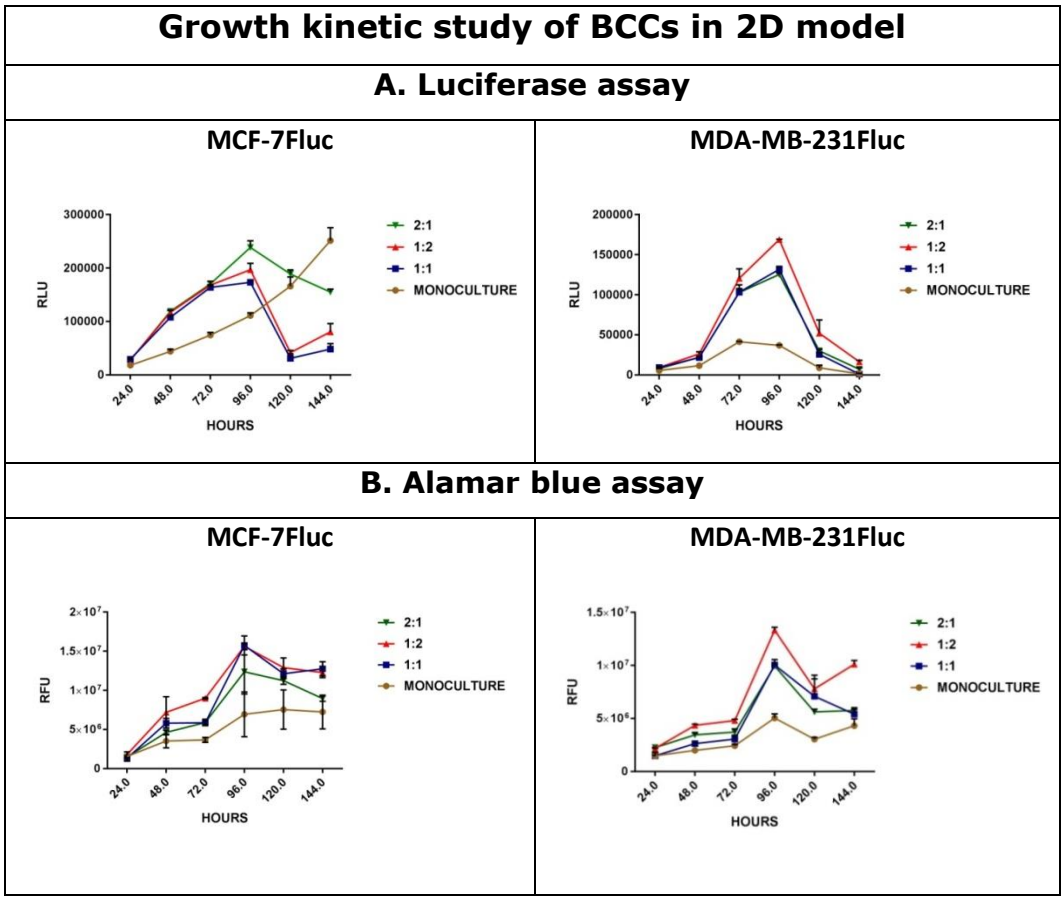

Figure 3-3: Growth kinetic study of BCC in 2D monoculture and co-culture: MCF7-fluc and MDA-MB231-fluc BCCs were grown in monolayer in the presence or absence of MSC-eGFPs at a range of BCC:MSC ratios: 2:1, 1:1 and 1:2. **A** Luciferase assay was used to assess the number of luciferase-expressing cancer cells, while the **B** Alamar blue assay was used to assess the total cell number, at specific time points in the study.

Images of 2D mono and co-culture at different time points

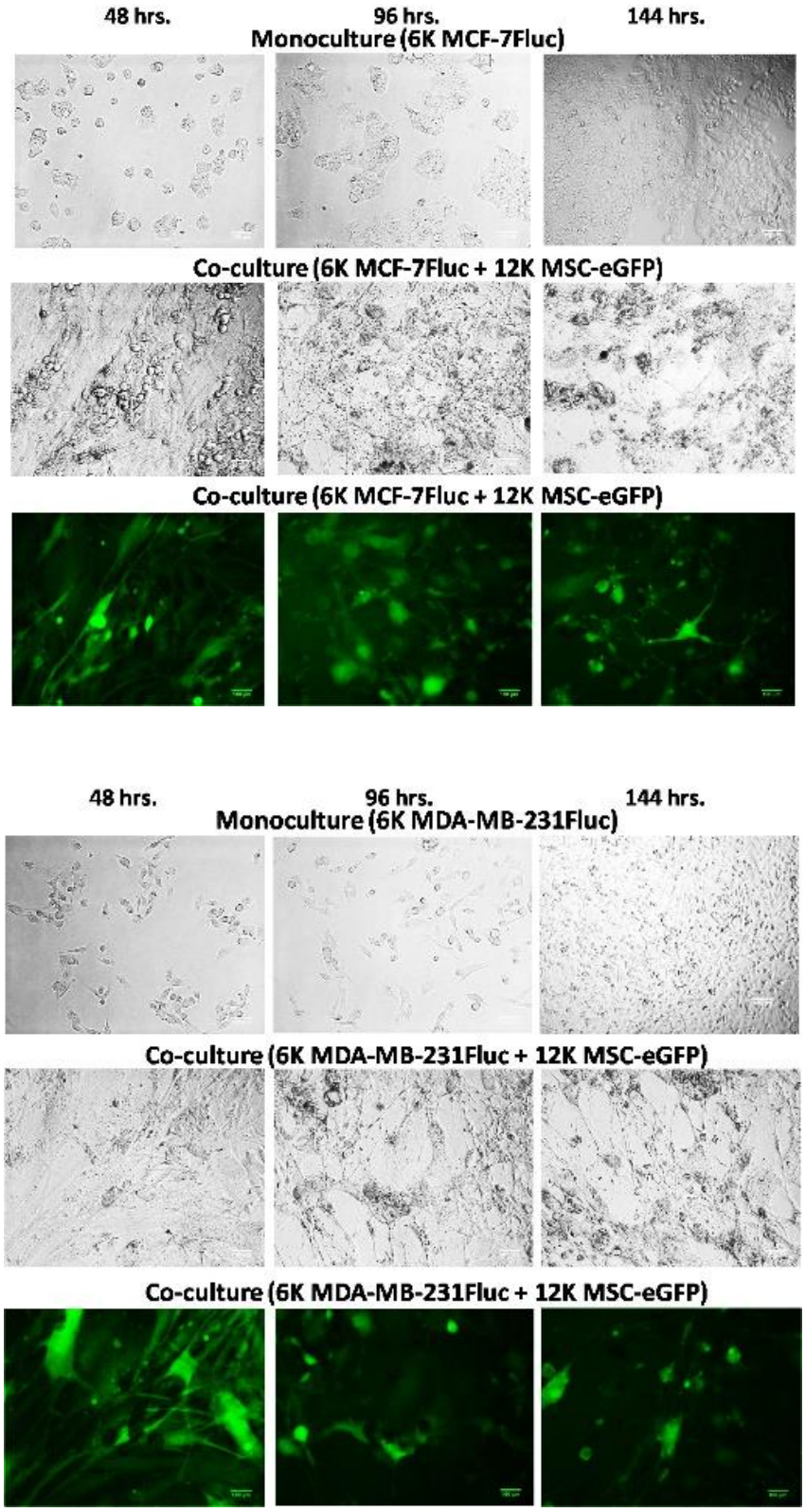

Figure 3-4: Microscopic images of increased cell population in 2D mono and co-culture: Brightfield microscopy images were used to assess cell confluency of BCCs in monoculture and co-culture, while fluorescent images were used to assess the presence of GFP-expressing MSCs (green) in BCC:MSC 1:2 co-cultures using a NikonTi brightfield microscope at 10X magnification.

Statistics for Growth kinetic study

MCF-7Fluc

Luciferase assay

	24hrs	48hrs	72hrs	96hrs	120hrs	144hrs
Monoculture vs. 1:1	Ns	***	****	***	****	****
Monoculture vs. 1:2	Ns	****	****	****	****	****
Monoculture vs. 2:1	Ns	****	****	****	Ns	****
1:1 vs. 1:2	Ns	Ns	Ns	Ns	Ns	Ns
1:1 vs. 2:1	Ns	Ns	Ns	***	****	****
1:2 vs. 2:1	Ns	Ns	Ns	*	****	****

Alamar blue assay

	24hrs	48hrs	72hrs	96hrs	120hrs	144hrs
Monoculture vs. 1:1	Ns	Ns	Ns	***	*	**
Monoculture vs. 1:2	Ns	*	**	***	**	**
Monoculture vs. 2:1	Ns	Ns	Ns	**	*	Ns
1:1 vs. 1:2	Ns	Ns	Ns	Ns	Ns	Ns
1:1 vs. 2:1	Ns	Ns	Ns	Ns	Ns	*
1:2 vs. 2:1	Ns	Ns	Ns	Ns	Ns	Ns

MDA-MB-231Fluc

Luciferase assay

	24hrs	48hrs	72hrs	96hrs	120hrs	144hrs
Monoculture vs. 1:1	Ns	Ns	****	***	Ns	Ns
Monoculture vs. 1:2	Ns	Ns	****	****	****	Ns
Monoculture vs. 2:1	Ns	Ns	****	****	*	Ns
1:1 vs. 1:2	Ns	Ns	Ns	***	*	Ns
1:1 vs. 2:1	Ns	Ns	Ns	Ns	Ns	Ns
1:2 vs. 2:1	Ns	Ns	Ns	****	*	Ns

Alamar blue assay

	24hrs	48hrs	72hrs	96hrs	120hrs	144hrs
Monoculture vs. 1:1	Ns	Ns	Ns	****	***	Ns
Monoculture vs. 1:2	Ns	*	*	****	****	****
Monoculture vs. 2:1	Ns	Ns	Ns	****	**	Ns
1:1 vs. 1:2	Ns	Ns	Ns	**	Ns	****
1:1 vs. 2:1	Ns	Ns	Ns	Ns	Ns	Ns
1:2 vs. 2:1	Ns	Ns	Ns	***	*	****

Table 3-1: Statistical analysis of MSC-driven proliferation of BCC at different time-points of the study: Luciferase assay and Alamar blue assay demonstrated significant increase of BCCs in co-culture comparing to the monoculture at different time-points of the study. Statistical analysis for the growth kinetic study of BCC in mono and co-culture were performed in the Prism. Significance of the study was determined using the Tukey's test in the Two-way ANOVA in the Prism. The Asterisk (*) symbol highlighted the significance of the study at 95% of confidence interval. *, **, ***, **** represent the P values 0.0101, 0.0027, 0.0002, and <0.0001 respectively.

3.3 Establishing and characterising spheroid co-culture model

Spheroids are assumed to imitate tumor behavior more effectively and are perhaps suitable for use as preclinical models in cancer research[220]. Although MSC-conditioned medium (MSC-CM) has been shown to increase BCC proliferation in 2D monolayer cultures[221], it was also of interest to investigate the effect of MSCs on BCC proliferation in the 3D spheroid model. However, certain potential factors including the necrotic core formation and cell viability, needed to be taken into account in order to have an optimal system available for studying BCC proliferation in the spheroid models. Unlike the 2D cell culture, the cell seeding density of the BCCs and MSCs for spheroid co-culture cannot be determined by observing cell confluency under the microscope. Instead, cells aggregate to form spheroids resulting in a gradient of oxygen and nutrition which can lead to formation of a necrotic core in spheroid culture[212]. Since the occurrence of a necrotic core in the spheroid depends on the initial cell seeding density, optimization was required to select the appropriate cell number to avoid the possibility of necrotic core formation. In the 2D monolayer, adhesion to the surface of the cell culture plate prevents apoptosis of cells, but the lack of such adhesion can reduce cell viability in spheroid culture. Therefore, the impact of the inclusion of the basement membrane extract (BME) on cell viability was also investigated in the spheroid culture. The purpose of using BME was to support initial cell-matrix and cell-cell interaction in the spheroid culture.

Thus, while comprehensive optimization to select the correct cell numbers based on cell confluence and the development of *in vitro*

assays was needed to successfully demonstrate BCC proliferation in 2D co-culture, understanding the complexity of the spheroid model itself is an essential aspect requiring further investigation prior to assessing the role of MSCs on BCC proliferation in the spheroid co-culture.

3.4 Spheroid formation using BCC lines

96-well ULA plates were used to initiate spheroid formation of BCC lines. ULA plates do not allow cells to adhere on the surface of the culture plate and thus facilitate the formation of spheroids in a time-dependent manner. The formation of spheroids is also dependent upon cell types in the culture[206,222]. In order to maintain the consistency of cell numbers used in 2D culture, 6K MCF-7Fluc and 6K MDA-MB-231Fluc were seeded separately and monitored until they formed spheroids.

On day 1, MCF-7Fluc appeared to form fairly tight aggregates of cells compared to the loosely-packed MDA-MB-231Fluc. On day 2, MDA-MB-231 became more tightly packed and finally, by day 3 both BCC lines had formed tight round spheroids (Figure 3-5). Therefore, day 3 was noted as the first day for spheroid formation in the monoculture system. However, spheroids formed from the 2 cell-types look very different even on day 3. The smooth-edge in MCF-7 spheroids indicates compactness of the cells but uneven edge in MDA-MB-231 spheroids highlighted potentially looser association between the cells.

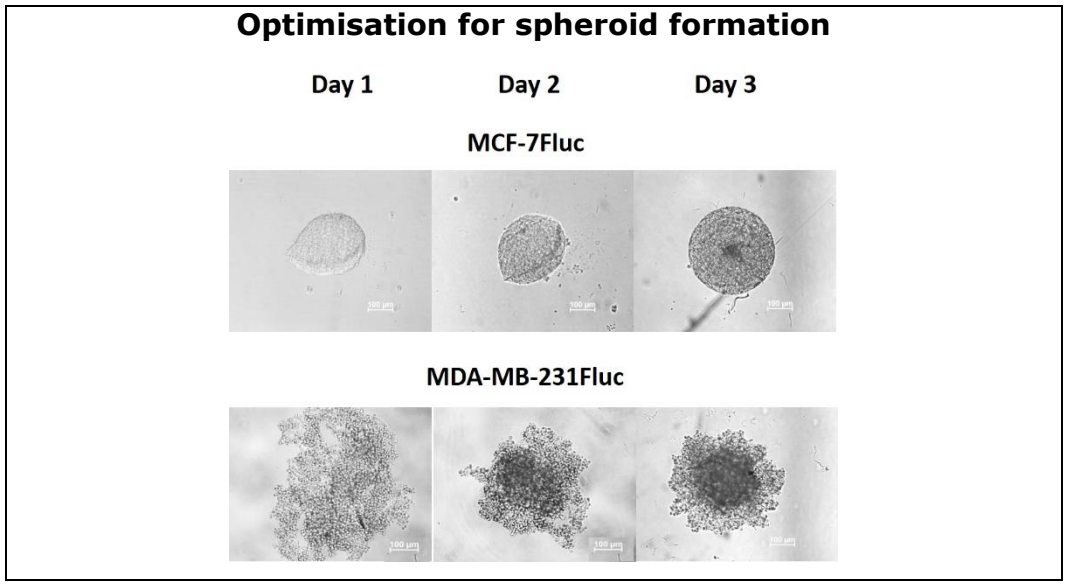

Figure 3-5: Spheroid formation in BCCs: MCF-7Fluc and MDA-MB-231Fluc were seeded in 96-well ULAplates. Microscopic observation demonstrated BCCs formed spheroids in a time-dependent manner. Images were captured with the assistance of a brightfield microscope at 10X magnification.

3.5 Cellular arrangement in the spheroid co-culture model

In order to investigate the distribution of MSCs in the spheroid co-culture, spheroid monoculture and co-culture were established using 6k MCF-7Fluc with varying ratios of MSCs as had been done for the 2D co-culture. Since day 3 was noted as the first day of spheroid formation in the monoculture system, the distribution of MSCs in the spheroid co-culture was investigated starting from that time point. In the spheroid co-culture, MSCs were observed in the core of the spheroid surrounded by MCF-7Fluc. Further microscopic investigation demonstrated co-culture (1:2) showed better retention of MSCs compared to other co-cultures (Figure 3-6). Hence, in order to maintain consistency with the cell numbers used in 2D cell culture and given the better retention of MSCs at a BCC:MSC ratio of 1:2, 6K BCC (MCF-7Fluc and MDA-MB-231Fluc) for spheroid monocultures and 6K BCC with 12K MSCs (BCC:MSC is 1:2) for the spheroid co-culture were used for the growth kinetic studies.

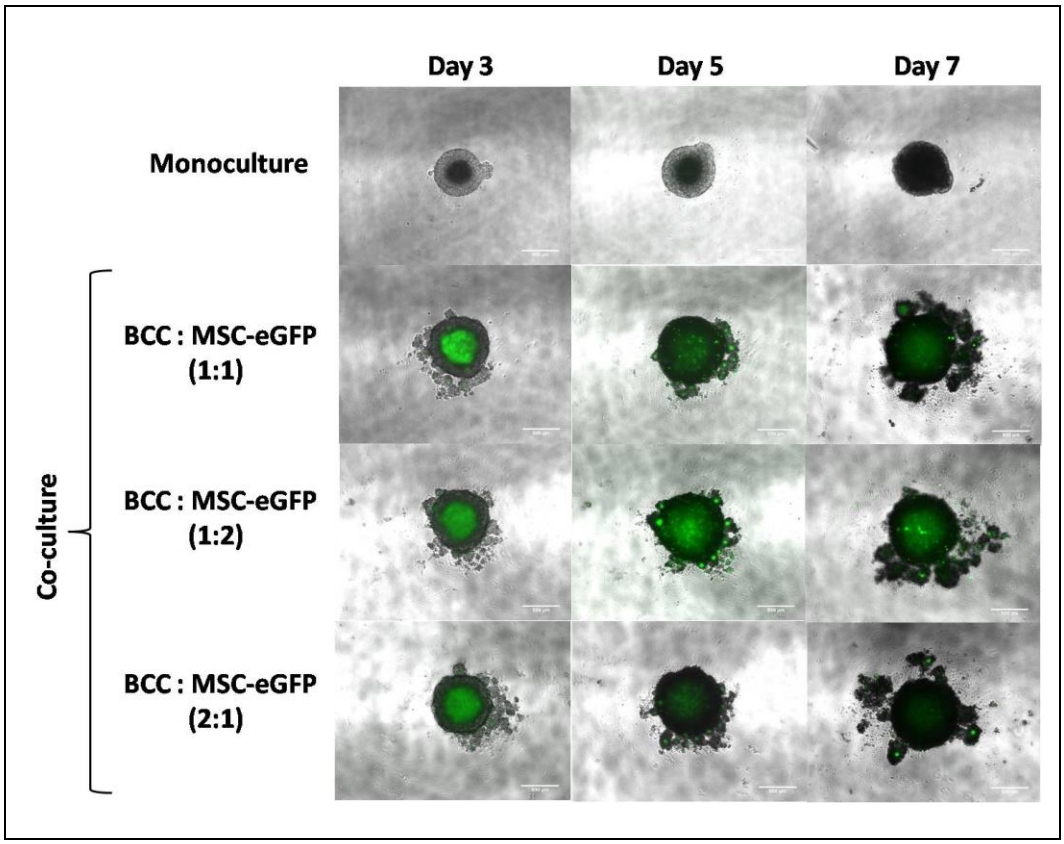

Figure 3-6: Retention of the MSC-eGFPs in spheroid co-culture: 6K MCF-7Fluc/wells were seeded for the monoculture, and for co-culture 6K BCCs with different numbers of MSCs to give ratios of 1:1, 1:2 and 2:1 were seeded. Images were captured at 4X magnification by fluorescent microscopy to observe the retention of MSCs in the spheroid co-culture based on the presence of GFP over the course of the study.

3.6 Necrotic core detection in the spheroid monoculture made using from 6K BCC

A dark mass appears in the center of spheroids potentially because of the presence of the quiescent or dead cells[211]. Since a dark region appeared in the core of the spheroid monoculture from 6K BCC (Figure 3-6), it was necessary to determine the cell viability in the core. In order to detect whether a necrotic core was present in the spheroids, Propidium iodide (PI) was added to the spheroids at day 3, day 5 and day 7, and microscopic images were captured under a fluorescent microscope. From the image analysis, the

presence of a necrotic core was observed in the spheroids of both BCCs on day 3 of the culture and it appeared that the diameter of the necrotic core increased with time (Figure 3-7). Therefore, in order to avoid the increased population of dead cells in spheroids, the formation of necrotic core in spheroids using lower total cell counts was investigated.

Cells	Day3	Day5	Day7
MCF-7Fluc	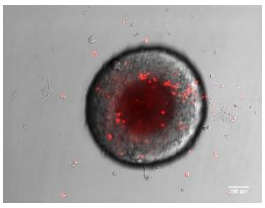	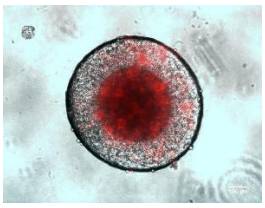	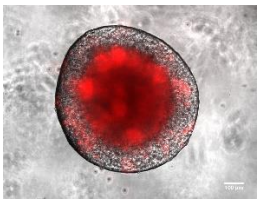
MDA-MB-231Fluc	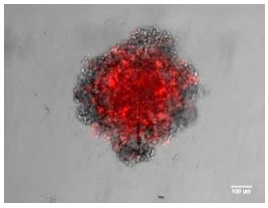	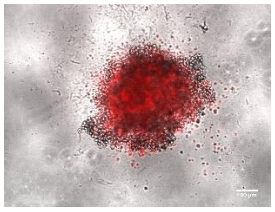	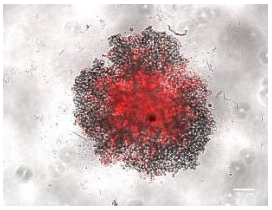

Figure 3-7: Detection of the necrotic core in the spheroid monoculture: Propidium iodide staining was performed to detect the presence of necrotic core in spheroids from 6K BCC in the monoculture. Population of dead cells in the center of the spheroids stained with Propidium iodide and appeared red in colour. Images were captured under a fluorescent microscope at 10X magnification.

3.6.1 Necrotic core detection in spheroids made using2K and 4K BCCs

The major purpose of avoiding the necrotic core formation in the spheroid is to investigate the BCC proliferation in the spheroid mono and co-culture model while all the BCC are alive over the course of the study. Since the formation of a necrotic core in spheroids is directly proportional to the increasing radius of the spheroids, probably due to the restriction of oxygen and nutrition

within the spheroids[213], spheroid monocultures were seeded with 2K and 4 K BCCs. Propidium iodide staining was performed at different time-points including day 3, 5 and 7 of seeding the spheroid monocultures with 2K and 4K BCC (Figure 3-8). Although some dead cells were observed, necrotic core formation was not observed at day 3 in the spheroid monoculture formed using 2K MCF-7Fluc but a region of dead cells appeared in the core at day 5 and 7. On the other hand, in the spheroid monocultures made using 4K MCF-7 and MDA-MB-231 demonstrated the presence of dead cells from day 3 onwards and the region of dead cells increased by day 7. Therefore, it seems that the low cell-seeding density decreased necrotic core formation in the MCF-7 spheroid model.

In contrast to 2K MCF-7 spheroid monocultures, the presence of dead cells in 2K MDA-MB-231 spheroid monoculture on day 3 indicated that the presence of dead cells was not only dependent on the cell numbers but also on the cell type. Studies have shown that E-cadherin-mediated cell-cell contact plays an important role in maintaining cell viability[223,224,225]. Hence, being triple negative BCCs, low expression of E-cadherin in MDA-MB-231 may result in early cell death in these spheroids compared to the MCF-7 spheroids. In order to promote cell-cell contacts in the spheroids, the ECM-rich BME was applied and further characterisation was performed to investigate the impact of ECM on cell viability in spheroid model.

Cells	Day3	Day5	Day7
MCF-7Fluc (2K)	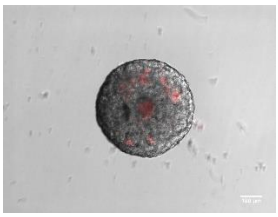	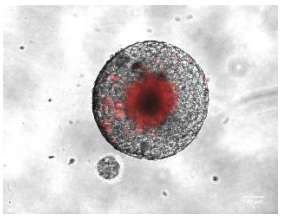	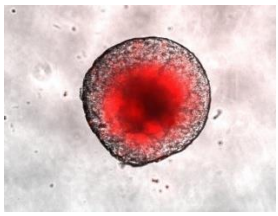
MCF-7Fluc (4K)	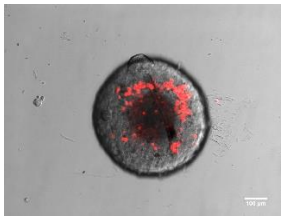	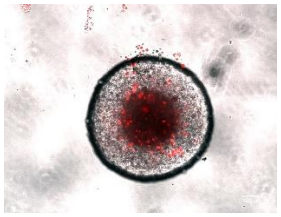	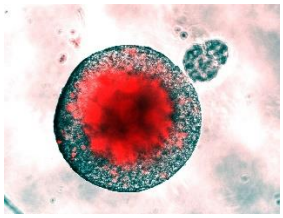
MDA-MB-231Fluc (2K)	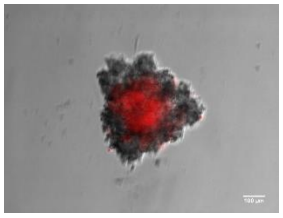	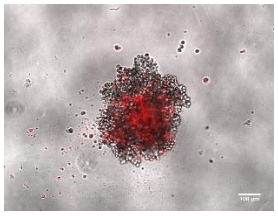	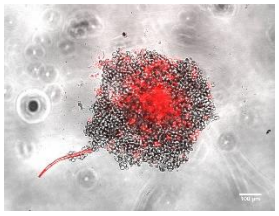
MDA-MB-231Fluc (4K)	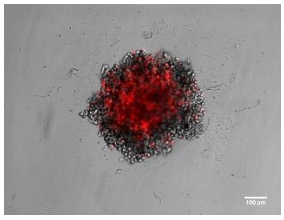	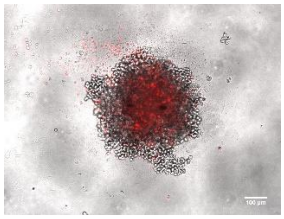	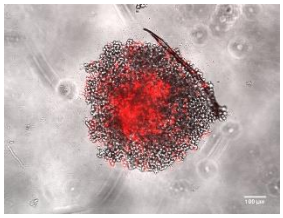

Figure 3-8: Propidium iodide staining in spheroid monoculture of BCCs: Propidium iodide detected the necrotic core in spheroids from 2K and 4K BCC in the monoculture. Population of dead cells in the center of the spheroids stained with Propidium iodide and appeared red in color. Images were captured under brightfield microscope at 10X magnification.

3.6.2 Impact of Basement membrane extract (BME) on spheroid formation

In order to observe the effect of ECM in spheroid formation and to investigate its effect on necrotic core, spheroids were seeded

using 2K BCC in the presence (BME-positive spheroids) and absence of BME (BME-negative spheroids) and the images were captured from day 1 of the culture onwards. The presence of BME helped in the formation of more compact spheroids in MCF-7 from day 1. Interestingly, BME also supported the formation of spheroids of MDA-MB-231 from day1 compared to the spheroids without BME and at day 3 the spheroids with the BME appeared more compact. Hence, day 3 was considered as a starting point to perform downstream experiments with the spheroids.

Cell no.	Day1	Day2	Day3
2K Without BME	**MCF-7** 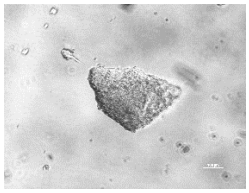	**MCF-7** 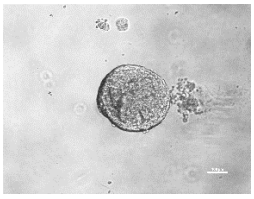	**MCF-7** 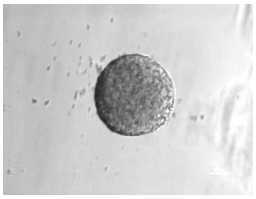
	MDA-MB-231 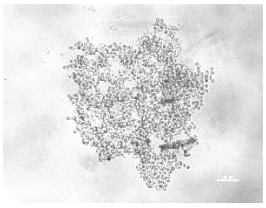	**MDA-MB-231** 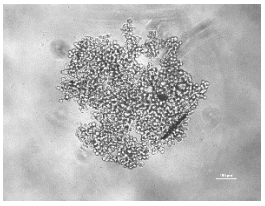	**MDA-MB-231** 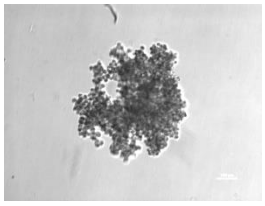
2K With BME	**MCF-7** 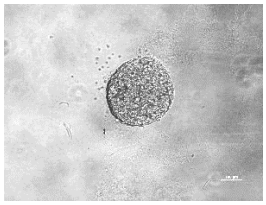	**MCF-7** 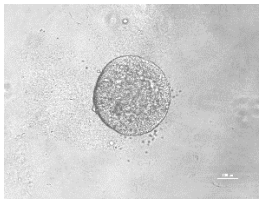	**MCF-7** 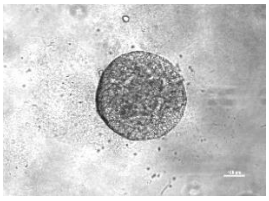
	MDA-MB-231 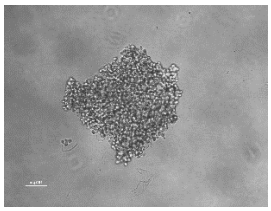	**MDA-MB-231** 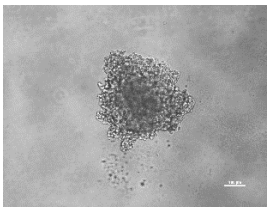	**MDA-MB-231** 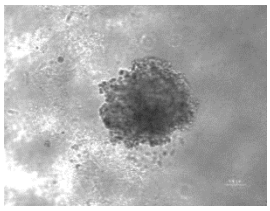

Figure 3-9: BME accelerated the spheroid formation in MCF-7 and MDA-MB-231: Investigating the impact of BME on spheroid formation in the BCC. Brightfield images were captured at 10X magnification.

3.6.3 Cellular compactness affects the formation of dead cell region in 2K BCC spheroid monoculture

Cell survival is dependent on cell-matrix interaction[226]. Hence, the impact of BME on maintaining the cell viability in spheroid model was investigated. Spheroid monocultures formed in the presence/absence of BME were stained with PI. In the absence of BME, no necrotic region appeared in the spheroid from 2K MCF-7 at day 3 but a population of dead cells started appearing in the core from day 5 and became more conspicuous at day 7 (Figure 3-10). In the case of MDA-MB-231-spheroids, the cells did not form spheroids in the absence of BME but formed a loose aggregate of cells (Figure 3-10) which may have resulted in dead cells observed to be present by day 3. In contrast, the presence of BME supported spheroid formation in MDA-MB-231 from day 3 and helped in the cell survival in the spheroid monoculture. In addition to helping maintain cell viability, increased radius in the MDA-MB-231 spheroids also indicated a positive role of BME in maintaining uniform growth of spheroids in the relevant time points (Figure 3-11). Similarly, in the presence of BME, no trace of necrotic core was detected in the MCF-7 spheroid mono and co-culture at day 3 and day 5 but red staining highlighted the presence of dead cells at different loci. However, at day 7 a dark mass appeared in the middle of spheroid monoculture indicating the presence of a necrotic core (Figure 3-10). The red signal over the entire spheroid monoculture of MCF-7 at day 7 indicated the possible non-specific binding of PI with BME. Hence, MCF-7 monoculture spheroids were again seeded but following PI

staining spheroids were washed carefully three times with phosphate buffer saline (PBS) in order to avoid the false-positive PI signal. Although the existence of the dead cells was not identified in the spheroids on day 3 and day 5, dead cells in the core of spheroids on day 7 were observed (Figure 3-10B).

Cell no.	Day3	Day5	Day7
2K MCF-7 Mono **Without BME**	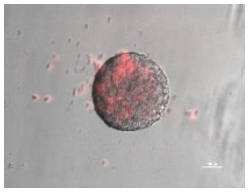	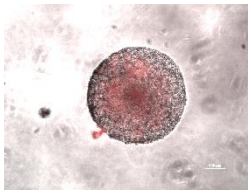	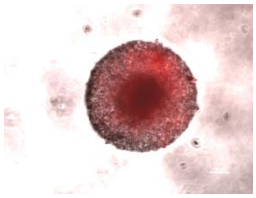
2K **Mono** (MDA-MB-231) **Without BME**	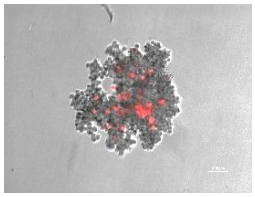	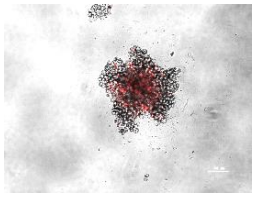	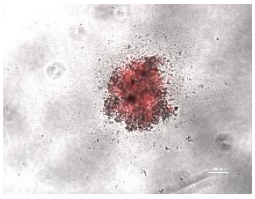
2K **Mono** (MCF-7) **With BME**	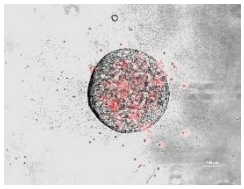	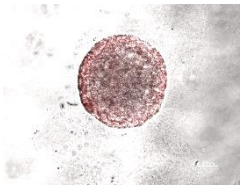	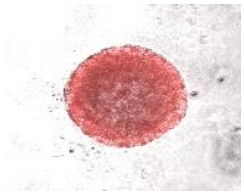
2K **Mono** (MDA-MB-231) With BME	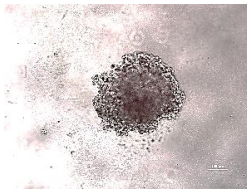	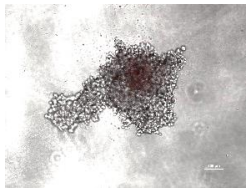	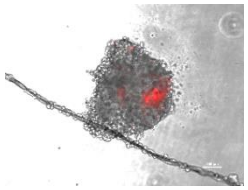
B. Spheroid monoculture washed with PBS for three times			
2K **Mono** (MCF-7) **With BME**	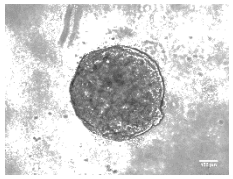	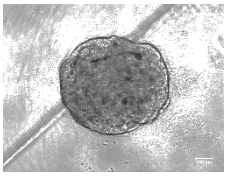	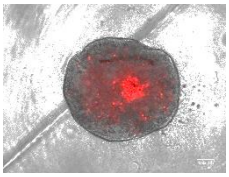

Figure 3-10: Impact of the BME on necrotic core formation in the spheroid monoculture: A. PI staining was performed in the spheroids from

2K MCF-7 and MDA-MB-231 in monoculture. Images were captured at 10X magnification. **B.** Spheroid monocultures were stained with PI and images were captured at 10X magnification after repeated washing the spheroids for three times with PBS.

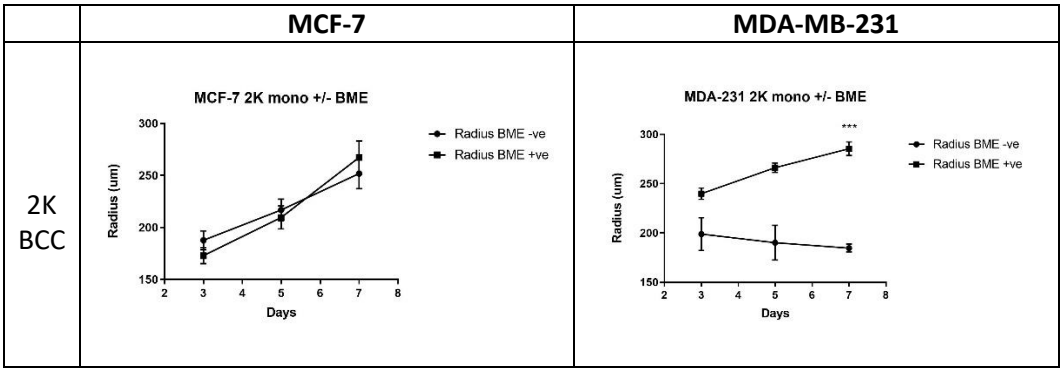

Figure 3-11: BME supported the structure of spheroids: The presence of BME did not make big differences in MCF-7-spheroid formation comparing to the monoculture seeded in the absence of BME. Presence of BME plays a significant role in clustering MDA-MB-231 to form the spheroid and keep the cells altogether during cell growth. *** represents the P value 0.0002, demonstrating the significant increase in the growth of BME-positive MDA-MB-231 spheroids at day 7.

3.6.4 Investigation of overall cell viability in the spheroid monoculture and co-culture

Although Propidium iodide staining assisted in detection of a necrotic core in the spheroid model, dual live/dead staining[211] was performed in order to further investigate the overall cell viability in the model. As the necrotic core was not observed in the spheroid monoculture made using 2K BCC, spheroid monocultures (2K BCC) and co-cultures (BCC:MSC in the ratio of 1:2) were subjected to Calcein AM and PI staining. Calcein AM crosses the cell membrane of live cells and gives green (G) fluorescence by reacting with intracellular esterases[227]. On the other hand, dead cells are permeable to Propidium iodide and appeared red (R)[228]. Therefore, the G/R ratio facilitates understanding the overall cell viability in the spheroid model. Hoechst staining was performed to

observe the presence of cell-nuclei in spheroid and to ensure the live/dead signal is from the cells in the spheroid but not from the background. After staining the spheroid cultures with the Calcein AM, PI and Hoechst 33342, the Z-stack fluorescent images were captured with a fluorescent microscope. In order to receive the maximum intensity from the Green and Red channels, central Z-stack image was taken into account to calculate the G/R at the relevant time points of the study.

In spheroids formed from 2K BCCs, the high intensity of green signal from the corresponding Hoechst positive cells suggested the presence of live cells (G/R is 6) in the core and the periphery at day 3 and day 5. However, at day 7 the reduced G/R value of 3 highlights the poor cell viability in the spheroid monoculture (Figure 3-12A).

In parallel to performing the dual staining in the monoculture, further investigation of cell viability was performed in the spheroid co-culture made using BCC: MSCs at a ratio of 1:2 (2K BCC and 4K MSCs). Unlike the monoculture of each BCC type, a decrease in the G/R-value in the corresponding co-cultures showed a reduction in the overall cell viability in a time-dependent manner (Figure 3-12A). Further investigation demonstrated that from day 5 onwards, an increase in the intensity of red-color in the core resulted in the reduction of G/R ratio in the spheroid co-culture. As it had been observed that MSCs resided in the core of spheroid co-culture (Figure 3-6), it seems that the red-signal was from dying MSCs.

In order to test this hypothesis, spheroid co-cultures were seeded with 2K BCC in the presence of 4K MSC-eGFPs and the

fluorescence intensity of the eGFP was measured from day 3 to day 7. Interestingly, the study showed a reduction in eGFP-intensity over the course of the study and the eGFP-intensity was significantly lower at day 7 compared to the day 3 in the spheroid co-cultures of both BCC types (Figure 3-12C). This suggests that the increased red signal in the core was because of the dead MSCs resulting in a reduction in the overall cell viability in spheroid co-culture.

A. Live/dead cell staining in spheroid mono and co-culture

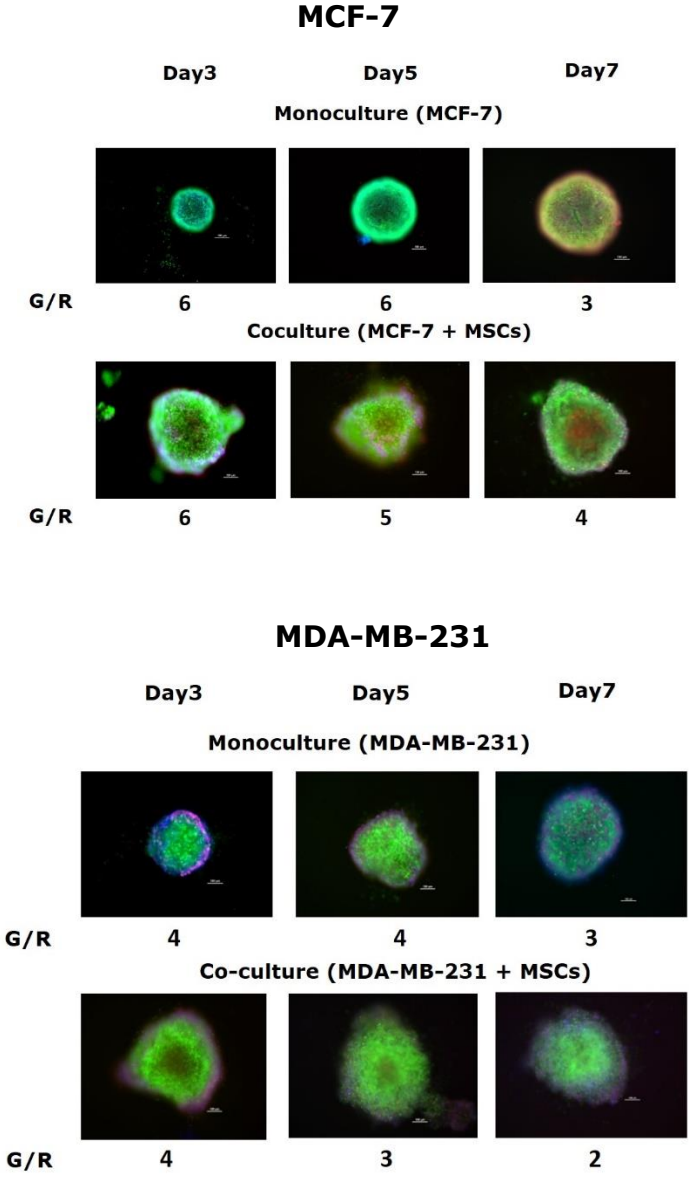

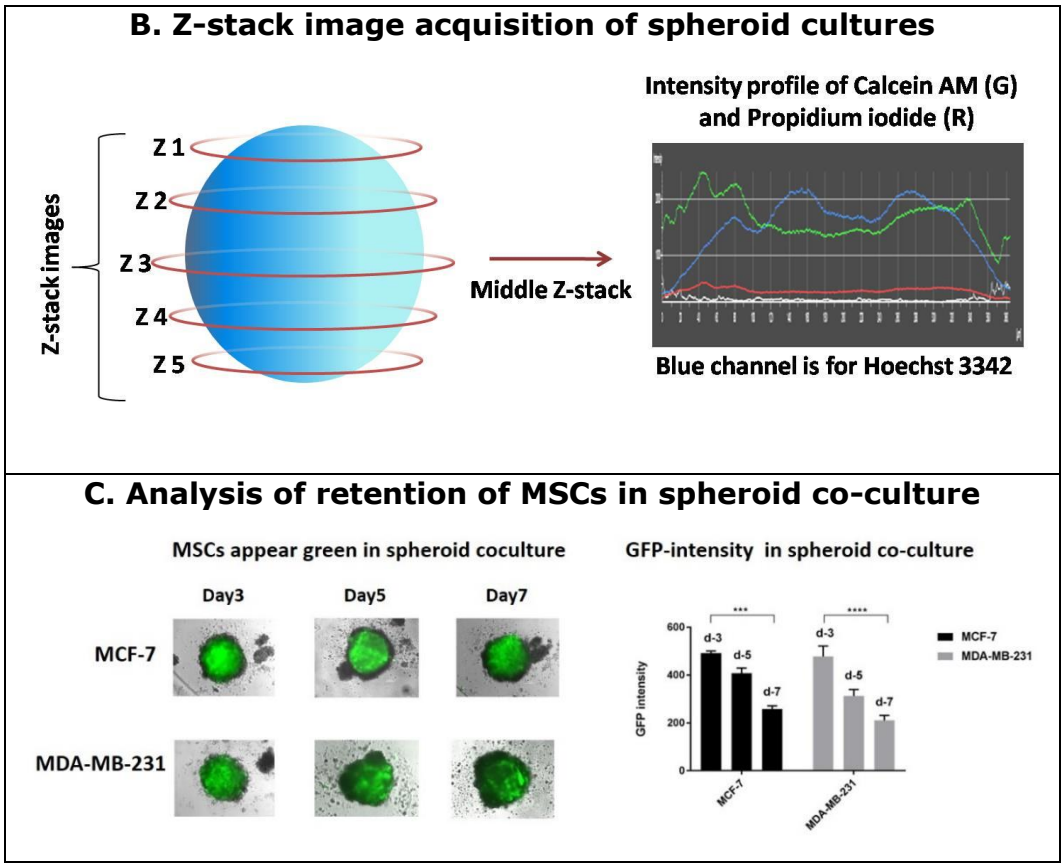

Figure 3-12: Cell viability in the spheroid mono- and co-culture: A. Spheroid mono and co-culture were stained with Calcein AM and PI to differentiate between live-dead cells in the course of the study. Intensity profiles represent the intensities of each channel in the spheroid at different time points of culture. G/R (Green/Red) represented the proportion of the live cells upon dead cells in the spheroid monoculture and co-culture. Images were captured under brightfield microscope at 10X magnification. **B.** Z-stack images of spheroid mono and co-cultures were captured by fluorescent microscopy. Fluorescent images at the central Z-stack were used to calculate the G/R in the spheroid mono and co-cultures at different time points of the study. **C**. The decreased intensity of eGFP in the spheroid co-culture highlighted loss of MSCs in the course of the study. The significant reduction of MSC-level in spheroid co-culture was represented the P value of <0.05 at 95% of confidence interval, analysed in the Prism using the concept of Two-way ANOVA. *** and **** represent the P values 0.0002 and <0.0001 demonstrating the significance of the study.

3.7 Summary

- In this study MCF-7 and MDA-MB-231 were directly cultured with MSCs in a 2D monolayer system. Since there are no known reference guideline for using the exact cell number for establishing a 2D co-culture, MCF-7 and MDA-MB-231 were seeded at various densities to observe the relevant time-points of their confluence. From the cell density study, 6K BCC was chosen for monoculture and the co-culture was established using 6K BCC with varying ratios of MSCs including 1:1, 1:2 and 2:1 for the growth kinetic study of BCCs. The Luciferase and Alamar blue assays demonstrated that the co-culture with BCC:MSC at a ratio of 1:2 results in an increase in the proliferation of BCCs. In parallel to investigating the growth-promoting effect of MSCs in BCC in 2D co-culture, the impact of MSCs on BCC proliferation in the spheroid co-culture was performed.

- There are different approaches to form spheroids including forced floating method, hanging drop method and agitation based method. Among all the aforementioned approaches, spheroids formed from the forced floating method are more convenient for high-throughput screening in the same cell culture plate because spheroids from two other approaches must be transferred to the other cell culture plate for the downstream assays. This transferring of spheroids may results in transfer-induced distortion in cell morphology and in addition, agitation based approach enforces sheer stress and gives non-uniformity in the spheroid size[229]. Another drawback of using hanging drop technique is the limitation

of using a small volume of the liquid drop, that is, 50µl containing cells. volumes over 50µl will not be accommodated in the hanging drop method because of the insufficient surface tension of the surface of the culture. In addition, changing culture media disturbed the spheroids in the hanging drop method. Another method such as microfluidic system is designed for 3D culture but because of the intricate design of the device, it is difficult to retrieve cells from the system. In contrast, the forced-floating method provides reproducibility in the sizes of spheroids seeded with the same number of cells, can accommodate larger spheroids and spheroids are easily accessible for the downstream assays[230]. Therefore, in this study, hydrogel-coated round bottom 96-well ULA plates were used for spheroid formation in BCCs. Because of the coating, cells dispensed in the wells did not get chance to adhere to the surface of cell culture plate and formed spheroids in the suspension consistent with the principle of forced floating method-based spheroid formation[230].

- In order to maintain the consistency with the cell number used in the 2D monolayer, 6K BCCs was used to set up the spheroid monoculture. 6K MCF-7 forms a cell cluster faster compared to the 6K MDA-MB-231. On day 3, the cell clusters of both BCCs appeared more circular and appeared as a mass of tissue (Figure 3-5). Therefore, day 3 was noted as the first day when the BCCs form spheroids. However, the edge of MDA-MB-231 spheroid appeared uneven compared

to the MCF-7. Therefore, it seems that the structure of spheroid is dependent upon the cell types.

- A thorough literature search revealed no precedent studies describing suitable cell density and the distribution of MSCs in the spheroid co-culture formed using the ULA 96-well plates. Hence, spheroid co-culture made using MCF-7:MSC-eGFPs in the ratio of 1:1, 1:2 and 2:1 were seeded. Among all the co-cultures, 1:2 was selected because of the better retention of MSCs over the course of study (Figure 3-6).

- In parallel, the chance of necrotic core formation in the spheroid culture was also taken into account before performing the growth kinetic study. The spheroid monocultures made using 6K MCF-7 and MDA-MB-231 were subjected to Propidium iodide (PI) staining. The presence of a necrotic core was detected in the center of the spheroids on day 3 and the population of dead cells increased in a time-dependent manner (Figure 3-7). As the formation of necrotic cores in the spheroids is dependent upon the cell seeding number, spheroid monocultures were seeded using 2K and 4K BCCs and stained with PI. Necrotic cores were detected in 4K spheroids of both BCCs since day 3 and therefore 4K was not suitable for the growth kinetic study. On the other hand, there was no necrotic core in the spheroids made using 2K MCF-7 but a necrotic core was observed in the spheroids of 2K MDA-MB-231 on day 3 (Figure 3-8).

- BME was included to support BCCs in the spheroid model. BME accelerated the formation of cell cluster in MDA-MB-231 (Figure 3-9) and supported uniform growth of spheroids at relevant time-points of the study (Figure 3-11). However, a sparsely distributed red signal suggests the presence of dead cells in the 2K spheroids of MCF-7 but no distinct necrotic core was observed resembling the necrotic core in the BME-negative spheroids on day 5 (Figure 3-10A). Therefore, it was assumed that there may be non-specific binding of PI with the BME that results in the appearance of red signal in the spheroids. Later, use of PBS washes decreased the non-specific binding of PI on day 3 and day 5, but, the presence of dead cells in the center indicate the necrotic core on day 7 in the 2K MCF-7 spheroid (Figure 3-10B).

- Although the PI staining procedure helps in the detection the dead cells, it is not efficient enough to provide information regarding the cell viability. On the other hand, the Calcein-AM detects early apoptosis events[227] which facilitates investigating cell viability. Hence, in order to investigate overall cell viability in the spheroid mono (2K MCF-7) and co-cultures (2K MCF-7 with 4K MSCs), BME-positive spheroids were stained with dual live/dead cell staining. The Calcein AM stained live cells green (G) and PI stained the dead cells red (R) in the spheroid. The G/R ratio in the spheroid monoculture showed viability was consistent between day 3 and day 5, but at day 7 cell viability reduced in the monoculture (Figure 3-12A). However, as the MSCs

progressively degenerated in the spheroid co-culture, the G/R ratio decreased gradually (Figure 3-12C).

CHAPTER 4: MSCs SUPPORT BCC PROLIFERATION AND INVASION IN SPHEROID CO-CULTURE

The aim of this chapter was to investigate the impact of MSCs on BCC (BCC) proliferation and invasion in the spheroid co-culture. In the previous chapter the characterisation of spheroid models demonstrated that using 2K BCCs avoids the formation of a necrotic core in spheroid monocultures and addition of BME improved the cell viability in the spheroid models. Therefore, in the first part of this chapter the aim was to use these models to study the effect of the MSCs on BCC proliferation. Unlike cells in the 2D monolayer system, cells in the spheroid models are not uniformly exposed to the reagents. Therefore, to trace BCC proliferation by means of luciferase assay in the spheroid model, incubation time for luciferin in spheroid culture needed to be determined. The purpose of this optimisation was to investigate the time required for the luciferin to enter into the spheroid model so the luciferin can reach BCCs buried inside the spheroid. The Alamar blue assay was also performed in parallel to the luciferase assay in order to investigate the consistency between the two cell proliferation assays. Although luciferase and Alamar blue assays are promising and reliable in terms of detecting cell proliferation, limitations of using these assays in spheroid culture were addressed. The bioluminescence (RLU) produced in the luciferase assay is dependent on the oxidation of luciferin catalysed by the luciferase in the presence of oxygen, Mg^{2+} and ATP[231]. On the other hand, the fluorescence produced in the Alamar blue assay is dependent on the cellular metabolism[219]. Since the cells in some spheroids experience gradients of nutrition and oxygen, cells

inside the spheroid may have different metabolic rates. The resulting RFU and RLU may therefore vary, which may not reflect the overall proliferation of BCCs in the spheroid culture. Hence, an experiment was designed to track proliferation of BCCs in the spheroid model using a non-metabolic dye, CellTrace violet.

Carboxy-fluorescein diacetate succinimidyl ester (CFSE) is used to determine the proliferation of B and T-lymphocytes. Upon antigen stimulation, reduction in the intensity of the CFSE-level in the parental lymphocytes give rise to the CFSE-peaks for daughter lymphocytes on flow cytometry analysis[232]. Hence, borrowing the concept of CFSE-mediated determination of cell proliferation and following the staining guideline, the BCCs were stained with the CellTrace Violet and seeded for the spheroid formation. Therefore, the intensity of the dye determined by flow cytometry would allow analysis of the presence of proliferative cells in the spheroid model.

Since flow cytometry analyses cells in suspension, optimization of enzyme-mediated dissociation of the spheroid culture was also required to prepare a single cell suspension ensuring good cell viability. Otherwise, dead cells might interfere with analysis. Further, immunohistochemistry for Ki-67 in spheroid was required in order to investigate the accuracy of aforementioned cell culture-based assays intended to use for investigating the impact of mesenchymal cells on BCC proliferation in the spheroid model. Although uncontrolled proliferation is one of the unique features of cancer cells, dissemination of cancer cells to distant organs in patients is lethal. Therefore, in parallel to the investigation of the impact of mesenchymal cells on BCC proliferation, the impact of

mesenchymal cells on BCC invasion in the spheroid co-culture was also studied.

4.1 Optimisation of luciferase assay in spheroids

Unlike the monolayer culture, the clustering of cells in spheroids may restrict the diffusion of any reagents inside the spheroid model. Hence, the incubation time for luciferin in spheroid cultures may need to be different than that for monolayers. Therefore, spheroids made using 2K MCF-7Fluc were seeded for three independent replicates. Each independent replicate contained four technical replicates of MCF-7 spheroids to monitor the reproducibility of the analysis. Since it was intended to study the BCC proliferation in spheroids from day 3 to day 7, and the spheroid radius increases over time, day 7 was chosen to optimize the incubation time with luciferin in the spheroid culture for luciferase assay. Therefore, day 7 spheroid monocultures were incubated with luciferin and the resulting luminescence (RLU) was measured at various incubation times. In each independent replicate of the study, increased signal of luminescence (relative luminescence unit or RLU) was observed over time, which was greatest at 90 minutes of incubation and thereafter the RLU decreased (Figure 4-1). Therefore, 90 minutes was selected as an incubation time for luciferin to investigate the role of mesenchymal cells in BCCs proliferation in the spheroid co-culture model.

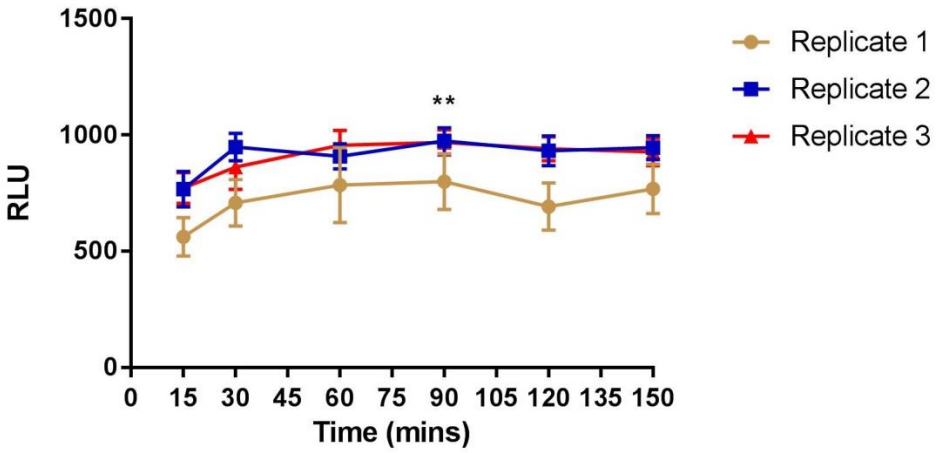

Figure 4-1 : Optimisation of luciferin incubation time in spheroids: Optimisation was carried out by incubating day 7 spheroid monocultures of MCF-7Fluc at different incubation times with luciferin. Analysis of the RLU assessed the statistical difference between the RLU at each time-point of the study in the biological replicates. '**' represented the statistical significance of the study having the P value 0.0051 at 95% of confidence interval.

4.2 Luciferase assay-mediated study of mesenchymal cell-driven proliferation of BCCs in spheroid co-culture

As the spheroid co-culture with a 1:2 ratio demonstrated better retention of MSCs in the course of the study, a growth kinetic curve was created by plotting the RLU values from the spheroid mono and co-cultures using 90 minutes luciferin incubation. In order to compare the BCC proliferation between the 2D and spheroid model at a similar incubation time with luciferin, the proliferation of BCC in the monolayer using luciferase assay was investigated. Interestingly, it was observed that, in contrast to 2D co-culture, the resulting RLU decreased in the spheroid co-culture in a time-dependent manner (Figure 4-2A). Therefore, it seems that the mesenchymal cells suppressed BCC proliferation in the spheroid co-culture. On the other hand, the increased volume of spheroid co-cultures suggested mesenchymal-driven proliferation of the BCCs (Figure 4-3). Therefore, it was hypothesized that luciferin could be accessed in 90 minutes of incubation by most of

the BCCs in spheroid monoculture, but the presence of mesenchymal cells, ECM and larger volume of the spheroid co-cultures, compared to the monoculture, might obstruct the diffusion of luciferin resulting in the loss of luciferase signal (Figure 4-2B). In order to avoid the problem of luciferin penetration in the spheroid co-culture, it was decided to extend the incubation time of luciferin so that the BCC in the core of spheroid co-culture can access luciferin.

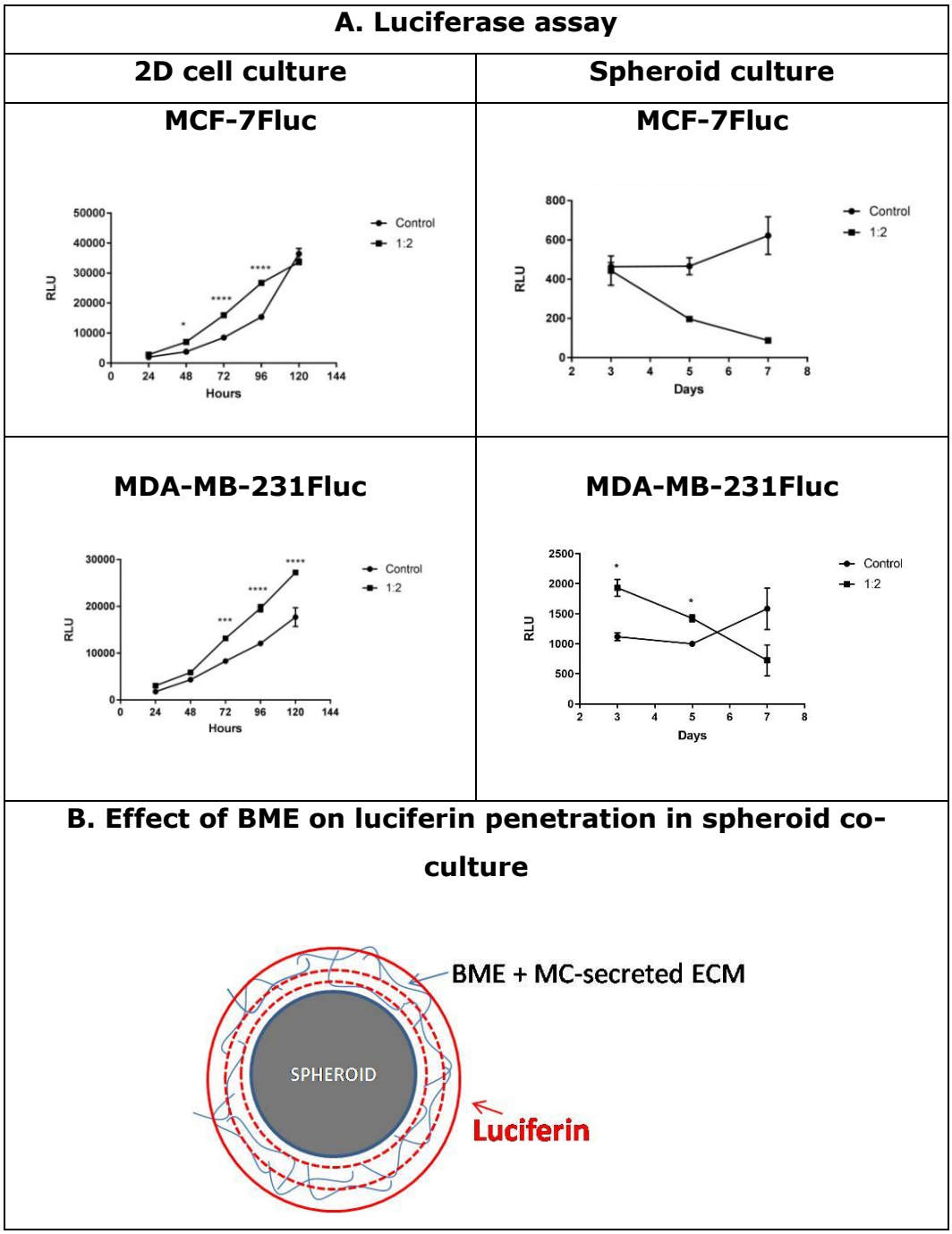

Figure 4-2: Investigation of BCC proliferation in the 2D and spheroid models by Luciferase assay: A. 2D monolayer and spheroid were incubated with luciferin for 90 minutes. RLU were quantified by a plate reader from BMGlabtech. '*' at day 3 and 5 represents the P values 0.04 and 0.01 signify an increased proliferation in MDA-MB-231 in the spheroid co-culture compare to monocultures. In contrast, no such significant increase in the proliferation was observed in the MCF-7 spheroid co-culture. However, '*', '***', '****' reflect significant increase in BCCs proliferation in 2D co-culture. 0.0126, 0.0004 and <0.0001 are the P values of corresponding asterisks in the 2D growth curves of BCCs. Growth curves and significance of the study were determined by Two-way ANOVA in the Prism. **B.** Schematic diagram of luciferin

penetration in spheroid co-culture represented the limitation in the diffusion of luciferin inside the spheroid co-culture model because of the cell aggregation, BME and MSC-secreted ECM in the spheroid co-culture. The wavy blue lines symbolise the presence of BME/MSC-secreted extracellular matrix (ECM) in the spheroid co-culture. While the solid and dotted red lines represent the inaccessibility of luciferin by BCCs in the spheroid co-culture.

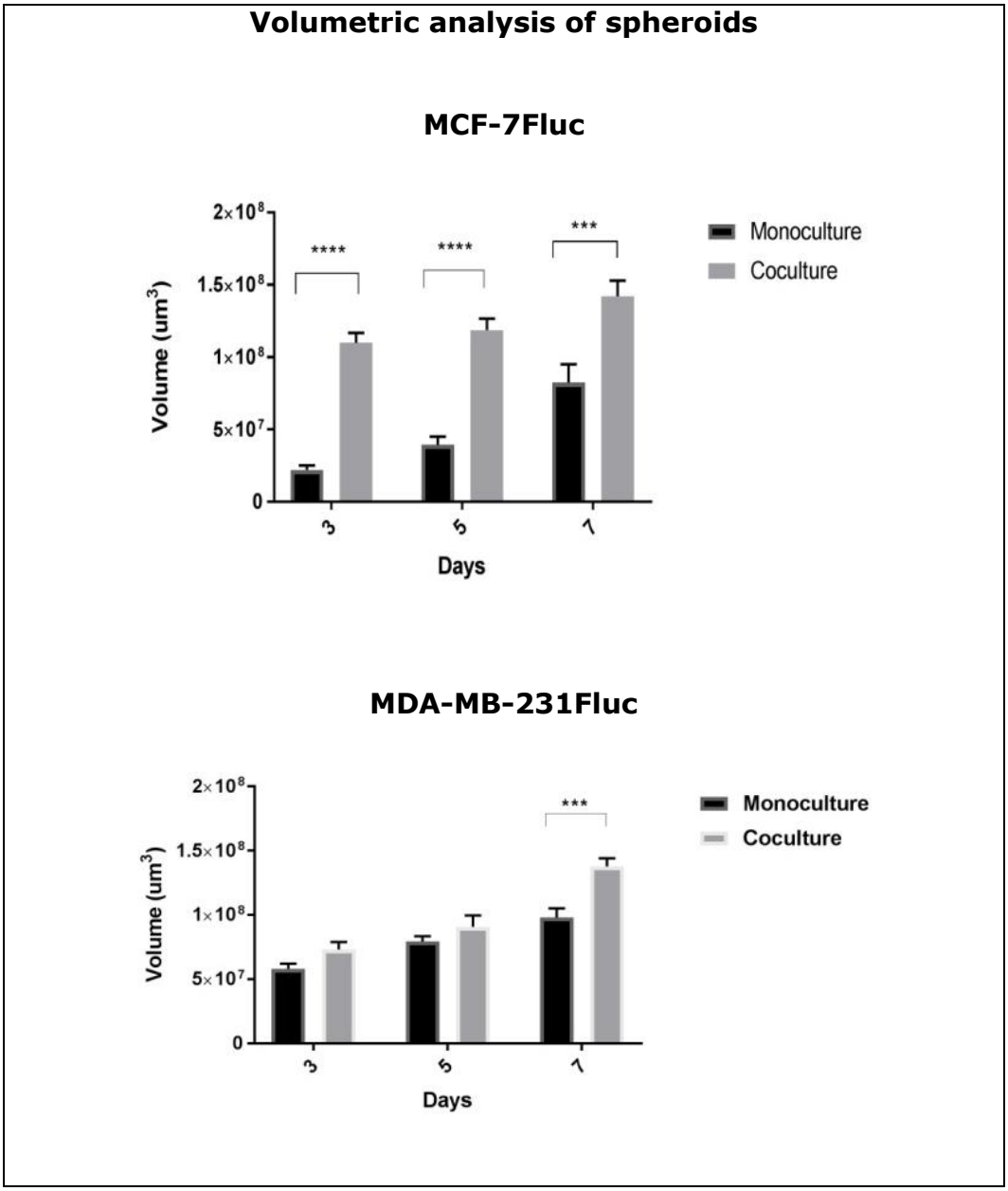

Figure 4-3: Volumetric analysis of spheroid mono and co-cultures of MCF-7 and MDA-MB-231: Images of the spheroid mono and co-cultures were captured and the radii of spheroids analysed by macros in imageJ. The volumes of spheroids were determined by using the formula $4/3*\Pi*R^3$. The bar graph and the volumetric analysis were performed in the Prism. Statistical significance (*) in the increased spheroid volume was analysed by the Two-way ANOVA in

the Prism. *,***,**** represented the P values 0.0126, 0.0004 and <0.0001 respectively.

4.3 Comparative studies of Luciferase and Alamar blue assay to investigate BCC proliferation capacity of MSCs in spheroid co-culture

In order to investigate the MSC-driven BCC proliferation with the Luciferase assay, the spheroid co-culture from day 3 was incubated with luciferin for 180 minutes so that the luciferin can diffuse to the centre of spheroid. However, it was again observed that instead of increasing, the value of RLU in spheroid co-culture decreased on prolonged incubation with luciferin (Figure 4-4A). Interestingly, in the same study, it was observed that on prolonged incubation of spheroid co-culture with the Alamar blue the resulting RFU increased. These results demonstrated that the luciferin is perhaps less stable than the Alamar blue in culture and the prolonged incubation resulted in the degradation of the luciferin. Therefore, new sets of the spheroid mono and co-cultures were seeded and BCC proliferation was measured from day 3 to day 7 using luciferin and Alamar blue by incubating spheroids for 90 minutes to compare the two assays. Although RLU decreased, the increase in the RFU from day 3 to day 5 demonstrated an increased cell proliferation in the spheroid co-cultures (Figure 4-4B). Nevertheless, on day 7 the resulted RFU in the co-culture was decreased may be because of the poor cell viability. However, compared with luciferin, Alamar blue in co-culture is not specific for the BCCs therefore it is not possible to tell which cell types have produced the observed fluorescence. But, as we demonstrated in the previous experiment (Figure 3-12C), MSCs in co-culture were lost in a time-dependent manner,

so it is more likely that the elevated RFU in the spheroid co-culture originates from the BCCs.

A. RLU vs. RFU

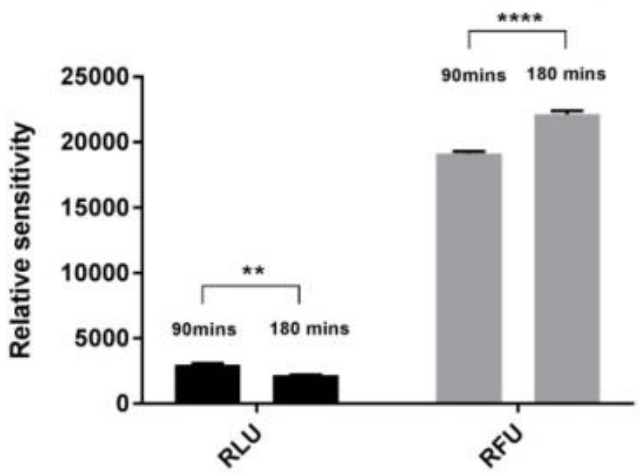

B. Luciferase and Alamar blue assay in spheroids

MCF-7Fluc

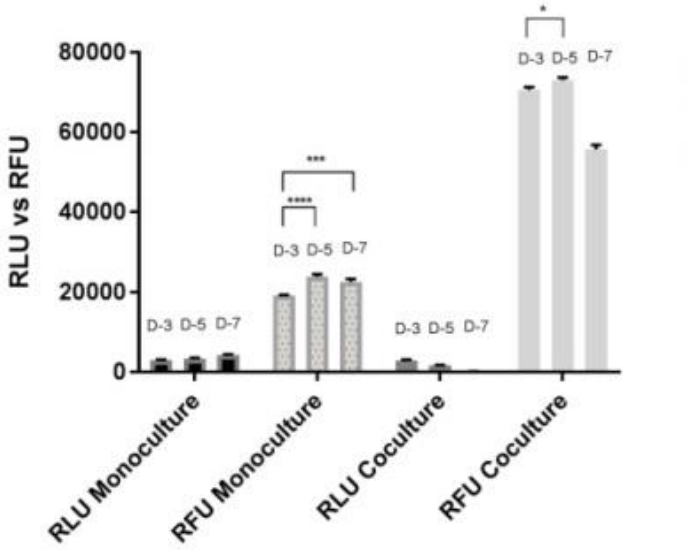

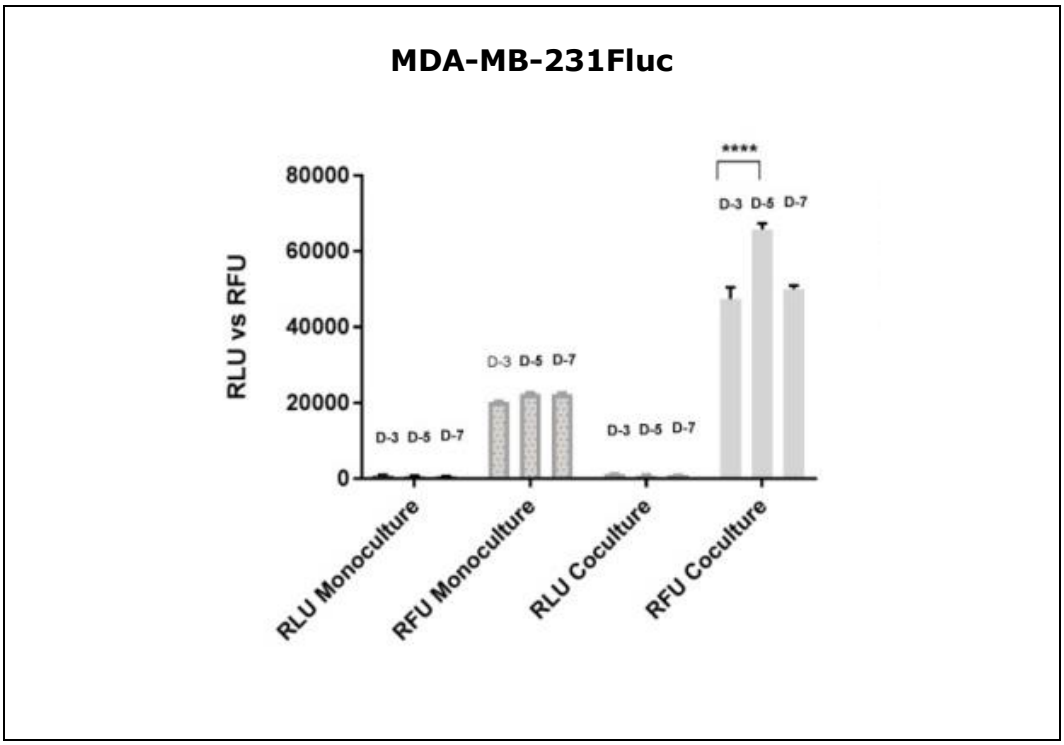

Figure 4-4: Comparative study between the Luciferase and Alamar blue assay in the spheroid model: A. Spheroid co-culture was incubated with the Luciferin and Alamar blue. The resulting RLU and RFU were quantified at different incubation time points including 90 mins. and 180 mins. The differential responses of spheroid co-cultures toward Luciferase and Alamar blue assay at different time points were determined in Prism. ** and **** represented the significance of the study and the P-values 0.0076 and <0.0001 respectively. **B.** Spheroid mono and co-cultures were incubated with Alamar blue and luciferin. After 90 minutes of incubation, RLU and RFU were determined by the plate reader. The bar graphs and significance (*) in the growth kinetic study were determined in Prism using Two-way ANOVA.

4.4 Flow cytometry-based analysis of BCC proliferation in spheroid co-culture

Luciferin and Alamar blue assays are dependent on the availability of oxygen and metabolism of cells[231,219]. Therefore, the alteration in the resulting RLU and RFU may mask the understanding about the true nature of MSCs on the proliferation of BCC in the spheroid model. Therefore, the CellTrace violet assay, which is independent of oxygen and metabolism, was introduced to investigate the BCC proliferation capacity of MSCs in the spheroid model. CellTrace Violet diffuses into cells where it is cleaved by intracellular

esterases to yield a highly fluorescent compound. This compound covalently binds to intracellular amines resulting in fluorescent staining. Hence, cell division results in sharing of the dye between the daughter cells which appear as a distinct peak separate from the parental cells on flow cytometry analysis[233]. Therefore, staining BCC with the CellTrace violet before seeding the spheroid has the advantage in circumventing the problem associated with the accessibility of the reagents once spheroids have formed. However, the CellTrace violet-based analysis of spheroids requires their dissociation into a single cell suspension for flow cytometry analysis. Therefore, optimisation was required to dissociate spheroids into a single cell suspension.

4.4.1 Enzymatic dissociation of spheroids

The major difficulty with dissociating spheroids into a single cell suspension is the presence of ECM. As the ECM consists of proteoglycan and fibrous proteins[42] it was necessary to find a potential enzyme to degrade the ECM for preparing a single cell suspension from the spheroid model. In this study, two different enzymes, Accutase and Accumax, were used to dissociate the spheroid into the single cell suspension. Following addition of the enzymes separately, spheroids were subjected under continuous shaking at 37^{O}C in the water bath for 3 minutes with the aim that, together with enzymatic reaction, mechanical turbulence may help in dissociation of spheroids. Although spheroid monocultures were disintegrated by both enzymes (Figure 4-5A), cell aggregates were still observed in the cell suspension of spheroid co-cultures digested by Accutase (Figure 4-5B). In contrast, Accumax treatment resulting in better dissociation of the spheroid co-cultures and no intact cell aggregates were observed after

digestion (Figure 4-5B). Therefore, it seems that Accutase is less efficient in dissociating the spheroid co-culture compared to the Accumax.

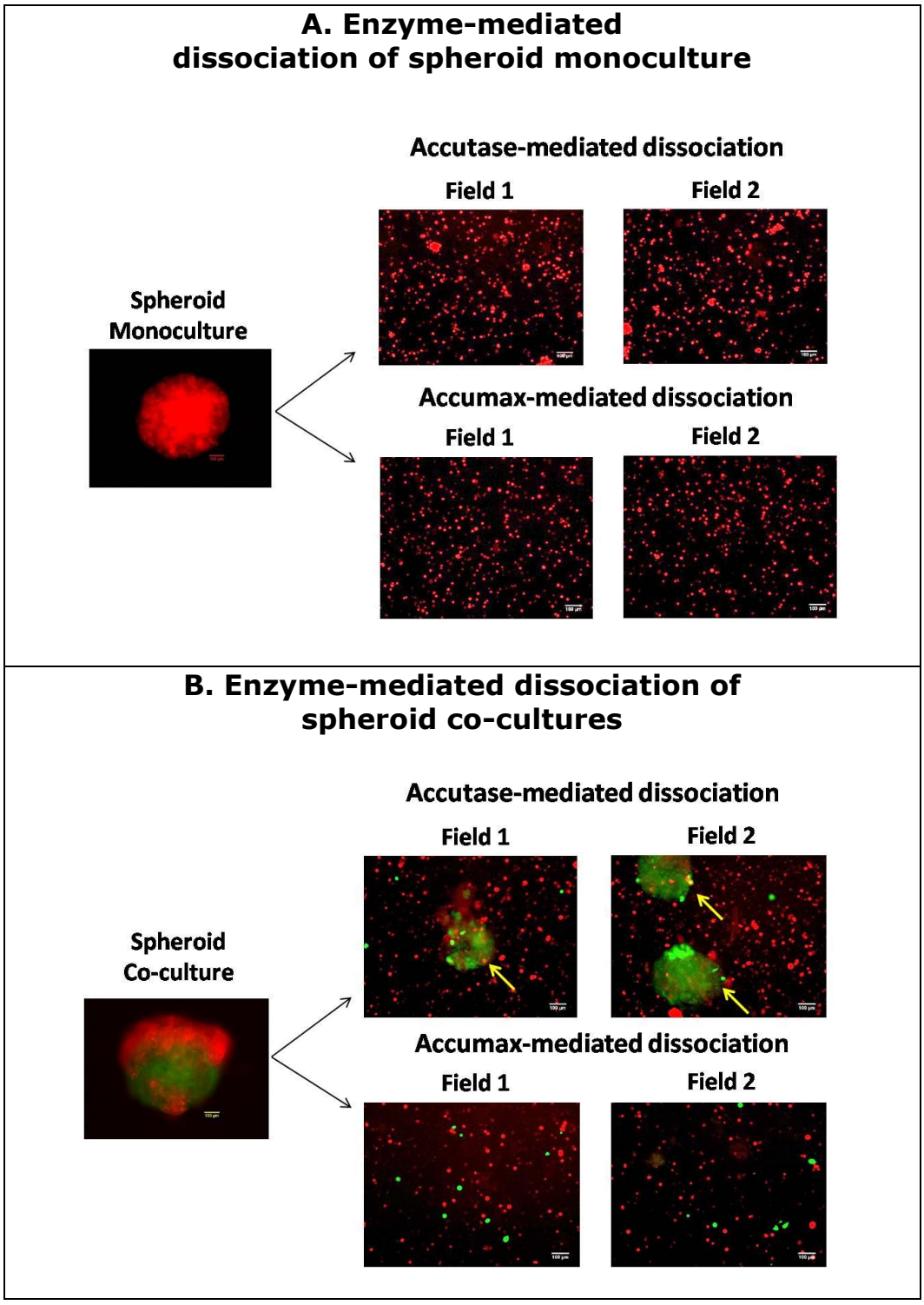

Figure 4-5: Dissociation of spheroid culture: A. Representing the Accutase and Accumax-mediated dissociation of spheroid monoculture. Images were captured under 10X objective of fluorescent microscope. **B.** The remnants of intact spheroid co-cultures (yellow arrows) were observed under Accutase treatment compared to the Accumax treatment. MCF-7tdTomato and MSC-eGFP were used to set up the spheroid co-culture in order to differentiate between MCF-7 and MSCs in the cell suspension of digested spheroids. Images were captured under fluorescent microscope at 10X magnification.

4.4.2 Investigation of the cell viability in single cell suspension resulted from the Accumax-mediated digestion of spheroids

Although Accumax demonstrated better digestion efficiency of the spheroid co-culture compared to the Accutase, experimental evidence was still required regarding cell viability (CV) following Accumax digestion of spheroids. Spheroids seeded with MCF-7tdTomato in the presence and absence ofthe MSC-eGFPs were digested with accumax by three different approaches. In Method 1, Accumax addition was followed by continuous shaking of spheroids in the water bath for 3 minutes. Although this resulted in the formation of cell suspension with the cell viability of 94% from spheroid monoculture, the resulting cell viability in the cell suspension from digested spheroid co-culture was only 73%. Hence, in order to increase the cell viability after dissociation of the spheroid co-culture, Method 2 was applied. Here, prior to shaking for 3 minutes in the water bath, spheroids were incubated with the Accumax at $37^{O}C$ in the incubator for 2 minutes; this improved the cell viability to 88% while cell viability of spheroid monocultures was maintained. Since the optimisation steps above enhanced the cell viability in the cell suspension of spheroid co-culture, Method 3 was designed to improve the viability on post-digestion of spheroid co-culture. The reasoning behind use of method 3 was that stepwise digestion of the spheroids may protect the cells from the enzymatic-action of the Accumax and

improve the cell viability in the cell suspension on spheroid digestion. Therefore in Method 3, spheroids (mono and co-cultures) were digested with Accumax in two steps with a short incubation time of 90 seconds per step. In the first 90 seconds of incubation with Accumax, the cell viability in the cell suspensions from spheroid mono and co-culture was 59% and 41%. However, Accumax-mediated digestion of remaining cell aggragates in step 2 increased the cell viability in the cell suspensions of spheroid monocultures (CV was 88%) and co-cultures (CV was 80%) and MCF-7tdTomato in the suspension was clearly visible under the microscope. Hence, the overall calculated average cell viabilities (ACV) from the method 3-directed digestion of spheroid mono and co-culture were 73.5% and 60.5%. Therefore, it seems that Method 2 for digestion of spheroid co-culture maintained better cell viability compared to the Methods 1 or 3.

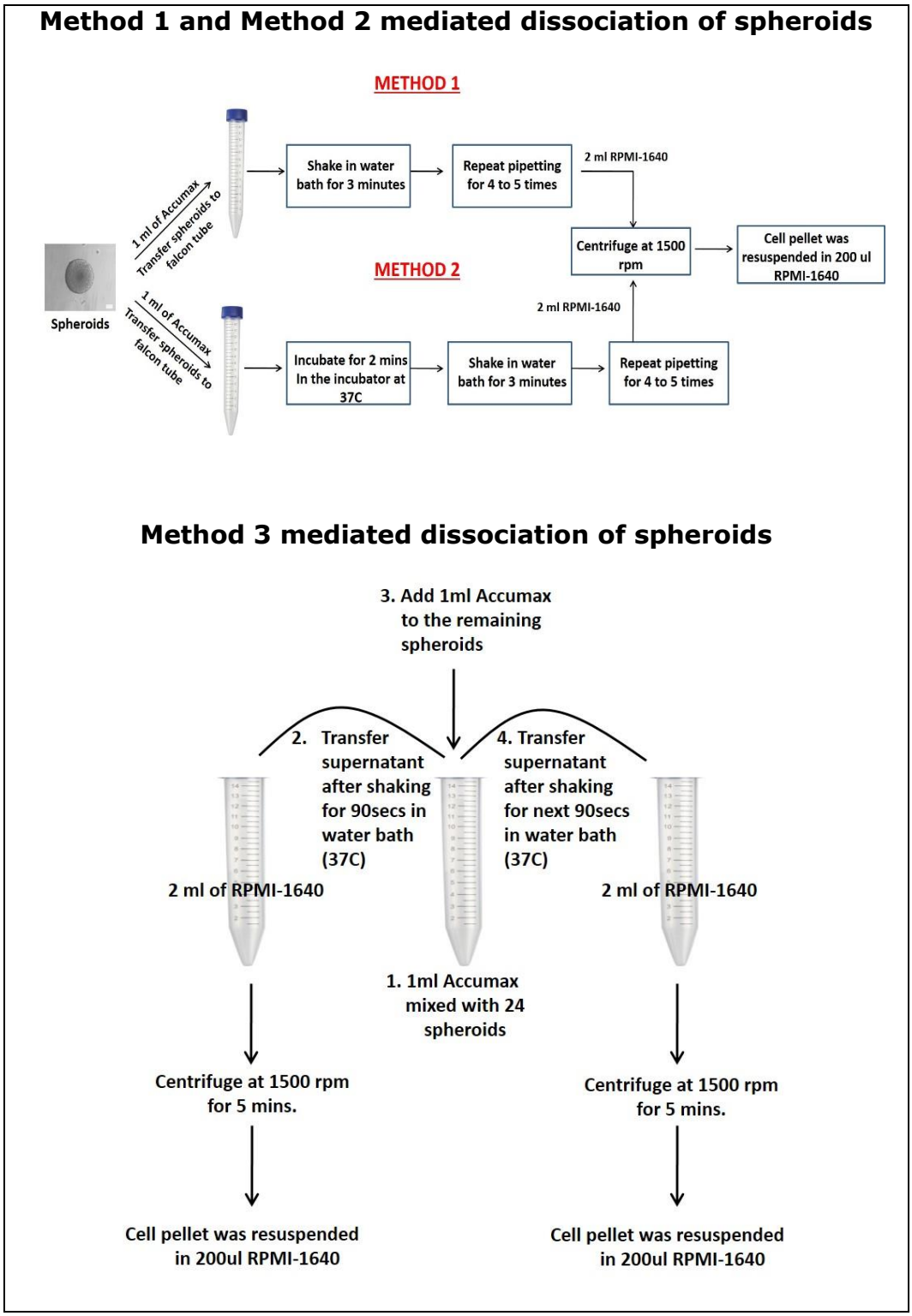

Figure 4-6: Schematic diagrams of the Method 1, Method 2 and Method 3 used for dissociating spheroid mono and co-cultures.

Cell suspension on post-digestion of spheroids

METHOD 1

Monoculture

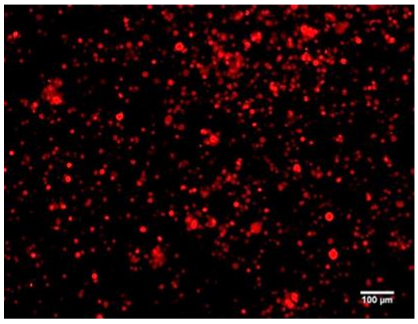

CV = 94%

Co-culture

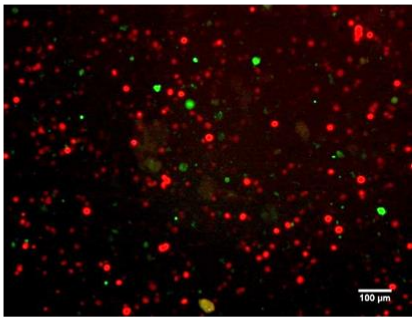

CV = 73%

METHOD 2

Monoculture

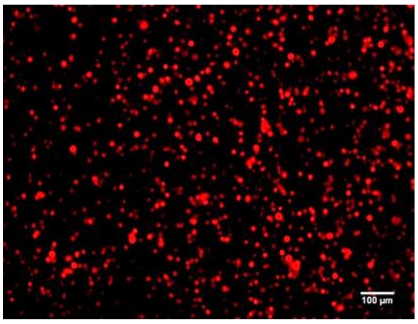

CV = 92%

Co-culture

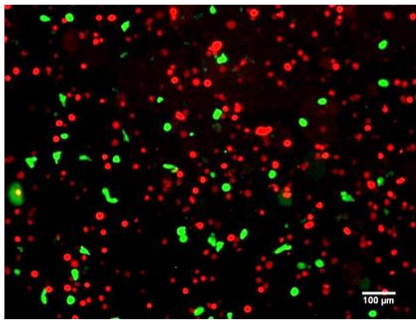

CV = 88%

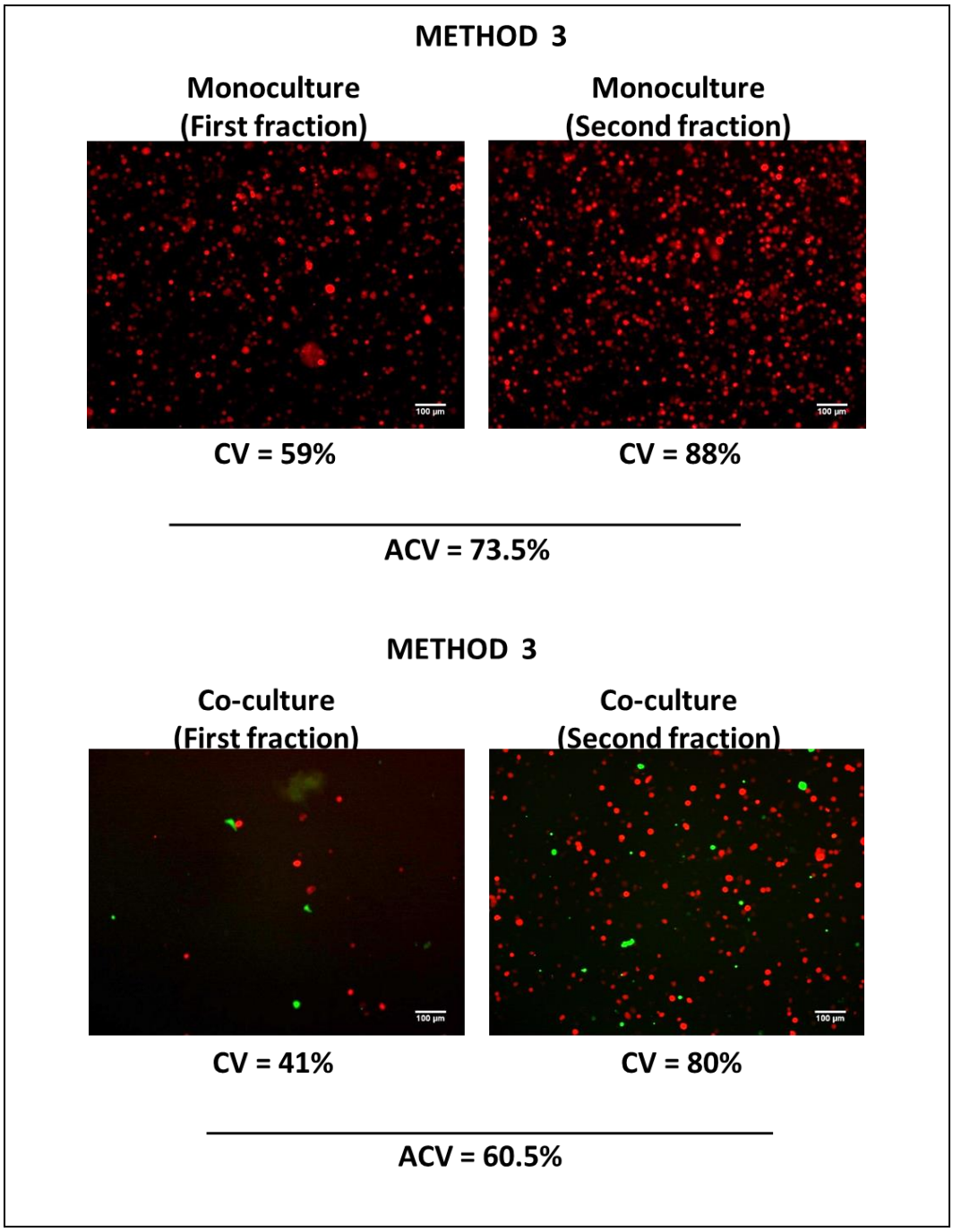

Figure 4-7: Accumax-mediated dissociation of spheroid: Spheroid mono and co-cultures were dissociated by Accumax following the work flow of each method separately. Presence of cells (MCF-7tdTomato) in the cell suspensions were observed under fluorescent microscope at 10X magnification. The cell viability (CV) in the cell suspensions was determined by trypan blue exclusion method with the assistance of TC20 automated cell counter machine.

In addition to determining the CV in the cell suspensions, the total number of live cells was also investigated in order to confirm the yield of cells prepared from the spheroid model digested in each method. Method 1 and 2 provided a good number of live cells on digestion of spheroid monoculture. In contrast, the yield of total cells and live cells decreased in Method 1 compared to the Method 2-mediated digestion of the spheroid co-culture. Similarly, Method 3-based digestion decreased the yield of viable cells in the first fraction of the corresponding digested spheroid mono and co-culture. Although an improvement in the yield of total and live cells was observed in the second fraction of Method 3-based digestion, the overall cell viability decreased compared to the Method 1 and 2-mediated digestion. In addition, the yield of live cells in each fraction of Method 3-mediated digestion was strikingly less compared to the number of viable cells produced by the Method 1 and 2-based digestion of spheroid monoculture. It seems that transferring the fraction of cell suspension into the new tube may increase the chance of losing cells in Method 3. Therefore, from the perspective of the yield of total cells and live cells, and cell viability, Method 2-mediated digestion stands as a best method for digestion of spheroid monoculture and co-culture.

<table>
<tr><th colspan="5">Monoculture</th></tr>
<tr><th>Methods</th><th>Total cells</th><th>Live cells</th><th colspan="2">CV</th></tr>
<tr><td>Method 1</td><td>$1.97X10^6$ cells/ml</td><td>$1.84X10^6$ cells/ml</td><td colspan="2">94%</td></tr>
<tr><td>Method 2</td><td>$1.6X10^6$ cells/ml</td><td>$1.47X10^6$ cells/ml</td><td colspan="2">92%</td></tr>
<tr><td rowspan="4">Method 3</td><td colspan="2">First fraction</td><td>59%</td><td rowspan="4">ACV

73.5%</td></tr>
<tr><td>$5.23X10^5$ cells/ml</td><td>$3.06X10^5$ cells/ml</td><td rowspan="2">88%</td></tr>
<tr><td colspan="2">Second fraction</td></tr>
<tr><td>$4.90X10^5$ cells/ml</td><td>$4.29X10^5$ cells/ml</td></tr>
</table>

<table>
<tr><th colspan="5">Co-culture</th></tr>
<tr><td>Method 1</td><td>1.19X10^6 cells/ml</td><td>8.74X10^5 cells/ml</td><td colspan="2">73%</td></tr>
<tr><td>Method 2</td><td>1.35X10^6 cells/ml</td><td>1.19X10^6 cells/ml</td><td colspan="2">88%</td></tr>
<tr><td rowspan="5">Method 3</td><td colspan="2">First fraction</td><td>41%</td><td rowspan="3">ACV

60.5%</td></tr>
<tr><td>1.22X10^5 cells/ml</td><td>5.01X10^4 cell/ml</td><td rowspan="2"></td></tr>
<tr><td colspan="2">Second fraction</td><td>80%</td></tr>
<tr><td>1.54X10^6 cells/ml</td><td>1.24X10^6 cells/ml</td><td colspan="2"></td></tr>
</table>

Table 4-1: Details of live cells, dead cells and corresponding cell viability in the cell suspensions prepared from the dissociation of the spheroid mono and co-cultures by Method 1, Method and Method 3.

In parallel with the cell viability screening, the efficiency of each method in preparing the single cell suspension on following spheroid dissociation was investigated using the automated cell counter machine TC20. Since the diameter of a single cancer cell has been shown to be≥10um using a Particle size analyzer[234], a gate of between 10um to 16um was used to indicate the presence of single cells in the cell suspension and the height of the histogram inside the gate represented the number of single cells in the suspension. This approach was applied to the cell suspensions prepared using the different methods of spheroid co-culture digestion. Since the histogram height within the gate in Method 2 appeared larger than the histograms in Method 1 and 3, the Method 2-directed digestion of the spheroid co-culture appeared to increase the population of single cells in the cell suspension (Figure 4-8). Therefore, along with maintainance of the CV, the gate-based single cell analysis demonstrated that Method 2 was an efficient approach in terms of preparing single cell suspension from the spheroid co-cultures.

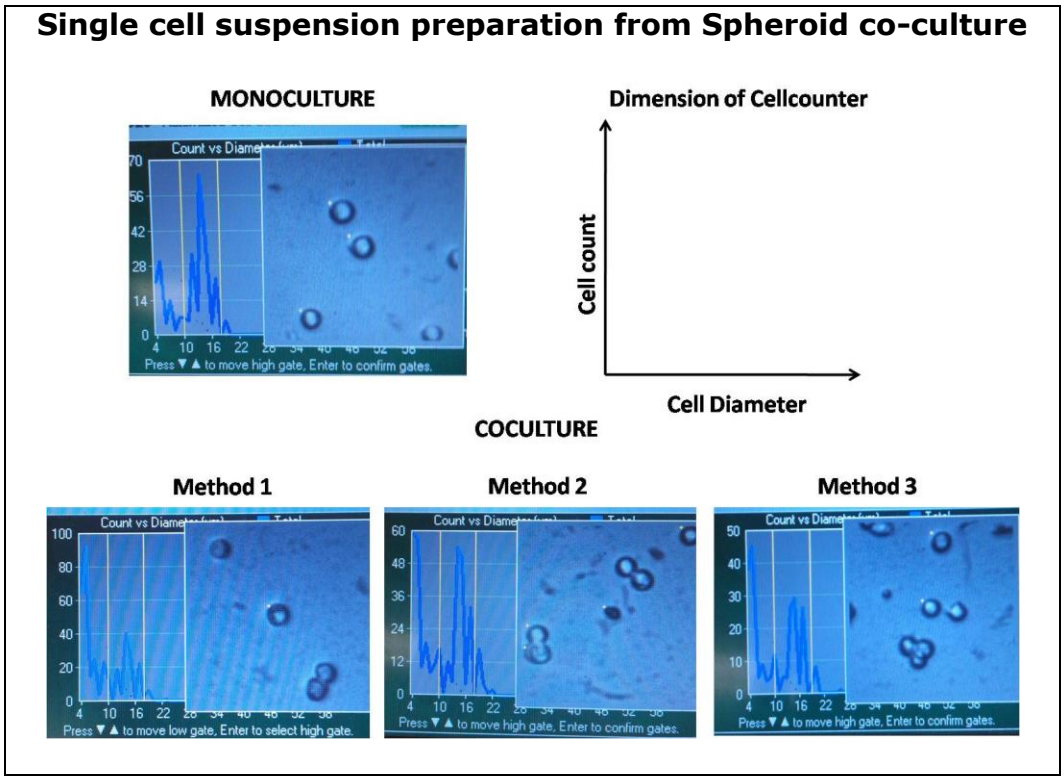

Figure 4-8: Analysis for the presence of single cell on Accumax-mediated spheroid dissociation in different methods: Histogram appeared inside the gate represented the presence of single cell in the suspension of MCF-7tdTomato from the monoculture. Cell suspensions prepared from spheroid co-cultures using different methods were analysed to investigate the presence of a single cell population. Height of the histogram inside the gate represented the number of single cells in the cell suspension and the cells within the gate between 10um to 16um in the X-axis were singlet.

4.4.3 CellTrace violet assay-mediated determination of the effect of Mesenchymal cells on the proliferation of BCC in spheroid co-cultures

The CellTrace violet-based detection of BCC proliferation in the spheroid culture was carried out on day 3 and day 5. Due to the poor cell viability, day 7 was excluded from this study. On day 0, BCC was stained with CellTrace Violet and the fluorescence intensity in BCC was ensured by the flow cytometry at the excitation and emission wavelengths of 405nm and 448/50nm before using them for the spheroid culture. H2 in the histogram represented the brighter population of BCC on day 0 and, due to

autofluorescence, non-labelled MSCs appeared in the H1 region at the same excitation wavelength. The difference of fluorescence intensity between the MCs and BCCs was highlighted in the overlap histogram. Since the co-culture was made using the MSCs and BCC in the ratio of 1:2; 33% of BCC was positive for CellTrace violet at day 0. In order to investigate the BCC proliferation capacity of MCs, the spheroid monoculture and co-culture on day 3 and 5 were digested with the Accumax and the BCC population positive for the CellTrace was analysed by the flow cytometry. The generated histograms and the statistical analysis of parental BCC in the spheroid monoculture demonstrated that 75% and 17% of MCF-7 and MDA-MB-231 remained positive for the CellTrace Violet at day 3, suggesting that 25% and 83% of the original population had divided prior to this time point. However, in the co-culture the number of positively stained cells was just 15% of the total population in the case of MCF-7 and 9% for MDA-MB-231; this means that considering that only total 33% of the cells in the co-culture were BCCs at the start of the experiment, 55% [100x(33-15)/33] of the MCF7s and 73% [100x(33-9)/33] of the MDA-MB231s had divided. Prolonged culture up to day 5 resulted in 50% and 14% of CellTrace Violet positive MCF-7 and MDA-MB-231 in the monoculture or 50% and 86% of the cells had divided, whereas in the co-cultures there were only 11% and 7% positive MCF-7 and MDA-MB-231 were positive, or 66% [100x(33-11)/33] and 79% [100x(33-7)/33] respectively had divided. Therefore, the resulting decrease of the fluorescent intensity in the BCC in the co-culture compared to the monoculture indicated the increased BCC proliferation in the spheroid co-culture. In parallel of determining the BCC proliferation in the co-culture, the

CellTrace Violet analysis also confirmed the differences of the proliferation rate between the MCF-7 and MDA-MB-231 in the spheroid monocultures. Since the fluorescence intensity in MDA-MB-231 reduced faster than the MCF-7 in the monocultures; it reflected the high proliferative nature of MDA-MB-231.

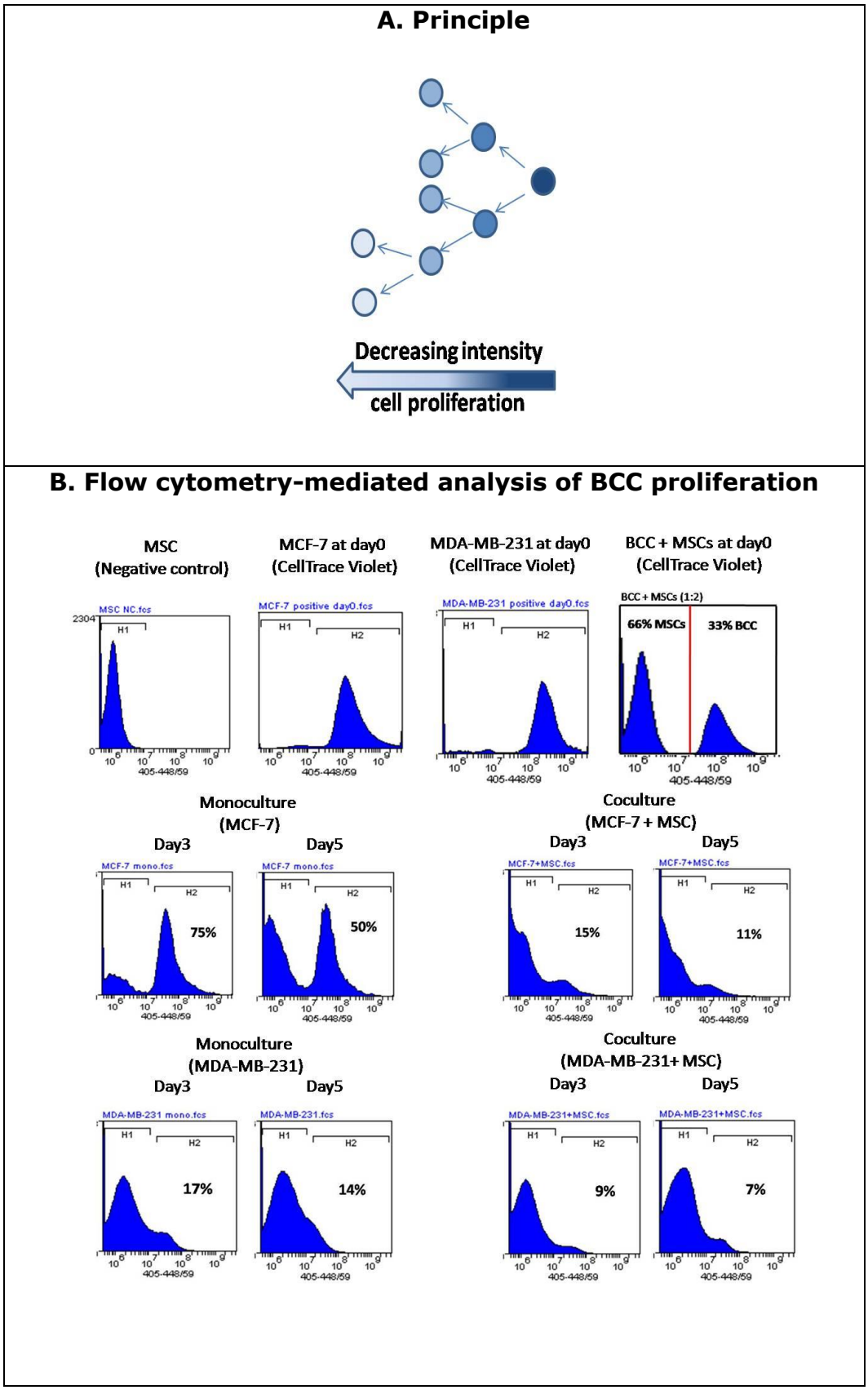
A. Principle
Decreasing intensity
cell proliferation
B. Flow cytometry-mediated analysis of BCC proliferation
MSC
(Negative control)
MCF-7 at day0
(CellTrace Violet)
MDA-MB-231 at day0
(CellTrace Violet)
BCC + MSCs at day0
(CellTrace Violet)
MSC NC.fcs
MCF-7 positive day0.fcs
MDA-MB-231 positive day0.fcs
BCC + MSCs (1:2)
66% MSCs
33% BCC
H1
H2
405-448/59
Monoculture
(MCF-7)
Coculture
(MCF-7 + MSC)
Day3
Day5
MCF-7 mono.fcs
MCF-7+MSC.fcs
75%
50%
15%
11%
Monoculture
(MDA-MB-231)
Coculture
(MDA-MB-231+ MSC)
MDA-MB-231 mono.fcs
MDA-MB-231.fcs
MDA-MB-231+MSC.fcs
17%
14%
9%
7%

C. Statistical Analysis

CellTraceViolet positive MCF-7 and MDA-MB-231 at H2 region in the histogram at different time-points				
MCF-7	Monoculture day 3	Co-culture day 3	Monoculture day 5	Co-culture day 5
Cell Positive for CellTrace violet at H2	75%	15%	50%	11%
Cell divided	25%	55%	50%	66%
MDA-MB-231	Monoculture day 3	Co-culture day 3	Monoculture day 5	Co-culture day 5
Cell Positive for CellTrace violet at H2	17%	9%	14%	7%
Cell divided	83%	73%	86%	79%

Figure 4-9: CellTrace Violet proliferation assay: A. The intensity of cell-trace violet decreased once the cells start expanding in the culture medium. **B.** BCCs positively stained with Cell-trace violet were analysed by flow cytometry and seeded for spheroid mono and co-culture. Spheroids were harvested on day 3 and day 5 respectively and digested in the presence of Accumax in order to prepare single cell suspension. Intensity deterioration of Cell-trace violet in BCCs was determined by the flow-cytometry. H2 is the area allotted for positively stained MCF-7. MSCs were used as a negative control and resided in H1. **C.** Statistical analysis demonstrated the presence of BCC population in the H2 region spheroid mono and co-culture at different time points of the study. Histograms and statistical analysis were performed with the assistance of the flow cytometry software named Weasel.

4.5 MSCs increased the expression of proliferation marker, Ki-67 in MCF-7 in spheroid co-culture

Since the CellTrace violet assay demonstrated an increased proliferation in the MCF-7 compared to the MDA-MB-231 in the co-culture models, the differential expression level of Ki-67 in MCF-7 spheroid mono and co-cultures was investigated. As mentioned earlier, Ki-67 is used as a cancer cell proliferation marker routinely in cancer pathology. An increased expression of nuclear Ki-67 in the BCC is associated with worse prognosis in BC patients[11]. Therefore, in order to investigate the Ki-67 expression in MCF-7 in the spheroid model, paraffin sections of 5um thickness from the

spheroid microarrays were prepared. Immunohistochemical characterisation of the sections demonstrated an increased Ki-67 expression in the spheroid co-culture over the course of the study. A close inspection demonstrated a major population of nuclei outside the spheroid core stained positive for Ki-67 (Figure 4-10C). Since the fluorescent images showed BCC resided at the peripheral region of spheroid co-culture (Figure 3-6), it was confirmed that the Ki-67 in the spheroid co-culture was from the proliferating MCF-7s. On the other hand, few BCCs stained positive for Ki-67 in the spheroid monoculture. Therefore, in parallel to the CellTrace violet proliferation assay, the Ki-67 analysis confirmed the BCC proliferation capacity of the MCs in the spheroid co-culture.

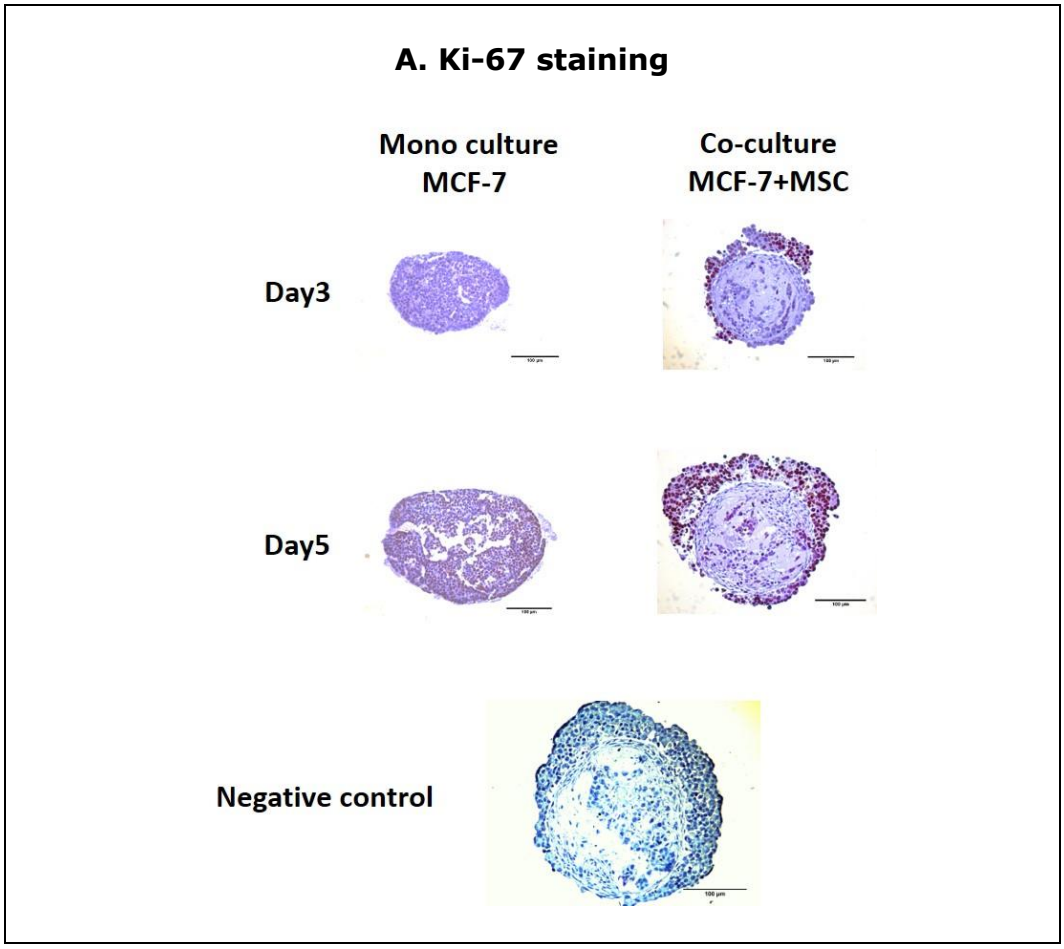

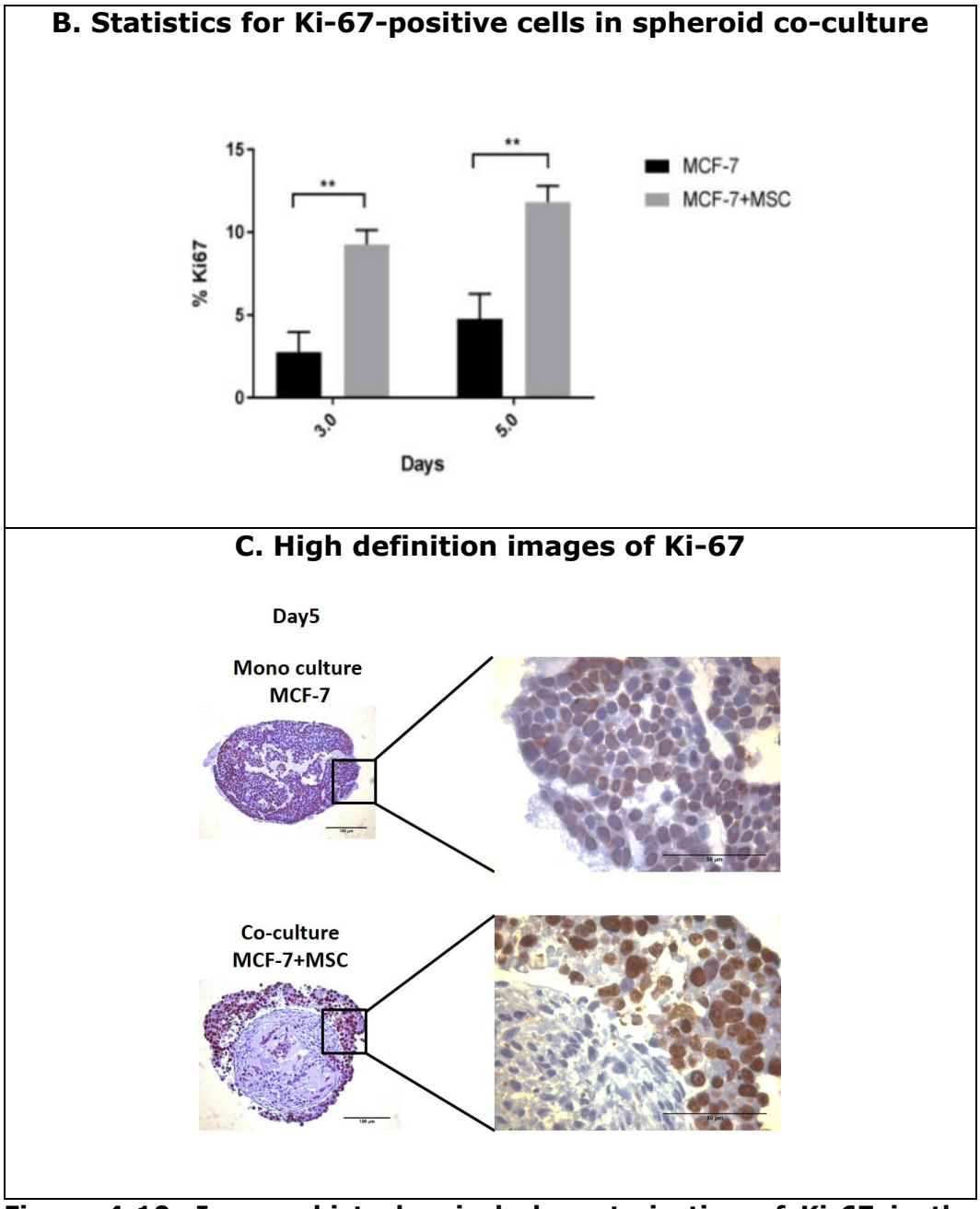

Figure 4-10: Immunohistochemical characterisation of Ki-67 in the spheroid: A. Spheroid mono and co-cultures were probed with the Ki-67 antibody. Brown color indicated the presence of the Ki-67 in the nuclei of MCF-7. Images were captured at 20X magnification under the Leica DFC480 microscope. **B.** Bar graph representing the quantitative expression of Ki-67 staining. '**' represented the P value <0.005, highlighting the statistical significance of the study. **C.** The oil immersion images of spheroid mono and co-culture were captured with the assistance of Nikon DFC480 microscope. The nuclei of MCF-7 are round in shape whereas the nuclei of MCs are flat and elongated. Nuclei of MCF-7 appeared brown in color due to the Ki-67 staining.

4.6 Impact of the MSCs on the BCC invasion

Metastasis is a potential reason for death of most cancer patients, which takes place through the events of invasion, intravasation and extravasation in the course of the disease progression. Invasion is an early event of metastasis where the cancer cells lose association with the primary tumor-mass and invade the surrounding stroma[235]. Since the increased Ki-67 is associated with aggressive BCCs and inversely correlated with ER status in BC patients[11], the impact of MCs on MCF-7 invasion in the spheroid co-culture model was investigated.

4.6.1 Optimisation for the concentration of BME (Cultrex) to investigate BCC invasion in the spheroid model

Tumor rigidity due to ECM accumulation[236] and the presence of hyaluronic acid and fibronectin in the ECM plays an essential role in facilitating the invasion of cancer cells[237]. Therefore, choosing the right concentration of BME was essential to observe cancer cell invasion *in vitro*. An optimisation experiment was carried out using the MDA-MB-231 spheroids to determine the concentration of the BME that supports the invasion in the culture. The optimized concentration of the BME was subsequently incorporated in the spheroid co-culture invasion studies to investigate the impact of the mesenchymal cells on the phenotypic changes of the non-invasive BCC, MCF-7 into an invasive cell type. The MDA-MB-231 spheroid monocultures were formed by seeding in a round bottom ULA 96-well plates supplemented with a low gelling BME (100µg/ml) and on day 3, spheroids were transferred to a high gelling BME of different concentrations including 1mg/ml, 2mg/ml and 3mg/ml in serum-free medium. Serum-free media used in this study was RPMI-1640 with 2mM Glutamine but contained no fetal

bovine serum (FBS). The reason for using serum-free media was to exclude any possible FBS-mediated invasion effects that could interfere with BME concentration optimization. Following incorporation of the MDA-MB-231 spheroids in the high gelling BME, images were captured at 24hrs, 48hrs and 72hrs in order to investigate the BME concentration supporting spheroid invasion in a time-dependent manner. The MDA-MB-231 spheroids embedded in 3mg/ml BME showed the presence of the migrated cells from the peripheral region at 72 hours compared to the spheroids embedded in 1mg/ml and 2mg/ml of high gelling Cultrex (Figure 4-11). However, the invasion was completely impaired in spheroids not embedded in the high gelling Cultrex. It can, therefore be said that the presence of ECM is necessary for invasion studies and BME at a concentration of 3mg/ml supported invasion of MDA-MB-231. Hence, 3mg/ml was chosen as the optimised concentration of the BME to investigate the MSC-driven invasion of non-invasive luminal BCC, MCF-7 in the spheroid co-culture.

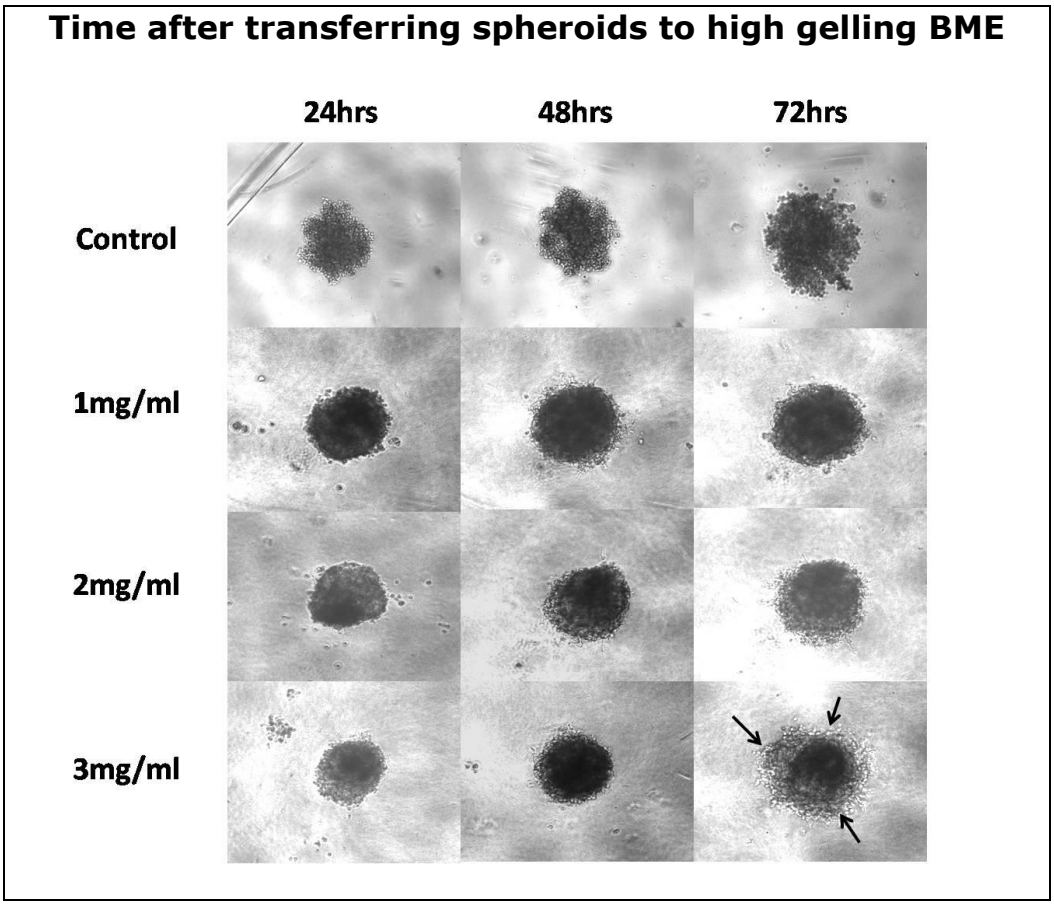

Figure 4-11: Invasion of cancer cells in spheroid model was concentration-dependent of BME: On day3, MDA-MB-231 spheroid monocultures were embedded in the high gelling BME of different concentrations including 1mg/ml, 2mg/ml and 3mg/ml. Images were captured for next 72hrs to observe the dispersion of MDA-MB-231 at the peripheral region of the spheroids embedded at different concentrations of the BME. Arrow heads pointing the migratory cells in the spheroid. In control, spheroids were suspended in the serum-free medium without a supplementation of the high-gelling BME. Images were captured at 4X magnification under brightfield microscope.

4.6.2 The presence of nutrition facilitates cell migration in the invasive BCCs, MDA-MB-231 in the spheroid model

In order to migrate through the ECM in tumor stroma, cancer cells consume huge amounts of energy supplied by ATP (adenosine triphosphate) generated in the course of metabolic process inside mitochondria[238]. Therefore, it was decided to study the MDA-MB-231 invasion in the spheroid in the presence of 10% FBS-supplemented culture media which will be used as a resource of

nutrition for invading cells in the invasion assay. Hence, once the spheroid formed on day 3, spheroids were embedded into the optimised BME concentration (3mg/ml) and images were captured under the microscope over the next 72 hrs, in order to observe cell migration. Strikingly, in the presence of FBS-supplemented media MDA-MB-231 migrated greater distances, resulting in the formation of finger-like projections which were clearly visible under the microscope in the spheroid at 72 hours (Figure 4-12A). In addition, the presence of the serum in the cell culture media supported invadopodia formation in the spheroid at earlier time-points (Figure 4-12A) in contrast to the high gelling BME-embedded spheroids in serum-free media (Figure 4-11). Further, in order to avoid any false interpretation of the invasion due to background-associated artefacts such as a crack in the gel or scratch underneath the wells of the cell culture plate, spheroids on day 7 were stained with a nuclear stain, Hoechst 33342. The presence of the nuclei in the projections of the invaded spheroid confirmed the presence of migrated cells (Figure 4-12B).

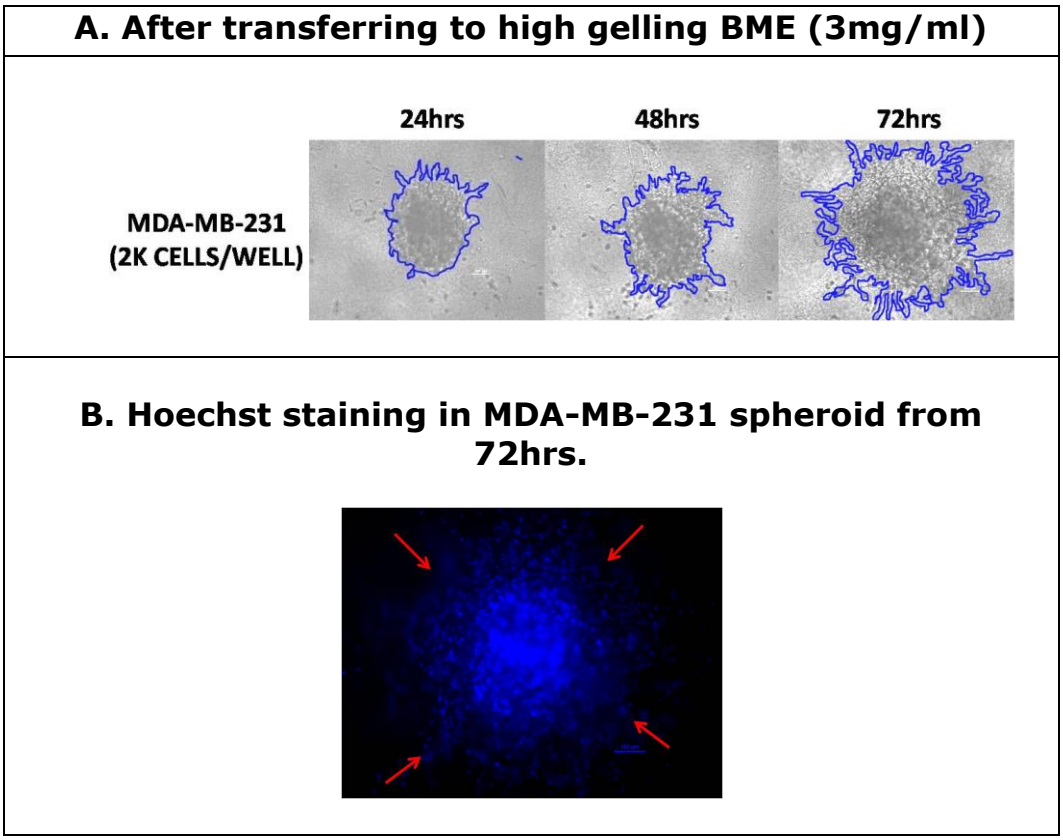

Figure 4-12: Impact of nutrition on invasion: A. On day 3, MDA-MB-231 spheroid monocultures were embedded in the high gelling BME supplemented with the serum containing medium and images were captured under brightfield microscope at 10X magnification. The migrated cells were highlighted by the blue border line drawn in the imageJ. **B.** MDA-MB-231 spheroid monoculture at 72 hours was stained with the nuclear stain Hoechst 33342. Nuclei of the cells in the primary site and migrated cells projecting outside (Red arrow pointed) from the periphery of the spheroid appeared blue. Image was captured under the fluorescent microscope at 10X magnification.

4.7 MSCs support cell migration of the non-invasive BCC, MCF-7 in spheroid co-culture

Since MDA-MB-231 is an invasive BCC line, cell migration is consistent with its invasive nature. On the other hand, MCF-7 is a well-differentiated and poorly metastatic BCC line[239]. The question was therefore asked if MSCs could convert non-invasive BCC to invasive cancer cells in the spheroid co-culture. In response to the question, spheroid co-culture was seeded with MCF-7tdTomato in the presence of MSC-eGFPs. Once the spheroid was formed on day 3, the spheroids were transferred to the high-gelling BME

(3mg/ml) and serum-containing medium was added to the culture to provide nutrition and energy for invading cells, if any. Interestingly, finger-like projections from the peripheral region of spheroid co-culture began after 48hours of embedding in the high gelling BME. However, no such structures were observed in the monoculture embedded in the same way. Image analysis of invasion in the spheroid co-culture demonstrated that the invading cells were red-fluorescent, showing that it is MCF-7tdTomato migrating out of the spheroid (Figure 4-13A). At the same time, a significant increase in the volume demonstrated mesenchymal cell-driven tumor growth in the co-culture (Figure 4-13B). Therefore, it seems that in parallel to inducing cancer cell growth, MSCs induced BC migration in the MCF-7 spheroid co-culture.

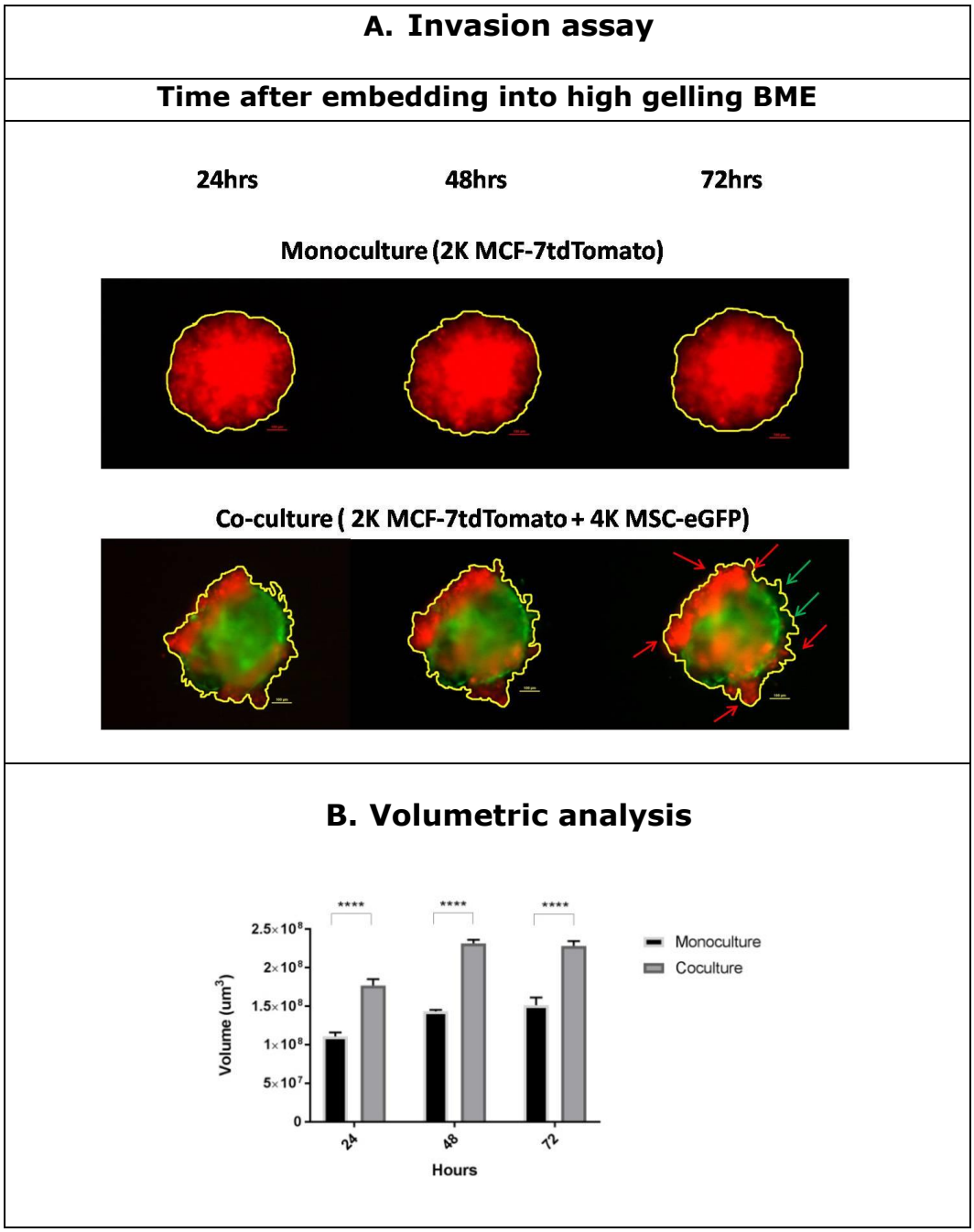

Figure 4-13: MSCs induced invasion in MCF-7 in the spheroid co-culture: A. MCF-7 spheroid monoculture and co-culture on day 3 embedded in high gelling BME and the images were captured at 10X magnification with a fluorescent microscope at different time points. The uneven borderline at the peripheral region in the spheroid co-culture highlighted the migrated cells. Red and green arrows are pointing to the migrated MCF-7 and MSCs in the spheroid co-culture. **B.** Volumetric analysis demonstrated increased tumor growth in MCF-7 spheroid co-culture compared to the monoculture over the course of the study. Volumetric analysis was performed in Prism. **** represents a significant increase in the volume of spheroid co-culture compared to the monoculture at the relevant time-points of the study. The P value is <0.0001 determined by the Two-way ANOVA.

4.8 Summary

- Once the characterisation of the spheroid model was accomplished, the impact of MSCs on BCC proliferation was investigated. The optimal incubation time for luciferin with spheroid cultures was 90 minutes, determined by measuring the RLU at different time-points of incubation of day 7 spheroid with luciferin.

- Luciferase assay demonstrated the decreased proliferation of BCCs in spheroid co-culture compared to the 2D co-culture (Figure 4-2A). Therefore, it was apparent that the role of MSCs altered in the spheroid model. In contrast, the increased spheroid volume (Figure 4-3) and the resulting RFU in the Alamar blue assay (Figure 4-4) highlighted the MSC-driven BCC proliferation in the spheroid co-culture in a time-dependent manner. However, the decreased RFU in the spheroid co-culture at day 7 may be due to poor cell viability (Figure 3-12A).

- In order to ensure the BCC proliferation capacity, CellTrace Violet assay was used as an alternative *in vitro* cell proliferation assay to compare the observations between the Luciferase and Alamar blue assay in the spheroid model. Since the analysis of the CellTrace violet test is carried out in the flow cytometry, the appropriate enzyme and workflow for spheroid digestion have been chosen based on the digestive efficiency, the cell viability followed by spheroid

digestion and the efficacy of single cell suspension generation. Therefore, following digestion of the spheroid mono and co-culture on day 3 and day 5, flow cytometry analysis was performed to investigate the status of the CellTrace violet-positive cells in the cell suspensions from each condition. Over the course of the study, the rapid decrease in the CellTrace violet-positive parental BCC population in the cell suspension from the digested spheroid co-culture comparing to the monoculture demonstrated the positive impact of MSCs on the BCC proliferation. Hence, the inference drawn in the CellTrace violet assay was consistent with the outcome of the Alamar blue assay performed in the spheroid model.

- Further, the paraffin-embedded sections of spheroid microarray of MCF-7 spheroid mono and co-culture were probed with the Ki-67 antibody. Due to the high proliferation capacity in the monoculture determined from the CellTrace Violet assay, MDA-MB-231 spheroid was excluded from the IHC characterisation of Ki-67. The following analysis of the Ki-67-positive cells demonstrated an increased MCF-7 proliferation in the spheroid co-culture in a time-dependent manner (Figure 4-10). Therefore, from the Alamar blue assay, CellTrace Violet assay and Ki-67 characterisation taken together, it was concluded that there is a positive impact of MSCs on BCC proliferation in the spheroid co-culture.

- In parallel to investigating BCC proliferation, invasion-inducing capacity of MSCs in the BCC was also investigated

in the spheroid co-culture. Since MCF-7 is less invasive BCC type; invasion assay was performed in the spheroid co-culture made using MCF-7 and MSCs. MCF-7 spheroid monoculture and co-culture were embedded in the optimised BME concentration which provide a platform for cancer cells to invade the surrounding stroma. In addition, the invasion set up was supplemented with the complete cell culture medium as a source of nutrition required for invading BCC. The migrated MCF-7 from the peripheral region of the spheroid co-culture suggested the acquisition of invasive phenotype in MCF-7 (Figure 4-13).

CHAPTER 5: INVESTIGATING MSC-DRIVEN EPITHELIAL-MESENCHYMAL TRANSFORMATION (EMT) AND THE ASSOCIATED MSC-EXERTED PARACRINE SIGNALLING RESPONSIBLE FOR BCC PROLIFERATION AND INVASION IN CO-CULTURE

The aim of this chapter was to investigate MSC-driven EMT in BCCs and to understand the paracrine signalling associated with BCC proliferation and invasion. Cancer cells undergoing EMT acquire a mesenchymal phenotype and become more invasive in nature[240]. Therefore, in parallel to investigating the morphological alteration in the BCC it was required to FACS-sort the BCCs from the co-culture in order to investigate the alteration in the expression of E-cadherin and vimentin by the Western blot technique to assess MSC-driven EMT in BCC. Along with the investigation of EMT-promoting effect in BCCs, the impact of MSCs on SnON was also investigated. Gene knockdown studies have shown that downregulation of SnON is related to invasion in BCCs[161]; however, the role of the TME in regulation of SnON in BCCs is largely unknown. Therefore, it was attempted to investigate whether MSC-mediated SnON downregulation results in BCC invasion via EMT. Originally, use of a protein microarray was also planned in order to investigate the broader MSC-exerted paracrine signalling responsible for BC progression. Although the role of MSCs in the proliferation and invasion of BCC was previously demonstrated using the standard BCC lines MCF-7 and MDA-MB-231, in this chapter, BC patient-derived xenografts (PDXs) including BR8 and BR15 were also included in the study. The purpose of using PDXs was to extend the data generated using the standard BCC lines and identify potential paracrine signalling

pathways associated with MSC-driven BC progression in a model system which is potentially more relevant to that of patient tumors.

5.1 Alteration in BCC morphology in the 2D co-culture model

Initially, EMT in MCF-7 in co-culture was investigated in a 2D setting. Studies have shown that the reorganisation of F-actin/stress fiber is associated with the morphological changes in the cancer cells undergoing EMT[241]. MCF-7 was therefore stained with the phalloidin to observe the structural changes in mono and co-culture at day 5 of the culture. It was observed that F-actin resided immediately underneath the plasma membrane of MCF-7 in the 2D monoculture and cells were attached with each other in a cluster. Interestingly, in the co-culture, F-actin was reorganised within the MCF-7 cells and decreased cell-cell interaction was observed (Figure 5-1A). In addition, at day 5 co-culture, MCF-7 obtained MDA-MB-231-like phenotype and the distribution of the F-actin in the MCF-7 appeared very similar to the MSCs in the co-culture (Figure 5-1B). Therefore, it seems that the presence of MSCs induced EMT in MCF-7 cells in co-culture.

A. F-actin staining in MCF-7tdTomato in 2D mono and co-culture

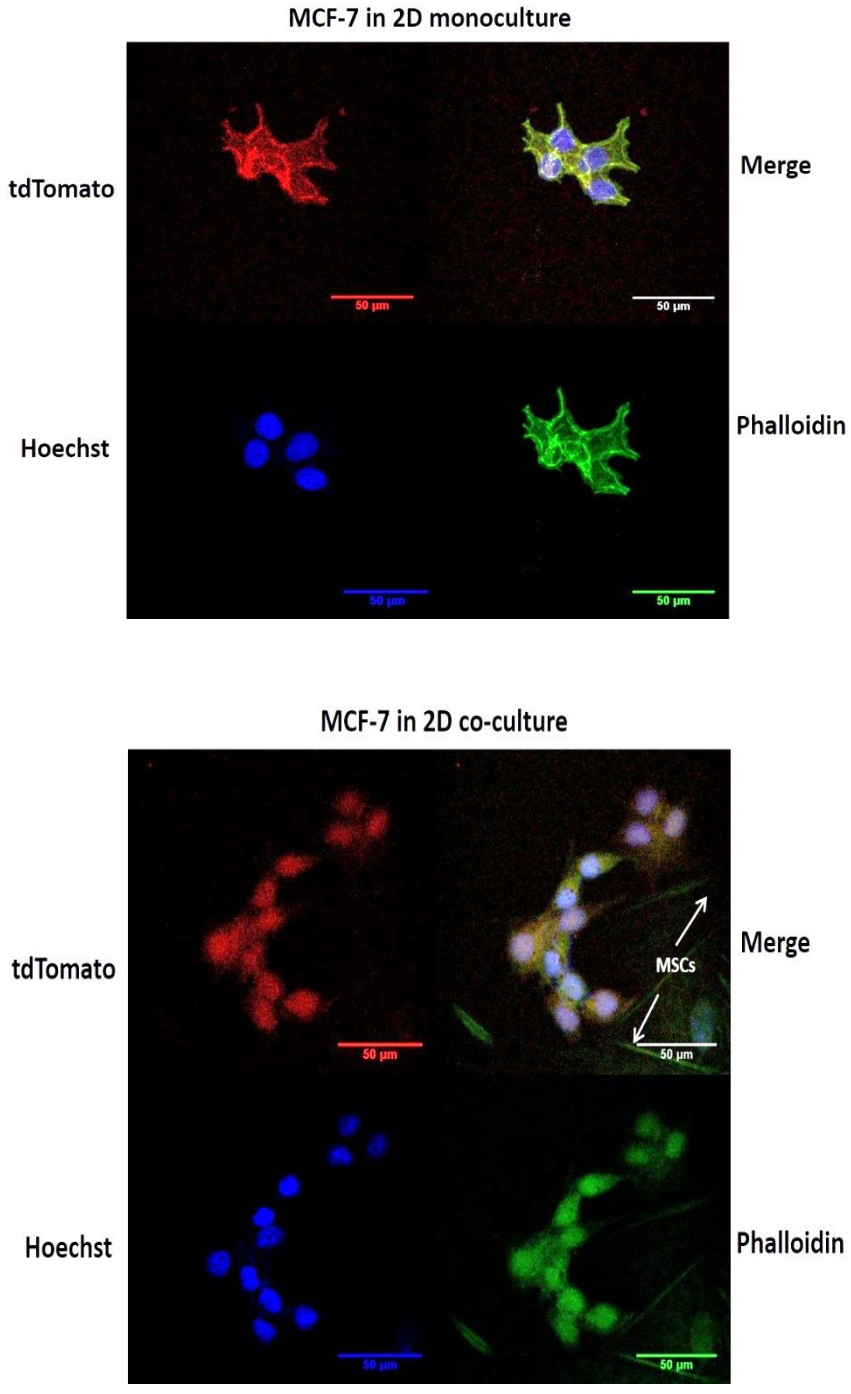

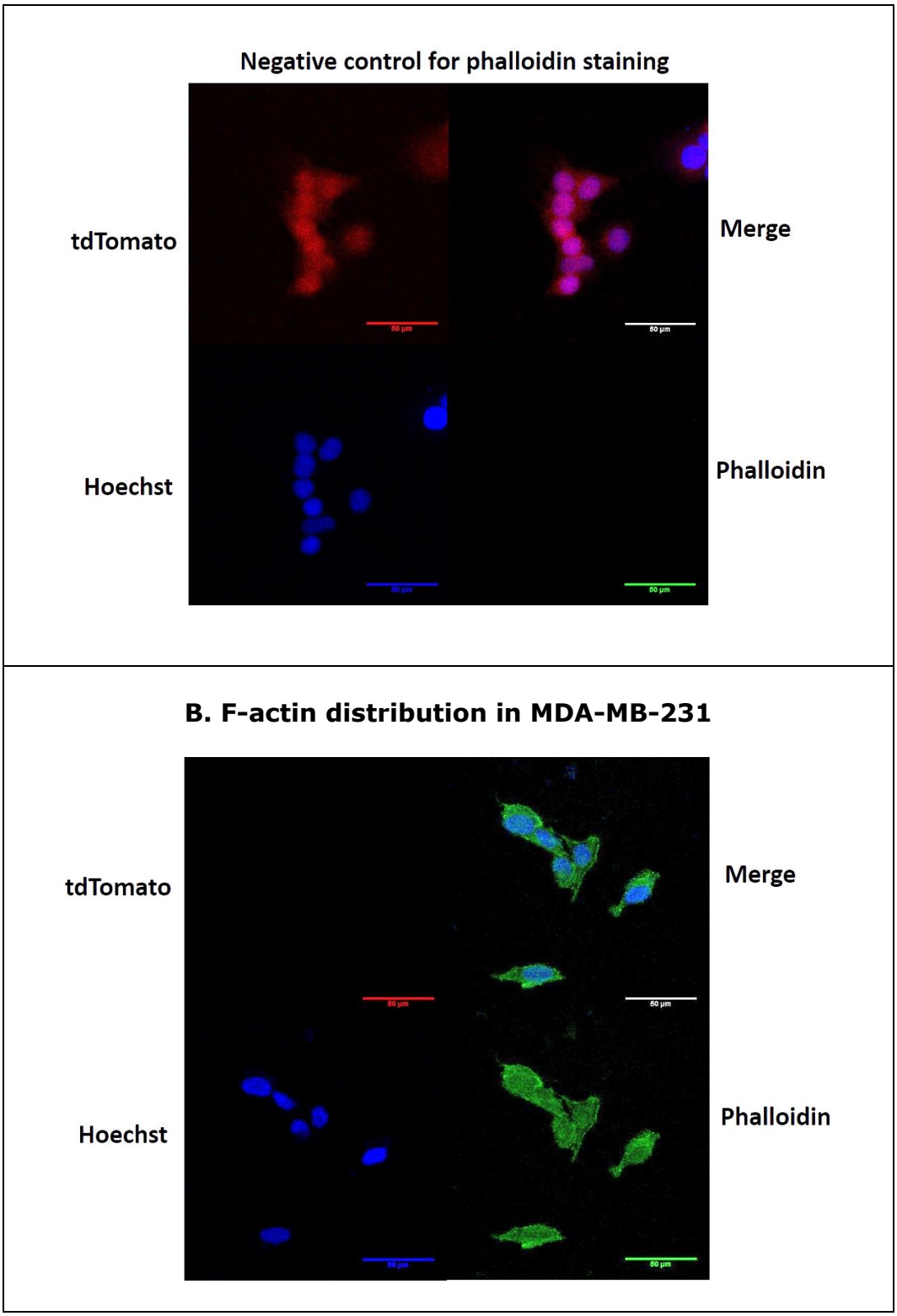

Figure 5-1: Distribution of F-actin in the BCC: A. MCF-7 was seeded with and without MSCs and the images were captured at day 5. The structural changes corresponded to the distribution of F-actin (green) in MCF-7 in the 2D mono and co-culture was investigated. MCF-7 was tagged with tdTomato to identify the BCC in the co-culture. Phalloidin facilitated observation of F-actin

distribution in MSCs along with the MCF-7 in the co-culture. **B.** Phalloidin staining in MDA-MB-231 was performed to observe the arrangement of the F-actin (green) in invasive BCC. A slide of MF-7tdTomato monoculture in the experiment was used as a negative control prepared by using PBS instead of Phalloidin. Images were captured with the assistance of a confocal microscope at 40X magnification.

5.2 Fluorescence-activated cell sorting (FACS) of the BCCs from the 2D co-culture

Since the presence of MSCs in the co-culture induced F-actin rearrangement, morphological alteration and reduced cell-cell interaction in the MCF-7, changes in E-cadherin and vimentin expression in MCF-7 in the 2D co-culture were investigated. Flow cytometry-mediated sorting (FACS) was used to obtain a pure population of MCF-7 from the 2D co-culture and spheroid co-culture. The task was initially complex, however, because the MSCs promote the expression of the mesenchymal surface-marker in BCCs through physical interaction in the co-culture[74]. Thus, if the BCCs underwent EMT in the co-culture, cancer cells may express surface markers similar to the MSCs that may obstruct the FACS-sorting of pure population of BCC from co-culture. Therefore, instead of sorting BCCs based on the presence of a cell surface marker, one of the cells in the co-culture must be labelled with a fluorochrome to FACS-sort the pure population of BCCs followed by the protein extraction in order to investigate the alteration in the expression of E-cadherin and vimentin in the BCCs in the co-culture. Therefore, MSC-eGFP and MCF-7tdTomato were used individually and alternatively for optimisation to select the best method to isolate MCF-7 from the co-culture.

5.2.1 Optimisation for sorting MCF-7 from the GFP-tagged MSCs in a mixed cell population

Initially the strategy chosen was to retrieve a pure population of non-fluorochrome labelled MCF-7 from the eGFP-tagged MSCs (MSC-eGFP) in a mixed cell suspension. However, in an initial analysis of the fluorescence profiles of the two populations of cells, the histogram of the MSC-eGFP showed a heterogeneous cell population with different GFP intensities (Figure 5-2). Across the entire population of MSC-eGFP, the histogram of the low intensity GFP-expressing MSCs overlapped with the histogram (H1) of GFP-negative BCCs, which would obscure the retrieval of the BCCs from a mixed population. Therefore, the high intensity GFP-expressing MSCs residing in H3 were gated, sorted and collected in the MSCM media (Figure 5-2) in order to try to expand them for later experiments. However the number of the FACS-sorted high eGFP-intensity MSCs was less compared to the total population of MSCs, that is 13,271 in H3 (Table 5-1) and, because of instrument-derived bacterial infection, the FACS-sorted MSC-eGFP stopped growing and died within a week before becoming confluent. Hence, the experiment was repeated and the FACS-sorted MSC-eGFP was cultured in antibiotic/antimycotic (Ab/Am) supplemented MSCM media. Although there was no trace of infections detected this time, MSCs still did not expand in the culture.

Hence, treating the MSC-eGFP with puromycin (0.5µg/ml) was used as a next strategy to select for and expand a population of MSCs expressing high levels of eGFP uniformly in the culture. However, the administration of puromycin unfortunately suppressed the growth of MSC-eGFP. Therefore, it seems that the

eGFP-expressing MSCs was not a good choice for this particular application.

Therefore, another alternative strategy was attempted involving using MCF-7s labelled with tdTomato (MCF-7tdTomato) and unlabelled MSCs to sort a pure population of MCF-7 from the co-culture.

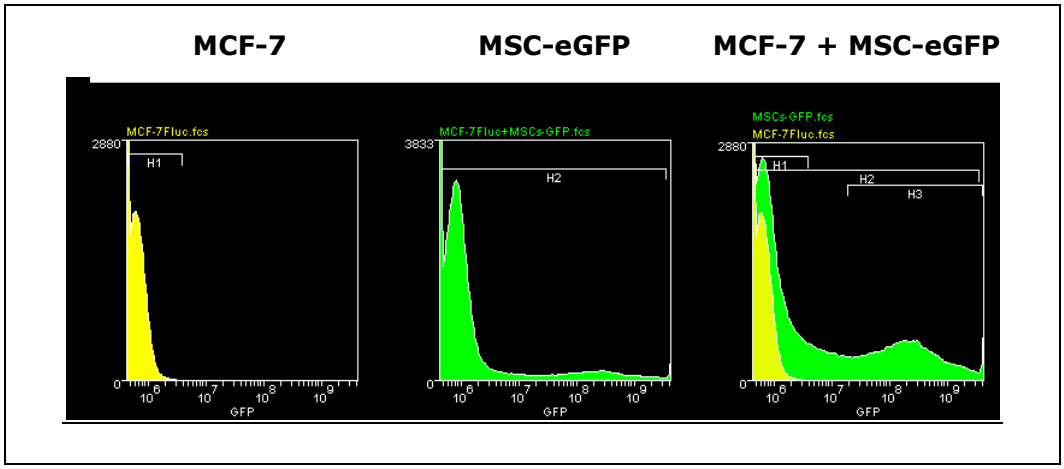

Figure 5-2: Flow cytometry analysis of MCF-7 and MSC-eGFP: Non-labelled MCF-7 was used as a negative control to observe and for analysing the relative intensity and the histogram for GFP expressing MSCs. H1 representing the region of MCF-7-GFP-negative cells in the histogram. H2 represented the entire region of MSCs-GFP, overlapped with the region H1. H3 is the region represented the high GFP-expressing MSCs which was gatedand FACS-sorted.

STATISTICS			
Windows	Cells	%Total	Median
H1	89185	63.05	847034
H2	105415	74.52	969118
H3	13271	9.38	2288929

Table 5-1: The Cell numbers and relative GFP-intensity of MSCs in the selected regions H1, H2 and H3 in the Figure 5-2. Window stats represented the cells in the selected areas in the histograms. Median value in the table represented the relative intensity of GFP of MSCs resided in each region. GFP was excited by the laser beam having the wavelength of 488nm and the emission wavelegth was detected in the 513/26 bandpass filter. The analysis was performed with the assistance of Beckman Coulter Astrios EQ cell sorter.

5.2.2 Optimisation for FACS-sorting the MCF-7tdTomato from the MSCs in a mix population of cells

In order to assess whether a pure population of BCC could be sorted from the MSCs in co-culture using this new strategy, MCF-7tdTomato was analysed in the presence or absence of non-labelled MSCs. The flow cytometry analysis of the MCF-7tdTomato demonstrated a heterogeneous cell population with a varying expression level of the td-Tomato. Therefore, in order to investigate the difference of fluorescence intensity between the MSCs and MCF-7tdTomato, the FACS analysis was performed in a cell suspension constituted of MCF-7tdTomato mixed with the MSCs. The FACS analysis showed a distinct region, H1 in the histogram, residing 7866 MCF-7 with the highest spectral intensity of tdTomato (Figure 5-3A). As the number of the cells in the H1 region was only around 9% (Table 5-2) of the total cell population, there was a high chance of losing large population of MCF-7tdTomato on FACS sorting in the co-culture. Hence, in order to increase the yield of MCF-7 on sorting in the co-culture, MCF-7tdTomato resided in the H1 region was gated, and FACS-sorted. The FACS-sorted cells were collected in the Ab/Am-supplemented complete RPMI-1640 medium and expanded in a monolayer (Figure 5-3B) to make the cell stock and for using in the co-culture.

A. Flow cytometry analysis of MCF-7tdTomato

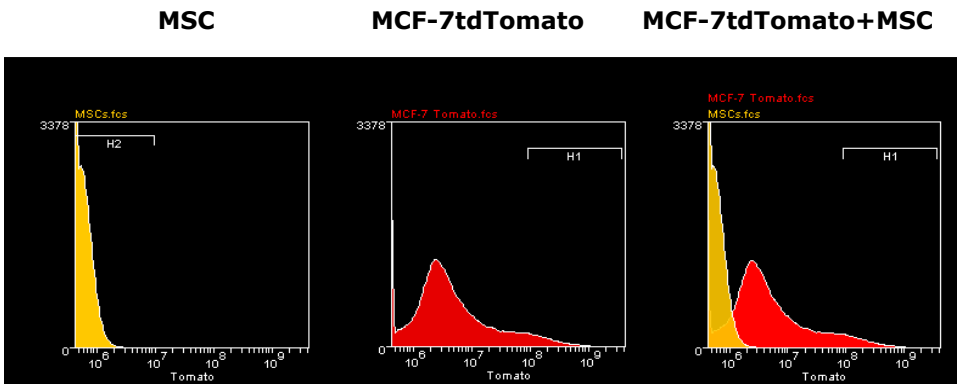

B. Sorting and expanding of high intensity tdTomato expressing MCF-7

Expanded sorted MCF-7tdTomato

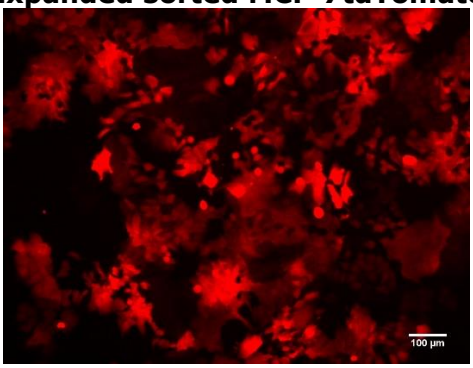

Figure 5-3: FACS sorting and expanding the MCF-7tdTomato: A. H1 in the histogram represented the region for the high intensity td-Tomato expressing MCF-7 cells. **B.** Cells from H1 were gated, FACS-sorted and allowed to expand in the culture. Sorted MCF-7tdTomato was expanded succesfully in monolayer in 24-well cell culture plate.

STATISTICS			
Windows	Cells	%Total	Median
H1	7866	8.67	2209792

Table 5-2: The cell numbers and the relative intensity of the MCF-7tdTomato in the selected region H1 in the Figure 5-3. Window stats demonstrated the cells in the selected areas in the histogram. Median values represented the spectral intensity of tdTomato positive MCF-7. tdTomato was excited by the laser beam having the wavelength of 561nm and the emission wavelegth was detected in the 579/16 bandpass filter. The analysis of the tdTomato-positive cells was performed by the Beckman Coulter Astrios EQ cell sorter.

5.2.3 Flow cytometry analysis of sorted MCF-7tdTomato in a mixed population of cells

Once the sorted MCF-7tdTomato became confluent in the monolayer, cells were re-analysed in the presence or absence of the td-Tomato negative MSCs. The FACS analysis demonstrated the presence of the two distinct populations of two cell types, MSCs and MCF-7tdTomato, in the mixed-cell suspension. The FACS analysis demonstrated an increased MCF-7tdTomato population in the H1 region of the histogram (Figure 5-4). In addition, the statistical analysis showed that using expanded sorted-MCF-7tdTomato in a co-culture can increase the yield of MCF-7 by almost 9 fold (Table 5-3) on FACS-sorting in respect to the previous analysis (Table 5-2). Although the yield was increased, the histogram highlighted the presence of a population of lesser strength tdTomato expressing MCF-7 in the region (H2) of td-Tomato negative MSCs. Although the overlapping of the low intensity tdTomato expressing MCF-7 with the MSCs may still obscure the retrieval of the entire BCCs from the co-culture, a reasonable cell yield could be obtained in this way.

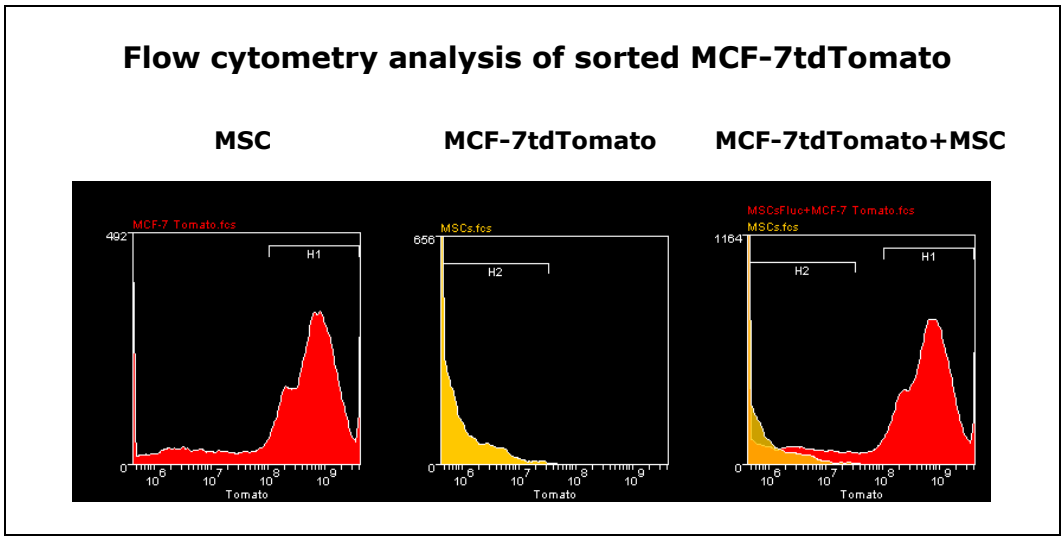

Figure 5-4: Flow cytometry-based analysis of the fluorescence intensity of the expanded MCF-7tdTomato in the mixed cell population of MCF-7tdTomato and MSCs: FACS-sorted high td-Tomato expressing MCF-7 were analysed in the presence or absence of the tdTomato-negative MSCs. H1 is the region for the high tdTomato expressing MCF-7. However, a few of the td-Tomato expressing MCF-7 cells seems lose their intensity and merged with the td-Tomato negative MSCs in the region H2.

STATISTICS			
Windows	Cells	%Total	Median
H1	18701	75.58	6360850

Table 5-3: Cell numbers and relative td-Tomato intensity of sorted high intensity td-Tomato positive MCF-7 cells in the selected region H1.

5.3 Mesenchymal cells downregulate the expression of E-cadherin and increased Vimentin expression in MCF-7 in the co-culture

The downregulation of E-cadherin and upregulation of Vimentin is the hallmark of the cells undergoing EMT and invasion[242]. Morphological alteration and F-actin distribution in MCF-7 cells in the 2D co-culture demonstrated phenotypic switch in MCF-7. Hence, in order to investigate the EMT in MCF-7tdTomato cells in the 2D co-culture, following sorting they would be subjected to protein extraction and Western Blotting to investigate the expression alteration of E-cadherin and vimentin in MCF-7 in the co-culture.

5.3.1 Sorting of MCF-7tdTomato from the 2D co-culture

Since the mono and co-culture were performed in 96 well culture plates, further optimisation was required to ensure the least number of wells in the culture plate to harvest the cells for FACS sorting the pure population of BCCs for preparing the protein lysates. Therefore, 2D monoculture and co-culture were established using MCF-7tdTomato without or with MSCs. On day 3, co-cultures were harvested from 12, 24, 48 and 80 wells of the cell culture plate and the pure population of MCF-7tdTomato was FACS-sorted. It was noted that sorting cells from 48 wells onwards provide sufficient numbers of MCF-7tdTomato from the co-culture in order to achieve good amount of protein for the Western blot analysis.

A. Flow cytometry-mediated sorting of MCF-7tdTomato from 2D co-culture

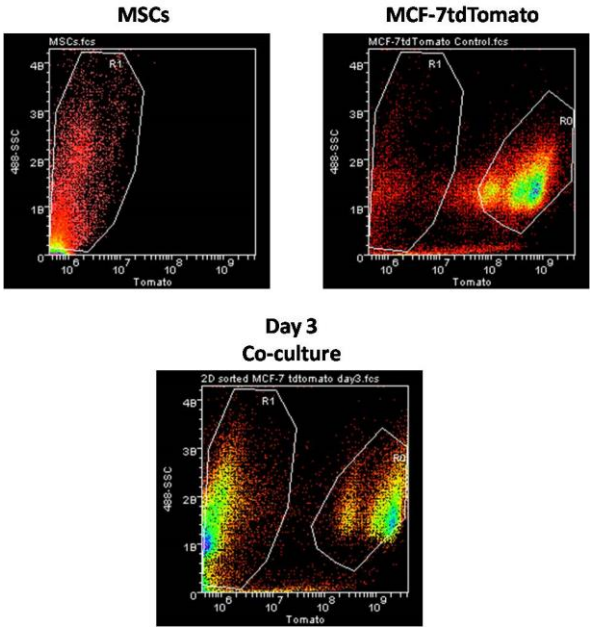

B. Numbers of wells selected for sorting

MCF-7dTomato sorted from 12 wells into 96-well plate

Gate	cells
0:R0	10511

MCF-7dTomato sorted from 24 wells into 96-well plate

Gate	cells
0:R0	12155

MCF-7dTomato sorted from 48 wells into 96-well plate

Gate	cells
0:R0	329343

MCF-7dTomato sorted from 80 wells into 96-well plate

Gate	cells
0:R0	690041

Figure 5-5: Optimisation for selecting minimum numbers of wells in the 96 well cell culture plates to achieve prudent numbers of MCF-7tdTomato cells on sorting: A. tdTomato-labelled MCF-7s were seeded for 2D mono and co-cultures with MSCs. Cells were harvested at day 3 and MCF-7tdTomato was sorted from the co-culture. R0 in the dot plot represented the sorting-region for pure population of MCF-7tdTomato. **B.** MCF-7tdTomato was sorted from the 2D co-cultures harvested from different numbers of wells at 96-well plate to investigate the yield of sorted cells.

5.3.2 Optimisation of protein extraction by comparing Standard protein extraction with Snap freezing or Sonication

Next, in order to achieve a higher yield of protein from the sorted cells, a pilot study was performed using 300K MCF-7 using standard approach[75], snap-freezing protocol[243] and sonication method[244]. In this study it was demonstrated that the Snap-freezing approach significantly increased ($P<0.05$) the yield of protein compared to the standard protein extraction procedure (Figure 5-6A). On the other hand, the Snap-freezing showed an insignificant increase in protein yield in the low number of cells (30,000 cells) compared with sonication, but both Snap-freezing and sonication provided similar amounts of protein from 300,000 cells (Figure 5-6B). Further, in order to confirm the quality of extracted protein using the snap freezing and sonication, protein was separated in SDS-PAGE gel, transferred onto the PVDF membrane and probed for alpha-tubulin. Staining of the protein-smear in the gel with Coomassie blue confirmed successful running of protein in the gel (Figure 5-6C). The bands of alpha-tubulin on the PVDF membrane ensured proper transfer of protein from the gel to the membrane, good quality of protein lysates and identified alpha-tubulin as an acceptable control for the Western blot (Figure 5-6D).

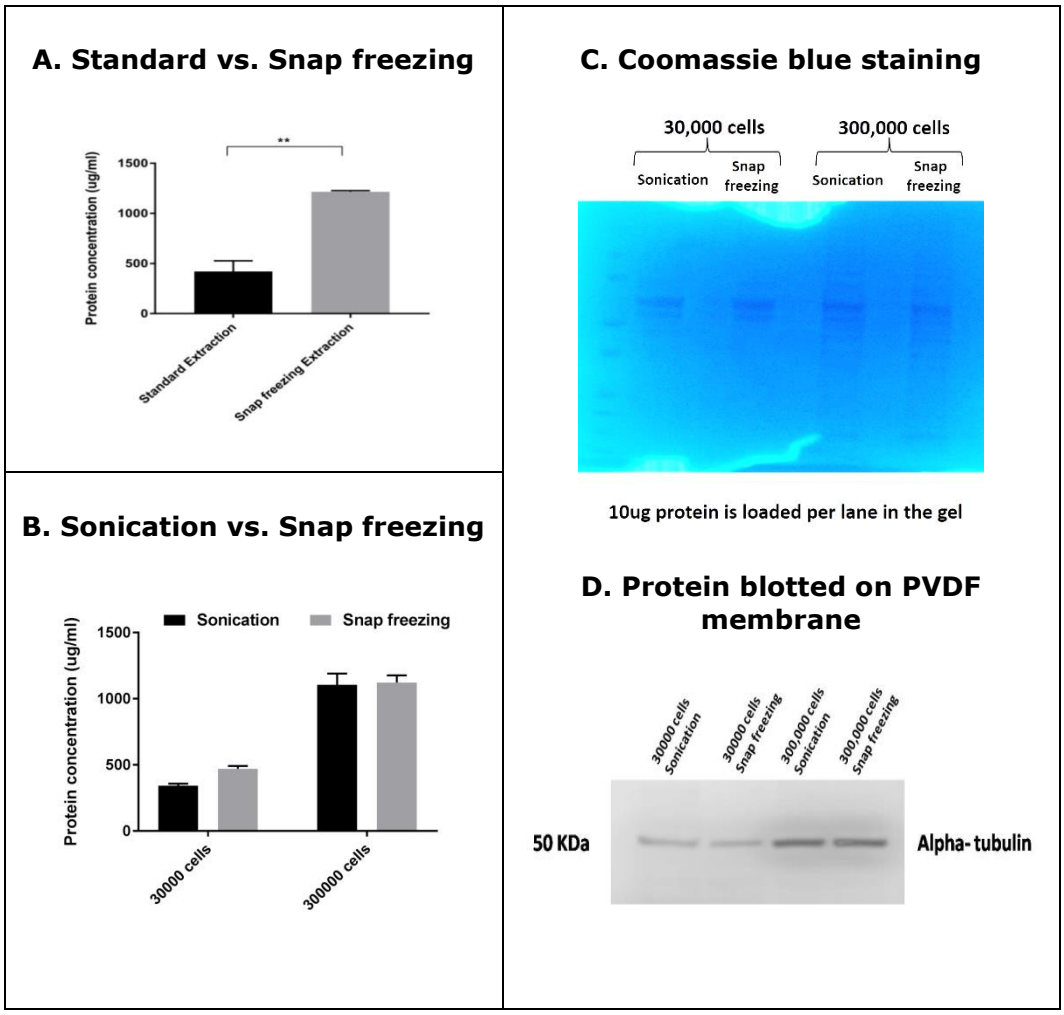

Figure 5-6: Optimisation of protein extraction from MCF-7 by different approaches: A. The Snap freezing procedure allowed significant ($P<0.05$) increased protein yield from the cells in 2D cell culture in compare to the standard protein extraction. ** represented the significance of the study determined by the unpaired t-test in Prism. **B.** Since the sonication process used in the protein extraction in some studies, the efficiency of snap-freezing and sonication was compared using different cell number. 30,000 and 300,000 cells were subjected to the snap freezing and sonication for protein extraction. Bar graphs demonstrated the protein yield from the given cell numbers. Later, the protein lysates were separated on SDS-PAGE gels. **C.** Coomassie blue staining detected the presence of protein smear in the SDS-PAGE gel. D. Appearance of alpha-tubulin bands on probing the PVDF membrane with the alpha-tubulin antibody.

Although the sonication and snap-freezing demonstrated similar efficiency in preparing the protein lysates, snap-freezing approach was applied throughout the study in order to avoid the risk of protein degradation due to the heat generated in the sonication[244].

In order to assess the quality of the protein lysates prepared by the snap-freezing from the MCF-7 tdTomato, lysates were run in the SDS-PAGE and transferred to the PVDF membrane to probe with alpha-tubulin antibody. Although the bands of alpha-tubulin appeared in the lysates prepared from the 2D monoculture, 2D co-culture and spheroid monoculture, none was detected in the lysates of MCF-7tdTomato sorted from the spheroid co-culture (Figure 5-7). Hence, to ensure the presence of protein in the lysates the gel was stained with Coomassie blue. Strikingly, staining of the gel demonstrated the presence of protein smear in the lysates of MCF-7tdTomato from each condition. However, the protein smear in the last track appeared fainter and displayed small number of particularly prominent bands. Since the reason for such disparity was not well understood, the Western blot analysis was performed only in the 2D monolayer model in order to investigate the MSC-driven expression of EMT markers in the BCC.

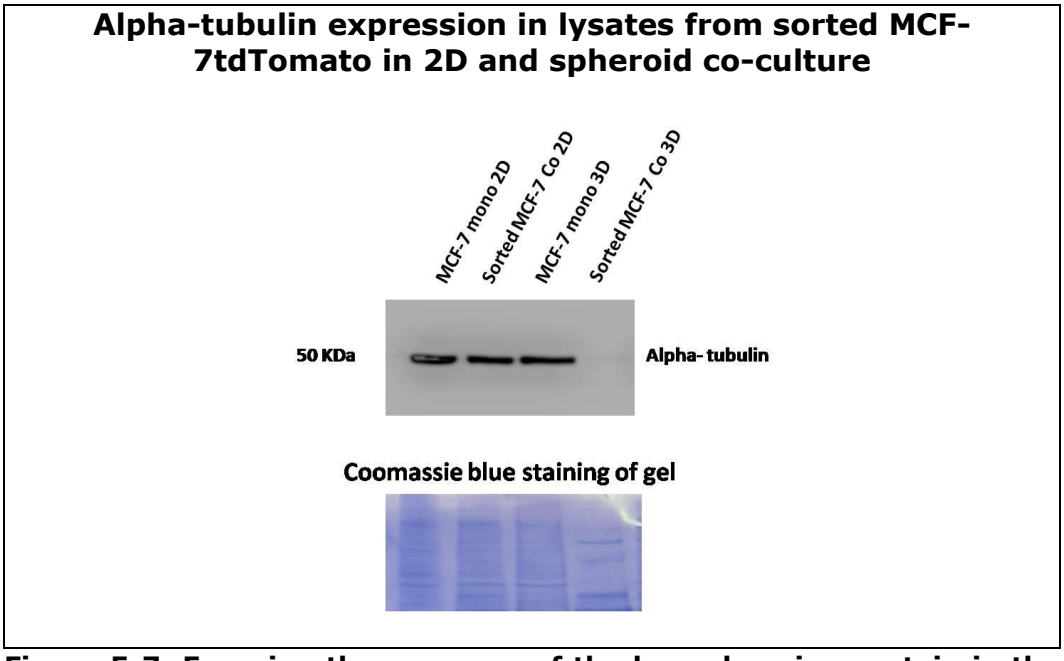

Figure 5-7: Ensuring the presence of the housekeeping protein in the lysates from the sorted MCF-7tdTomato: Lysates from the 2D and spheroid

mono and co-cultures were prepared, separated in SDS-PAGE and probed with alpha-tubulin after transferring on PVDF membrane. Coomassie blue staining highlighted the presence of protein in each lane of the gel.

5.3.3 Investigating the expression of the EMT markers in MCF-7 in the presence of the MSCs in the 2D co-culture

E-cadherin is a protein which resides in the plasma membrane of MCF-7 and is responsible for cell-cell interactions[245]. The presence of E-cadherin is characteristic of non-invasive tumor cells. Therefore, the downregulation in the expression of E-cadherin in the sorted MCF-7 reflected the loss of epithelial characteristics in the MCF-7 in co-culture (Figure 5-8A). On the other hand, the expression of vimentin increased in the MCF-7 retrieved from the 2D co-culture (Figure 5-8A). In adult tissue, vimentin, a type 3 intermediate filament, is generally expressed in the cells of mesenchymal origin and in cancer cells undergoing EMT[246]. Therefore, the increased expression of vimentin in the MCF-7 in the 2D co-culture highlighted the acquisition of the mesenchymal feature in the non-invasive BCC, MCF-7. Hence, these expression-alternations of the E-cadherin and vimentin in MCF-7 suggest MSC-driven EMT in MCF-7 cells in 2D co-culture.

A. Western blot analysis of E-cadherin and vimentin in MCF-7 in the 2D model

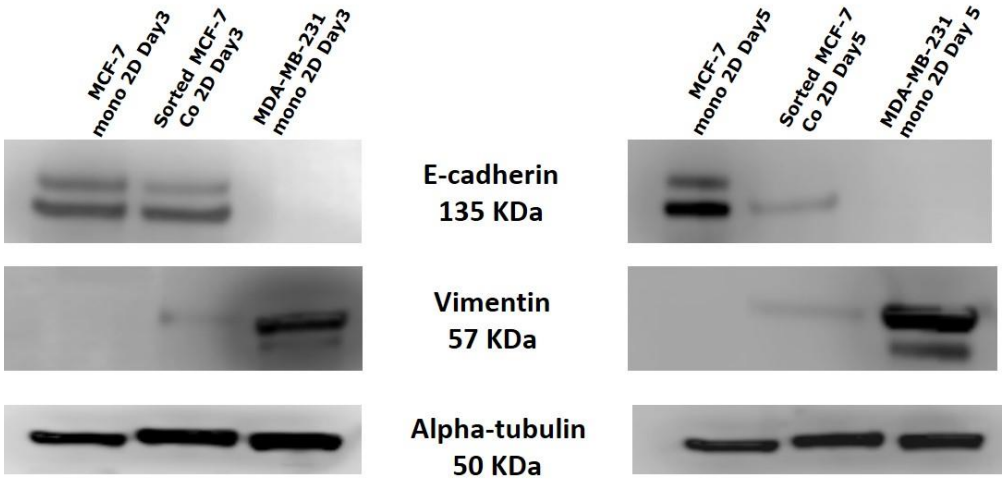

B. Statistics for E-cadherin and vimentin expression

E-cadherin

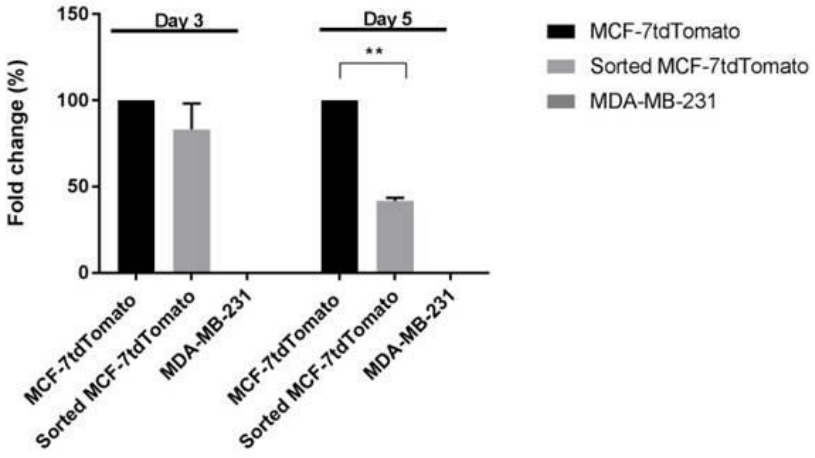

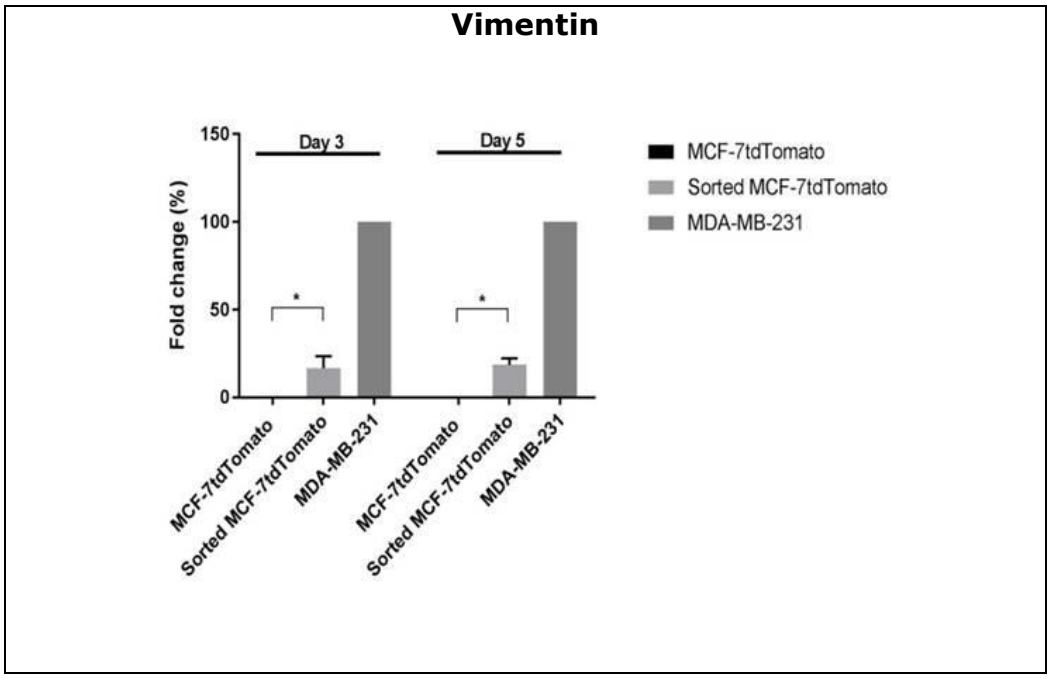

Figure 5-8: MSC-mediated alteration in the expression of E-cadherin and vimentin in MCF-7 in the 2D co-culture: A. On day 3 and 5 of the 2D culture, protein lysates were prepared from MCF-7tdTomato.Next, the lysates were run on SDS-PAGE and then the separated protein in the SDS-PAGE was transferred on PVDF membrane to probe with the antibodies to investigate the alteration in the expression of E-cadherin and vimentin. The protein lysate from MDA-MB-231 was used as a negative control for E-cadherin and positive control for vimentin. **B.** Generated data for E-cadherin and vimentin expression were analysed using Two-way ANOVA in Prism.** and * represented the significance of the study having the P values 0.0016 and 0.0130 at 95% confidence interval.

5.4 Expression of the E-cadherin and vimentin in non-invasive BCC, MCF-7 in the spheroid monoculture and co-culture

Since the housekeeping gene did not appear in the lysates of FACS-sorted MCF-7 from the spheroid co-culture, the expression of E-cadherin and vimentin in spheroids was investigated by performing immunohistochemistry in paraffin-embedded spheroid microarray. Consistent with 2D co-culture, an overall downregulation of E-cadherin in spheroid co-culture compared with its monoculture (Figure 5-9A) was observed. Since the statistical analysis compared the total E-cadherin expression in MCF-7 between the spheroid monoculture and co-culture while the

absolute number of MCF-7 in the co-culture is unknown, direct comparison of the expression alteration in E-cadherin in the spheroid seems not to be accurate. However, high magnification of the spheroid co-culture demonstrated faint staining for E-cadherin in a few populations of cancer cells at the edge of the spheroid. On the other hand, the cancer cells in the core completely lost the expression of E-cadherin (Figure 5-9B). Therefore, it seems that the heterogeneity in terms of the E-cadherin expression in the BCC correlates with the distance between the cancer cells and MSCs in co-culture.

A. IHC for E-cadherin in spheroid model

E-cadherin staining

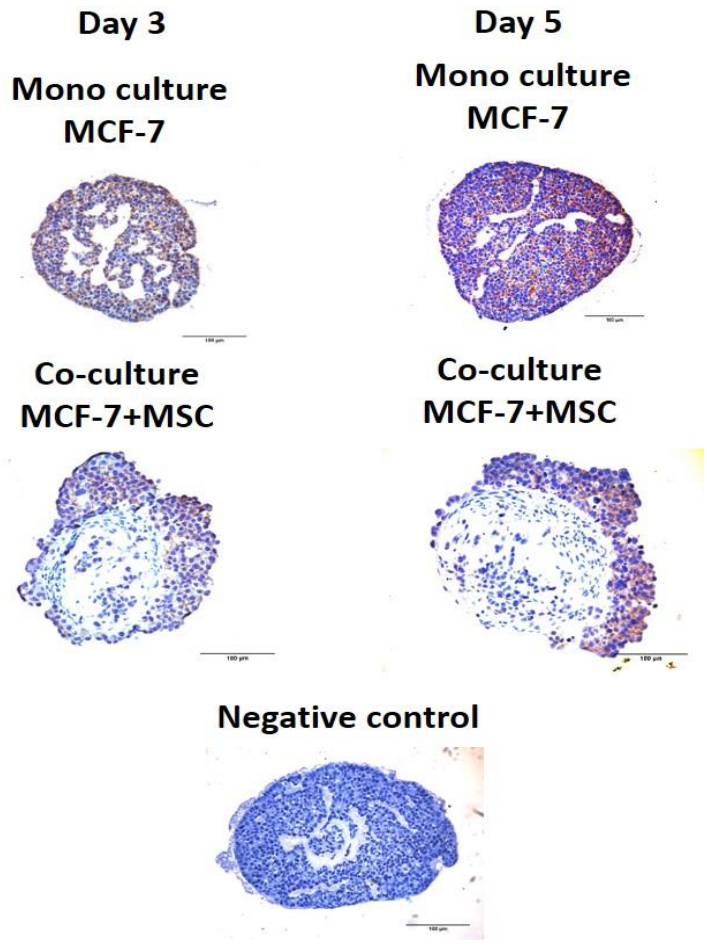

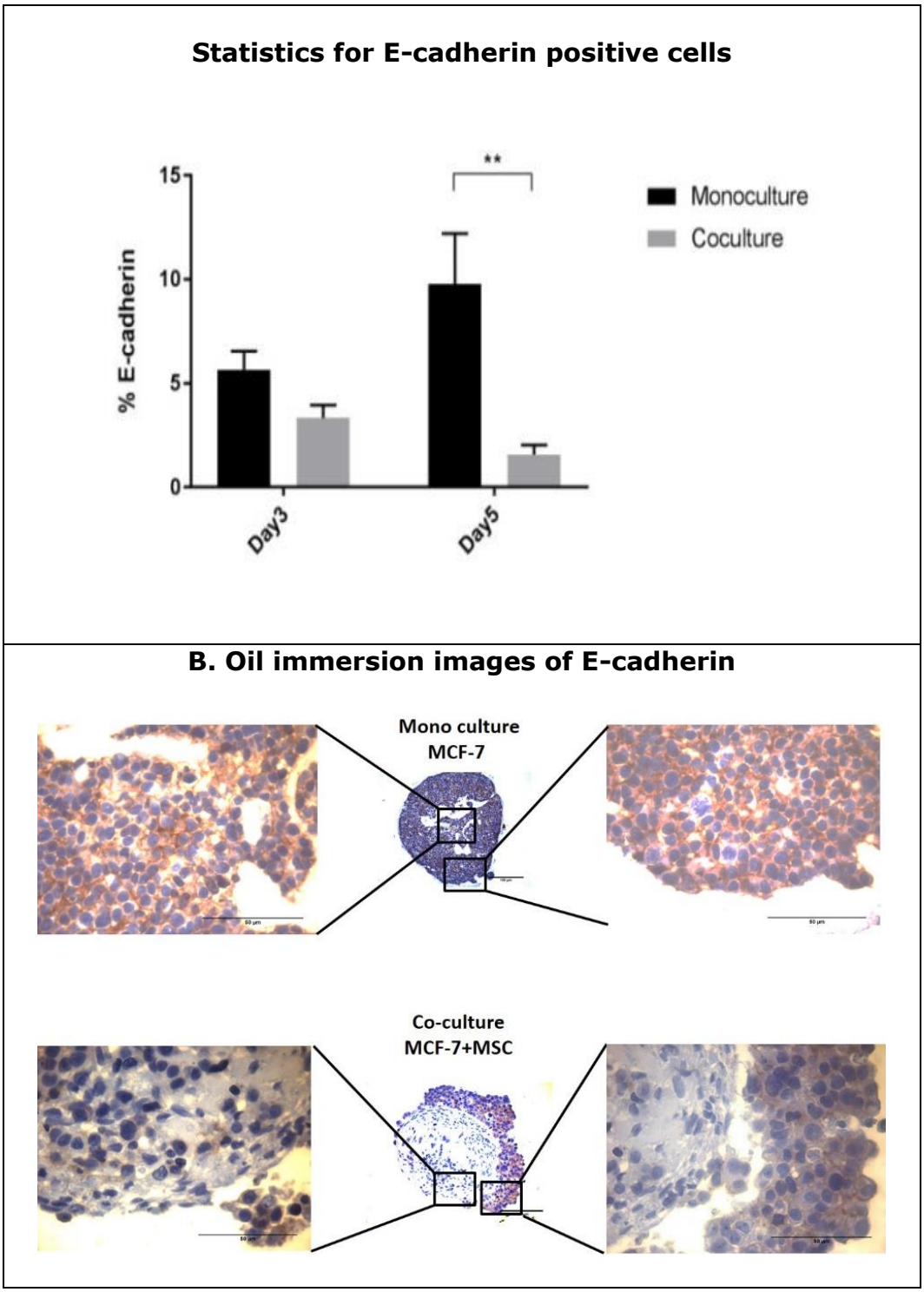

Figure 5-9: Immunostaining of E-cadherin in the paraffin-embedded spheroid microarray: A. IHC for E-cadherin was performed using 5um sections of paraffin-embedded array of spheroid mono and co-cultures. Statistical analysis was performed in order to investigate the percentage of DAB positive cells in the spheroids on day 3 and 5. While the absence of signal in MCF-7 monoculture used as a negative control probed with Mouse IgG1 demonstrated specificity of secondary antibody towards primary antibody in

positive-stained tissue. The significant of the study was performed using Two-way ANOVA in Prism. ** represented the P value 0.0021. **B.** High power images of the spheroid monoculture and co-culture were captured at 60x magnification with oil immersion under the Leica DFC480 microscope.

On the other hand, although an increased expression of vimentin was observed in the core, no trace of vimentin was observed in the cancer cells outside the core of spheroid in co-culture (Figure 5-10A). Since MSCs express vimentin[246] and occupy the core in spheroid co-culture (Figure 3-6) it seems that the increased expression of vimentin in the spheroid co-culture may be from the MSCs residing in the core of the spheroid co-culture. Therefore, in order to determine whether the vimentin positive cells are MSCs or MCF-7 in the spheroid co-culture, high magnification images were captured (Figure 5-10B). Since the high power images of the spheroid co-culture were not useful enough to differentiate between the cancer cells and MSCs; H&E staining was performed on consecutive sections of the spheroid microarray. The nuclei of the cancer cells in the peripheral region were circular but the cell nuclei in the spheroid core appeared more oval and elongated. Since the MSC-GFP decreased (Figure 3-12C) and the vimentin expression increased over time in the co-culture; it seems that the vimentin positive cells in the core are the cancer cells. However, in order to differentiate between the cancer cells and MSCs in the spheroid core, IHC staining for MSC-eGFP and *in situ* hybridization for luciferase-labelled MSCs are required.

A. IHC for vimentin in spheroid model

Vimentin

Day 3

Mono culture
MCF-7

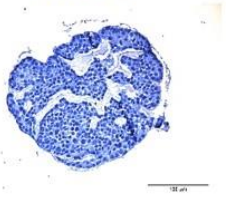

Day 5

Mono culture
MCF-7

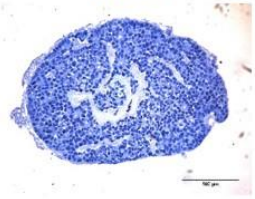

Co-culture
MCF-7+MSC

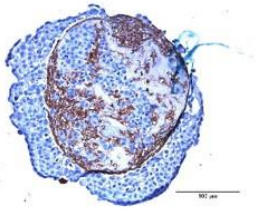

Co-culture
MCF-7+MSC

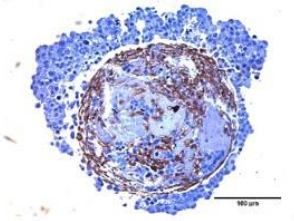

Negative control

Co-culture
MCF-7+MSC

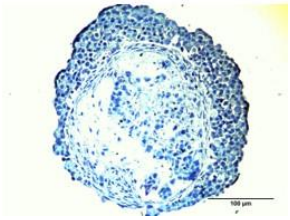

Statistics for vimentin positive cells

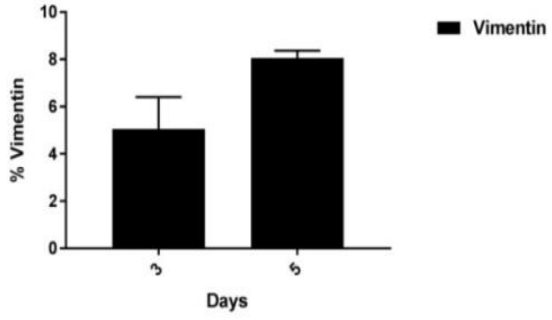

B. Oil immersion images of spheroid

IHC staining in the spheroid co-culture

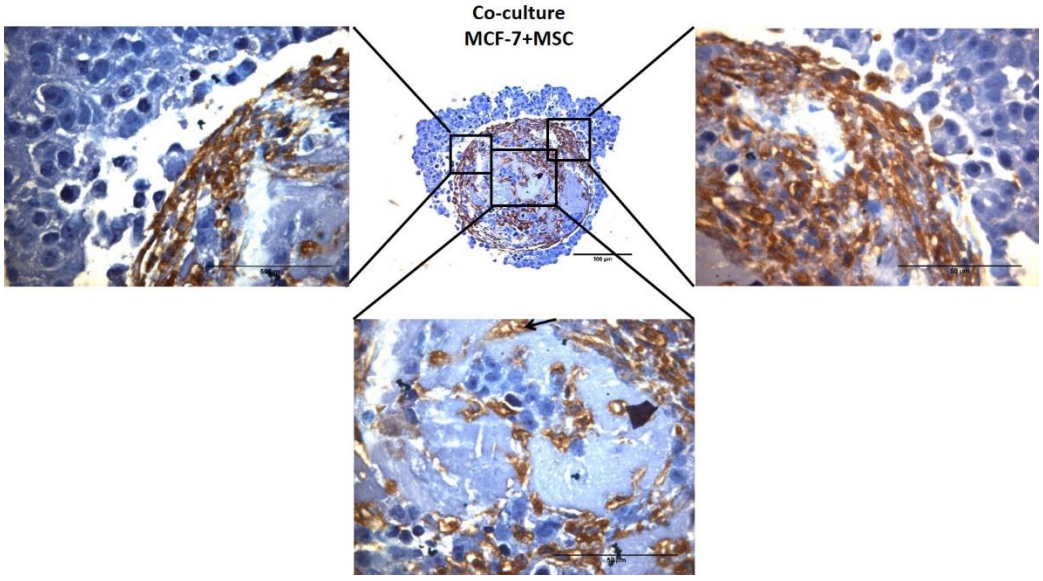

H&E staining in the spheroid co-culture

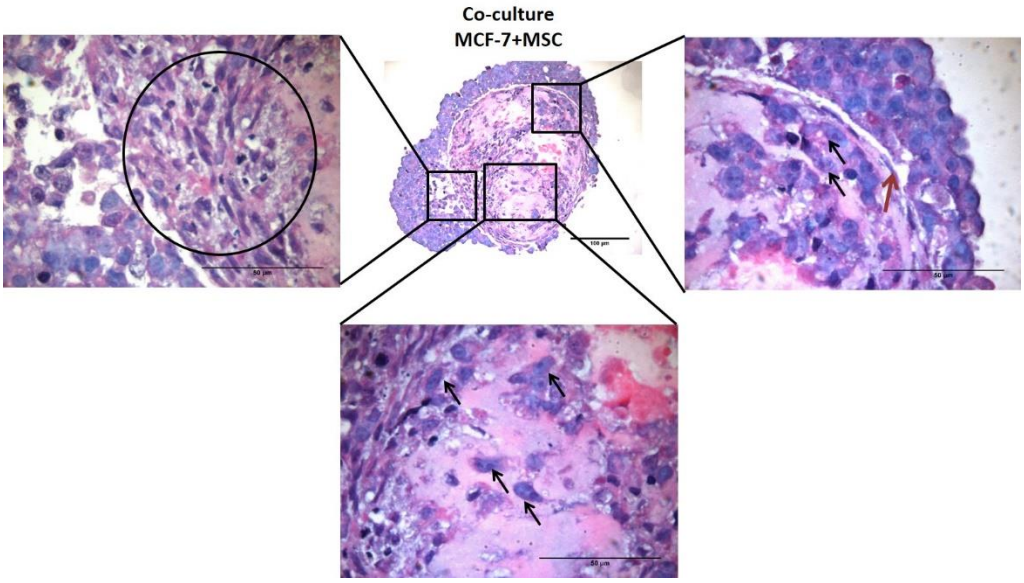

Figure 5-10: Immunostaining of vimentin in paraffin-embedded spheroid block: A. IHC for vimentin was performed using 5µm sections of paraffin-embedded array block of spheroid mono and co-cultures. In negative control, absence of signal in co-culture probed with Mouse IgG1 demonstrated specific binding of secondary antibody towards primary antibody in vimentin-positive samples. Statistical analysis was performed in order to investigate the

percentage of DAB positive cells in the spheroids on day 3 and 5. **B.** High power images of the spheroid co-culture were captured at 60x magnification with oil immersion under the Leica DFC480 microscope. Black arrows indicated the nuclei of BCCs. The nuclei of the MSCs were pointed by brown arrow in the high power field of the sections stained with H&E. Cells in the circle represented the presence of the mixed-cell population and technically challenging in order to differentiate between the cancer cells and MSCs.

5.5 Mesenchymal stem cells downregulated the expression of SnON in 2D co-culture

SnON (also known as Skil) acts as a negative regulator of the TGF-β signalling axis, by repressing the activity of Smad proteins. Previous studies showed that knockdown of SnON increased cell motility, increased extracellular matrix production, reduced cell-cell interactions and enhanced TGF-β-induced EMT in breast and lung cancer cells[161]. In the same study, researchers also demonstrated that the knockdown of SnON reduced tumor growth in breast and lung cancer *in vivo* models. Hence, it seems that the alteration in SnON expression is associated with EMT and tumor growth in BCCs. Although, the shRNA-mediated knockdown studies helped in understanding the role of SnON in EMT, very little is known about the TME-driven alteration of SnON expression in BCCs.

Since MSC-induced alteration in morphology and EMT markers (E-cadherin and vimentin) had been observed in MCF-7s in the 2D co-culture, the expression of SnON was investigated in that model. Interestingly, the Western blot analysis of the lysates of MCF-7 from the 2D mono and co-culture demonstrated decreased expression of SnON in the FACS-sorted MCF-7 in the 2D co-culture compared with the monoculture, and, overall lower SnON expression was observed in the invasive BCC, MDA-MB-231, than in MCF7s. Therefore, it seems that there was an association

between the downregulation of SnON and an invasive phenotype governed by the MSCs in BCCs.

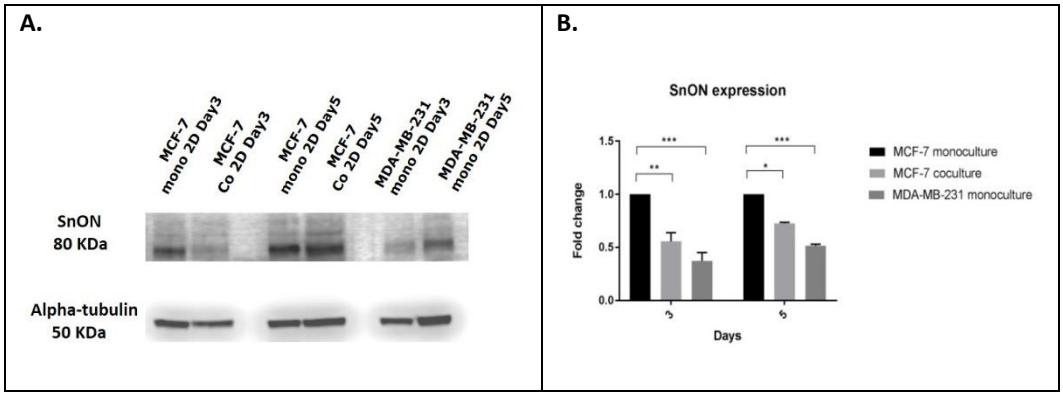

Figure 5-11: MCs influence the expression of SnON in MCF-7 in the 2D co-culture: A. The expression of the SnON was investigated in MCF-7 in the 2D monolayer at day 3 and day 5. The protein lysates of MDA-MB-231 in the 2D monoculture was included to investigate the expression of SnON in the invasive BCC. **B.** Intensities of each band from different conditions were measured by ImageJ and the generated data were normalized against the intensity of alpha-tubulin. Normalised data were plotted and the significance of the study was analysed by using the Two-way ANOVA in the Prism.*, ** and *** represented the P values 0.0172, 0.0015, 0.0002 at the 95% confidence interval.

5.6 Cytoplasmic shift of SnON in MCF-7 spheroid co-cultures

SnON is mainly a nuclear protein but becomes more cytoplasmic in ER/PR negative grade III ductal breast tumors with high expression of Ki67 and HER2 amplification[247], representing a more aggressive subtype of BC[9]. Since the MSCs increased the expression of Ki-67 and invasion in MCF-7 cells, IHC for SnON expression was performed in spheroids. The IHC revealed nuclear localisation of SnON in MCF-7 in the spheroid monoculture. On the other hand, in the spheroid co-culture on day 3 the cytoplasmic localisation of SnON in MCF-7 imitated the location of SnON observed in high-grade breast tumor in patients. However, on day 5 spheroid co-culture, the intensity of SnON decreased in MCF-7. Since SnON was weakly stained in the spheroid monoculture of

invasive BCC, MDA-MB-231, possibly the MSC-driven alteration in the SnON expression may be an underlying mechanism responsible for MCF-7 invasion in the spheroid co-culture. However, further invasion assay in the spheroid culture of SnON-knockdown MCF-7 is required in order to understand the link between the SnON and invasion in the ductal carcinoma.

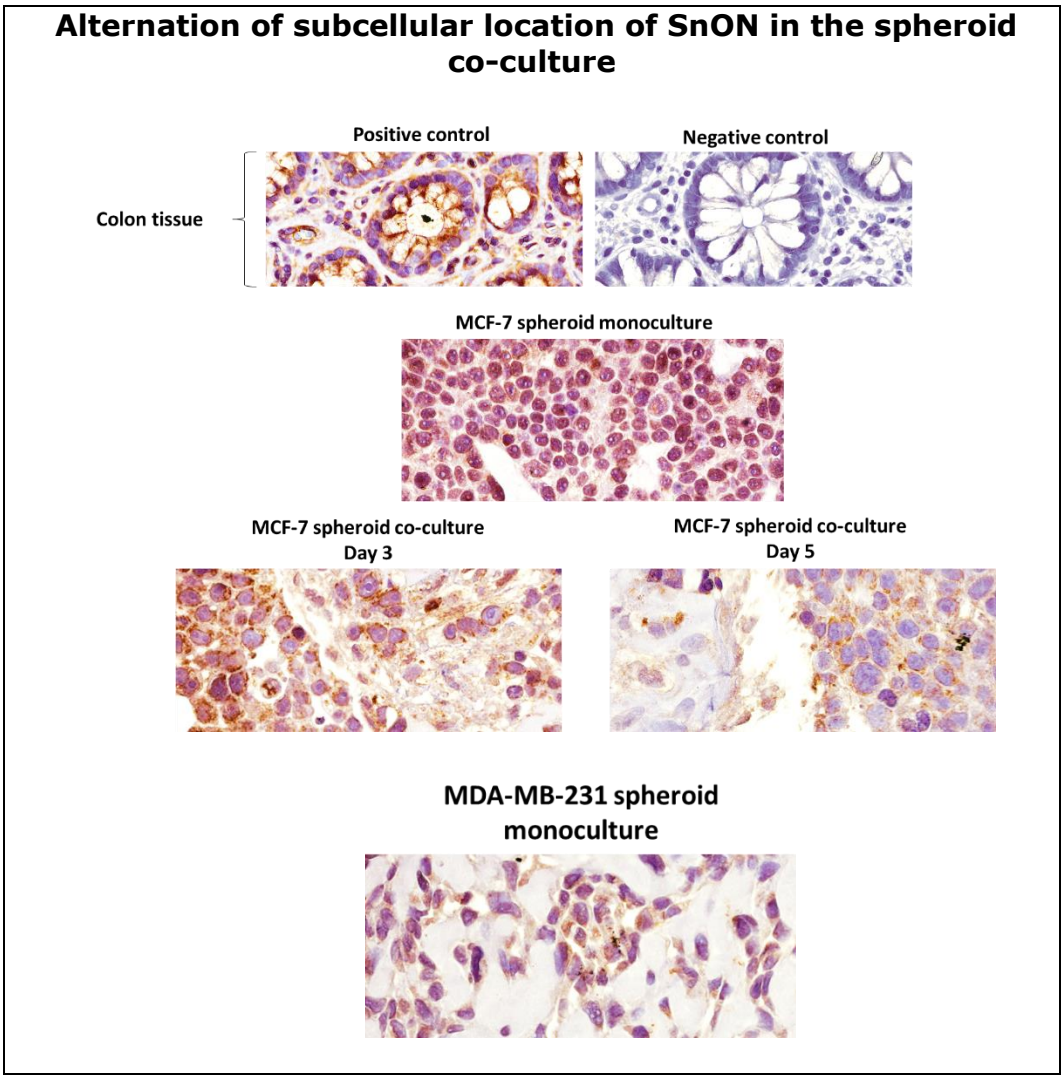

Figure 5-12: MSCs altered subcellular localisation of SnON in MCF-7 cells in spheroid co-culture: The spheroid monoculture was probed with SnON antibody to observe the expression of SnON. Spheroid co-cultures on day 3 and 5 were included in the study to investigate the expression alteration of SnON in MCF-7. Spheroid monoculture of MDA-MB-231 was stained in order to observe the expression of SnON in the invasive BCC. Colon tissue was used as a positive control in the experiment. Images were captured at 60X magnification using slide scanner.

5.7 Mesenchymal stem cells activate β-catenin in MCF-7 in co-culture

Since the housekeeping gene was not detected by the Western blot in the lysates of the FACS-sorted MCF-7 from the spheroid co-culture, and the protein concentration was low compared to the desired protein concentration (1mg/ml); the RPPA was not possible to perform for differential study of the paracrine signalling in the BCC in 2D and spheroid model. However, from the interactive model of the paracrine signalling network (Figure 1-3) it has been observed that β-catenin served as a common downstream target of various signalling pathways. It was reported that the cytoplasmic and nuclear level of β-catenin increased in S and G2/M phase of proliferating cells[248]. Studies in colorectal cancer cells demonstrated that nuclear localisation of β-catenin resulted in the activation of cyclin-D1, important in regulation of the cell cycle[249]. Although aberrant expression of β-catenin was observed in several cancers, impact of the MSCs on β-catenin activation in MCF-7 was not reported before.

Therefore, an immunofluorescence (IFC) study was carried out to investigate the localisation of β-catenin in MCF-7 in the co-culture models. IFC studies demonstrated that β-catenin resided in the plasma membrane of MCF-7tdTomato in 2D monoculture (Figure 5-13). On the other hand, in co-culture, β-catenin became more cytoplasmic and nuclear in MCF-7tdTomato. Hence, the cytoplasmic and nuclear presence of β-catenin in MCF-7tdTomato in 2D co-culture represented MSC-mediated activation of β-catenin. However, due to the lack of time required for optimising the immunofluorescence study for the activation of β-catenin in the spheroid co-culture was not performed, the activation of β-

catenin in BCC proliferation in the spheroid co-culture was investigated through an inhibitor study.

A. MSCs activate β-catenin in MCF-7 in 2D co-culture

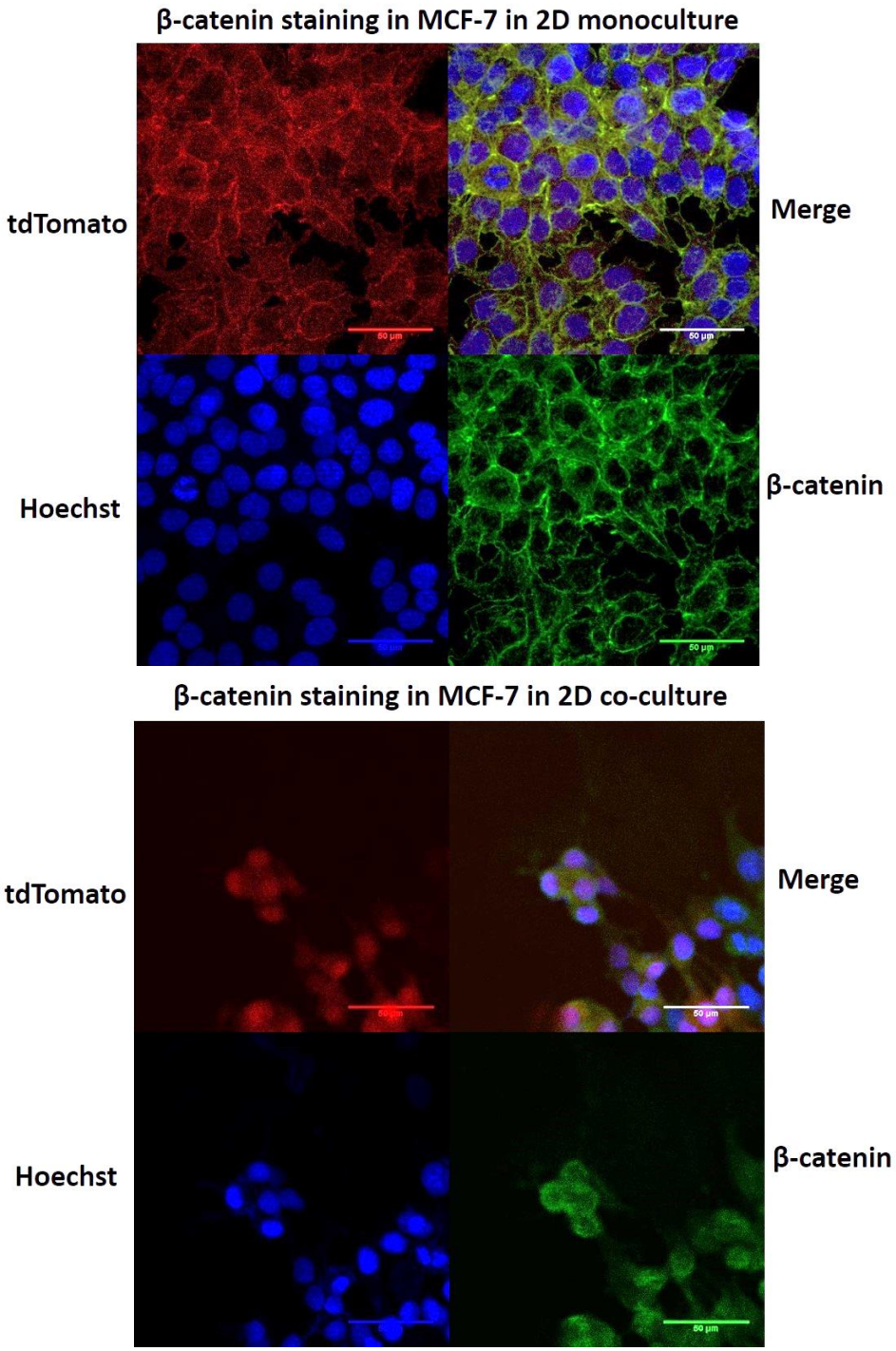

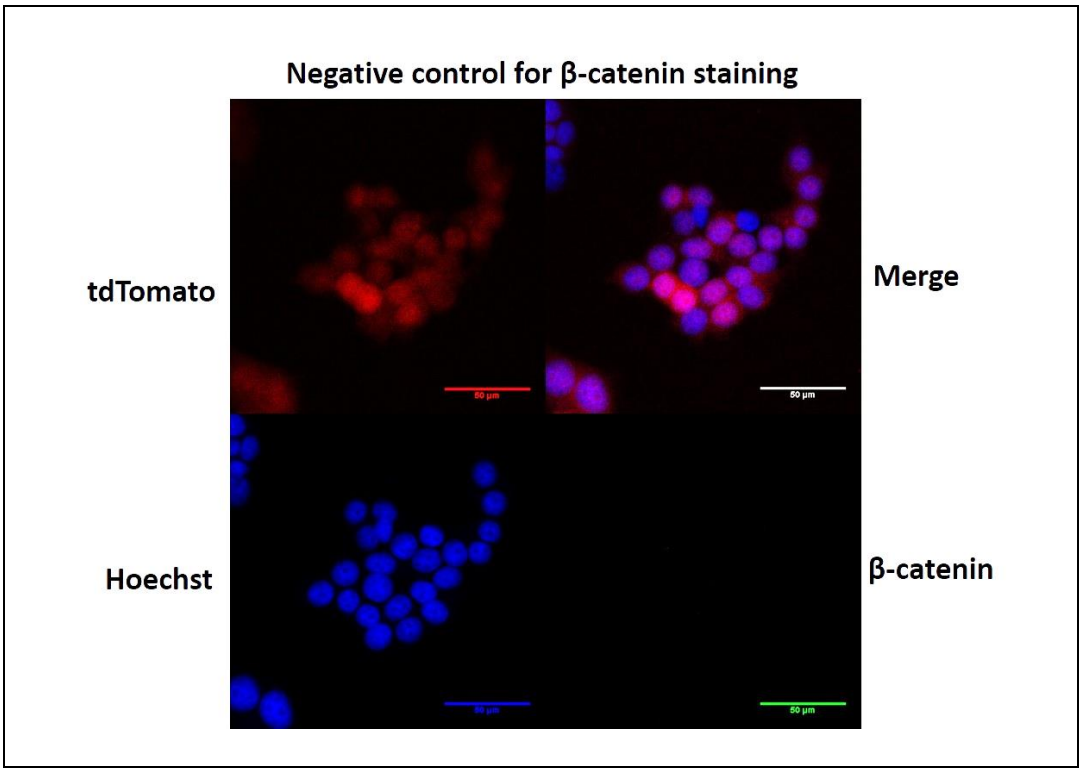

Figure 5-13: MSCs activate β-catenin in MCF-7: In monoculture, β-catenin resided in the cell membrane but β-catenin became more cytoplasmic and nuclear in the 2D co-culture. MCF-7 appeared red because of the presence of the tdTomato protein and thus facilitated identification of MCF-7 in the co-culture. While absence of signal in green channel in negative control of MCF-7tdTomato monoculture demonstrated the specificity of the secondary antibody towards primary antibody used for investigating the localisation of β-catenin in MCF-7 in 2D mono and co-culture. Nuclei appeared blue because of the Hoechst 33342 staining. Images were captured by confocal microscope at 40X magnification.

5.8 Inhibition of the β-catenin resulted in the MSC-driven BCC proliferation in the 2Dand spheroid co-cultures

The β-catenin inhibitor, MSAB, was used to investigate whether the activation of β-catenin driven by MSCs was associated with BCC proliferation in the co-culture. It has been observed that the MSAB-mediated degradation of the β-catenin resulted in the decreased proliferation in the canonical Wnt/β-catenin-dependent cancer cells[250].

DMSO was recommended as the solvent for MSAB. Since DMSO is toxic to cells, a DMSO tolerance test was performed to determine the cell viability at DMSO concentrations ranging from 0% to 14%, using the Alamar blue assay. It was observed that the cell viability was maintained between the DMSO concentrations ranging from 0% to 1% but thereafter the viability decreased on increasing the concentration of the DMSO (Figure 5-14A). Hence, to avoid DMSO-exerted toxicity, 2.44µl of the main stock of the MSAB (81.9mM in 100%DMSO) was first diluted in 2 ml PBS to prepare the working concentration of 100µM that gives the DMSO concentration of 0.12%, which was less than the cytotoxic concentration of DMSO, that is, 3%.

In order to investigate the impact of the β-catenin on MCF-7 proliferation, the mono and co-culture of 2D and spheroid models were treated with different concentrations of MSAB and Alamar blue assay was performed after 48hrs. The final concentrations of DMSO in the corresponding doses of MSAB were calculated accordingly (Table 5-4). Since the highest concentration of DMSO in the assay was 0.05% and DMSO concentrations over 20 times this high had no effect on cell viability (Figure 5-14a), the

observed dose-dependent effect (Figure 5-14B.1 and 2) must be solely due to MSAB. The experiment was repeated in the same setup ensuring the reproducibility of the IC50 values of the MSAB. The IC50 values of the MSAB in 2D monocultures were 2.5μM and 4.5μM, whereas in the 2D co-culture the IC50 values were 4.6 and 4.9 in two different experiments. Similarly, the IC50 values in the spheroid monoculture were 1.1μM and 1.9μM but in the spheroid co-culture the IC50 values were 6.4μM and 6.4μM. Therefore, the analysis of the generated bar graphs demonstrated a significant increase (P value 0.0059; unpaired t-test) in the MSAB dose in the spheroid co-culture compared to its monoculture (Figure 5-14B.4). In contrast, no significant difference was observed between the IC50 values of MSAB in the 2D co-culture compared to its monoculture (Figure 5-14B.3). Since the standard error between the IC50 values of the replicates in the 2D monoculture was high; higher number of replicate is required to determine whether the effect is significant in the 2D monolayer model. However, the increased dose of the MSAB in co-culture models highlighted the MSC-driven activation of β-catenin was associated with the increased proliferation of MCF-7. But the reason behind the increased IC50 of MSAB (P value 0.0089; unpaired t-test) in the spheroid co-culture compared to the 2D co-culture also needs to be further investigated (Figure 5-14B.5).

A. DMSO tolerance test

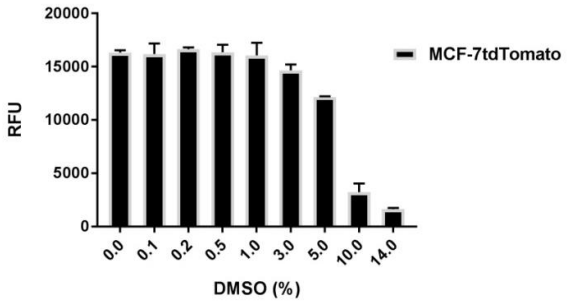

B. Drug response curve in 2D and spheroid culture

1. Drug response curve in 2D monolayer

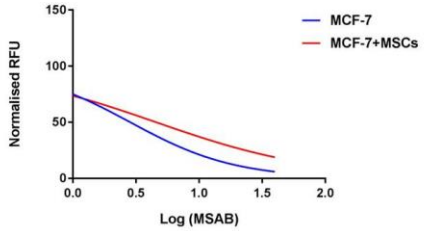

2. Drug response curve in spheroid culture

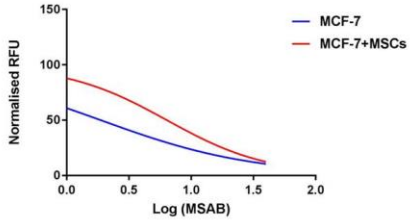

3. Bar graph of IC50 value of MSAB in 2D monolayer

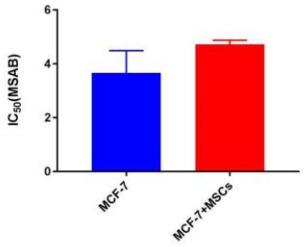

4. Bar graph of IC50 value of MSAB in spheroid model

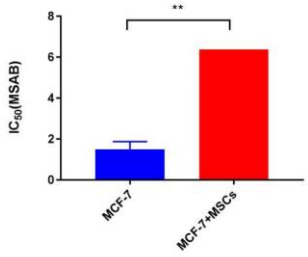

5. Bar graph of IC50 value of MSAB in 2D and spheroid co-culture

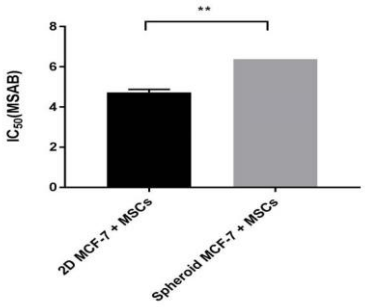

Figure 5-14: Inhibition of β-catenin suppressed the BCC proliferation in 2D and spheroid co-culture: A. A DMSO tolerance test was performed in the 2D monoculture of MCF-7 by following treatment with different concentrations of DMSO including 0%, 0.1%, 0.2%, 0.5%, 1%, 3%, 5%, 10% and 14% and incubated for 48 hrs. Cytotoxic concentration of DMSO was determined with the assistance of the Alamar blue assay. **B.** 1 and 2 represented the non-linear regression curves developed by plotting the log values of MSAB dose against the normalised RFU values in the prism. The IC_{50} was calculated by transforming the Log value of the MSAB. 3 and 4 represented the analysis of the IC_{50} values from the independent replicates determined the increased dose of MSAB in the co-cultures compared to the monocultures. 5. Represent the differences of the IC_{50} values of MSAB between the 2D and spheroid co-culture. The significance of the study in the bar graphs was determined by the unpaired t-test in the prism.

Drug concentration (μM)	Drug concentration Log_{10}(μM)	Final concentration of the DMSO (%)
1	0	0.001
3	0.5	0.003
5	0.7	0.006
10	1.0	0.012
15	1.2	0.018
20	1.3	0.024
25	1.4	0.030
30	1.5	0.037
40	1.6	0.049

Table 5-4: Final DMSO concentrations in the corresponding MSAB doses.

5.9 Inhibition of the β-catenin suppressed MSC-driven BCC invasion in spheroid co-culture

The role of β-catenin is not only restricted to cell proliferation but growing evidence suggests a role in EMT and invasion in several cancer types. For example, it was observed that EGF-driven activation of β-catenin was associated with EMT in glioblastoma[108]. Another study explained the regulatory role of β-catenin in vimentin expression in BCCs[251]. Therefore, it was hypothesised that the activation of β-catenin may be associated with the MSC-driven BCC invasion in the spheroid co-culture. Therefore, the spheroid co-cultures embedded in the high-gelling BME were treated with the MSAB concentrations of 6μM and 8μM. The

purpose of using two different doses of MSAB, as well as no treatment, was to observe whether the drug was able to suppress BCC invasion at a similar dose used for inhibiting the MCF-7 proliferation in the spheroid co-culture or required a higher dose while keeping below the concentration that could result in toxicity of the DMSO vehicle. As a 'no invasion' control, a spheroid co-culture was not embedded in Cultrex but maintained in standard cell culture medium (Figure 5-15).

Images were captured at 72 hours after the MSAB treatment to observe the invasion in MCF-7 in the co-culture. The invasion status in the spheroid co-culture from different conditions was analysed using ImageJ. The anterior projection of invasion demonstrated an invasive front in the BME-embedded spheroid co-culture not treated with the MSAB. On the other hand, the presence of MSAB suppressed the outgrowth from the peripheral region of the spheroid co-culture and the structure of these spheroids appeared similar to the negative control. In addition, analysis of the lateral projection of invasion demonstrated an increased core-edge distance in spheroid resulting from the BCC invasion but the MSAB treatment decreased the core-edge distance which appeared similar with the core-edge distance in the negative control. Therefore, it seems that the inhibition of β-catenin suppressed MSC-driven invasion of MCF-7 in the spheroid co-culture.

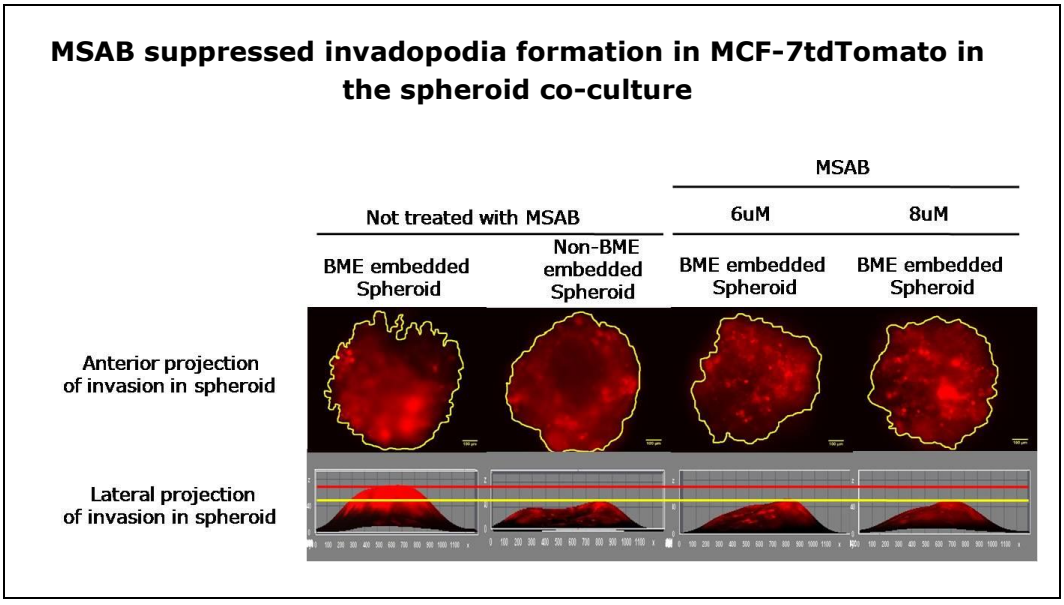

Figure 5-15: MSAB suppressed MSC-driven invasion of MCF-7 in the spheroid co-culture: The anterior projection of invasion assay demonstrated invasion in the spheroid co-culture in the presence or absence of the MSAB. Images were captured under a fluorescence microscope at 10X magnification. The analysis of the core-edge distance resulted from the BCC invasion in the spheroid co-culture in the presence or absence of MSAB was analysed by the imageJ. The spheroid co-culture not embedded in the BME used as a negative control in the invasion assay.

5.10 MSCs promote proliferation in Patient-derived xenografts (PDXs) in spheroid co-culture

Although studies with standard cancer cell lines helped us in understanding the underlying mechanisms of the disease, drawbacks of using standard cell lines were also addressed. In a study it was observed that passaging altered the differential potential and growth rate in multipotent murine bone marrow stromal cells, D1 in the cell culture[252]. Similarly, Comparative Genomic Hybridization (CGH) demonstrated copy number variation in MCF-7. Further, morphological differences and differential response to estradiol in MCF-7 highlighted the risk of reproducibility of the data using standard cell lines[253].

Therefore, in parallel to using MCF-7 and MDA-MB-231, the impact of MSCs on the proliferation of patient-derived xenograft (PDX) samples BR15 and BR8 was investigated. According to the pathological analysis at the Queens Medical Centre, BR15 and BR8 are DCIS and TNBC BCCs derived from the BC patients. Tissues from the BC patients were collected and implanted in the mammary fat pad of CD1nude and RAG2G mice to grow and maintained via *in vivo* passage.

For spheroid formation, tissues were isolated from the mice and dissociated into a single cell suspension. Next, the spheroid monoculture of 2K PDXs and co-culture of PDXs : MSC-eGFP at a ratio of 1:2 were seeded and growth proliferation from day 3 to day 7 in mono and co-culture determined using the Alamar blue assay. There was increased proliferation of PDXs in the co-culture compared to monoculture at the early time points. However, similar to that observed in the cell-line models, there was poor cell

viability by day 7 in the PDX spheroid co-culture (Figure 5-16A). In addition, studies regarding the retention of MSCs in PDXs spheroid co-culture demonstrated that although the GFP-intensity decreased in the BR8 spheroid co-culture as had been observed in the cell-line models, GFP-intensity was maintained in the spheroid co-culture of BR15 over the course of the study. Hence, it seems that the retention of MSCs in the spheroid co-culture is dependent on the type of BCCs.

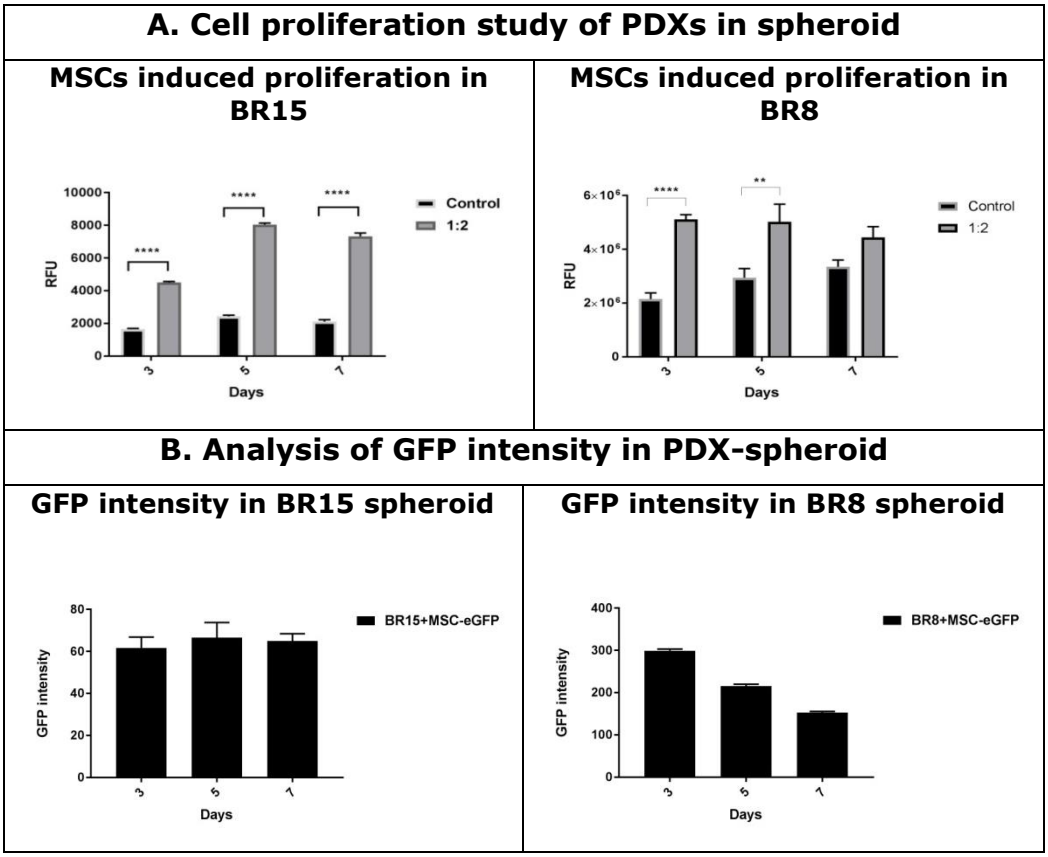

Figure 5-16: Investigating the MSC-driven proliferation of PDXs and retention of MSCs in the spheroid co-culture: A. Spheroid monocultures were seeded using 2K PDXs and their corresponding co-cultures were established using PDXs: MSC-eGFPs at the ratio of 1:2. The Alamar blue assay was used to determine the MSC-driven proliferation of PDXs in the spheroid co-culture. Statistical significances in the proliferation studies were determined by following the Two-way ANOVA in the Prism. ** and **** represented the P values 0.0030 and <0.0001. **B.** GFP intensities across the PDX spheroid co-cultures were measured at different time points with the assistance of fluorescence microscope.

5.11 MSCs induced invasion in non-invasive ductal PDX, BR15 in the spheroid co-culture

In parallel to investigating the effect of MSCs on the proliferation of PDXs, the impact of MSCs on the invasion of BC PDXs was demonstrated. Of the two PDXs used, BR15 was derived from a DCIS BC patient. Therefore, the influence of MSCs on the transformation of DCIS into invasive breast carcinoma was investigated in the spheroid co-culture made using of BR15: MSC-eGFP at the ratio of 1:2. Once the spheroids had formed on day 3, they were embedded in a high-gelling BME and images were taken under the brightfield microscope to observe the formation of invasive front in the spheroids. Although the edges of the BR15 spheroid monocultures appeared smooth after embedding in the high-gelling BME, finger-like projections from the peripheral region in the spheroid co-culture were observed starting from 48 hours of embedding in high-gelling cultrex (Figure 5-17). Since the fluorescent images demonstrated the presence of MSC-eGFP in the core; the resulted projections at the peripheral region of the spheroid co-culture was because of the migrated BR15. Therefore, it appears that the MSCs promote invasion in non–invasive PDX, BR15, consistent with the results observed in the MCF-7 in the spheroid co-culture (Figure 4-13).

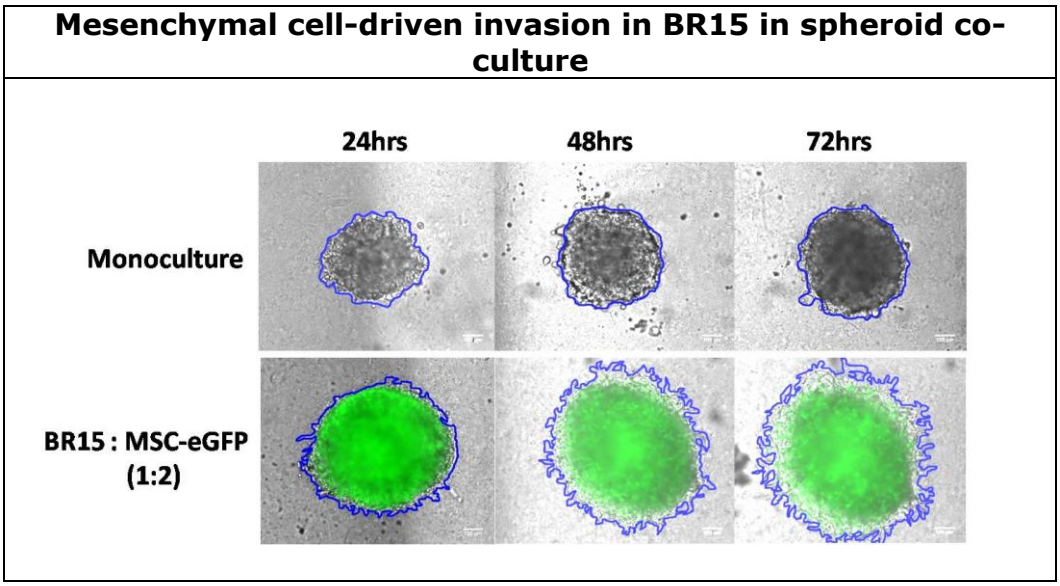

Figure 5-17: MSCs transform BR15 into invasive PDX in the spheroid co-culture: BR15 spheroid monocultures and co-cultures were embedded in high-gelling BME on day 3 and thereafter images were captured at different time-points to observe the invasion. MSC-eGFP appeared green in the co-culture and resided in the core of the spheroids. Images were captured at 10X magnification.

5.12 Summary

- Phalloidin staining demonstrated the phenotypic alteration of MCF-7 into spindle shapes in the 2D co-culture. In addition, the loss of cell-cell interaction in the MCF-7 highlighted the potentially EMT inducing property of MSCs in the MCF-7 in the 2D monolayer (Figure 5-1).

- In order to investigate the expression of EMT markers in MCF-7, the protein lysates were prepared from the FACS-sorted MCF-7. FACS sorting of MCF-7 was performed based on use of fluorescently tagged cells. Since, the use of the MSC-eGFP was not promising approach to FACS-sort MCF-7 from the mixed cell population in the co-culture, an alternative approach was adopted. Instead of tagging MSCs, MCF-7 was fluorescently tagged with tdTomato and the

spectral difference between MCF-7tdTomato and MSCs was analysed by flow cytometry. Due to the presence of heterogenous populations of tdTomato-expressing MCF-7, high intensity MCF-7tdTomato cells were FACS-sorted and expanded to enrich their population. Later, the flow cytometry analysis in the expanded population confirmed the presence of a homogenous population of high intensity tdTomato-expressing MCF-7 displaying a great spectral difference from the MSCs. Therefore, the co-cultures in both *in vitro* models were established and MCF-7tdTomato was FACS-sorted from 80 wells of the cell culture plate at different time points of the study.

- Since the Snap-freezing process provided better yield of protein from a low cell number; the lysates were prepared from the FACS-sorted MCF-7tdTomato by snap freezing and analysed by Western blot technique. The decreased expression of E-cadherin and increased vimentin highlighted the induction of the EMT in the FACS-sorted MCF-7 in the 2D co-culture (Figure 5-8). In contrast, the western blot analysis failed in detecting the housekeeping protein, alpha-tubulin in the lysates from the spheroid co-culture. Therefore, the alteration in the expression of E-cadherin and vimentin in MCF-7 in the spheroid co-culture was detected by IHC instead of western blot.

- The IHC analysis revealed a gradual reduction in the E-cadherin but increased vimentin in the spheroid co-culture (Figure 5-9 and Figure 5-10). Further analysis of the high power images of the spheroid co-culture demonstrated that

although the E-cadherin expression was greatly reduced in the MCF-7 dwelling outside the core, the expression of E-cadherin was completely abolished in the BCCs residing in the spheroid core. On the other hand, the positive staining of vimentin in the core raised a doubt of staining of MSCs in the spheroid co-culture. However, the fluorescent-based analysis (Figure 3-12C) demonstrated the degeneration of the MSCs in a time-dependent manner in the spheroid co-culture. Therefore, in order to differentiate between the cancer cells and MCs in the core, H&E staining was performed in the spheroid co-culture model. Although from the shape of the nuclei it seems that the vimentin positive cells may be MCF-7s (Figure 5-10B), due to the lack of information regarding the appearance of MSCs in the spheroid model it is not possible for now to state conclusively that vimentin positive cells are MCF-7 and not MSCs. Therefore, it was hypothesised that further IHC characterisation of MSC-GFP and *in situ* hybridisation for luciferase-labelled MSCs in the spheroid co-culture altogether may help us to provide the answer in the future.

- In parallel to confirming the EMT inducing property of MSCs in the MCF-7, the underlying mechanism triggers EMT in the co-culture was further investigated. The downregulation of SnON in MCF-7 in the *in vitro* co-cultures gives a clue regarding the possible mechanism by which MSCs transformed MCF-7 into invasive BCC. Although the EMT regulatory role of SnON in the MCF-7 was not illuminated, the degradation of SnON in the MCF-7 inside and outside

the core of the spheroid co-culture highlighted the possible E-cadherin regulatory role of SnON in the non-invasive BCCs. Since the expression of other EMT markers was not investigated it is too early to make the hypothesis concerning the E-cadherin regulatory role of SnON in BCC.

- The cytoplasmic and nuclear localisation of β-catenin in MCF-7 indicated the MSC-driven paracrine activation of β-catenin in the co-culture. Hence with the agreement of the observation, inhibition by a β-catenin inhibitor MSAB resulted in the suppression of BCC proliferation in the *in vitro* co-culture models. In addition, the high IC50 of MSAB in the co-culture relative to the monoculture may be a result of relatively high level of β-catenin in the MCF-7 in the co-culture. Interestingly, the inhibition of β-catenin not only arrested the proliferation of MCF-7 but also suppressed the MCF-7 invasion in the spheroid co-culture. Therefore, it seems that the active β-catenin in the co-culture may have a dual role in regulating proliferation and invasion of BCC.

- While direct co-culture of MCF-7 facilitated understanding of the impact of MSCs on BC progression; the incorporation of the BC PDX samples in the spheroid co-culture helped in validating the accuracy of the data generated using the established BCC lines. In an agreement with the proliferation study in MCF-7 spheroid co-culture, the Alamar blue assay demonstrated an increased proliferation in PDXs in the co-culture. Similarly, the transformation of the non-invasive PDX, BR15 into invasive subtype in the co-culture supported the BCC invasion property of MSCs. Therefore,

the data collectively highlighted the homing of MSCs in the TME may transform the DCIS BC into invasive ductal carcinoma (IDC) in BC patients. On the other hand, the retention of MSCs in the spheroid co-cultures of BR15 not observed with the MCF-7 cells, provide a clue regarding differential interaction nature of MCF-7 and BR15 with MSCs.

CHAPTER 6: DISCUSSION AND CONCLUSION

The effect of MSCs on BC progression was investigated in three stages in this study. Initially, the role of MSCs in BCC proliferation was investigated in 2D co-culture, and differences between 2D and spheroid culture model demonstrated. The next part of the thesis described the role of MSCs in BCC proliferation and invasion in the spheroid co-cultures. Finally, MSC-driven EMT in BCCs and the underlying mechanism of the MSC-induced effects on BC progression were illustrated. Spheroid co-culture using patient-derived xenografts (PDXs) with MSCs was included in order to validate the effect of MSCs on BC in a more clinically-relevant setting.

Uncontrolled cell proliferation in low-mitotic tissue results in the onset of neoplasia and therefore abnormal cell proliferation in tissue is a risk factor in patients[254]. The alteration of cell cycle-related proteins due to mutation or constitutive activation of signalling pathways play a crucial role in stimulating cell proliferation in the target cells[255]. From a systematic literature review, it was noted that MSCs migrate from the bone marrow to the BC niche and secrete a broad range of paracrine factors[70] and therefore, the role of MSCs in BCC proliferation was investigated. Although previous studies had demonstrated that MSC-derived conditioned media (MCM) promotes MCF-7 proliferation[221], the anti-tumorigenic properties of bm-MSCs in direct co-culture has also been documented. In one study, bromodeoxyuridine (BrDU) analysis demonstrated that the direct *in vitro* co-culture of bm-MSCs suppressed proliferation in hematopoietic and non-

hematopoietic cell-lines[256]. Similar anti-tumorigenic effects of bm-MSCs have been observed in Glioblastoma cell-lines in a direct *in vitro* co-culture model[257]. In parallel to such *in vitro* models, anti-tumorigenic effects of bm-MSCs have been illustrated *in vivo*. It was observed that the presence of bm-MSCs suppressed the tumor volume in an athymic nude mouse model of Kaposi's sarcoma[258]. Therefore, it seems that, although indirect co-culture promotes BCC proliferation, the physical presence of MSCs may have tumor suppressive effects in BC.

Hence, to understand the BCC proliferation capacity of MSCs, a direct co-culture was established in 2D monolayer culture. The increased proliferation of BCC in the direct co-culture was consistent with observations in indirect co-culture systems in the literature[221]. Although the reasons behind the anti-tumorigenic properties of MSCs in some studies are unknown, the passage number of MSCs could be a potential reason for such disparity in the outcome. Up to 10 passages, MSCs retain their stemness, and proliferation capacity[74]. Therefore, documenting the passage number of the MSCs used for a particular study may be useful in understanding the inconsistencies regarding the outcome of the studies performed in different laboratories.

Since MSCs promote BCC proliferation in 2D co-culture, the analysis of the underlying paracrine signalling pathways in BCC may facilitate identification of targeted therapeutics with potential to inhibit BCC proliferation. Frequently, following testing of inhibitors of cancer targets in 2D co-cultures, the drug is tested in BC mouse models in order to test the efficiency of the targeted therapeutics in a more physiological setting. However, drugs developed for targeted therapeutics based upon an active

signalling axis detected in conventional cell culture model are found not to be effective[188], or sometimes exert serious side-effects[187]. Failure of drugs tested in mouse cancer models in clinical trials[198] has negative impacts for patients and on the economy, and are wasteful of animals. Therefore, in order to reduce the use of animal models to situations where valuable information can be obtained, a robust preclinical model is required to serve as a platform to test the outcome of studies performed in 2D monolayer systems before taking them forward into *in vivo* studies. Since 3D spheroids have important characteristics of tumors *in vivo* including intricate cellular arrangement, stemness, and limited diffusion of mass (nutrients and drugs) spheroid models have received attention as preclinical tools for drug discovery[212].

The spheroid is a 3D model where the cells aggregate whilst in suspension[259]. In this model, cells grow in a tissue-like structure allowing greater cell-cell contact, with increased intercellular communication, and more uniform distribution of receptors and adhesion molecules over the cell surface[260]. In addition, due to the similarity between 3D culture and tissue in terms of slow growth rate of cancer cells, increased glycolysis, altered gene expression profile, increased drug resistance, and the morphological similarity[205], BCC proliferation capacity of MSCs was investigated in the spheroid co-culture.

In this study, spheroids were formed using round bottom 96-well ultra-low attachment plates and in the spheroid co-cultures, MSCs were shown to reside in the core whereas MSCs and BCCs were uniformly distributed on the flat surface of the 2D co-culture. In contrast, in spheroid co-cultures formed using the hanging drop

technique the BCCs were surrounded by the MSCs[261]. Therefore, it seems that the arrangement of cells in spheroid co-cultures is technique-dependent.

In coculture spheroid model, MSCs were lost over time; the reason behind this is not understood but the observation is consistent with a previous study performed in the hanging drop spheroid co-culture system[261]. Due to the better retention of MSCs in this experimental set-up, a ratio of 1:2 (cancer cells: MSCs) was chosen for the growth kinetic study of BCCs in the spheroid co-culture. In addition, the number of BCCs used was selected to avoid necrotic core formation and it was found that inclusion of BME helped to maintain cell viability, potentially through cell-ECM interaction in the spheroid.

Following characterisation of the cell viability in the spheroid model, the Luciferase and Alamar blue assay were performed in the spheroid mono- and co-cultures. The resulting decrease in luminescence in the spheroid co-culture compared to the 2D co-culture suggested the tumor suppressive role of MSCs in the spheroid co-culture (Figure 4-2). In contrast, the increased spheroid volume and the RFU in the Alamar blue assay (Figure 4-3 and Figure 4-4) suggested a growth promoting effect of MSCs in the spheroid co-culture. We hypothesised that the decreased luminescence may be artefactual, resulting from the presence of hypoxic areas within the spheroids[212]. The Luciferase enzyme produced by the Luciferase-labelled BCCs, acts on luciferin only in the presence of oxygen, producing luminescence which can be quantified using a luminometer[231]. However, because of the oxygen-gradient, some BCCs in the spheroid co-culture are not detected because the luciferase-mediated light production can not

occur. In contrast, the Alamar blue contains resazurin which is reduced by nicotinamide adenine dinucleotide (NADH) and nicotinamide adenine dinucleotide phosphate (NADPH) in living cells and the resulting fluorescence is measured by fluorometry[219]. As low oxygen levels increase production of NADH and NADPH[192], BCC in the spheroid co-culture can readily reduce the Alamar blue resulting in the increased RFU. Although, the BCC metabolism in the spheroid co-culture has not been studied so far, the aforementioned literature may help in explaining the apparently different results obtained using the Luciferase and Alamar blue assays in 2D and spheroid co-culture.

Hence, in order to investigate the BCC proliferation capacity of MSCs in the spheroid co-culture independent of metabolic considerations, the CellTrace Violet assay was included in the study. Flow cytometry-mediated analysis of the intensity of CellTrace Violet fluorescent signal in the single cell suspensions of the digested spheroids demonstrated an increased proliferation of BCC in the spheroid co-culture compared to the BCC in the spheroid monoculture (Figure 4-9B). Sharing of the dye between the daughter cells results in the production of sharp peaks of lower dye-intensity compared to the parental cells[233]. Therefore, unlike the luciferase and Alamar blue assay, the CellTrace Violet assay allowed the percentage of cells in the spheroid models, which had or had not proliferated by the relevant time points of the study to be determined. Thus, from the calculation of the CellTrace Violet positive cells it appeared that MSCs exert a strong effect on the proliferation of MCF-7 cells compared to the MDA-MB-231s (Figure 4-9C). The analysis of conditioned-medium (CM) from MDA-MB-231 demonstrated the presence of IGF, EGF and TGF-β, which

induce proliferation in MDA-MB-231 in a autocrine fashion[262]. Therefore, the self-sufficiency in producing growth factors, may mean that MDA-MB-231s, compared to the MCF-7s, are less dependent on MSCs in terms of proliferation in the co-culture. In addition, the presence of mutant P53[263], BRCA1 gene[264] and lack of functional retinoblastoma (Rb) protein, the regulator of synthesis phase (S-phase) in the cell cycle, together result in high mitotic indices in the TNBC cell lines[263]. Hence, differential mutation studies on P53, BRCA 1 and Rb genes across the DCIS cell lines (MCF-7, T47D, SUM 185, SKBR3) and TNBC cell lines (MDA-MB-231, MDA-MB-468, SUM190, BT549)[265], combined with proliferation studies in the spheroid model, may allow improved understanding of the correlation of mutation with BCC proliferation and provide an insight regarding the differential growth proliferation impact of MSCs in different BC subtypes.

Understanding of the role of MSCs in ductal carcinoma *in* situ (DCIS) BCC proliferation was not only based on live cell assays, but demonstrated through IHC which showed increased Ki-67 expression in the MCF-7 spheroid co-culture. However, in the *in vitro* model, whether the expansion of BCC was dependent on the MSC-driven paracrine signalling is still to be revealed. In the 2D co-culture, MSCs and BCCs were distributed on the flat surface of the cell culture plate in a way that allows both direct cell-cell contact between the two populations as well as paracrine signalling. Therefore, it is not possible to distinguish effects driven by these two different types of cell communication. In contrast, MSCs reside in the core of the spheroid co-culture surrounded by the BCCs (Figure 3-6). Therefore, the increased expression of Ki-

67 in BCC at the outside edge of the spheroid co-culture highlighted the MSC-exerted paracrine effect on BCC proliferation.

Although using the standard BCC lines helped in improving knowledge of the proliferation-promoting nature of MSCs, potential alterations in the functions of genes, risk of Mycoplasma infection and passaging of standard cell lines in the laboratory may alter their native characteristics and response towards stimuli[266]. Therefore, in order to validate the growth-promoting effect of MSCs in BCC, the DCIS-patient-derived xenograft (PDX), BR15 and TNBC-PDX, BR8 were included in the study. Since, the observations with the Alamar blue assay were similar to those from the CellTrace Violet assay in the spheroid co-cultures of MCF-7 and MDA-MB-231, the Alamar blue assay was performed to determine the proliferation of BR15 and BR8 in the spheroid mono and co-cultures. The increased proliferation of PDX-derived cells in a time-dependent manner (Figure 5-16) provided additional evidence regarding the impact of MSCs on BCC proliferation. Overall, this study in BCCs and a previous study in our laboratory[216] on lung cancer PDXs demonstrated the positive impact of MSCs on the proliferation of various cancers.

Interestingly, although the MSCs demonstrated similar impact on the proliferation of standard BCC lines and PDXs, in terms of retention of MSCs there was an interesting difference between the MCF-7 and DCIS-PDX BR15. Although MSCs were retained in the BR15 spheroid co-culture (Figure 5-16), MSCs were lost in the spheroid co-culture of MCF-7 (Figure 3-12) over the course of the study. Therefore, it was hypothesised that due to differences in the derivation of MCF-7s and BR15 cells, there are difference in their ability to interact with MSCs. The MCF-7 cell-line was

established in 1973 from BCCs derived from a patient and maintained in the laboratory conditions through passaging[245]. Prolonged culturing in a synthetic environment may compromise the native characteristics required for the interaction between the MCF-7 and MSCs. In contrast, BR15 was obtained from BC patients and maintained in-house in immunodeficient mice as PDXs and used at low passage numbers. Therefore, they were maintained in a more physiological milieu, in which recruitment of MSCs is still required for them to obtain important growth factors and cytokines, resulting in maintenance of characteristics that allow them to interact with MSCs and mutually promote their survival.

Cellular heterogeneity in PDXs may be another reason for differential retention of MSCs in the spheroid co-cultures of BR15 and MCF-7. PDXs may have both heterogeneity in terms of different clonal populations of the cancer cells themselves, and the presence of stromal cells derived from the host species. In relation to the latter, the BR15 and BR8 used in this study were grown in different immundeficient mouse strains which may make different contributions to the xenograft stroma. Immune cells in the TME play a supportive role in cancer progression. In CD1 nude mice BR15 grows in the midst of MDSCs, macrophages, B-cells, and NK cells, as well as T-cells which are immature due to lack of thymus[267]. Such cells may be transferred into the spheroid models along with the cancer cells.

In contrast to BR15, the TNBC-PDX BR8 was harvested from the eRAG mice. Recombination-activating genes or RAGs encode enzymes help in the expression of T-cell receptors and immunoglobulins and therefore, RAG-deficient mice have T and B-

lymphocyte deficiency[268] and there may also be an effect on expansion of NK cells[269]. Thus, different populations of mouse stromal cells may be transferred into the models when such PDXs are used. Further characterisation of the PDX spheroids to determine whether any immune cells are present is required to test this hypothesis.

Since an effect of MSCs on proliferation has been shown, we next investigated the impact of MSCs on BCC invasion in the spheroid co-culture. In one study, the BCC metastasis-promoting properties of MSCs were determined by using MDA-MB-231 cells[82]. However, previous studies demonstrated overexpression and mutation in KRAS (Kirsten rat sarcoma viral oncogene homolog) in MDA-MB-231s contribute toward their invasiveness[270] and so they may not be dependent on external factors. Consistent with this, invasion in the spheroid monoculture further indicates MSC-independent invasive nature of MDA-MB-231 cells.

Hence, the main focus of this study was to investigate the invasion-inducing property of MSCs in the non-invasive DCIS BCCs with low innate metastasis potential[245], was included in this study to investigate the impact of the MSCs on the BCC invasion. The presence of cells migrating from the outer edge of the spheroid co-cultures highlighted the MSC-driven effects on MCF-7s (Figure 4-13), apparently contradicting the observations regarding the BCC invasion-suppressing role of MSCs in non-invasive hormone receptor positive BCC, T47D[271]. However, since the source of the MSCs in the above study was not clearly described, possibly use of different types of MSCs may underlie the disparity between observations from different laboratories. As well as the source of MSCs, copy number variations in the chromosomes of MCF-7[253],

the cell culture medium and the cell passage number may be the factors that induce the inconsistency in the observations[245,252].

In order to extend the data generated using the MCF-7, BC invasion-inducing properties of MSCs was investigated in the spheroid co-culture invasion assay using DCIS PDX-derived cells, BR15. Consistent with its non-invasive nature, no migrating cells were observed in the BR15 spheroid monoculture. In contrast, outgrowth beyond the edge of the spheroid co-culture demonstrated the presence of a population of migrating BR15 cells able to invade the surrounding stroma (Figure 5-17).

Hence, from the data of the proliferation and invasion assays in the standard DCIS BCC-line and PDX it was highlighted that bm-MSCs may play an important role in switching the DCIS into invasive ductal carcinoma (IDC). However, further *in vitro* and *in vivo* studies using a larger panel of DCIS-PDXs with bm-MSCs are required in order to confirm the impact of MSCs on transforming DCIS into IDC subtypes.

Although the invasion assay was performed in the spheroid co-culture, invasion-inducing properties of MSCs in BCCs in 2D co-culture were not investigated in this study. A transwell chamber assay was performed in the previous studies to investigate the MSC-induced migration of BCCs. In the transwell chamber assay, MCF-7 migrated from the upper chamber through the permeable membrane toward the lower chamber contains MCM[221]. In contrast, in the physiological situation, MSCs travel towards the BC niche under the influence of inflammatory molecules[71]. Further, the stroma and cancer cells are mixed together in a tumor sample and do not exist as a separate compartment as in the transwell

set-up. Therefore, due to differences in the cellular arrangement between transwell chambers and real tumors, assessment of the invasion-inducing properties of MSCs in BCC was only performed in the spheroid co-culture model. However, transformation of MCF-7 from epithelial to spindle-shaped cells resulting from the reorganisation of F-actin in 2D co-culture (Figure 5-1), as determined by phalloidin staining, was consistent with the MSC-driven phenotypic switch in the BCC, T47D, which underwent EMT[272].

Since EMT is characterized by destabilisation of molecules responsible for tight and adherence junctions, including Claudin, Occludin and E-cadherin[273], MCF-7 was FACS-sorted from the 2D and spheroid co-culture to investigate the expression alteration of E-cadherin. The decreased expression of E-cadherin in MCF-7s in the 2D co-culture (Figure 5-8) was concluded as a potential underlying reason behind the loss of cell-cell interaction in MCF-7 observed by phalloidin staining (Figure 5-1). Although the loss of E-cadherin in MCF-7 in the 2D co-culture represented the loss of cell-cell contact, it may not sufficient for a cancer cells to become an invasive cell-type. Invasion is an early step of metastasis where cancer cells invade the surrounding stroma and migrated to the distant part of the body[235]. Studies showed that the interaction between vimentin and the actin bundles resulted in the activation of Focal adhesion kinase (FAK) responsible for migration[274]. Therefore, the expression of vimentin is required for cancer cell invasion along with the loss of E-cadherin. In agreement with the aforementioned literature, the increased expression of vimentin in MCF-7 in the 2D co-culture determined by the Western blot

analysis highlighted the acquisition of invasive characteristics in MCF-7 (Figure 5-8).

In parallel to investigating alteration in expression of E-cadherin and vimentin in MCF-7 in 2D co-culture, MCF-7 was FACS-sorted from the spheroid co-culture. However, due to inability to detect the housekeeping gene in the lysates of MCF-7, FACS-sorted from the spheroid co-culture, by Western blot (Figure 5-7), the MSC-driven expression alteration of E-cadherin and vimentin in MCF-7 was analysed by IHC in the paraffin-embedded spheroid microarrays. IHC revealed that the E-cadherin was clearly visible in the membrane of MCF-7 in the spheroid monoculture but loss of E-cadherin expression in MCF-7 in the spheroid co-culture reflected the MSC-driven alteration of the epithelial characteristics in MCF-7 (Figure 5-9). However, the expression of vimentin was restricted to the spheroid core. Since no trace of vimentin outside the core was observed in the spheroid co-culture, it was assumed that the cells positive for vimentin in the core were the MSCs. Although indirect approaches, including H&E staining and MSC-eGFP analysis, indicated the expression of vimentin in MCF-7, the IHC characterisation of MSC-GFP and vimentin and calculating the ratio of vimentin-positive cells compared to GFP positive cells in consecutive sections of the co-culture spheroids may answer this question more clearly.

Although IHC is a well-established approach in order to detect the presence of protein in tissues through application of antibody, certain factors including the time of tissue fixation and processing, variability in the specificity and sensitivity of the antibodies and scoring criteria can affect the accuracy of IHC data[275]. Therefore, to strengthen the IHC data, *in situ* hybridisation (ISH) has been

developed and classified into chromogenic-ISH (CISH) or fluorescence-ISH (FISH). Although no discrepancy observed between the CISH and FISH, the difference between the ISH and IHC data was identified in a comparative study[276]. Unlike IHC, ISH, which detects nucleic acids (DNA and RNA) rather than protein, is more consistent and accurate than IHC when tested for Her2 amplification in the BC tissues[277,278]. In addition, commercially available antibodies used in IHC can show variable affinity towards targets from other species but probes used in ISH bind to a specific sequence of the target gene in a species-specific manner if designed appropriately, that might make ISH more reliable technique than antibody-mediated target localisation in IHC, especially to detect cells of human or mouse origin; the latter may be particularly important for studying spheroids based on cells from xenografts. Hence, ISH for Luciferase-labelled MSCs and vimentin in a different set of spheroid microarray is required to observe the consistency of the IHC data. Thus, the IHC data and ISH together provide complementary methods to understand whether the vimentin-positive cells in the spheroid core are the MCF-7 or MSCs, or in the case of PDX-based spheroids, vimentin-positive cells of mouse origin.

Since vimentin is associated with cell migration[274], it seems that the cells expressing vimentin in the core had migratory properties during invasion compared to the MCF-7s outside the core. As well as vimentin, expression of N-cadherin has been associated with cell motility in a collagen matrix[279] including in BCCs[280]. Therefore, further analysis of N-cadherin expression in the spheroids may provide a clue regarding the underlying mechanism responsible for BCC motility residing at the outer edge of the spheroid co-

culture. However, the downregulation of E-cadherin and increased expression of vimentin in the MCF-7 together suggest MSC-driven EMT in BCCs. In addition, the unequal distribution of vimentin between the cells residing outside and inside the core may reflect heterogeneity in the spheroid model. Therefore, it appears that as well as staining for N-cadherin, analysing the expression of EMT markers Snail, Zeb and Twist[14,281], because of their E-cadherin-suppressing role and association with IDC tissues, would allow us to get a clearer picture of heterogeneity in terms of the expression of EMT markers in cancer cells in the spheroid co-culture.

Although the downregulation of E-cadherin, increased vimentin and morphology alteration in MCF-7 altogether provide a clue regarding the EMT-inducing property of MSCs in BCCs, the underlying mechanism by which MSCs transform the non-invasive into invasive BCC is unknown so far. The downregulation of SnON in MCF-7 in the co-culture highlighted a possible role for SnON in maintaining the non-invasive characteristics in the BCC. SnON is a component of the histone deacetylase complex (HDAC)[162] and the expression of SnON is lower in patients with advanced breast cancer[282]. In addition, shRNA-mediated knockdown of SnON has been shown to increase migration and invasion in breast and lung cancer cells including MDA-MB-231 and A549[161]. However, a role for the TME in regulating SnON in BCC has not been investigated before.

Since SnON appears to be a suppressor of invasion in BCCs and MSCs induce morphological alterations in MCF-7 in the 2D co-culture and invasion in MCF-7 spheroid co-culture, the impact of MSCs on SnON in MCF-7 was investigated. The reduced expression of SnON in MCF-7 in the 2D co-culture (Figure 5-11) highlighted

a possible MSC-driven mechanism underlying EMT in the BCC. IHC revealed SnON residing in the nuclei of MCF-7 cells in the spheroid monoculture. Therefore it seems that being a component of HDAC, SnON may play a role in maintaining the epithelial characteristics through the epigenetic pathway. However, it is important to note that the intercellular localisation of SnON varies depending upon the location of the epithelial cells in the ductal network and the origin of cancer in the breast. SnON is more cytoplasmic in the epithelial cells residing on the luminal side of the ductules in normal breast. On the contrary, SnON is more nuclear in the epithelial cells lining the large ducts in normal breast, lobular tumors and low grade tumors expressing hormone receptors with low proliferation index of Ki-67[247]. Therefore, further immunohistochemical characterization is required to investigate the variation in the intracellular location of SnON in the spheroid monoculture of other ductal BCC lines. However, the cytoplasmic presence of SnON in MCF-7 in the spheroid co-culture on day 3 (Figure 5-12) aligned with the study which showed an increased level of SnON in the cytoplasm in grade III ductal BC with the high expression level of Ki-67[247]. Later, on day 5, the faint staining-intensity of SnON in the cytoplasm of MCF-7 compared to the day 3 indicated the downregulation of SnON in the spheroid co-culture (Figure 5-12). Since a significant reduction in the SnON[282] is observed in metastatic BC, the downregulation of SnON and transformation of MCF-7 into an invasive phenotype in the spheroid co-culture (Figure 4-13) is consistent with this clinical observation. Although, the subcellular localisation of SnON in MCF-7 in the 2D mono and co-culture was not investigated, an overall reduction in the expression of SnON in MCF-7 in the 2D

and spheroid co-cultures together demonstrated for the first time the possibility that MSCs regulate SnON in BCCs.

Hence, it appears that downreguation of SnON may be a prognostic marker for invasiveness in DCIS BC. However, a study showing a favourable outcome in SnON-reduced ER-positive BC tissue[247], contradicts the obervations of a significant reduction in the SnON expression in grade II, III and metastatic samples of infiltrating ductal carcinoma[282]. Therefore, although the exact role of SnON is not clear, TGF-β-mediated increased production of ECM, and MMPs in the SnON-knockdown cancer cells suggest SnON's role as a negative regulator of TGF-β[161]. In the same study, it was demonstrated that along with increased cancer cell migration, EMT and invasion, knock-down of SnON suppressed the growth of cancer cells *in vitro* and *in vivo*. On the other hand, the increased MCF-7 proliferation in the 2D and spheroid co-culture indicated the association of MSC-exerted signalling pathways compensating the cell-cycle arrest even though the expression of SnON was suppressed in the MCF-7.

The presence of several growth factors, chemokines and cytokines in MCM highlight the potential paracrine role of MSCs, but the exact signalling axis responsible for BC malignancy is not well defined. Some of the growth factors, including Insulin growth factor (IGF), IL-6, CXCL12 and CCL5, were identified previously[90,82]. Other growth factors including EGF, HGF, and TGF-β in the stroma of BC[283] mainly expressed by the CAFs[284] also may be involved in paracrine signalling-driven BC progression.

Although the impact of all these growth factors in BC progression was not investigated individually in this study, MSC-driven

activation of the β-catenin in the BCC was demonstrated by the inhibitor study. β-catenin is a well-known downstream signalling molecule of Wnt signalling[285]. The non-phosphorylated form of β-catenin is a transcriptionally active molecule which translocates inside the nucleus and increases the expression of oncoproteins including Jun, c-Myc and Cyclin-D[286]. Interestingly, phosphorylation of β-catenin at serine 552 by EGF/AKT signalling axis induced tumor inavsion in epidermoid carcinoma cell line[186]. Although the multifunctional role of β-catenin in cell proliferation and invasion is dependent upon its phosphorylation status and location in the cell, the impact of MSCs on β-catenin in BCCs is unknown. β-catenin was shown to reside at the plasma membrane of MCF-7 in 2D monoculture but it became mainly cytoplasmic and nuclear in the MCF-7 in the 2D co-culture (Figure 5-13). Since, the cytoplasmic and nuclear β-catenin represent the functionally active form[287], the effect of β-catenin-inhibitor, MSAB, in the proliferation of MCF-7 in 2D mono and co-culture was investigated. The increased IC50 value of the MSAB in the MCF-7 2D co-culture compared to the monoculture suggests MSC-driven, β-catenin activation-mediated effects on cell proliferation and/or survival (Figure 5-14.1 and 3). On the other hand, the increase in the IC50 value of MSAB in the spheroid co-culture compared to the spheroid monoculture (Figure 5-14.2 and 4) and the 2D co-culture (Figure 5-14.5) demonstrated the possible hyperactivation of β-catenin in the spheroid co-culture. Studies showed that MSCs induce drug resistance in various kinds of haematological malignancies, and in head and neck squamous cell carcinoma, in a cell-cell contact independent manner[288]. Therefore, as well as the hyperactivation of β-catenin, MSCs may induce drug

resistance in cancer cells and this may be another reason for the increased dose in the spheroid co-culture.

To verify MSC-driven, β-catenin-dependent proliferation in the MCF-7s in the co-culture, it would be necessary to analyse the presence of non-phosphorylated and phosphorylated (Serine 552) forms of β-catenin in the nuclear and cytoplasmic fraction of BCC. However, since the housekeeping gene in the MCF-7 lysates from the spheroid co-culture could not be detected in the Western blot, the role of β-catenin in the MCF-7 proliferation in the spheroid co-culture could not be further investigated in this way. Therefore, for the future, this technical issue needs to be resolved.

The impact of β-catenin inhibition was not only studied in the context of suppression of MCF-7 proliferation in the co-culture but, since β-catenin is associated with vimentin expression in BCCs[251], and vimentin is one marker of EMT, the effect of MSAB on invasion was also studied in spheroid co-cultures. Interestingly, MSAB treatment also decreased MCF-7 invasion in the spheroid co-culture (Figure 5-15). Therefore, from the inhibitor study it was concluded that the MSC-mediated activation of β-catenin plays an important role in BCC proliferation and invasion in co-culture. However, the underlying mechanism by which β-catenin regulates invasion still remains to be investigated. In previous studies, it has been observed that knowckdown of SnON results in EMT induction but decreased proliferation, whereas β-catenin is associated both with EMT and proliferation. Therefore, this appears contradictory and needs further investigation.

Although, the standard cancer cell lines allowed gain of practical knowledge regarding the various aspects of the disease and have

contributed to the emergence of new treatment regimens, the limitations with the standard cancer cell lines cannot be overlooked. Therefore, the status of SnON and β-catenin in the spheroid co-cultures needs to be investigated using PDX-derived cells as well.

In summary, BC spheroid co-culture models display higher degree of complex cellular arrangment compared to the 2D monolayer. Despite being a 3D model, the positive impact of MSCs on BCC proliferation was consistent with the observations in the 2D co-culture. However, both models displayed certain advantagages and disadvantages for use in research. Invasion assays in the spheroid co-culture imitates the invasion in a physiological setting more accurately than the transwell invasion assay. On the other hand, compared to the spheroid co-culture, the protein lysates prepared from the cells in 2D co-culture are more compatible with western blot analysis. However, spheroids can be harvested intact, maintaining cell-cell contacts and histological features, and used for IHC characterisation but harvesting the cells from the 2D co-culture disrupts cell distribution. Apart from the technical aspects, both *in vitro* models display suppression of E-cadherin and increased expression of vimentin in MCF-7s consistently confirming the EMT-inducing property of MSCs in BCC. Furthermore, the downregulation of SnON in MCF-7 in the *in vitro* co-culture models, provided a potential new direction for investigating the underlying mechanism by which MSCs transform non-invasive BCC into an invasive phenotype. On the other hand, the suppression of MCF-7 proliferation and invasion in the co-culture model on β-catenin inhibition suggests a possible SnON regulatory role for β-catenin in BCC. Since MSCs secrete several

growth factors in the TME, a further comprehensive study on MSC-exerted paracrine signalling is required to investigate whether the regulation of the SnON is β-catenin dependent or controlled by different signalling axes. Therefore, on successful extraction of protein from the FACS-sorted BCC from the spheroid co-culture a comparative study of the paracrine signalling in the BCCs in the 2D and spheroid may provide an insight regarding the model-based alteration in the paracrine network. Further validation of the drugs developed based upon the identified targets in 2D and spheroid models is required and could be tested in the PDX models. In addition, the expression of the targets should be studied in patient samples in order to get a clear picture to justify spheroid models as an appropriate preclinical tool for use in drug discovery to identify better treatments for patient with invasive breast cancer.

CHAPTER 7: FUTURE WORKS

So far this study makes an important contribution to understanding the role of MSCs in BCC proliferation, EMT and invasion using 2D and spheroid co-culture models. In addition, further experiments using DCIS-PDX in the spheroid co-culture give clues about the impact of MSCs in transformation of DCIS into IDC using more clinically-relevant BCs. However, due to a number of practical issues, relating to the nature of this type of work using 3D models and primary cells (e.g. unavailability of MSCs of low passage, slow growth rate of MSCs, irregular availability of BC PDXs, long incubation times for spheroid formation) and the need to optimise the experimental setup in order to obtain meaningful data (e.g. characterisation of spheroid co-culture model, optimisation of cell proliferation and invasion assays in spheroid co-culture, FACS-sorting of BCCs from the co-cultures) as well as time constraints, a fully comprehensive study of the underlying mechanism by which MSCs drive proliferation and invasion in BC was not possible. Hence, based upon the current findings in this study structuring the future work may provide deeper insight to decipher the role of MSCs in BC progression and lead to improved understanding of the importance of using more clinically-relevant models for BC research.

- Epithelial-mesenchymal transition (EMT) is a crucial step during which epithelial cells lose their polarity via destabilisation of molecules including Claudin, Occludin and E-cadherin responsible for tight and adherence junctions[273]. The expression of EMT-associated transcription factors such as Twist and Snail have been linked to high-grade invasive BC and lymph node

metastasis in patient tumors, while expression of other EMT markers including N-cadherin and Vimentin have been observed in patients with basal-like BC[289]. Since the suppression of E-cadherin and upregulation of vimentin in MCF-7 in the 2D and spheroid co-cultures provide a hint of the EMT-promoting nature of MSCs, further RNA studies followed by proteomics studies on the expression of EMT markers including N-cadherin, Snail, Zeb, and Twist may provide deeper insight of MSC-driven EMT-induction in BCCs. In addition, investigating the expression of EMT markers in BCCs in the co-cultures may also facilitate in differentiating the pattern of expression of EMT markers in different *in vitro* co-culture systems in order to understand the influence of such factors for selection of appropriate models in the future.

- Studies have revealed that growth factors, cytokines and chemokines in the TME play an important role in EMT induction responsible for cancer invasion[290]. Therefore, along with investigating the EMT-promoting nature of MSCs, detecting the paracrine axis responsible for BC progression is of major importance. Previous 2D cell culture studies demonstrated the presence of growth factors including CXCL12, CCL5[221], IL-6[90] in the MCM whereas HGF, FGF, TGF-β, CXCL12 and EGF are secreted largely from CAFs[40]. Since MSCs promote proliferation, invasion and alter cytoskeletal arrangment in the non-invasive BCCs in the 2D and spheroid co-culture, using RayBio Human Cytokine Antibody Array Kit[90] for investigation of the differential expression of growth factors and cytokines in the MCM derived from 2D and spheroid co-culture may provide a more

comprehensive picture of MSC-secreted factors influenced by differences in, for example, the nature of cell-cell contacts and geometry of different *in vitro* models. In addition, the information regarding MSC-secreted factors in the stromal compartment may be used to guide understanding of the important nodes in the paracrine signalling network and help in finding new targets other than the β-catenin as a therapeutic intervention in BC progression.

- Analysing the corresponding paracrine signalling axes relevant to the EMT may help in emergence of novel targeted therapeutics for preventing or treating BC invasion, but the characterisation of IBC derived from DCIS could be another interesting aspect of this study. So far the transformation of non-invasive DCISs into IDCs in the co-culture was observed but the phenotype of the IBC is not known. *In vitro* studies have shown that TGF-β and HGF induce the expression of CXCR4 which in turn induces the expression of Her2 receptor in BCCs under the influence of CXCL12[85,86,87]. Therefore, laboratory-based studies of the phenotypic switch of the hormone receptor in DCIS-luminal A BCC into Her2-enriched or TNBC subtype in the co-culture may provide an insight into MSC-mediated paracrine-driven molecular switch in breast tumor. Hence, along with the understanding of MSC-driven paracrine signalling in EMT, scrutinising the paracrine signalling axes that alters the molecular subtypes in DCIS-BC could contribute to a more efficient therapeutic approach to stop the BC from becoming invasive subtype.

- Along with the direct effect, MSCs influence BC progression by transdifferentiating into CAFs[72]. Therefore, investigating the appearance of CAFs in the direct co-cultures may shed light on the factors driving this differentiation/activation process. This could be performed either by analysing CAF-specific markers in the lysates of FACS-sorted MSCs by western blot in the case of 2D co-culture or by IHC in case of spheroid co-culture. Since preparing spheroid microarray for IHC characterisation is time-consuming and requires great effort, further optimisation of protein extraction from spheroid co-culture-derived, FACS-sorted MSCs may facilitate protein analysis for CAF-specific markers including FAP-α, FSP-1 and α-SMA[80]. Similarly, Reverse phase protein microarray (RPPA) analysis[291] in good quality lysates from the BCCs in spheroid co-culture may allow us to understand the potential MSC-exerted paracrine signalling axes responsible for BC progression and also help in investigating the expression of MSC markers (CD90, CD73 and CD105) in BCCs resulting from the direct co-culture[74].

- Although this study is mainly focused on investigating the role of MSC-mediated paracrine signalling in BC progression, the Notch signalling pathway generated via physical contact between MSCs and BCCs in co-culture cannot be underestimated. Notch is a transmembrane protein acts as a receptor for ligands including Delta-Like 1, 2, 3, 4, Jag1 and Jag2 on the surface of a adjacent cells. The binding of ligand leads to a proteolytic cleavage of Notch by γ-secretase. This releases the Notch intracellular domain (NICD), which translocates to the nucleus and switches transcription

repressor, CSL into transcription activator induces the expression of downtream target genes including NF-κβ, cyclin D1, c-myc, AKT, m-TOR, VEGF and transcription facors of Hes and Hey family[292]. In a normal cell, Notch signalling plays a crucial role in the process of development, but the association of Notch-activation with stemness, EMT and drug resistance has been described in several solid and blood cancers[293]. Although the effect of Notch signalling in angiogenesis in breast tumor has been investigated[294] the resulting growth arrest and suppression of the expression of mesenchymal stem cell surface marker CD90 in BCCs due to the inhibition of γ-secretase in the co-culture incorporating MSCs[74], confirms the proliferation and mesenchymal-like phenotype inducing capacity of MSCs in BCCs through Notch pathway. Hence, a comparative inhibition studies targetting Notch signalling and the paracrine axes may be an unique chance to observe the most robust approach by which MSCs promote proliferation, EMT and invasion in DCIS BC subtypes.

Conclusions

BC is a complex disease and MSCs may play a crucial role in BCC proliferation, EMT and invasion in direct 2D and spheroid co-culture system. Therefore, further detailed analysis of MSC-exerted paracrine signalling is required in order to understand the underlying mechanism responsible for BCC proliferation, EMT and invasion in the co-culture models. In parallel, comparative studies between signalling axes resulting from physical and paracrine interactions in 2D and spheroid co-culture of standard BC-cell lines and PDXs are essential in order to identify most suitable therapeutic targets for advanced BC-cases. Such studies may also

shed light on the influence of BCCs on MSC recruitment and maintenance highlighting additional potential therapeutic approaches.

CHAPTER 8: APPENDICES

8.1 Appendix A: Validation of *in situ* hybridisation (ISH) for luciferase and vimentin in xenografts

Aim: In order to investigate the retention of MSCs and to differentiate between the vimentin-positive cells in the core of spheroid co-culture models, xenograft tissue (CSU1613) of luciferase-labelled MDA-MB-231 (MDA-MB-231Fluc) was used for validating the *in situ* hybridisation (ISH) staining for luciferase and vimentin.

Materials and methods:

Deparaffinisation of slides: Xenograft tissues of luciferase-labelled MDA-MB-231 were fixed in 4% paraformaldehyde (PFA) for 24 hours (16-32 hours is recommended for ISH) and paraffin-embedded by following the standard laboratory protocol. Next, 5um sections of embedded-block of the tissues were prepared on superfrost slides. Once dried, slides were deparaffinised in xylene (2 baths for 5 mins each) and transferred into fresh 95% ethanol (2 baths for 1 min. each), and left for air-drying at room temperature.

ISH staining for luciferase and vimentin using RNAscope® 2.5 Assay system from Advanced Cell Diagnostics (ACD): ISH staining was performed by following the manufacturer protocol classified into Part A and Part B. While the Part A characterises with deparaffinisation, dehydration, and drying, Part B characterises with the staining.

Part A: In order to exhaust the endogenous peroxidase, tissue sections were treated with RNAscope® hydrogen peroxide for 10

minutes. Following washing, tissue sections were processed for 30 minutes at 98^0C for antigen retrieval using RNAscope® Target retrieval reagent and then washed in cold distilled water for 3-5 times followed by 100% ethanol wash and air dry at room temperature. Hydrophobic barrier was created surrounding the air-dried sections on the slides and either processed immediately for staining or can be stored in cold room before proceeding into staining in the following day.

Part B: Dried slides were placed on the hybridisation rack (HybEZ™ slide rack) and baked with RNAscope® Protease Plus at 40^0C inside the moist chamber of hybridisation oven (HybEZ™ Oven). After 30 minutes of incubation, slides were washed with distilled water and sections were covered with pre-warmed (40^0C for 10 min in a water bath) RNAscope® Probes for luciferase, vimentin and negative control, and incubated for 2 hours inside the humid hybridisation chamber at 40^0C. Slides were then washed with 1x wash buffer (2 times for 2 min each) at room temperature and incubated sequentially with pre-warmed Hybridize AMP 1 probe (30 min at 40^0C), AMP 2 (15 min at 40^0C), AMP 3 (30 min at 40^0C), AMP 4 (15 min at 40^0C), HRP-labelled AMP 5 (30 min at room temperature) and HRP-labelled AMP 6 (15 min at room temperature). Slides were washed with the wash buffer (2 washes for 2 min each) between each incubation in order to remove excess probe from the previous incubation. In the end, slides were incubated for 10 minutes at room temperature with DAB reagent prepared by mixing of equal volume of RNAscope® 2.5 DAB A and RNAscope® 2.5 DAB B for chromogenic reaction followed by tap water washing and hematoxylin counterstaining. Thereafter, excess hematoxylin was removed by washing under

tap water and slides dehydrated with 70% ethanol for 2 minutes were treated with 95% ethanol (2 bathes for 2 min each) and mounted with cover slip using DPX as a mounting medium.

Results: ISH staining for luciferase in xenografts tissue demonstrated the expression of luciferase in MDA-MB-231 cells, which are confirmed by positive staining of vimentin. Further hematoxylin and eosin staining in the tissue helps differentiating between cancer cells and stromal compartment, which is neither show positive staining for luciferase nor for vimentin. In addition, the absence of stain in the negative control demonstrated the specificity of the target probes to their targets.

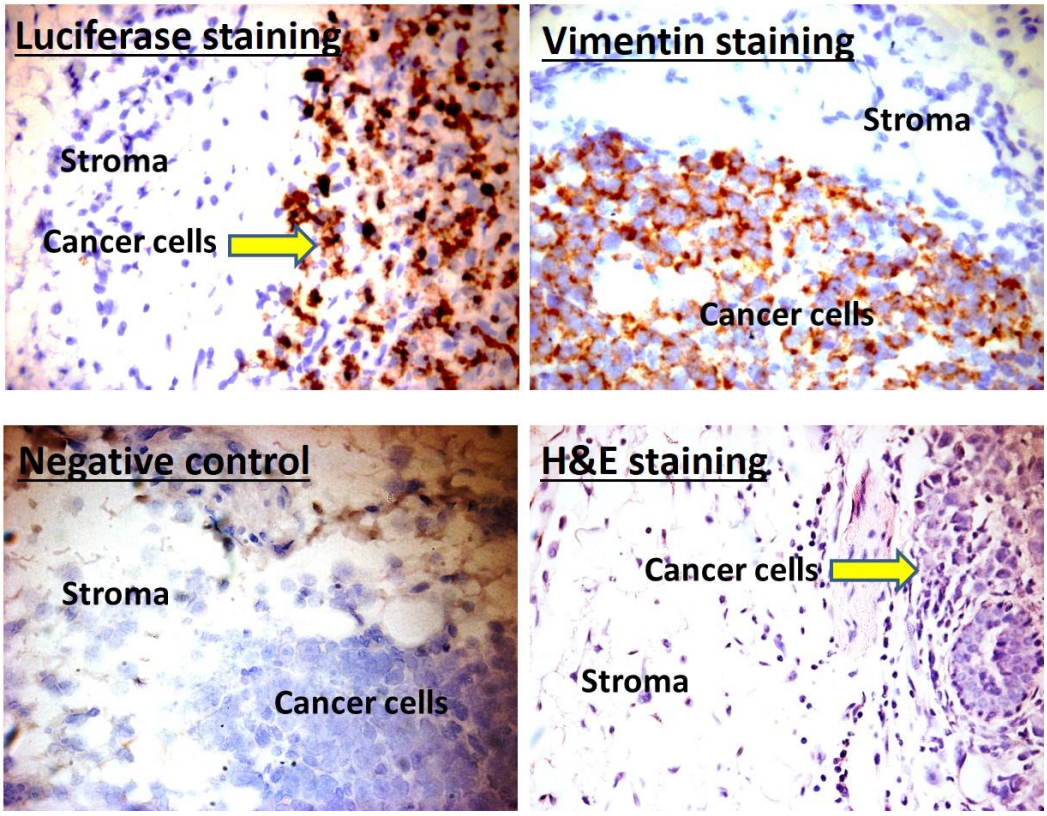

Figure 8-1: ISH staining of luciferase and vimentin in MDA-MB-231 xenografts: Xenograft tissue of MDA-MB-231Fluc was probed against luciferase and vimentin. Targets appeared brown due to chromogenic reaction between Horseradish peroxidase (HRP) and DAB in the staining process. While no such signal was observed in section from same tissue probed with negative

control probe. H&E staining was performed to observe the cancer cells and stromal compartment in the tissue. Images were captured at 40X magnification.

Discussion:

Since characterisation of luciferase and vimentin by ISH demonstrated high specificity of the probes toward their targets in human cancer cells, this xenograft tissue should be included as a positive control while performing ISH in spheroid co-culture of MCF-7 with MSC-Fluc. Later, the ratio of vimentin to luciferase-positive cells in the spheroid co-culture may provide a deeper understanding regarding the vimentin expression of MCF-7 in the core of spheroid co-culture.

Although in this study, the application of ISH is solely dedicated to serve the purpose of investigating the vimentin expression of BCCs in spheroid co-culture, ISH may be further applied in order to identify the growth factor-producing cells in spheroid co-culture. In a co-culture, cell-secreted growth factors present in the culture media can be detected through human cytokine array kit but it is difficult to identify the cell responsible for the production of a specific growth factor in a mixed cell population. Since the probes in ISH are designed for targeting the nucleic acids (DNA and RNA), ISH staining for gene of interest (GOI) may allow in differentiating the cells that produce the target growth factors in co-culture. As well as also help in understanding the nature (paracrine or autocrine) of exerted signalling pathway in BCCs.

8.2 Appendix B: Cytoskeletal reorganisation in MCF-7 in spheroid co-culture

Aim: Phalloidin staining was performed in order to investigate the impact of MSCs on reorganisation of cytoskeletal structure in MCF-7 in spheroid co-culture.

Materials and methods: On day 5, spheroid mono and co-culture of MCF-7tdTomato were harvested from 96 wells ULA plate and transferred to eppendorf tubes separately. Following three washes in PBS, spheroids were fixed in the presence of fixative solution constituted of 4% PFA, 0.3% Triton X-100 and 5% sucrose in PBS. After 10 minutes of incubation, spheroids were washed thrice with PBS in order to avoid the risk of over fixation due to the presence of PFA in the fixative solution. Next, spheroids were incubated for 90 minutes in 200ul of 1x phalloidin solution prepared by diluting 1ul of the stock in 1ml of permeabilisation solution (0.3% Triton X-100 and 5% sucrose in PBS). For negative control, spheroid monoculture was incubated in the permeabilising solution without phalloidin and used as a reference to adjust the exposure time of green channel while imaging the phalloidin-positive sample. 33uM Hoechst 33342 was supplemented in the permeabilising solution to observe the cell nuclei. Meanwhile, hydrophobic barrier was prepared on clean glass slides and 50ul-100ul of Cultrex (6mg/ml) was placed inside the hydrophobic barrier. Glass slides were then incubated at 37^0C allowing Cultrex to polymerise which was confirmed by face-down the slide.

Following incubation of spheroid in 1X phalloidin solution, spheroids were washed with PBS four times to remove unbound dye aiming toward achieving good quality images. Next, spheroids

were placed on the centre top of the polymerised cultrex on the glass slide and incubated for 45mins-60mins at 37^0C to allow cultrex in gripping the spheroid tightly. Each drop of Cultrex should contain no more than one spheroid and while incubation; slides were face-down in order to retain the spheroid in space instead of touching the base of glass slide. Finally, cover slip was mounted with great care over the embedded spheroid and fluorescent images were captured under confocal microscope. The workflow of F-actin staining in spheroid co-culture was borrowed from the previous study where the remodeling of F-actin in invasive cancer cells in 3D model was investigated[295].

Result: MSCs promote invasion in BCCs. Therefore, in spheroid co-culture F-actin-reorganisation in MCF-7 was investigated. Phalloidin staining of spheroid monoculture showed a honeycomb structure resulting from well differentiated epithelial structure of MCF-7 cells and F-actin resided at the plasma membrane surrounding the cells while the nuclei in the middle. Since cells in spheroid experience gradients of oxygen and nutrients, separate images were captured for cells located inside and outside the spheroid core. Consistency in cell-geometry apparently demonstrated no differences in cells at corresponding locations in spheroid monoculture. In contrast, arrangement of F-actin in MCF-7 altered in spheroid co-culture. In addition, acquisition of a spindle shape demonstrated loss of epithelial characteristics in MCF-7 results in destruction of honeycomb structure in spheroid co-culture. Since reorganisation of F-actin is one of the features in cells undergoing EMTs[241], Phalloidin staining provide additional clues regarding the EMT-inducing property of MSCs. Further, the signal in the red channel confirms the coexistence of MCF-7 and

MSCs inside the spheroid core and the cell-cell interaction in cancer cells seems severely compromised compared to the cancer cells outside the edge. The variable difference of cell-cell interaction inside and outside core of spheroid co-culture may be artefactual as MSCs possibly acts as a barrier influencing the proximity between cancer cells inside the core. In contrast, the spheroid edge is dominated by cancer cells and therefore, cancer cells remain close to each other, even though the arrangement of F-actin was altered.

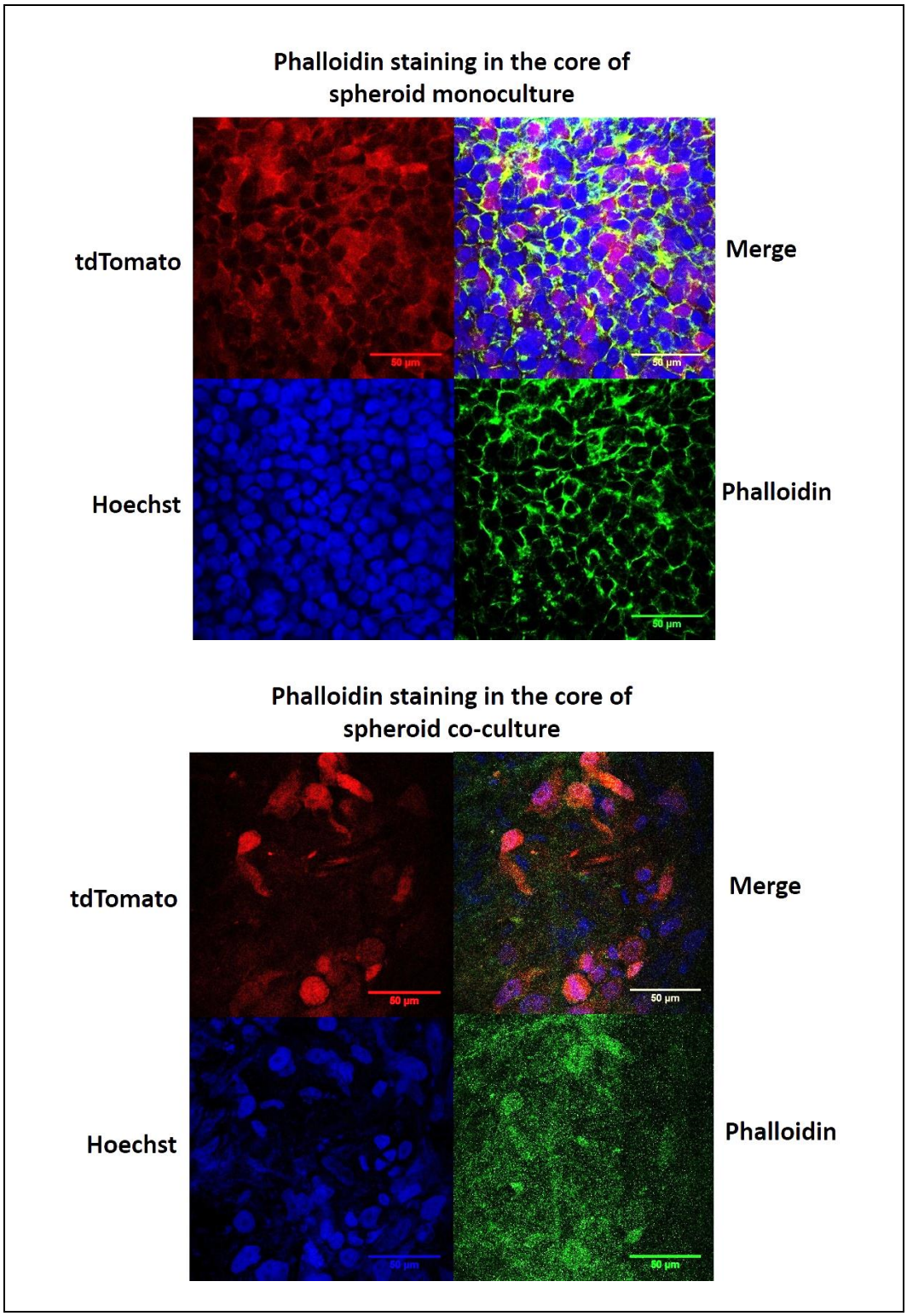

Figure 8-2: Phalloidin staining for F-actin distribution in cells inside spheroid core: Spheroid mono and co-culture were stained with phalloidin to investigate the impact of MSCs on F-actin reorganisation in MCF-7. MCF-7 cells

appeared red because of the expression of tdTomato gene transduced by viral transduction. Phalloidin stains F-actin green while the cell nuclei appeared blue because of Hoechst. Z-stack confocal images were captured under 40x objectives.

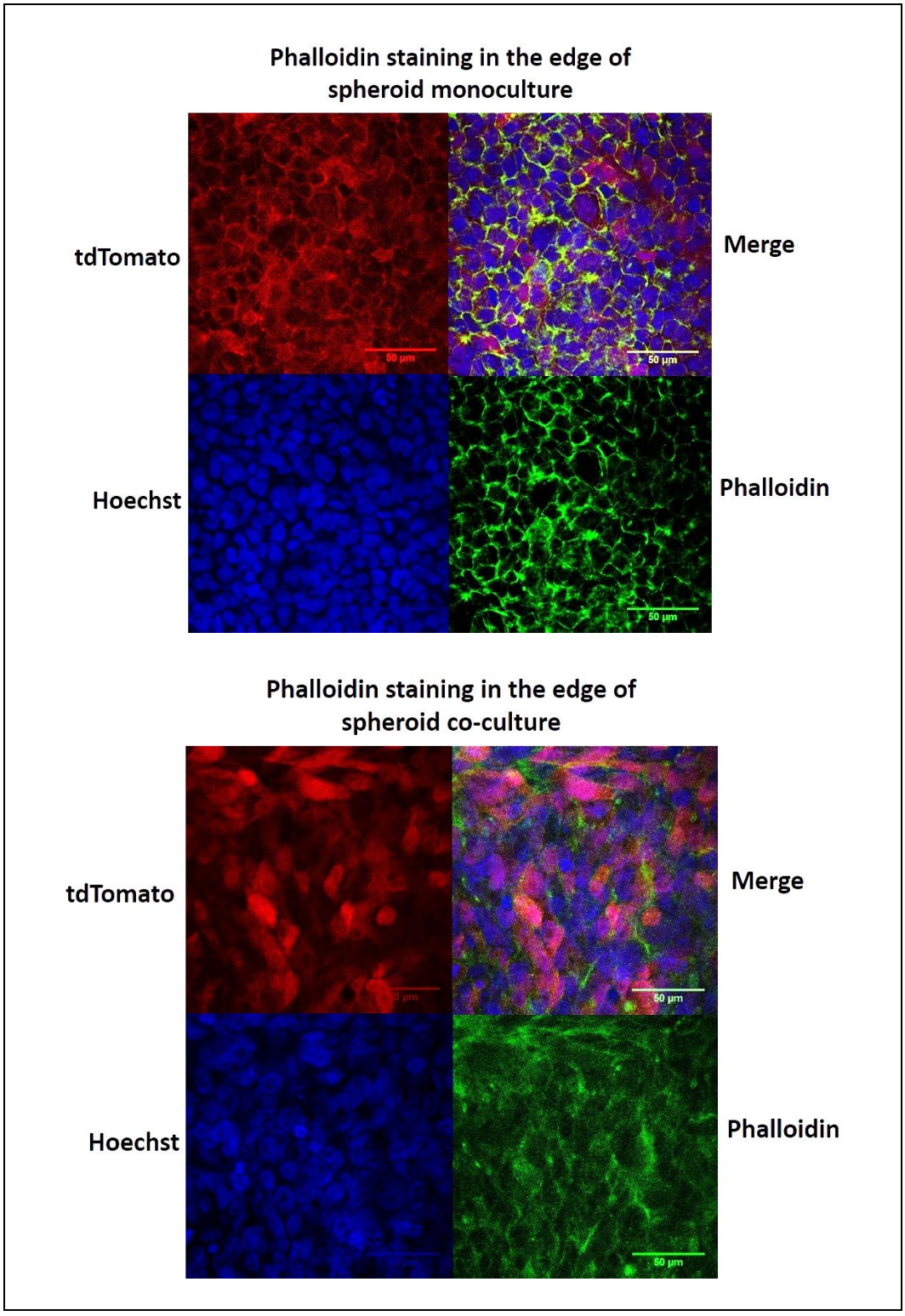

Figure 8-3: Phalloidin staining for F-actin distribution in cells outside spheroid core: Spheroid mono and co-culture were stained with phalloidin to investigate the impact of MSCs on F-actin reorganisation in MCF-7. MCF-7 cells appeared red because of the expression of tdTomato gene transduced by viral transduction. Phalloidin stains F-actin green while the cell nuclei appeared blue because of Hoechst. Z-stack confocal images were captured under 40x objectives.

Discussion:

Rho A is a cytoskeletal regulatory protein associates with the formation of F-actin/stress fibre. In the course of EMT, activation of Rho A promotes cell migration through remodelling of actin filaments. While administration of actin depolymerisation substance reinstates the epithelial structure in EMT cells[296]. Therefore, along with analysing the MSC-secreted paracrine factors responsible for BCC proliferation and EMT, targeting upstream signalling molecule associates with cytoskeletal reorganisation may suppress MSC-driven invasion of BCCs in co-culture.

Along with understanding the influence of MSCs on F-actin arrangement in MCF-7, this study provides an insight to answer a critical argument raised regarding the vimentin-positive cells inside the core of spheroid co-culture. Since BCCs inside the core are spindle shaped, it seems there is a possibility of mixed vimentin-positive cell population instead of MSCs alone. In contrast, absence of vimentin in the cells outside the core of spheroid co-culture determined from IHC but phenotypic switch in cancer cells suggests the possibility of the presence of other EMT markers.

Studies suggest acquisition of stemness occurs in a small population of cancer cells in a tumor and accompanied with the

expression of vimentin and stem cell markers including Nanog, Sox2 and Oct4[196]. Since MSCs are the predominant cell-type in the core of spheroid co-culture, investigation of expression of stem cell markers in this small population of co-existing cancer cells may provide a novel understanding regarding the stemness-inducing property of MSCs in BCCs in a 3D setting.

8.3 Appendix C: Lentivirus transduction for constitutive expression of tdTomato, Firefly luciferase (Fluc) and e-GFP in mammalian cells

Aim: Standard BCC lines and MSCs were stably transduced with Fluc, tdTomato and e-GFP in order to serve the objectives including growth kinetic assay of BCCs in co-culture, FACS sorting of BCCs from co-culture, and characterisation of BCCs and MSCs in co-culture.

Materials and methods:

Constructs of e-GFP, Fluc and tdTomato: Stable transductions of e-GFP, Fluc and tdTomato were performed by following the principle of lentiviral infections where attenuated virus particles act as a vehicle for inserting the plasmids carrying the gene of interest (GOI) in target cells. The details of each construct are attached at the end of the thesis.

GOI	Plasmid carrying GOI	Provider of plasmids
e-GFP	LVX-eGFP	Teresa Coughlan
tdTomato	LVX-Tomato	
Fluc	LVX-Luc	

Table 8-1: Plasmids carrying the gene of interest (GOI) for constitutive expression of e-GFP, tdTomato, and Fluc on lentivirus infection in mammalian cells.

Lentivirus-mediated transduction of the plasmids in cells: Lentivirus-mediated transduction was performed using Lenti-X™ 293T cell line (#632180) from Takara. HEK 293 is a human embryonic kidney cell line used for producing virus and grown in Tetracyclin-free FBS. Following is the workflow of lentiviral production, followed by transduction of GOI in target cells:

Day before transfection:

Plate out 4-5x10^6 LentiX HEK293T Cells in 100mm tissue culture plate, in 10 ml media and incubated until they reach 80-90% confluence.

Day of Transfection:

Transfection of plasmid DNA into HEK293T cells was performed using Xfect™ transfect reagent (Xfect Polymer + Xfect Reaction buffer) (# 631318) from Takara. Transfection was performed by following the workflow described below:

- Thoroughly vortex Xfect Polymer.
- Two eppendorf tubes were prepared as follows:

Tube 1 (Plasmid DNA)	Tube 2 (Polymer)
557ul Xfect reaction buffer 36µl Lenti X HTX Packaging Mix 7µl Lenti-X Vector DNA (1µg/µl)	592.5µl Xfect Reaction Buffer 7.5µl Xfect Polymer

- Vortex each tube well to mix.
- Add polymer solution (tube 2) to the DNA solution (tube 1).
- Vortex at medium speed for 10 seconds.

- Incubate DNA-Xfect mixture for 10 minutes at room temperature.
- Add ALL of the 1200µl DNA-Xfect solution dropwise onto the cultured LentiX HEK293T cells – a slight change in media-color is normal.
- Incubate the plate at 37°C.
- After a minimum of 4 hours replace transfection media with 10ml fresh growth media (Tet system approved FBS).
- Incubate at 37^0C for 48 hours.
- Harvest lentiviral supernatants.
- Centrifuge briefly (500g for 10 minutes).
- Verify virus production with Go-Stix.
- Store Virus at -80°C.

Determining Lentiviral Titre with Go-Stix

- Remove 10µl of virus.
- Drop onto the sample window.
- Add 4 drops of chase buffer.
- Wait for up to 10 minutes.
- Control line should light up when and a line should be visible for the titre.

Transducing Target Cells

- Plate target cells day before transduction at $3x10^5$ cells/well in a 6 well plate.
- Thaw aliquots of virus, mixing gently, but do not vortex.
- Adjust volume of medium in the target cell cultures to accommodate the addition of virus and polybrene – we use a final concentration of 8µg/ml.
- Lentiviral stock was diluted to obtain correct MOI. Typically, 1 & 3 MOI are used for transduction.

- Add supernatant to the cells, and transducer for 24 hours.
- Remove and discard the media and replace with fresh media.
- Incubate cells for 24-48 hours.
- Proceed to selection (puromycin typically) and expansion of cell lines.

8.4 Appendix D: Symposiums and workshops

- Delivered an oral presentation at Nottingham Breast Cancer Research Center (NBCRC conference) on 14th May 2019.
- Presented a Scientific poster at EACR conference (European Association of Cancer Research) of Mechanisms to Therapies on 9th October 2018.
- Delivered talk based on a selected abstract at BACR (British Association of Cancer Research) student conference in Francis Crick Institute on 8th October 2018.
- Delivered talk at CRN symposium (Cancer Research Nottingham) on 19th September 2018.
- Delivered an oral presentation at Sue Watson on 27th March 2018 at City Hospital, University of Nottingham.
- Presented scientific poster at BACR Tumor microenvironment conference and 3D workshop on 14th June 2017.
- Delivered short talk and presented scientific poster at Faculty Postgraduate Research Forum (Medicine and Health Sciences Faculty) on 29th June 2016.

8.5 Appendix E: Certifications

- Vice chancellor scholarship (December 2015 to December 2018).
- Best PhD research Student talk at the NBCRC symposium

(2019).

- BACR and EACR membership (February 2017 to 2019).

8.6 Appendix F: Planned publication

Title: *Spheroid co-culture studies investigating the role of mesenchymal stem cells in breast cancer progression*.

8.7 References

1. Boyle, P. The globalisation of cancer. *Lancet* **368**, 629–630 (2006).

2. Li, Q. *et al.* 3D Models of Epithelial-Mesenchymal Transition in Breast Cancer Metastasis: High-Throughput Screening Assay Development, Validation, and Pilot Screen. *J. Biomol. Screen.* **16**, 141–154 (2011).

3. Allred, D. C. Ductal Carcinoma In Situ: Terminology, Classification, and Natural History. *JNCI Monogr.* **2010**, 134–138 (2010).

4. Malhotra, G. K., Zhao, X., Band, H. & Band, V. Histological, molecular and functional subtypes of breast cancers. *Cancer Biol. Ther.* **10**, 955–960 (2010).

5. Shoker & Sloane. DCIS grading schemes and clinical implications. *Histopathology* **35**, 393–400 (1999).

6. Shawarby, M., Al-Tamimi, D. & Ahmed, A. Molecular classification of breast cancer: An overview with emphasis on ethnic variations and future perspectives. *Saudi J. Med. Med. Sci.* **1**, 14 (2013).

7. Aktaş, S., Eliyatkin, N., Vardar, E., Zengel, B. & Yalcin, E. Molecular Classification of Breast Carcinoma: From Traditional, Old-Fashioned Way to A New Age, and A New Way. *J. Breast Heal.* **11**, 59–66 (2015).

8. Eliyatkin, N., Yalcin, E., Zengel, B., Aktaş, S. & Vardar, E. Molecular Classification of Breast Carcinoma: From Traditional, Old-Fashioned Way to A New Age, and A New Way. *J. Breast Heal.* **11**, 59–66 (2015).

9. Liu, Z., Zhang, X.-S. & Zhang, S. Breast tumor subgroups reveal diverse clinical prognostic power. *Sci. Rep.* **4**, (2014).

10. Elkablawy, M. A. *et al.* Ki67 expression in breast cancer: Correlation with prognostic markers and clinicopathological parameters in Saudi patients. *Saudi Med. J.* **37**, 137–141 (2016).

11. Nishimura, R. *et al.* Ki-67 as a prognostic marker according to breast cancer subtype and a predictor of recurrence time in primary breast cancer. *Exp. Ther. Med.* **1**, 747–754 (2010).

12. Masoud, V. & Pagès, G. Targeted therapies in breast cancer: New challenges to fight against resistance. *World J. Clin. Oncol.* **8**, 120 (2017).

13. Allred, D. C. *et al.* Ductal Carcinoma In situ and the Emergence of Diversity during Breast Cancer Evolution. *Clin. Cancer Res.* **14**, 370–378 (2008).

14. Liu, F., Gu, L.-N., Shan, B.-E., Geng, C.-Z. & Sang, M.-X. Biomarkers for EMT and MET in breast cancer: An update. *Oncol. Lett.* **12**, 4869–4876 (2016).

15. Bissell, M. J., Radisky, D. C. & Nistico, P. Epithelial-Mesenchymal Transition : General Principles and Pathological Relevance with Special Emphasis on the Role of Matrix Metalloproteinases. *Cold Spring Harb. Perspect. Biol.* **4**, 1–12 (2016).

16. Foroni, C., Broggini, M., Generali, D. & Damia, G. Epithelial–mesenchymal transition and breast cancer: Role, molecular mechanisms and clinical impact. *Cancer Treat. Rev.* **38**, 689–697 (2012).

17. Balkwill, F. R., Capasso, M. & Hagemann, T. The tumor microenvironment at a glance. *J. Cell Sci.* **125**, 5591–5596 (2012).

18. Li, H., Fan, X. & Houghton, J. Tumor microenvironment: The role of the tumor stroma in cancer. *J. Cell. Biochem.* **101**, 805–815 (2007).

19. Dmitry I. Gabrilovich1 & Srinivas Nagaraj1. Myeloid-derived suppressor cells as regulators of the immune system. *Nat. Rev. Immunol.* (2009). doi:10.1038/nri2506

20. Foo, J. *et al.* The Impact of Microenvironmental Heterogeneity on the Evolution of Drug Resistance in Cancer Cells. *Cancer Inform.* 19 (2015). doi:10.4137/CIN.S19338

21. Vona-Davis, L. *et al.* Triple-Negative Breast Cancer and Obesity in a Rural Appalachian Population. *Cancer*

Epidemiol. Biomarkers Prev. **17**, 3319–3324 (2008).

22. Carter, J. C. & Church, F. C. Mature breast adipocytes promote breast cancer cell motility. *Exp. Mol. Pathol.* **92**, 312–317 (2012).

23. Gyamfi, J., Eom, M., Koo, J.-S. & Choi, J. Multifaceted Roles of Interleukin-6 in Adipocyte–Breast Cancer Cell Interaction. *Transl. Oncol.* **11**, 275–285 (2018).

24. Mordoh, J. & Levy, E. M. Biological role of NK cells and immunotherapeutic approaches in breast cancer. **3**, (2012).

25. Hoffmann, C. C. & Garner, W. L. Human Breast Cancer and Impaired NK Cell Function. **66**, 64–66 (1983).

26. Murdoch, C., Giannoudis, A. & Lewis, C. E. Mechanisms regulating the recruitment of macrophages into hypoxic areas of tumors and other ischemic tissues. *Blood* **104**, 2224–2234 (2004).

27. Quail, D. & Joyce, J. Microenvironmental regulation of tumor progression and metastasis. *Nat. Med.* **19**, 1423–1437 (2013).

28. Qiu, S.-Q. *et al.* Tumor-associated macrophages in breast cancer: Innocent bystander or important player? *Cancer Treat. Rev.* **70**, 178–189 (2018).

29. Lewis, C. & Murdoch, C. Macrophage responses to hypoxia: implications for tumor progression and anti-cancer therapies. *Am. J. Pathol.* **167**, 627–35 (2005).

30. Popovic, P. J., Zeh, H. J. & Ochoa, J. B. Arginine and immunity. *J. Nutr.* **137**, 1681S-1686S (2007).

31. Hoechst, B. *et al.* A New Population of Myeloid-Derived Suppressor Cells in Hepatocellular Carcinoma Patients Induces CD4+CD25+Foxp3+ T Cells. *Gastroenterology* **135**, 234–243 (2008).

32. S. Cole, A. Montero, E. Garret-Mayer, G. Onicescu, T. Vandenberg, S. Hutchens, and C. D.-M. Elevated Circulating Myeloid Derived Suppressor Cells (MDSC) Are Associated with Inferior Overall Survival (OS) and Correlate with Circulating Tumor Cells (CTC) in Patients with Metastatic Breast Cancer. *Cancer Res.* (2009).

doi:10.1158/0008-5472

33. Bruchard, M. *et al.* Chemotherapy-triggered cathepsin B release in myeloid-derived suppressor cells activates the Nlrp3 inflammasome and promotes tumor growth. *Nat. Med.* **19**, 57–64 (2013).

34. Dudley, A. C. Tumor Endothelial Cells. *Cold Spring Harb. Perspect. Med.* **2**, a006536–a006536 (2012).

35. Hoeben, A. *et al.* Vascular endothelial growth factor and angiogenesis. *Pharmacol. Rev.* **56**, 549–580 (2004).

36. Hirschi, K. K. & D'Amore, P. A. Pericytes in the microvasculature. *Cardiovasc. Res.* **32**, 687–98 (1996).

37. Patan, S. *et al.* Vascular morphogenesis and remodeling in a human tumor xenograft: blood vessel formation and growth after ovariectomy and tumor implantation. *Circ. Res.* **89**, 732–9 (2001).

38. Medici, D. *et al.* Conversion of vascular endothelial cells into multipotent stem-like cells. *Nat. Med.* **16**, 1400–1406 (2010).

39. Bergers, G. & Song, S. The role of pericytes in blood-vessel formation and maintenance. *Neuro. Oncol.* **7**, 452–464 (2005).

40. Frances R. Balkwill. The tumor microenvironment at a glance. *J. Cell Sci.* (2012). doi:10.1242/jcs.116392

41. Cooke, V. G. *et al.* Pericyte Depletion Results in Hypoxia-Associated Epithelial-to-Mesenchymal Transition and Metastasis Mediated by Met Signaling Pathway. *Cancer Cell* **21**, 66–81 (2012).

42. Frantz, C., Stewart, K. M. & Weaver, V. M. The extracellular matrix at a glance. *J. Cell Sci.* **123**, 4195–4200 (2010).

43. Bosman, F. T. & Stamenkovic, I. Functional structure and composition of the extracellular matrix. *J. Pathol.* **200**, 423–428 (2003).

44. Nanda, D. P. *et al.* Matrix metalloproteinase-9 as a potential tumor marker in breast cancer. *J. Environ. Pathol. Toxicol. Oncol.* **32**, 115–29 (2013).

45. Giussani, M., Merlino, G., Cappelletti, V., Tagliabue, E. & Daidone, M. G. Tumor-extracellular matrix interactions: Identification of tools associated with breast cancer progression. *Semin. Cancer Biol.* **35**, 3–10 (2015).

46. Pellegrini, L., Burke, D. F., von Delft, F., Mulloy, B. & Blundell, T. L. Crystal structure of fibroblast growth factor receptor ectodomain bound to ligand and heparin. *Nature* **407**, 1029–34 (2000).

47. Bade, L. K., Goldberg, J. E., Dehut, H. a, Hall, M. K. & Schwertfeger, K. L. Mammary tumorigenesis induced by fibroblast growth factor receptor 1 requires activation of the epidermal growth factor receptor. *J. Cell Sci.* **124**, 3106–17 (2011).

48. Tang, L. & Han, X. The urokinase plasminogen activator system in breast cancer invasion and metastasis. *Biomed. Pharmacother. = Biomédecine pharmacothérapie* **67**, 179–82 (2013).

49. Mao, Y., Keller, E. T., Garfield, D. H., Shen, K. & Wang, J. Stromal cells in tumor microenvironment and breast cancer. *Cancer Metastasis Rev.* **32**, 303–15 (2013).

50. Desmoulière, A., Guyot, C. & Gabbiani, G. The stroma reaction myofibroblast: A key player in the control of tumor cell behavior. *Int. J. Dev. Biol.* **48**, 509–517 (2004).

51. Weber, C. E. *et al.* Osteopontin mediates an MZF1-TGF-β1-dependent transformation of mesenchymal stem cells into cancer-associated fibroblasts in breast cancer. *Oncogene* **34**, 4821–33 (2015).

52. Kraman, M. *et al.* Suppression of Antitumor Immunity by Stromal Cells Expressing Fibroblast Activation Protein-. *Science (80-.).* **330**, 827–830 (2010).

53. Fang, J. *et al.* A potent immunotoxin targeting fibroblast activation protein for treatment of breast cancer in mice. *Int. J. Cancer* **138**, 1013–23 (2016).

54. Cirri, P. & Chiarugi, P. Cancer associated fibroblasts: the dark side of the coin. *Am. J. Cancer Res.* **1**, 482–97 (2011).

55. Jackson, W. M., Nesti, L. J. & Tuan, R. S. Mesenchymal stem cell therapy for attenuation of scar formation during

wound healing. *Stem Cell Res. Ther.* **3**, 20 (2012).

56. Tanabe, S. Role of mesenchymal stem cells in cell life and their signaling. *World J. Stem Cells* **6**, 24 (2014).

57. Chamberlain, G., Fox, J., Ashton, B. & Middleton, J. Concise Review: Mesenchymal Stem Cells: Their Phenotype, Differentiation Capacity, Immunological Features, and Potential for Homing. *Stem Cells* **25**, 2739–2749 (2007).

58. Ling, L., Nurcombe, V. & Cool, S. M. Wnt signaling controls the fate of mesenchymal stem cells. *Gene* **433**, 1–7 (2009).

59. Ridge, S. M., Sullivan, F. J. & Glynn, S. A. Mesenchymal stem cells: key players in cancer progression. *Mol. Cancer* **16**, 31 (2017).

60. Karnoub, A. E. *et al.* Mesenchymal stem cells within tumour stroma promote breast cancer metastasis. *Nature* **449**, 557–563 (2007).

61. Cheng, J. *et al.* The role of mesenchymal stem cells in promoting the transformation of androgen-dependent human prostate cancer cells into androgen-independent manner. *Sci. Rep.* **6**, 1–10 (2016).

62. Chen, B. *et al.* Human Bone Marrow Mesenchymal Stem Cells Promote Gastric Cancer Growth via Regulating c-Myc. *Stem Cells Int.* **2018**, 9501747 (2018).

63. Ramsay, D. T., Kent, J. C., Hartmann, R. A. & Hartmann, P. E. Anatomy of the lactating human breast redefined with ultrasound imaging. *J. Anat.* **206**, 525–534 (2005).

64. Brisken, C. & O'Malley, B. Hormone action in the mammary gland. *Cold Spring Harb. Perspect. Biol.* **2**, a003178 (2010).

65. Rosen, J. M. & Roarty, K. Paracrine signaling in mammary gland development: what can we learn about intratumoral heterogeneity? *Breast Cancer Res.* **16**, 202 (2014).

66. Watson, C. J. & Khaled, W. T. Mammary development in the embryo and adult: a journey of morphogenesis and commitment. *Development* **135**, 995–1003 (2008).

67. Robinson, G. W. Cooperation of signalling pathways in embryonic mammary gland development. *Nat. Rev. Genet.*

8, 963–972 (2007).

68. Hennighausen, L. & Robinson, G. W. Signaling Pathways in Mammary Gland Development. *Dev. Cell* **1**, 467–475 (2001).

69. Javed, A. & Lteif, A. Development of the human breast. *Semin. Plast. Surg.* **27**, 5–12 (2013).

70. Räsänen, K. & Herlyn, M. Paracrine signaling between carcinoma cells and mesenchymal stem cells generates cancer stem cell niche via epithelial-mesenchymal transition. *Cancer Discov.* **2**, 775–777 (2012).

71. Yagi, H. & Kitagawa, Y. The role of mesenchymal stem cells in cancer development. *Front. Genet.* **4**, 1–6 (2013).

72. Cuiffo, B. G. & Karnoub, A. E. Mesenchymal stem cells in tumor development. *Cell Adh. Migr.* **6**, 220–230 (2012).

73. Ullah, I., Subbarao, R. B. & Rho, G. J. Human mesenchymal stem cells - current trends and future prospective. *Biosci. Rep.* **35**, 1–18 (2015).

74. Melzer, C., Yang, Y. & Hass, R. Interaction of MSC with tumor cells. *Cell Commun. Signal.* **14**, 20 (2016).

75. Martin, F. T. *et al.* Potential role of mesenchymal stem cells (MSCs) in the breast tumour microenvironment: stimulation of epithelial to mesenchymal transition (EMT). *Breast Cancer Res. Treat.* **124**, 317–326 (2010).

76. Kwon, H. M. *et al.* Multiple paracrine factors secreted by mesenchymal stem cells contribute to angiogenesis. *Vascul. Pharmacol.* **63**, 19–28 (2014).

77. Coussens, L. M. & Werb, Z. Inflammation and cancer. *Nature* **420**, 860–867 (2002).

78. Karagiannis, G. S. *et al.* Cancer-Associated Fibroblasts Drive the Progression of Metastasis through both Paracrine and Mechanical Pressure on Cancer Tissue. *Mol. Cancer Res.* **10**, 1403–1418 (2012).

79. Weber, C. E. *et al.* Osteopontin mediates an MZF1-TGF-β1-dependent transformation of mesenchymal stem cells into cancer-associated fibroblasts in breast cancer. *Oncogene* **34**, 4821–33 (2015).

80. De Veirman, K. *et al.* Cancer Associated Fibroblasts and Tumor Growth: Focus on Multiple Myeloma. *Cancers (Basel).* **6**, 1363–1381 (2014).

81. Orimo, A. *et al.* Stromal Fibroblasts Present in Invasive Human Breast Carcinomas Promote Tumor Growth and Angiogenesis through Elevated SDF-1/CXCL12 Secretion. *Cell* **121**, 335–348 (2005).

82. Karnoub, A. E. *et al.* Mesenchymal stem cells within tumour stroma promote breast cancer metastasis. *Nature* **449**, 557–63 (2007).

83. Green, J. L. *et al.* Paracrine Wnt signaling both promotes and inhibits human breast tumor growth. *Proc. Natl. Acad. Sci.* **110**, 6991–6996 (2013).

84. Noh, M. Interleukin-17A increases leptin production in human bone marrow mesenchymal stem cells. *Biochem. Pharmacol.* **83**, 661–670 (2012).

85. Zhao, X. P. *et al.* Transforming growth factor-B1 upregulates the expression of CXC chemokine receptor 4 (CXCR4) in human breast cancer MCF-7 cells. *Acta Pharmacol. Sin.* **31**, 347–354 (2010).

86. Huang, S. *et al.* HGF-induced PKCζ activation increases functional CXCR4 expression in human breast cancer cells. *PLoS One* **7**, (2012).

87. Cabioglu, N. *et al.* CXCL-12/Stromal Cell–Derived Factor-1α Transactivates HER2-neu in Breast Cancer Cells by a Novel Pathway Involving Src Kinase Activation. *Cancer Res.* **65**, 6493–6497 (2005).

88. Mukherjee, D. & Zhao, J. The Role of chemokine receptor CXCR4 in breast cancer metastasis. *Am. J. Cancer Res.* **3**, 46–57 (2013).

89. Lo, H. W. & Ali-Osman, F. Cyclic AMP mediated GSTP1 gene activation in tumor cells involves the interaction of activated CREB-1 with the GSTP1 CRE: A novel mechanism of cellular GSTP1 gene regulation. *J. Cell. Biochem.* **87**, 103–116 (2002).

90. Clarke, M. R., Imhoff, F. M. & Baird, S. K. Mesenchymal stem cells inhibit breast cancer cell migration and invasion

through secretion of tissue inhibitor of metalloproteinase-1 and -2. *Mol. Carcinog.* **54**, 1214–1219 (2015).

91. Salazar, K. D., Lankford, S. M. & Brody, A. R. Mesenchymal stem cells produce Wnt isoforms and TGF- 1 that mediate proliferation and procollagen expression by lung fibroblasts. *AJP Lung Cell. Mol. Physiol.* **297**, L1002–L1011 (2009).

92. Scaltriti, M. The Epidermal Growth Factor Receptor Pathway : A Model for T argeted Therapy. **12**, 5268–5273 (2006).

93. Kim, J., Kong, J., Chang, H., Kim, H. & Kim, A. EGF induces epithelial-mesenchymal transition through phospho-Smad2/3-Snail signaling pathway in breast cancer cells. *Oncotarget* **7**, (2016).

94. Masuda, H. *et al.* Role of epidermal growth factor receptor in breast cancer. *Breast Cancer Res. Treat.* **136**, 331–345 (2012).

95. Turner, N. & Grose, R. Fibroblast growth factor signalling: from development to cancer. *Nat. Rev. Cancer* **10**, 116–129 (2010).

96. Pond, A. C. *et al.* Fibroblast growth factor receptor signaling dramatically accelerates tumorigenesis and enhances oncoprotein translation in the mouse mammary tumor virus-Wnt-1 mouse model of breast cancer. *Cancer Res.* **70**, 4868–4879 (2010).

97. Nguyen, P. T. *et al.* The FGFR1 inhibitor PD173074 induces mesenchymal–epithelial transition through the transcription factor AP-1. *Br. J. Cancer* **109**, 2248–2258 (2013).

98. EL-Attar, H. & Sheta, M. Hepatocyte growth factor profile with breast cancer. *Indian J. Pathol. Microbiol.* **54**, 509 (2011).

99. You, W.-K. *et al.* Development of antibody-based c-Met inhibitors for targeted cancer therapy. *ImmunoTargets Ther.* 35 (2015). doi:10.2147/ITT.S37409

100. Organ, S. L. & Tsao, M.-S. An overview of the c-MET signaling pathway. *Ther. Adv. Med. Oncol.* **3**, S7–S19 (2011).

101. Zarzynska, J. M. Two Faces of TGF-Beta1 in Breast Cancer. *Mediators Inflamm.* **2014**, 1–16 (2014).

102. Izzi, L. & Attisano, L. Regulation of the TGFbeta signalling pathway by ubiquitin-mediated degradation. *Oncogene* **23**, 2071–8 (2004).

103. Hwangbo, C. *et al.* Syntenin regulates TGF-β1-induced Smad activation and the epithelial-to-mesenchymal transition by inhibiting caveolin-mediated TGF-β type I receptor internalization. *Oncogene* **35**, 389–401 (2016).

104. Neil, E., Justin, M., Teresa, C. & Gabriela, M. TGF- [Beta] Inhibition enhances chemotherapy action against triple-negative breast cancer. **123**, (2013).

105. Polakis, P. Wnt signaling in cancer. *Cold Spring Harb. Perspect. Biol.* **4**, 9 (2012).

106. Clements, W. M., Lowy, A. M. & Groden, J. Adenomatous polyposis coli/beta-catenin interaction and downstream targets: altered gene expression in gastrointestinal tumors. *Clin. Colorectal Cancer* **3**, 113–20 (2003).

107. Sethi, J. K. & Vidal-Puig, A. Wnt signalling and the control of cellular metabolism. *Biochem. J.* **427**, 1–17 (2010).

108. Wang, X. *et al.* The critical role of EGF-β-catenin signaling in the epithelial-mesenchymal transition in human glioblastoma. *Onco. Targets. Ther.* **10**, 2781–2789 (2017).

109. Chen, K. *et al.* Human MSCs promotes colorectal cancer epithelial-mesenchymal transition and progression via CCL5/β-catenin/Slug pathway. *Cell Death Dis.* **8**, e2819 (2017).

110. Le, P. N., McDermott, J. D. & Jimeno, A. Targeting the Wnt pathway in human cancers: Therapeutic targeting with a focus on OMP-54F28. *Pharmacol. Ther.* **146**, 1–11 (2015).

111. Klopocki, E. *et al.* Loss of SFRP1 is associated with breast cancer progression and poor prognosis in early stage tumors. *Int. J. Oncol.* **25**, 641–9 (2004).

112. Xu, L. *et al.* WNT pathway inhibitor pyrvinium pamoate inhibits the self-renewal and metastasis of breast cancer stem cells. *Int. J. Oncol.* (2016).

doi:10.3892/ijo.2016.3337

113. Schlange, T., Matsuda, Y., Lienhard, S., Huber, A. & Hynes, N. E. Autocrine WNT signaling contributes to breast cancer cell proliferation via the canonical WNT pathway and EGFR transactivation. *Breast Cancer Res.* **9**, R63 (2007).

114. Kohli, S. & Kohli, V. Role of RANKL-RANK/osteoprotegerin molecular complex in bone remodeling and its immunopathologic implications. *Indian J. Endocrinol. Metab.* **15**, 175 (2011).

115. Kim, N.-S. *et al.* Survival and Differentiation of Mammary Epithelial Cells in Mammary Gland Development Require Nuclear Retention of Id2 Due to RANK Signaling. *Mol. Cell. Biol.* **31**, 4775–4788 (2011).

116. Thomas, R. J. *et al.* Breast cancer cells interact with osteoblasts to support osteoclast formation. *Endocrinology* **140**, 4451–8 (1999).

117. Tan, W. *et al.* Tumour-infiltrating regulatory T cells stimulate mammary cancer metastasis through RANKL–RANK signalling. *Nature* **470**, 548–553 (2011).

118. González Ricarte, M., Castro Pérez, A. de, Tarín, J. J. & Cano, A. Progestogens and risk of breast cancer: a link between bone and breast? *Gynecol. Endocrinol.* **32**, 6–8 (2016).

119. Horwood, N. J., Elliott, J., Martin, T. J. & Gillespie, M. T. Osteotropic agents regulate the expression of osteoclast differentiation factor and osteoprotegerin in osteoblastic stromal cells. *Endocrinology* **139**, 4743–6 (1998).

120. Burtis, W. J. *et al.* Identification of a novel 17,000-dalton parathyroid hormone-like adenylate cyclase-stimulating protein from a tumor associated with humoral hypercalcemia of malignancy. *J. Biol. Chem.* **262**, 7151–6 (1987).

121. Bundred, N. J. *et al.* Parathyroid hormone related protein and hypercalcaemia in breast cancer. *BMJ* **303**, 1506–9 (1991).

122. Wang, W., Nag, S. A. & Zhang, R. Targeting the NFκB signaling pathways for breast cancer prevention and

therapy. *Curr. Med. Chem.* **22**, 264–89 (2015).

123. Yellowley, C. CXCL12/CXCR4 signaling and other recruitment and homing pathways in fracture repair. *Bonekey Rep.* **2**, (2013).

124. Mukherjee, D. *et al.* Krüppel-like factor 8 activates the transcription of C-X-C cytokine receptor type 4 to promote breast cancer cell invasion, transendothelial migration and metastasis. *Oncotarget* (2016). doi:10.18632/oncotarget.8083

125. Peng, S.-B. *et al.* Identification of LY2510924, a Novel Cyclic Peptide CXCR4 Antagonist That Exhibits Antitumor Activities in Solid Tumor and Breast Cancer Metastatic Models. *Mol. Cancer Ther.* **14**, 480–490 (2015).

126. Zlotnik, A. & Yoshie, O. The Chemokine Superfamily Revisited. *Immunity* **36**, 705–716 (2012).

127. Quint??s-Cardama, A. & Verstovsek, S. Molecular pathways: JAK/STAT pathway: Mutations, inhibitors, and resistance. *Clin. Cancer Res.* **19**, 1933–1940 (2013).

128. Zhou, J. *et al.* Activation of the PTEN/mTOR/STAT3 pathway in breast cancer stem-like cells is required for viability and maintenance. *Proc. Natl. Acad. Sci. U. S. A.* **104**, 16158–16163 (2007).

129. Esquivel-Velázquez, M. *et al.* The Role of Cytokines in Breast Cancer Development and Progression. *J. Interf. Cytokine Res.* **35**, 1–16 (2015).

130. Wang, H. Signal Transducer and Activator of Transcription 3 in Liver Diseases: A Novel Therapeutic Target. *Int. J. Biol. Sci.* 536–550 (2011). doi:10.7150/ijbs.7.536

131. Perera, C. N., Chin, H. G., Duru, N. & Camarillo, I. G. Leptin-regulated gene expression in MCF-7 breast cancer cells: mechanistic insights into leptin-regulated mammary tumor growth and progression. *J. Endocrinol.* **199**, 221–233 (2008).

132. Noh, M. Interleukin-17A increases leptin production in human bone marrow mesenchymal stem cells. *Biochem. Pharmacol.* **83**, 661–670 (2012).

133. Koul, H. K., Pal, M. & Koul, S. Role of p38 MAP Kinase Signal Transduction in Solid Tumors. *Genes Cancer* **4**, 342–359 (2013).

134. Katz, M., Amit, I. & Yarden, Y. Regulation of MAPKs by growth factors and receptor tyrosine kinases. *Biochim. Biophys. Acta - Mol. Cell Res.* **1773**, 1161–1176 (2007).

135. Guyon, A. CXCL12 chemokine and its receptors as major players in the interactions between immune and nervous systems. *Front. Cell. Neurosci.* **8**, 1–10 (2014).

136. Santen, R. J. *et al.* The role of mitogen-activated protein (MAP) kinase in breast cancer. *J. Steroid Biochem. Mol. Biol.* **80**, 239–256 (2002).

137. Azzam, D. G., Tay, J. W. T., Greeve, M. A., Harvey, J. M. & Bentel, J. M. ERK/MAPK Regulation of the Androgen Responsiveness of Breast Cancer Cells. in 429–435 (2008). doi:10.1007/978-0-387-69080-3_41

138. Yun, M.-S. Both ERK and Wnt/ -catenin pathways are involved in Wnt3a-induced proliferation. *J. Cell Sci.* **118**, 313–322 (2005).

139. Hatsell, S., Rowlands, T., Hiremath, M. & Cowin, P. Beta-catenin and Tcfs in mammary development and cancer. *J. Mammary Gland Biol. Neoplasia* **8**, 145–58 (2003).

140. Wang, Z. *et al.* Clinical implications of β-catenin protein expression in breast cancer. *Int. J. Clin. Exp. Pathol.* **8**, 14989–14994 (2015).

141. Lévy, L., Wei, Y., Labalette, C. & Wu, Y. Acetylation of beta-catenin by p300 Regulates beta-catenin-Tcf4 Interaction. *Mol. Cell. Biol.* **24**, 3404–3414 (2004).

142. Zhong, H., Voll, R. E. & Ghosh, S. Phosphorylation of NF-κB p65 by PKA Stimulates Transcriptional Activity by Promoting a Novel Bivalent Interaction with the Coactivator CBP/p300. *Mol. Cell* **1**, 661–671 (1998).

143. Van Laere, S. J. *et al.* NF-κB activation in inflammatory breast cancer is associated with oestrogen receptor downregulation, secondary to EGFR and/or ErbB2 overexpression and MAPK hyperactivation. *Br. J. Cancer* **97**, 659–669 (2007).

144. Helbig, G. *et al.* NF-κB promotes breast cancer cell migration and metastasis by inducing the expression of the chemokine receptor CXCR4. *J. Biol. Chem.* **278**, 21631–21638 (2003).

145. Smith, S. M., Lyu, Y. L. & Cai, L. NF-κB affects proliferation and invasiveness of breast cancer cells by regulating CD44 expression. *PLoS One* **9**, (2014).

146. Tsubaki, M. *et al.* Activation of NF-κB by the RANKL/RANK system up-regulates snail and twist expressions and induces epithelial-to-mesenchymal transition in mammary tumor cell lines. *J. Exp. Clin. Cancer Res.* **32**, 62 (2013).

147. Xu, C., Zhao, H., Chen, H. & Yao, Q. CXCR4 in breast cancer: oncogenic role and therapeutic targeting. *Drug Des. Devel. Ther.* **9**, 4953–4964 (2015).

148. Hou, T., Ray, S., Lee, C. & Brasier, A. R. The STAT3 NH2-terminal domain stabilizes enhanceosome assembly by interacting with the p300 bromodomain. *J. Biol. Chem.* **283**, 30725–30734 (2008).

149. Palianopoulou, M., Papanikolaou, V., Stefanou, N. & Tsezou, A. The activation of leptin-mediated survivin is limited by the inducible suppressor SOCS-3 in MCF-7 cells. *Exp. Biol. Med.* **236**, 70–76 (2011).

150. Banerjee, K. & Resat, H. Constitutive activation of STAT3 in breast cancer cells: A review. *Int. J. Cancer* **138**, 2570–2578 (2016).

151. Nakagawa, T. *et al.* Decreased expression of SOCS-3 mRNA in breast cancer with lymph node metastasis. *Oncol. Rep.* **19**, 33–39 (2008).

152. Ishitani, T. *et al.* letters to nature The TAK1 ± NLK ± MAPK-related pathway antagonizes signalling between b -catenin and transcription factor TCF. **399**, (1999).

153. Komiya, Y. & Habas, R. Wnt signal transduction pathways. *Organogenesis* **4**, 68–75 (2014).

154. Katoh, M. Canonical and non-canonical WNT signaling in cancer stem cells and their niches: Cellular heterogeneity, omics reprogramming, targeted therapy and tumor plasticity (Review). *Int. J. Oncol.* **51**, 1357–1369 (2017).

155. Sugimura, R. & Li, L. Noncanonical Wnt signaling in vertebrate development, stem cells, and diseases. *Birth Defects Res. Part C - Embryo Today Rev.* **90**, 243–256 (2010).

156. Ornitz, D. M. & Itoh, N. The fibroblast growth factor signaling pathway. *Wiley Interdiscip. Rev. Dev. Biol.* **4**, 215–266 (2015).

157. Scaltriti, M. & Baselga, J. The epidermal growth factor receptor pathway: A model for targeted therapy. *Clin. Cancer Res.* **12**, 5268–5272 (2006).

158. Renema, N., Navet, B., Heymann, M.-F., Lezot, F. & Heymann, D. RANK-RANKL signalling in cancer. *Biosci. Rep.* **36**, e00366–e00366 (2016).

159. WÃ¼rth, R., Bajetto, A., Harrison, J. K., Barbieri, F. & Florio, T. CXCL12 modulation of CXCR4 and CXCR7 activity in human glioblastoma stem-like cells and regulation of the tumor microenvironment. *Front. Cell. Neurosci.* **8**, (2014).

160. Sengupta, S., Jana, S., Biswas, S., Mandal, P. K. & Bhattacharyya, A. Cooperative involvement of NFAT and SnoN mediates transforming growth factor-β (TGF-β) induced EMT in metastatic breast cancer (MDA-MB 231) cells. *Clin. Exp. Metastasis* **30**, 1019–1031 (2013).

161. Zhu, Q. *et al.* Dual Role of SnoN in Mammalian Tumorigenesis. *Mol. Cell. Biol.* **27**, 324–339 (2007).

162. Nomura, T. *et al.* Ski is a component of the histone deacetylase complex required for transcriptional repression by Mad and thyroid hormone receptor. *Genes Dev.* **13**, 412–423 (1999).

163. Deheuninck, J. & Lou, K. Ski and SnoN, Potent Negative Regulators of TGF-beta Signalling. *Cell Res.* **19**, 47–57 (2009).

164. Li, J. *et al.* The anti-proliferative function of the tgf-β1 signaling pathway involves the repression of the oncogenic tbx2 by its homologue tbx3. *J. Biol. Chem.* **289**, 35633–35643 (2014).

165. Li, J., Weinberg, M. S., Zerbini, L. & Prince, S. The oncogenic TBX3 is a downstream target and mediator of

the TGF- 1 signaling pathway. *Mol. Biol. Cell* **24**, 3569–3576 (2013).

166. Gervasi, M. *et al.* JunB contributes to Id2 repression and the epithelial–mesenchymal transition in response to transforming growth factor–β. *J. Cell Biol.* **196**, 589–603 (2012).

167. Song, H., Ki, S. H., Kim, S. G. & Moon, A. Activating Transcription Factor 2 Mediates Matrix Metalloproteinase-2 Transcriptional Activation Induced by p38 in Breast Epithelial Cells. *Cancer Res.* **66**, 10487–10496 (2006).

168. Yao, J. *et al.* Multiple signaling pathways involved in activation of matrix metalloproteinase-9 (MMP-9) by heregulin-β1 in human breast cancer cells. *Oncogene* **20**, 8066–8074 (2001).

169. Ibrahim, S. A. *et al.* Hormonal-receptor positive breast cancer: IL-6 augments invasion and lymph node metastasis via stimulating cathepsin B expression. *J. Adv. Res.* **7**, 661–670 (2016).

170. Zhang, L., Wang, H. & Xu, J. Cathepsin S as a cancer target. *Neoplasma* **62**, 16–26 (2015).

171. Karanam, B. *et al.* Multiple Roles for Acetylation in the Interaction of p300 HAT with ATF-2 †. *Biochemistry* **46**, 8207–8216 (2007).

172. Zhan, T., Rindtorff, N. & Boutros, M. Wnt signaling in cancer. *Oncogene* **36**, 1461–1473 (2017).

173. Shi, W. *et al.* Inhibition of IL-6/STAT3 signaling in human cancer cells using Evista. *Biochem. Biophys. Res. Commun.* **491**, 159–165 (2017).

174. Saxena, N. K., Vertino, P. M., Anania, F. A. & Sharma, D. Leptin-induced Growth Stimulation of Breast Cancer Cells Involves Recruitment of Histone Acetyltransferases and Mediator Complex to CYCLIN D1 Promoter via Activation of Stat3. *J. Biol. Chem.* **282**, 13316–13325 (2007).

175. Danny N. Dhanasekaran & E. Premkumar Reddy. JNK signaling in apoptosis. *Oncogene* **27**, 6245–6251 (2008).

176. Olson, J. M. & Hallahan, A. R. p38 MAP kinase: A

convergence point in cancer therapy. *Trends Mol. Med.* **10**, 125–129 (2004).

177. Koul, H. K., Pal, M. & Koul, S. Role of p38 MAP Kinase Signal Transduction in Solid Tumors. *Genes Cancer* **4**, 342–359 (2013).

178. Song, G., Ouyang, G. & Bao, S. The activation of Akt/PKB signaling pathway and cell survival. *J Cell Mol Med* **9**, 59–71 (2005).

179. Farhan, M. *et al.* FOXO signaling pathways as therapeutic targets in cancer. *Int. J. Biol. Sci.* **13**, 815–827 (2017).

180. Hay, N. Interplay between FOXO, TOR, and Akt. *Biochim. Biophys. Acta - Mol. Cell Res.* **1813**, 1965–1970 (2011).

181. Xiao, G.-H. Anti-apoptotic signaling by hepatocyte growth factor/Met via the phosphatidylinositol 3-kinase/Akt and mitogen-activated protein kinase pathways. *Proc. Natl. Acad. Sci.* **98**, 247–252 (2001).

182. Wheler, J. J. *et al.* Presence of both alterations in FGFR/FGF and PI3K/AKT/mTOR confer improved outcomes for patients with metastatic breast cancer treated with PI3K/AKT/mTOR inhibitors. *Oncoscience* **3**, 164 (2016).

183. Cicenas, J. *et al.* Increased level of phosphorylated akt measured by chemiluminescence-linked immunosorbent assay is a predictor of poor prognosis in primary breast cancer overexpressing ErbB-2. *Breast Cancer Res.* **7**, 394–401 (2005).

184. Zhao, M., Mueller, B. M., DiScipio, R. G. & Schraufstatter, I. U. Akt plays an important role in breast cancer cell chemotaxis to CXCL12. *Breast Cancer Res. Treat.* **110**, 211–222 (2008).

185. Lee, B.-C., Lee, T.-H., Avraham, S. & Karsenty Avraham, H. Involvement of the Chemokine Receptor CXCR4 and Its Ligand Stromal Cell-Derived Factor 1-α in Breast Cancer Cell Migration Through Human Brain Microvascular Endothelial Cells. *Mol. Cancer Res.* **2**, 327–38 (2004).

186. Fang, D. *et al.* Phosphorylation of beta-catenin by AKT promotes beta-catenin transcriptional activity. *J. Biol. Chem.* **282**, 11221–11229 (2007).

187. Aggarwal, B. B., Sethi, G., Baladandayuthapani, V., Krishnan, S. & Shishodia, S. Targeting cell signaling pathways for drug discovery: An old lock needs a new key. *J. Cell. Biochem.* **102**, 580–592 (2007).

188. Wong, C. C., Cheng, K.-W. & Rigas, B. Preclinical Predictors of Anticancer Drug Efficacy: Critical Assessment with Emphasis on Whether Nanomolar Potency Should Be Required of Candidate Agents. *J. Pharmacol. Exp. Ther.* **341**, 572–578 (2012).

189. Holder, J. W., Elmore, E. & Barrett, J. C. Gap junction function and cancer. *Cancer Res.* **53**, 3475–85 (1993).

190. Bai, C. *et al.* Associations of chemo- and radio-resistant phenotypes with the gap junction, adhesion and extracellular matrix in a three-dimensional culture model of soft sarcoma. *J. Exp. Clin. Cancer Res.* **34**, 1–10 (2015).

191. Anton, D., Burckel, H., Josset, E. & Noel, G. Three-dimensional cell culture: A breakthrough in vivo. *Int. J. Mol. Sci.* **16**, 5517–5527 (2015).

192. Eales, K. L., Hollinshead, K. E. R. & Tennant, D. A. Hypoxia and metabolic adaptation of cancer cells. *Oncogenesis* **5**, e190 (2016).

193. Fantozzi, A. & Christofori, G. Mouse models of breast cancer metastasis. *Breast Cancer Res.* **8**, 212 (2006).

194. Zhang, Y. *et al.* Establishment of a murine breast tumor model by subcutaneous or orthotopic implantation. *Oncol. Lett.* **15**, 6233–6240 (2018).

195. Dai, L., Lu, C., Yu, X., Dai, L. J. & Zhou, J. X. Construction of orthotopic xenograft mouse models for human pancreatic cancer. *Exp. Ther. Med.* **10**, 1033–1038 (2015).

196. Yang, H. F. *et al.* Fentanyl promotes breast cancer cell stemness and epithelial-mesenchymal transition by upregulating α1, 6-fucosylation via Wnt/β-catenin signaling pathway. *Front. Physiol.* **8**, 1–12 (2017).

197. Khanna, C. Modeling metastasis in vivo. *Carcinogenesis* **26**, 513–523 (2004).

198. Mak, I. W. Y., Evaniew, N. & Ghert, M. Lost in translation:

Animal models and clinical trials in cancer treatment. *Am. J. Transl. Res.* **6**, 114–118 (2014).

199. Dong, X. *et al.* Patient-Derived First Generation Xenografts of Non-Small Cell Lung Cancers: Promising Tools for Predicting Drug Responses for Personalized Chemotherapy. *Clin. Cancer Res.* **16**, 1442–1451 (2010).

200. Zhang, X. & Lewis, M. T. Establishment of Patient-Derived Xenograft (PDX) Models of Human Breast Cancer. in *Current Protocols in Mouse Biology* (John Wiley & Sons, Inc., 2013). doi:10.1002/9780470942390.mo120140

201. Whittle, J. R., Lewis, M. T., Lindeman, G. J. & Visvader, J. E. Patient-derived xenograft models of breast cancer and their predictive power. *Breast Cancer Res.* **17**, 17 (2015).

202. Lai, Y. *et al.* Current status and perspectives of patient-derived xenograft models in cancer research. *J. Hematol. Oncol.* **10**, 1–14 (2017).

203. Jackson, S. J. & Thomas, G. J. Human tissue models in cancer research: Looking beyond the mouse. *DMM Dis. Model. Mech.* **10**, 939–942 (2017).

204. Festing, S. & Wilkinson, R. Talking Point: the ethics of animal research. *EMBO Rep.* (2007). doi:10.1038/sj.embor.7400993

205. Petrelli, N. J., Jia, X. & Farach-carson, M. C. Gursky 2010 3D matrices for anti-cancer Drug testing and Development. (2010).

206. Edmondson, R., Broglie, J. J., Adcock, A. F. & Yang, L. Three-Dimensional Cell Culture Systems and Their Applications in Drug Discovery and Cell-Based Biosensors. *Assay Drug Dev. Technol.* **12**, 207–218 (2014).

207. Tibbitt, M. W. & Anseth, K. S. Hydrogels as extracellular matrix mimics for 3D cell culture. *Biotechnol. Bioeng.* **103**, 655–663 (2009).

208. Kleinman, H. K. & Martin, G. R. Matrigel: Basement membrane matrix with biological activity. *Semin. Cancer Biol.* **15**, 378–386 (2005).

209. Worthington, P., Pochan, D. J. & Langhans, S. A. Peptide

Hydrogels – Versatile Matrices for 3D Cell Culture in Cancer Medicine. *Front. Oncol.* **5**, (2015).

210. Benton, G., Kleinman, H. K., George, J. & Arnaoutova, I. Multiple uses of basement membrane-like matrix (BME/Matrigel) in vitro and in vivo with cancer cells. *Int. J. Cancer* **128**, 1751–1757 (2011).

211. Zanoni, M. *et al.* 3D tumor spheroid models for in vitro therapeutic screening: a systematic approach to enhance the biological relevance of data obtained. *Sci. Rep.* **6**, 19103 (2016).

212. Mehta, G., Hsiao, Y. A., Ingram, M., Luker, G. D. & Takayama, S. Opportunities and Challenges for use of Tumor Spheroids as Models to Test Drug Delivery and Efficacy. *J. Control Release* **164**, 192–204 (2012).

213. Sirenko, O. *et al.* High-Content Assays for Characterizing the Viability and Morphology of 3D Cancer Spheroid Cultures. *Assay Drug Dev. Technol.* **13**, 402–14 (2015).

214. Ivanov, D. P. & Grabowska, A. M. Spheroid arrays for high-throughput single-cell analysis of spatial patterns and biomarker expression in 3D. *Sci. Rep.* **7**, 41160 (2017).

215. Varghese, F., Bukhari, A. B., Malhotra, R. & De, A. IHC profiler: An open source plugin for the quantitative evaluation and automated scoring of immunohistochemistry images of human tissue samples. *PLoS One* **9**, (2014).

216. Onion, D. *et al.* 3-Dimensional Patient-Derived Lung Cancer Assays Reveal Resistance to Standards-of-Care Promoted by Stromal Cells but Sensitivity to Histone Deacetylase Inhibitors. *Mol. Cancer Ther.* **15**, 753–763 (2016).

217. Feitelson, M. A. *et al.* Sustained proliferation in cancer: Mechanisms and novel therapeutic targets. *Semin. Cancer Biol.* **35**, S25–S54 (2015).

218. Soysal, S. D. & Muenst, S. E. Role of the Tumor Microenvironment in Breast Cancer. *pathobiology* 142–152 (2015). doi:10.1159/000430499

219. Rampersad, S. N. Multiple applications of alamar blue as an indicator of metabolic function and cellular health in cell viability bioassays. *Sensors (Switzerland)* **12**, 12347–

12360 (2012).

220. Friedrich, J., Seidel, C., Ebner, R. & Kunz-schughart, L. A. Spheroid-based drug screen : considerations and practical approach. *Nat. Protoc.* **4**, (2009).

221. Zhang, C. *et al.* Mesenchymal stem cells derived from breast cancer tissue promote the proliferation and migration of the MCF-7 cell line in vitro. *Oncol. Lett.* **6**, 1577–1582 (2013).

222. Kenny, P. A. *et al.* The morphologies of breast cancer cell lines in three-dimensional assays correlate with their profiles of gene expression. *Mol. Oncol.* **1**, 84–96 (2007).

223. Day, M. L. *et al.* E-cadherin mediates aggregation-dependent survival of prostate and mammary epithelial cells through the retinoblastoma cell cycle control pathway. *J. Biol. Chem.* **274**, 9656–9664 (1999).

224. Faussat, A. *et al.* Roza Kuleshova found peeping. *Nature* **227**, 543 (1970).

225. Peluso, J., Pappalardo, A. & Fernandez, G. E-Cadherin-Mediated Cell Contact Prevents Apoptosis of Spontaneously Immortalized Granulosa Cells by Regulating Akt Kinase Activity. *Biol. Reprod.* **64**, 1183–1190 (2001).

226. Moro, L. *et al.* Integrins induce activation of EGF receptor: role in MAP kinase induction and adhesion-dependent cell survival. *Embo J* **17**, 6622–6632 (1998).

227. Gatti, R. *et al.* Comparison of annexin V and calcein-AM as early vital markers of apoptosis in adherent cells by confocal laser microscopy. *J. Histochem. Cytochem.* **46**, 895–900 (1998).

228. Zhou, S., Cui, Z. & Urban, J. Dead cell counts during serum cultivation are underestimated by the fluorescent live/dead assay. *Biotechnol. J.* **6**, 513–518 (2011).

229. Fang, Y. & Eglen, R. M. Three-Dimensional Cell Cultures in Drug Discovery and Development. *SLAS Discov.* **22**, 456–472 (2017).

230. Breslin, S. & O'Driscoll, L. Three-dimensional cell culture: The missing link in drug discovery. *Drug Discov. Today* **18**,

240–249 (2013).

231. Dubuisson, M., Marchand, C. & Rees, J. F. Firefly luciferin as antioxidant and light emitter: The evolution of insect bioluminescence. *Luminescence* **19**, 339–344 (2004).

232. Lim, J. F., Berger, H. & Su, I. Isolation and Activation of Murine Lymphocytes. *J. Vis. Exp.* **2**, 1–8 (2016).

233. Filby, A., Begum, J., Jalal, M. & Day, W. Appraising the suitability of succinimidyl and lipophilic fluorescent dyes to track proliferation in non-quiescent cells by dye dilution. *Methods* **82**, 29–37 (2015).

234. Shashni, B. *et al.* Size-based Differentiation of Cancer and Normal Cells by a Particle Size Analyzer Assisted by a Cell-recognition PC Software. *Biol. Pharm. Bull.* **41**, 487–503 (2018).

235. Martin, T. A., Ye, L., Sanders, A. J., Lane, J. & Jiang, W. G. Cancer Invasion and Metastasis : Molecular and Cellular Perspective Cancer Invasion and Metastasis : The Role of Cell Adhesion Molecules. 1–37 (2016).

236. Gkretsi, V. & Stylianopoulos, T. Cell Adhesion and Matrix Stiffness: Coordinating Cancer Cell Invasion and Metastasis. *Front. Oncol.* **8**, (2018).

237. Stivarou, T. & Patsavoudi, E. Extracellular molecules involved in cancer cell invasion. *Cancers (Basel).* **7**, 238–265 (2015).

238. Zanotelli, M. R. *et al.* Regulation of ATP utilization during metastatic cell migration by collagen architecture. *Mol. Biol. Cell* **29**, 1–9 (2018).

239. Pérez-Yépez, E. A., Ayala-Sumuano, J.-T., Reveles-Espinoza, A. M. & Meza, I. Selection of a MCF-7 Breast Cancer Cell Subpopulation with High Sensitivity to IL-1 β : Characterization of and Correlation between Morphological and Molecular Changes Leading to Increased Invasiveness. *Int. J. Breast Cancer* **2012**, 1–12 (2012).

240. Felipe Lima, J., Nofech-Mozes, S., Bayani, J. & Bartlett, J. EMT in Breast Carcinoma—A Review. *J. Clin. Med.* **5**, 65 (2016).

241. Haynes, J., Srivastava, J., Madson, N., Wittmann, T. & Barber, D. L. Dynamic actin remodeling during epithelial-mesenchymal transition depends on increased moesin expression. *Mol. Biol. Cell* **22**, 4750–4764 (2011).

242. Sarrio, D. *et al.* Epithelial-Mesenchymal Transition in Breast Cancer Relates to the Basal-like Phenotype. *Cancer Res.* **68**, 989–997 (2008).

243. Yen T. Phung1, Dario Barbone2, V. Courtney Broaddus2 & Mitchell Ho1. Rapid Generation of In Vitro MulticellularSpheroids for the Study of Monoclonal Antibody Therapy. *J. Cancer* **2**, 507–514 (2011).

244. Zhao, R., Bean, S. R. & Wang, D. Sorghum protein extraction by sonication and its relationship to ethanol fermentation. *Cereal Chem.* **85**, 837–842 (2008).

245. Comşa, Ş., Cîmpean, A. M. & Raica, M. the Story of Mcf7. *Int. J. Cancer Res. Treat.* **3154**, 3147–3154 (2015).

246. Kidd, M. E., Shumaker, D. K. & Ridge, K. M. The role of Vimentin intermediate filaments in the progression of lung cancer. *Am. J. Respir. Cell Mol. Biol.* **50**, 1–6 (2014).

247. Zhang, F. *et al.* Ski-related novel protein N (SnoN), a negative controller of transforming growth factor-β signaling, is a prognostic marker in estrogen receptor-positive breast carcinomas. *Cancer Res.* **63**, 5005–5010 (2003).

248. Mbom, B. C., Nelson, W. J. & Barth, A. β-catenin at the centrosome: Discrete pools of β-catenin communicate during mitosis and may co-ordinate centrosome functions and cell cycle progression. *BioEssays* **35**, 804–809 (2013).

249. Shtutman, M. *et al.* The cyclin D1 gene is a target of the -catenin/LEF-1 pathway. *Proc. Natl. Acad. Sci.* **96**, 5522–5527 (1999).

250. Hwang, S. Y. *et al.* Direct Targeting of β-Catenin by a Small Molecule Stimulates Proteasomal Degradation and Suppresses Oncogenic Wnt/β-Catenin Signaling. *Cell Rep.* **16**, 28–36 (2016).

251. Gilles, C. *et al.* Transactivation of vimentin by β-catenin in human breast cancer cells. *Cancer Res.* **63**, 2658–2664

(2003).

252. Kwist, K., Bridges, W. C. & Burg, K. J. L. The effect of cell passage number on osteogenic and adipogenic characteristics of D1 cells. *Cytotechnology* **68**, 1661–1667 (2016).

253. Kleensang, A. *et al.* Genetic variability in a frozen batch of MCF-7 cells invisible in routine authentication affecting cell function. *Sci. Rep.* **6**, 1–10 (2016).

254. Farber, E. Cell proliferation as a major risk ractor for cancer: A concept of doubtful validity. *Cancer Res.* **56**, 4272–4274 (1996).

255. Feitelson, M. A. *et al.* Sustained proliferation in cancer: Mechanisms and novel therapeutic targets. *Semin. Cancer Biol.* **35**, S25–S54 (2015).

256. Ramasamy, R. *et al.* Mesenchymal stem cells inhibit proliferation and apoptosis of tumor cells: Impact on in vivo tumor growth. *Leukemia* **21**, 304–310 (2007).

257. Ho, I. A. W. *et al.* Human bone marrow-derived mesenchymal stem cells suppress human glioma growth through inhibition of angiogenesis. *Stem Cells* **31**, 146–155 (2013).

258. Khakoo, A. Y. *et al.* Human mesenchymal stem cells exert potent antitumorigenic effects in a model of Kaposi's sarcoma. *J. Exp. Med.* **203**, 1235–1247 (2006).

259. Haycock, J. W. 3D Cell Culture: A Review of Current Approaches and Techniques. in *3D Cell Culture: Methods and Protocols* (ed. Haycock, J. W.) 1–15 (Humana Press, 2011). doi:10.1007/978-1-60761-984-0_1

260. Knight, E. & Przyborski, S. Advances in 3D cell culture technologies enabling tissue-like structures to be created in vitro. *J. Anat.* **227**, 746–756 (2015).

261. Bartosh, T. J., Ullah, M., Zeitouni, S., Beaver, J. & Prockop, D. J. Cancer cells enter dormancy after cannibalizing mesenchymal stem/stromal cells (MSCs). *Proc. Natl. Acad. Sci.* **113**, E6447–E6456 (2016).

262. Martínez-Carpio, P. A., Mur, C., Rosel, P. & Navarro, M. A.

Constitutive and regulated secretion of epidermal growth factor and transforming growth factor-β1 in MDA-MB-231 breast cancer cell line in 11-day cultures. *Cell. Signal.* **11**, 753–757 (1999).

263. Perou, C. M. Molecular Stratification of Triple-Negative Breast Cancers. *Oncologist* **15**, 39–48 (2010).

264. Boyle, P. Triple-negative breast cancer: epidemiological considerations and recommendations. *Ann. Oncol.* **23**, vi7–vi12 (2012).

265. Holliday, D. L. & Speirs, V. Choosing the right cell line for breast cancer research. *Breast Cancer Res.* **13**, 215 (2011).

266. Kaur, G. & Dufour, J. M. Cell lines. Valuable tools or useless artifacts. *Spermatogenesis* **2**, 1–5 (2012).

267. Yan, F. *et al.* Thymic function in the regulation of T cells, and molecular mechanisms underlying the modulation of cytokines and stress signaling (Review). *Mol. Med. Rep.* **16**, 7175–7184 (2017).

268. Mombaerts, P. *et al.* RAG-1-deficient mice have no mature B and T lymphocytes. *Cell* **68**, 869–877 (1992).

269. Leavy, O. Natural killer cells: RAG keeps natural killers fit. *Nat. Rev. Immunol.* **14**, 716–717 (2014).

270. Kim, R. K. *et al.* Activation of KRAS promotes the mesenchymal features of Basal-type breast cancer. *Exp. Mol. Med.* **47**, e137-9 (2015).

271. Clarke, M. R., Imhoff, F. M. & Baird, S. K. Mesenchymal stem cells inhibit breast cancer cell migration and invasion through secretion of tissue inhibitor of metalloproteinase-1 and -2. *Mol. Carcinog.* **54**, 1214–1219 (2015).

272. Martin, F. T. *et al.* Potential role of mesenchymal stem cells (MSCs) in the breast tumour microenvironment: stimulation of epithelial to mesenchymal transition (EMT). *Breast Cancer Res. Treat.* **124**, 317–326 (2010).

273. Lamouille, S., Xu, J. & Derynck, R. Molecular mechanisms of epithelial–mesenchymal transition. *Nat. Rev. Mol. Cell Biol.* **15**, 178–196 (2014).

274. Tang, D. D. & Gerlach, B. D. The roles and regulation of the actin cytoskeleton, intermediate filaments and microtubules in smooth muscle cell migration. *Respir. Res.* **18**, 54 (2017).

275. Sui, W. *et al.* Comparison of immunohistochemistry (IHC) and fluorescence in situ hybridization (FISH) assessment for Her-2 status in breast cancer. *World J. Surg. Oncol.* **7**, 83 (2009).

276. Nwose, E. U. Comparison of immunohistochemistry with in situ hybridization methods: discrepancy resolution and implications for low-mid income countries. *J. Histotechnol.* **39**, 21–25 (2016).

277. Huber, D., Voith von Voithenberg, L. & Kaigala, G. V. Fluorescence in situ hybridization (FISH): History, limitations and what to expect from micro-scale FISH? *Micro Nano Eng.* **1**, 15–24 (2018).

278. Ellis, C. M., Dyson, M. J., Stephenson, T. J. & Maltby, E. L. HER2 amplification status in breast cancer: A comparison between immunohistochemical staining and fluorescence in situ hybridisation using manual and automated quantitative image analysis scoring techniques. *J. Clin. Pathol.* **58**, 710–714 (2005).

279. Shih, W. & Yamada, S. N-cadherin-mediated cell-cell adhesion promotes cell migration in a three-dimensional matrix. *J. Cell Sci.* **125**, 3661–3670 (2012).

280. Nieman, M. T., Prudoff, R. S., Johnson, K. R. & Wheelock, M. J. N-cadherin promotes motility in human breast cancer cells regardless of their E-cadherin expression. *J. Cell Biol.* **147**, 631–643 (1999).

281. Tan, R., Wang, L., Song, J., Li, J. & He, T. Expression and significance of Twist, estrogen receptor, and E-cadherin in human breast cancer cells and tissues. *J. Cancer Res. Ther.* **13**, 707 (2017).

282. Jahchan, N. S., Ouyang, G. & Luo, K. Expression Profiles of SnoN in Normal and Cancerous Human Tissues Support Its Tumor Suppressor Role in Human Cancer. *PLoS One* **8**, 1–13 (2013).

283. Peng, Q. *et al.* Biological Characteristics and Genetic

Heterogeneity between Carcinoma-Associated Fibroblasts and Their Paired Normal Fibroblasts in Human Breast Cancer. *PLoS One* **8**, (2013).

284. Kalluri, R. & Zeisberg, M. Fibroblasts in cancer. *Nat. Rev. Cancer* **6**, 392–401 (2006).

285. Clevers, H. Wnt/β-Catenin Signaling in Development and Disease. *Cell* **127**, 469–480 (2006).

286. Shang, S., Hua, F. & Hu, Z.-W. The regulation of β-catenin activity and function in cancer: therapeutic opportunities. *Oncotarget* **8**, 33972–33989 (2017).

287. Bertrade, M., Nelson, W. J. & Angela, B. B-catenin at the centrosome. *BioEssays* **35**, 804–809 (2013).

288. Houthuijzen, J. M., Daenen, L. G. M., Roodhart, J. M. L. & Voest, E. E. The role of mesenchymal stem cells in anti-cancer drug resistance and tumour progression. *Br. J. Cancer* **106**, 1901–1906 (2012).

289. Tomaskovic-Crook, E., Thompson, E. W. & Thiery, J. P. Epithelial to mesenchymal transition and breast cancer. *Breast Cancer Res.* **11**, 213 (2009).

290. Felipe Lima, J., Nofech-Mozes, S., Bayani, J. & Bartlett, J. EMT in Breast Carcinoma—A Review. *J. Clin. Med.* **5**, 65 (2016).

291. Sutandy, F. X. R., Qian, J., Chen, C.-S. & Zhu, H. Overview of Protein Microarrays. *Curr. Protoc. Protein Sci.* **72**, 27.1.1-27.1.16 (2013).

292. Wang, Z., Li, Y., Kong, D. & H. Sarkar, F. The Role of Notch Signaling Pathway in Epithelial-Mesenchymal Transition (EMT) During Development and Tumor Aggressiveness. *Curr. Drug Targets* **11**, 745–751 (2010).

293. Miele, L., Espinoza, I., Pochampally, Watabe & Xing, F. Notch signaling: targeting cancer stem cells and epithelial-to-mesenchymal transition. *Onco. Targets. Ther.* 1249 (2013). doi:10.2147/OTT.S36162

294. Kontomanolis, E. N. *et al.* The Notch Pathway in Breast Cancer Progression. *Sci. World J.* **2018**, 1–11 (2018).

295. Geraldo, S., Simon, A. & Vignjevic, D. M. Revealing the Cytoskeletal Organization of Invasive Cancer Cells in 3D. *J. Vis. Exp.* 2–7 (2013). doi:10.3791/50763

296. Shankar, J. & Nabi, I. R. Actin cytoskeleton regulation of epithelial mesenchymal transition in metastatic cancer cells. *PLoS One* **10**, 1–12 (2015).

Plasmid: LVX-eGFP
Made by: Teresa Coughlan
Users: Teresa Coughlan
Richard Argent
Nektaria Papadopoulou
Yin Yinfei
Anna Grabowska

Description of plasmid: This construct is based on 'pLVX-tomato' (Teresa). Expression of the fluorescent protein eGFP is constitutive under the CMV promoter. It was made by removing the BamHI/NotI 'tdTomato' ORF fragment from the original vector, and replacing it with a PCR-amplified BamHI/NotI eGFP ORF fragment from Lv-eGFP-neo (Genecopoeia). Clone 2 is the one to use.

Other relevant details: ABI sequencing shows construct is correct in respect of inserted fragment and patent insertion sites. No PCR-introduced mutational errors present.

Sequencing primers: - see sequence.

Restriction map: (showing only unique sites)

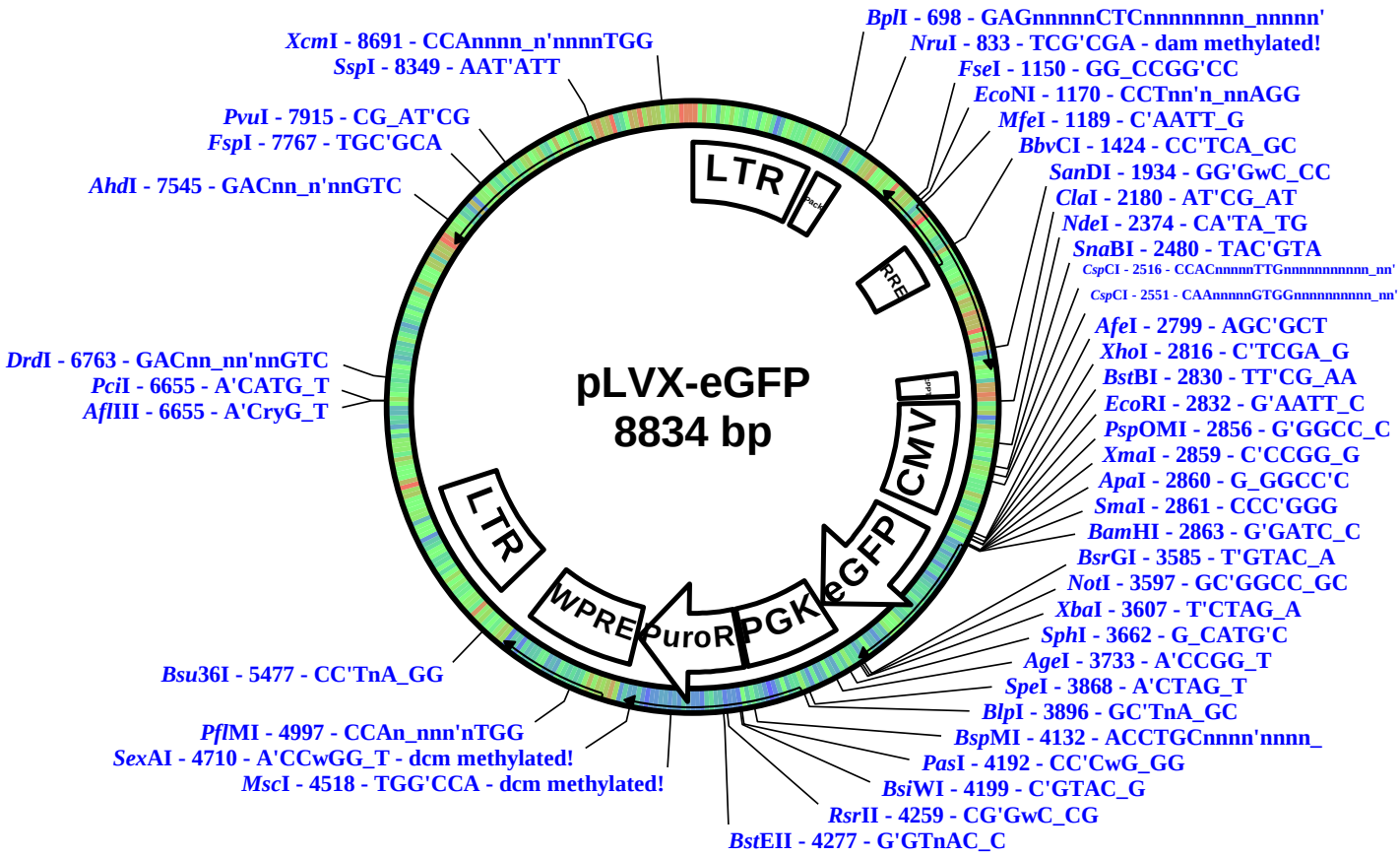

Sequence:

Green(dark)=CMV promoter
Green (light)=eGFP ORF, PuroR and WPRE
Teal=sequencing primers
Pink=PGKprom
Blue= packaging signal, RREreg and cPPT elements
Purple=LTRs

TGGAAGGGCTAATTCACTCCCAAAGAAGACAAGATATCCTTGATCTGTGGATCTACCACACACAAGGCTACT
TCCCTGATTAGCAGAACTACACACCAGGGCCAGGGGTCAGATATCCACTGACCTTTGGATGGTGCTACAAGC
TAGTACCAGTTGAGCCAGATAAGGTAGAAGAGGCCAATAAAGGAGAGAACACCAGCTTGTTACACCCTGTGA
GCCTGCATGGGATGGATGACCCGGAGAGAGAAGTGTTAGAGTGGAGGTTTGACAGCCGCCTAGCATTTCATC
ACGTGGCCCGAGAGCTGCATCCGGAGTACTTCAAGAACTGCTGATATCGAGCTTGCTACAAGGGACTTTCCG
CTGGGGACTTTCCAGGGAGGCGTGGCCTGGGCGGGACTGGGGAGTGGCGAGCCCTCAGATCCTGCATATAAG
CAGCTGCTTTTTGCCTGTACTGGGTCTCTCTGGTTAGACCAGATCTGAGCCTGGGAGCTCTCTGGCTAACTA
GGGAACCCACTGCTTAAGCCTCAATAAAGCTTGCCTTGAGTGCTTCAAGTAGTGTGTGCCCGTCTGTTGTGT
GACTCTGGTAACTAGAGATCCCTCAGACCCTTTTAGTCAGTGTGGAAAATCTCTAGCAGTGGCGCCCGAACA
GGGACTTGAAAGCGAAAGGGAAACCAGAGGAGCTCTCTCGACGCAGGACTCGGCTTGCTGAAGCGCGCACGG
CAAGAGGCGAGGGGCGGCGACTGGTGAGTACGCCAAAAATTTTGACTAGCGGAGGCTAGAAGGAGAGAGATG
GGTGCGAGAGCGTCAGTATTAAGCGGGGGAGAATTAGATCGCGATGGGAAAAAATTCGGTTAAGGCCAGGGG
GAAAGAAAAAATATAAATTAAAACATATAGTATGGGCAAGCAGGGAGCTAGAACGATTCGCAGTTAATCCTG
GCCTGTTAGAAACATCAGAAGGCTGTAGACAAATACTGGGACAGCTACAACCATCCCTTCAGACAGGATCAG
AAGAACTTAGATCATTATATAATACAGTAGCAACCCTCTATTGTGTGCATCAAAGGATAGAGATAAAAGACA
CCAAGGAAGCTTTAGACAAGATAGAGGAAGAGCAAAACAAAAGTAAGACCACCGCACAGCAAGCGGCCGGCC
GCTGATCTTCAGACCTGGAGGAGGAGATATGAGGGACAATTGGAGAAGTGAATTATATAAATATAAAGTAGT
AAAAATTGAACCATTAGGAGTAGCACCCACCAAGGCAAAGAGAAGAGTGGTGCAGAGAGAAAAAAGAGCAGT
GGGAATAGGAGCTTTGTTCCTTGGGTTCTTGGGAGCAGCAGGAAGCACTATGGGCGCAGCGTCAATGACGCT
GACGGTACAGGCCAGACAATTATTGTCTGGTATAGTGCAGCAGCAGAACAATTTGCTGAGGGCTATTGAGGC
GCAACAGCATCTGTTGCAACTCACAGTCTGGGGCATCAAGCAGCTCCAGGCAAGAATCCTGGCTGTGGAAAG
ATACCTAAAGGATCAACAGCTCCTGGGGATTTGGGGTTGCTCTGGAAAACTCATTTGCACCACTGCTGTGCC
TTGGAATGCTAGTTGGAGTAATAAATCTCTGGAACAGATTTGGAATCACACGACCTGGATGGAGTGGGACAG
AGAAATTAACAATTACACAAGCTTAATACACTCCTTAATTGAAGAATCGCAAAACCAGCAAGAAAAGAATGA
ACAAGAATTATTGGAATTAGATAAATGGGCAAGTTTGTGGAATTGGTTTAACATAACAAATTGGCTGTGGTA
TATAAAATTATTCATAATGATAGTAGGAGGCTTGGTAGGTTTAAGAATAGTTTTTGCTGTACTTTCTATAGT
GAATAGAGTTAGGCAGGGATATTCACCATTATCGTTTCAGACCCACCTCCCAACCCCGAGGGGACCCGACAG
GCCCGAAGGAATAGAAGAAGAAGGTGGAGAGAGAGACAGAGACAGATCCATTCGATTAGTGAACGGATCTCG
ACGGTATCGCCTTTAAAAGAAAAGGGGGGATTGGGGGGTACAGTGCAGGGGAAAGAATAGTAGACATAATAG
CAACAGACATACAAACTAAAGAACTACAAAAACAAATTACAAAAATTCAAAATTTTCGGGTTTATTACAGGG
ACAGCAGAGATCCAGTTTATCGATAAGCTTGGGAGTTCCGCGTTACATAACTTACGGTAAATGGCCCGCCTG
GCTGACCGCCCAACGACCCCCGCCCATTGACGTCAATAATGACGTATGTTCCCATAGTAACGCCAATAGGGA
CTTTCCATTGACGTCAATGGGTGGAGTATTTACGGTAAACTGCCCACTTGGCAGTACATCAAGTGTATCATA
TGCCAAGTACGCCCCCTATTGACGTCAATGACGGTAAATGGCCCGCCTGGCATTATGCCCAGTACATGACCT
TACGGGACTTTCCTACTTGGCAGTACATCTACGTATTAGTCATCGCTATTACCATGGTGATGCGGTTTTGGC
AGTACACCAATGGGCGTGGATAGCGGTTTGACTCACGGGGATTTCCAAGTCTCCACCCCATTGACGTCAATG
GGAGTTTGTTTTGGCACCAAAATCAACGGGACTTTCCAAAATGTCGTAACAACTCCGCCCCATTGACGCAAA
TGGGCGGTAGGCGTGTACGGTGGGAGGTCTATATAAGCAGAGCTCGTTTAGTGAACCGTCAGATCGCCTGGA
GACGCCATCCACGCTGTTTTGACCTCCATAGAAGACACCGACTCTAGCTAGAGGATCGCTAGCGCTACCGGA
CTCAGATCTCGAGCTCAAGCTTCGAATTCTGCAGTCGACGGTACCGCGGGCCCGGgatcccgccaccatggt
gagcaagggcgaggagctgttcaccggggtggtgcccatcctggtcgagctggacggcgacgtaaacggcca
caagttcagcgtgtccggcgagggcgagggcgatgccacctacggcaagctgaccctgaagttcatctgcac
caccggcaagctgcccgtgccctggcccaccctcgtgaccaccctgacctacggcgtgcagtgcttcagccg
ctaccccgaccacatgaagcagcacgacttcttcaagtccgccatgcccgaaggctacgtccaggagcgcac
catcttcttcaaggacgacggcaactacaagacccgcgccgaggtgaagttcgagggcgacaccctggtgaa
ccgcatcgagctgaagggcatcgacttcaaggaggacggcaacatcctggggcacaagctggagtacaacta

caacagccacaacgtctatatcatggccgacaagcagaagaacggcatcaaggtgaacttcaagatccgcca
caacatcgaggacggcagcgtgcagctcgccgaccactaccagcagaacaccccatcggcgacggccccgt
gctgctgcccgacaaccactacctgagcacccagtccgccctgagcaaagaccccaacgagaagcgcgatca
catggtcctgctggagttcgtgaccgccgccgggatcactctcggcatggacgagctgtacaagtaagcggc
cgcGACTCTAGATAATTCTACCGGGTAGGGGAGGCGCTTTTCCCAAGGCAGTCTGGAGCATGCGCTTTAGCA
GCCCCGCTGGGCACTTGGCGCTACACAAGTGGCCTCTGGCCTCGCACACATTCCACATCCACCGGTAGGCGC
CAACCGGCTCCGTTCTTTGGTGGCCCCTTCGCGCCACCTTCTACTCCTCCCCTAGTCAGGAAGTTCCCCCCC
GCCCCGCAGCTCGCGTCGTGCAGGACGTGACAAATGGAAGTAGCACGTCTCACTAGTCTCGTGCAGATGGAC
AGCACCGCTGAGCAATGGAAGCGGGTAGGCCTTTGGGGCAGCGGCCAATAGCAGCTTTGCTCCTTCGCTTTC
TGGGCTCAGAGGCTGGGAAGGGGTGGGTCCGGGGGCGGGCTCAGGGGCGGGCTCAGGGGCGGGGCGGGCGCC
CGAAGGTCCTCCGGAGGCCCGGCATTCTGCACGCTTCAAAAGCGCACGTCTGCCGCGCTGTTCTCCTCTTCC
TCATCTCCGGGCCTTTCGACCTGCAGCCCAAGCTTACCATGACCGAGTACAAGCCCACGGTGCGCCTCGCCA
CCCGCGACGACGTCCCCAGGGCCGTACGCACCCTCGCCGCCGCGTTCGCCGACTACCCCGCCACGCGCCACA
CCGTCGATCCGGACCGCCACATCGAGCGGGTCACCGAGCTGCAAGAACTCTTCCTCACGCGCGTCGGGCTCG
ACATCGGCAAGGTGTGGGTCGCGGACGACGGCGCCGCGGTGGCGGTCTGGACCACGCCGGAGAGCGTCGAAG
CGGGGGCGGTGTTCGCCGAGATCGGCCCGCGCATGGCCGAGTTGAGCGGTTCCCGGCTGGCCGCGCAGCAAC
AGATGGAAGGCCTCCTGGCGCCGCACCGGCCCAAGGAGCCCGCGTGGTTCCTGGCCACCGTCGGCGTCTCGC
CCGACCACCAGGGCAAGGGTCTGGGCAGCGCCGTCGTGCTCCCCGGAGTGGAGGCGGCCGAGCGCGCCGGGG
TGCCCGCCTTCCTGGAGACCTCCGCGCCCCGCAACCTCCCCTTCTACGAGCGGCTCGGCTTCACCGTCACCG
CCGACGTCGAGGTGCCCGAAGGACCGCGCACCTGGTGCATGACCCGCAAGCCCGGTGCCTGACCGCGTCTGG
AACAATCAACCTCTGGATTACAAAATTTGTGAAAGATTGACTGGTATTCTTAACTATGTTGCTCCTTTTACG
CTATGTGGATACGCTGCTTTAATGCCTTTGTATCATGCTATTGCTTCCCGTATGGCTTTCATTTTCTCCTCC
TTGTATAAATCCTGGTTGCTGTCTCTTTATGAGGAGTTGTGGCCCGTTGTCAGGCAACGTGGCGTGGTGTGC
ACTGTGTTTGCTGACGCAACCCCCACTGGTTGGGGCATTGCCACCACCTGTCAGCTCCTTTCCGGGACTTTC
GCTTTCCCCCTCCCTATTGCCACGGCGGAACTCATCGCCGCCTGCCTTGCCCGCTGCTGGACAGGGGCTCGG
CTGTTGGGCACTGACAATTCCGTGGTGTTGTCGGGGAAGCTGACGTCCTTTCCATGGCTGCTCGCCTGTGTT
GCCACCTGGATTCTGCGCGGGACGTCCTTCTGCTACGTCCCTTCGGCCCTCAATCCAGCGGACCTTCCTTCC
CGCGGCCTGCTGCCGGCTCTGCGGCCTCTTCCGCGTCTTCGCCTTCGCCCTCAGACGAGTCGGATCTCCCTT
TGGGCCGCCTCCCCGCCTGGAATTAATTCTGCAGTCGAGACCTAGAAAAACATGGAGCAATCACAAGTAGCA
ATACAGCAGCTACCAATGCTGATTGTGCCTGGCTAGAAGCACAAGAGGAGGAGGAGGTGGGTTTTTCCAGTC
ACACCTCAGGTACCTTTAAGACCAATGACTTACAAGGCAGCTGTAGATCTTAGCCACTTTTTAAAAGAAAAG
AGGGGACTGGAAGGGCTAATTCACTCCCAACGAAGACAAGATATCCTTGATCTGTGGATCTACCACACACAA
GGCTACTTCCCTGATTAGCAGAACTACACACCAGGGCCAGGGGTCAGATATCCACTGACCTTTGGATGGTGC
TACAAGCTAGTACCAGTTGAGCCAGATAAGGTAGAAGAGGCCAATAAAGGAGAGAACACCAGCTTGTTACAC
CCTGTGAGCCTGCATGGGATGGATGACCCGGAGAGAGAAGTGTTAGAGTGGAGGTTTGACAGCCGCCTAGCA
TTTCATCACGTGGCCCGAGAGCTGCATCCGGAGTACTTCAAGAACTGCTGATATCGAGCTTGCTACAAGGGA
CTTTCCGCTGGGGACTTTCCAGGGAGGCGTGGCCTGGGCGGGACTGGGGAGTGGCGAGCCCTCAGATCCTGC
ATATAAGCAGCTGCTTTTTGCCTGTACTGGGTCTCTCTGGTTAGACCAGATCTGAGCCTGGGAGCTCTCTGG
CTAACTAGGGAACCCACTGCTTAAGCCTCAATAAAGCTTGCCTTGAGTGCTTCAAGTAGTGTGTGCCCGTCT
GTTGTGTGACTCTGGTAACTAGAGATCCCTCAGACCCTTTTAGTCAGTGTGGAAAATCTCTAGCAGTAGTAG
TTCATGTCATCTTATTATTCAGTATTTATAACTTGCAAAGAAATGAATATCAGAGAGTGAGAGGCCTTGACA
TTGCTAGCGTTTTACCGTCGACCTCTAGCTAGAGCTTGGCGTAATCATGGTCATAGCTGTTTCCTGTGTGAA
ATTGTTATCCGCTCACAATTCCACACAACATACGAGCCGGAAGCATAAAGTGTAAAGCCTGGGGTGCCTAAT
GAGTGAGCTAACTCACATTAATTGCGTTGCGCTCACTGCCCGCTTTCCAGTCGGGAAACCTGTCGTGCCAGC
TGCATTAATGAATCGGCCAACGCGCGGGGAGAGGCGGTTTGCGTATTGGGCGCTCTTCCGCTTCCTCGCTCA
CTGACTCGCTGCGCTCGGTCGTTCGGCTGCGGCGAGCGGTATCAGCTCACTCAAAGGCGGTAATACGGTTAT
CCACAGAATCAGGGGATAACGCAGGAAAGAACATGTGAGCAAAAGGCCAGCAAAAGGCCAGGAACCGTAAAA
AGGCCGCGTTGCTGGCGTTTTTCCATAGGCTCCGCCCCCCTGACGAGCATCACAAAAATCGACGCTCAAGTC
AGAGGTGGCGAAACCCGACAGGACTATAAAGATACCAGGCGTTTCCCCCTGGAAGCTCCCTCGTGCGCTCTC
CTGTTCCGACCCTGCCGCTTACCGGATACCTGTCCGCCTTTCTCCCTTCGGGAAGCGTGGCGCTTTCTCATA
GCTCACGCTGTAGGTATCTCAGTTCGGTGTAGGTCGTTCGCTCCAAGCTGGGCTGTGTGCACGAACCCCCCG
TTCAGCCCGACCGCTGCGCCTTATCCGGTAACTATCGTCTTGAGTCCAACCCGGTAAGACACGACTTATCGC
CACTGGCAGCAGCCACTGGTAACAGGATTAGCAGAGCGAGGTATGTAGGCGGTGCTACAGAGTTCTTGAAGT
GGTGGCCTAACTACGGCTACACTAGAAGAACAGTATTTGGTATCTGCGCTCTGCTGAAGCCAGTTACCTTCG
GAAAAAGAGTTGGTAGCTCTTGATCCGGCAAACAAACCACCGCTGGTAGCGGTTTTTTTGTTTGCAAGCAGC
AGATTACGCGCAGAAAAAAAGGATCTCAAGAAGATCCTTTGATCTTTTCTACGGGGTCTGACGCTCAGTGGA

ACGAAAACTCACGTTAAGGGATTTTGGTCATGAGATTATCAAAAAGGATCTTCACCTAGATCCTTTTAAATT
AAAAATGAAGTTTTAAATCAATCTAAAGTATATATGAGTAAACTTGGTCTGACAGTTACCAATGCTTAATCA
GTGAGGCACCTATCTCAGCGATCTGTCTATTTCGTTCATCCATAGTTGCCTGACTCCCCGTCGTGTAGATAA
CTACGATACGGGAGGGCTTACCATCTGGCCCCAGTGCTGCAATGATACCGCGAGACCCACGCTCACCGGCTC
CAGATTTATCAGCAATAAACCAGCCAGCCGGAAGGGCCGAGCGCAGAAGTGGTCCTGCAACTTTATCCGCCT
CCATCCAGTCTATTAATTGTTGCCGGGAAGCTAGAGTAAGTAGTTCGCCAGTTAATAGTTTGCGCAACGTTG
TTGCCATTGCTACAGGCATCGTGGTGTCACGCTCGTCGTTTGGTATGGCTTCATTCAGCTCCGGTTCCCAAC
GATCAAGGCGAGTTACATGATCCCCCATGTTGTGCAAAAAAGCGGTTAGCTCCTTCGGTCCTCCGATCGTTG
TCAGAAGTAAGTTGGCCGCAGTGTTATCACTCATGGTTATGGCAGCACTGCATAATTCTCTTACTGTCATGC
CATCCGTAAGATGCTTTTCTGTGACTGGTGAGTACTCAACCAAGTCATTCTGAGAATAGTGTATGCGGCGAC
CGAGTTGCTCTTGCCCGGCGTCAATACGGGATAATACCGCGCCACATAGCAGAACTTTAAAAGTGCTCATCA
TTGGAAAACGTTCTTCGGGGCGAAAACTCTCAAGGATCTTACCGCTGTTGAGATCCAGTTCGATGTAACCCA
CTCGTGCACCCAACTGATCTTCAGCATCTTTTACTTTCACCAGCGTTTCTGGGTGAGCAAAAACAGGAAGGC
AAAATGCCGCAAAAAAGGGAATAAGGGCGACACGGAAATGTTGAATACTCATACTCTTCCTTTTTCAATATT
ATTGAAGCATTTATCAGGGTTATTGTCTCATGAGCGGATACATATTTGAATGTATTTAGAAAAATAAACAAA
TAGGGGTTCCGCGCACATTTCCCCGAAAAGTGCCACCTGACGTCGACGGATCGGGAGATCAACTTGTTTATT
GCAGCTTATAATGGTTACAAATAAAGCAATAGCATCACAAATTTCACAAATAAAGCATTTTTTTCACTGCAT
TCTAGTTGTGGTTTGTCCAAACTCATCAATGTATCTTATCATGTCTGGATCAACTGGATAACTCAAGCTAAC
CAAAATCATCCCAAACTTCCCACCCCATACCCTATTACCACTGCCAATTACCTAGTGGTTTCATTTACTCTA
AACCTGTGATTCCTCTGAATTATTTTCATTTTAAAGAAATTGTATTTGTTAAATATGTACTACAAACTTAGT
AGTTTTTAAAGAAATTGTATTTGTTAAATATGTACTACAAACTTAGTAGT

Plasmid: LVX-Luc
Made by: Teresa Coughlan
Users: Teresa Coughlan
Richard Argent
Nektaria Papadopoulou
Yin Yinfei
Anna Grabowska

Description of plasmid: This construct is based on 'pLVX-tomato' (Teresa). Expression of Firefly luciferase is constitutive under the CMV promoter. It was made by removing the BamHI/XbaI 'tdTomato' ORF fragment from the original vector, and replacing it with the BglII/XbaI Luciferase ORF fragment from pGL4.10[Luc2] (Promega). Clone 1 is the one to use.

Other relevant details: ABI sequencing shows construct is correct in respect of inserted fragment and patent insertion sites.

Sequencing primers: - see sequence.

Restriction map: (showing only unique sites)

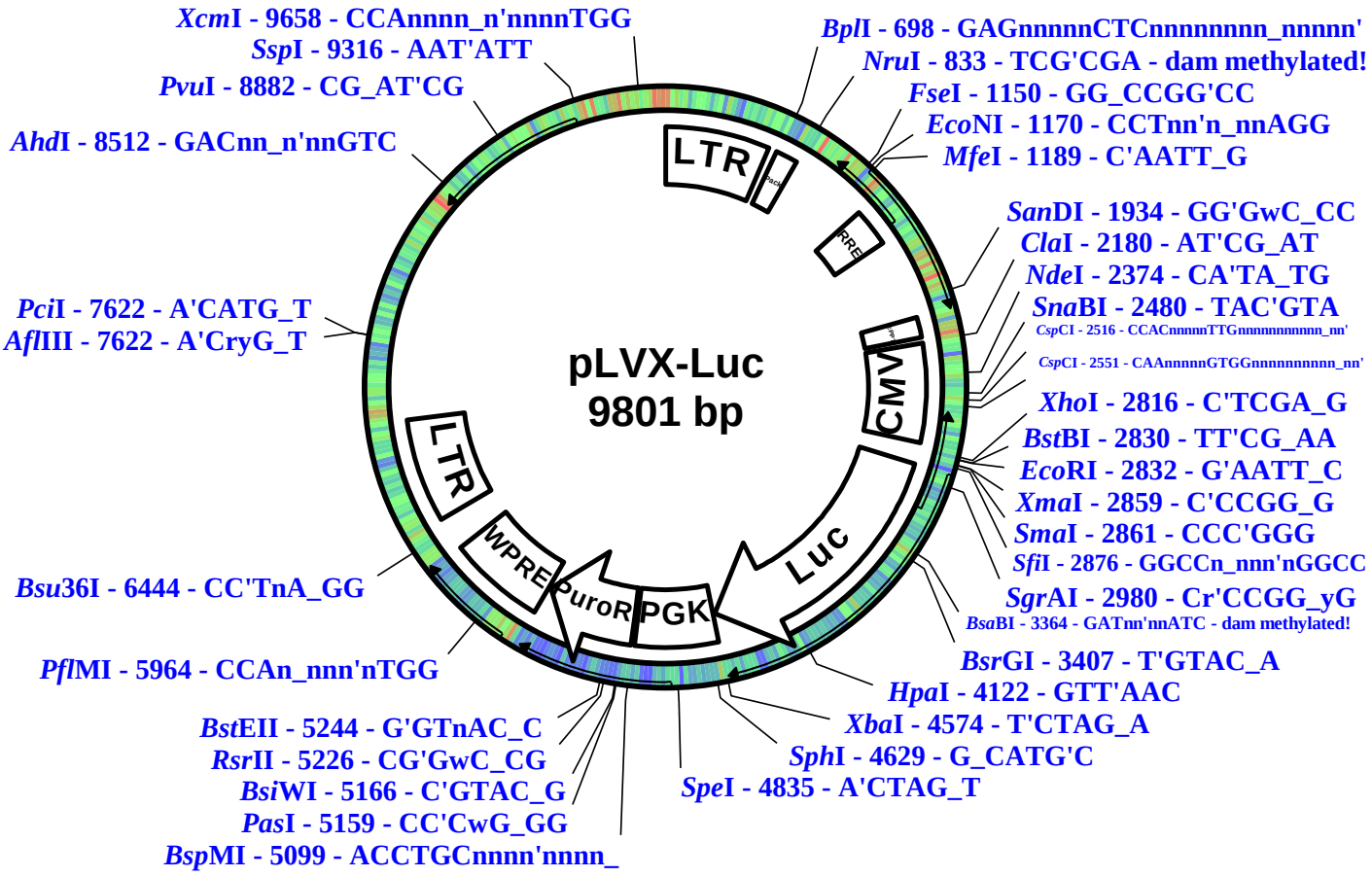

Sequence:

Green(dark)=CMV promoter
Turquoise=Luciferase ORF
Teal=sequencing primers
Pink=PGKprom
Green(light)=PuroR and WPRE
Blue= packaging signal, RREreg and cPPT elements
Purple=LTRs

TGGAAGGGCTAATTCACTCCCAAAGAAGACAAGATATCCTTGATCTGTGGATCTACCACACACAAGGCTACT
TCCCTGATTAGCAGAACTACACACCAGGGCCAGGGGTCAGATATCCACTGACCTTTGGATGGTGCTACAAGC
TAGTACCAGTTGAGCCAGATAAGGTAGAAGAGGCCAATAAAGGAGAGAACACCAGCTTGTTACACCCTGTGA
GCCTGCATGGGATGGATGACCCGGAGAGAGAAGTGTTAGAGTGGAGGTTTGACAGCCGCCTAGCATTTCATC
ACGTGGCCCGAGAGCTGCATCCGGAGTACTTCAAGAACTGCTGATATCGAGCTTGCTACAAGGGACTTTCCG
CTGGGGACTTTCCAGGGAGGCGTGGCCTGGGCGGGACTGGGGAGTGGCGAGCCCTCAGATCCTGCATATAAG
CAGCTGCTTTTTGCCTGTACTGGGTCTCTCTGGTTAGACCAGATCTGAGCCTGGGAGCTCTCTGGCTAACTA
GGGAACCCACTGCTTAAGCCTCAATAAAGCTTGCCTTGAGTGCTTCAAGTAGTGTGTGCCCGTCTGTTGTGT
GACTCTGGTAACTAGAGATCCCTCAGACCCTTTTAGTCAGTGTGGAAAATCTCTAGCAGTGGCGCCCGAACA
GGGACTTGAAAGCGAAAGGGAAACCAGAGGAGCTCTCTCGACGCAGGACTCGGCTTGCTGAAGCGCGCACGG
CAAGAGGCGAGGGGCGGCGACTGGTGAGTACGCCAAAAATTTTGACTAGCGGAGGCTAGAAGGAGAGAGATG
GGTGCGAGAGCGTCAGTATTAAGCGGGGGAGAATTAGATCGCGATGGGAAAAAATTCGGTTAAGGCCAGGGG
GAAAGAAAAAATATAAATTAAAACATATAGTATGGGCAAGCAGGGAGCTAGAACGATTCGCAGTTAATCCTG
GCCTGTTAGAAACATCAGAAGGCTGTAGACAAATACTGGGACAGCTACAACCATCCCTTCAGACAGGATCAG
AAGAACTTAGATCATTATATAATACAGTAGCAACCCTCTATTGTGTGCATCAAAGGATAGAGATAAAAGACA
CCAAGGAAGCTTTAGACAAGATAGAGGAAGAGCAAAACAAAAGTAAGACCACCGCACAGCAAGCGGCCGGCC
GCTGATCTTCAGACCTGGAGGAGGAGATATGAGGGACAATTGGAGAAGTGAATTATATAAATATAAAGTAGT
AAAAATTGAACCATTAGGAGTAGCACCCACCAAGGCAAAGAGAAGAGTGGTGCAGAGAGAAAAAAGAGCAGT
GGGAATAGGAGCTTTGTTCCTTGGGTTCTTGGGAGCAGCAGGAAGCACTATGGGCGCAGCGTCAATGACGCT
GACGGTACAGGCCAGACAATTATTGTCTGGTATAGTGCAGCAGCAGAACAATTTGCTGAGGGCTATTGAGGC
GCAACAGCATCTGTTGCAACTCACAGTCTGGGGCATCAAGCAGCTCCAGGCAAGAATCCTGGCTGTGGAAAG
ATACCTAAAGGATCAACAGCTCCTGGGGATTTGGGGTTGCTCTGGAAAACTCATTTGCACCACTGCTGTGCC
TTGGAATGCTAGTTGGAGTAATAAATCTCTGGAACAGATTTGGAATCACACGACCTGGATGGAGTGGGACAG
AGAAATTAACAATTACACAAGCTTAATACACTCCTTAATTGAAGAATCGCAAAACCAGCAAGAAAAGAATGA
ACAAGAATTATTGGAATTAGATAAATGGGCAAGTTTGTGGAATTGGTTTAACATAACAAATTGGCTGTGGTA
TATAAAATTATTCATAATGATAGTAGGAGGCTTGGTAGGTTTAAGAATAGTTTTTGCTGTACTTTCTATAGT
GAATAGAGTTAGGCAGGGATATTCACCATTATCGTTTCAGACCCACCTCCCAACCCCGAGGGGACCCGACAG
GCCCGAAGGAATAGAAGAAGAAGGTGGAGAGAGAGACAGAGACAGATCCATTCGATTAGTGAACGGATCTCG
ACGGTATCGCCTTTAAAAGAAAAGGGGGGATTGGGGGGTACAGTGCAGGGGAAAGAATAGTAGACATAATAG
CAACAGACATACAAACTAAAGAACTACAAAAACAAATTACAAAAATTCAAAATTTTCGGGTTTATTACAGGG
ACAGCAGAGATCCAGTTTATCGATAAGCTTGGGAGTTCCGCGTTACATAACTTACGGTAAATGGCCCGCCTG
GCTGACCGCCCAACGACCCCCGCCCATTGACGTCAATAATGACGTATGTTCCCATAGTAACGCCAATAGGGA
CTTTCCATTGACGTCAATGGGTGGAGTATTTACGGTAAACTGCCCACTTGGCAGTACATCAAGTGTATCATA
TGCCAAGTACGCCCCCTATTGACGTCAATGACGGTAAATGGCCCGCCTGGCATTATGCCCAGTACATGACCT
TACGGGACTTTCCTACTTGGCAGTACATCTACGTATTAGTCATCGCTATTACCATGGTGATGCGGTTTTGGC
AGTACACCAATGGGCGTGGATAGCGGTTTGACTCACGGGGATTTCCAAGTCTCCACCCCATTGACGTCAATG
GGAGTTTGTTTTGGCACCAAAATCAACGGGACTTTCCAAAATGTCGTAACAACTCCGCCCCATTGACGCAAA
TGGGCGGTAGGCGTGTACGGTGGGAGGTCTATATAAGCAGAGCTCGTTTAGTGAACCGTCAGATCGCCTGGA
GACGCCATCCACGCTGTTTTGACCTCCATAGAAGACACCGACTCTAGCTAGAGGATCGCTAGCGCTACCGGA
CTCAGATCTCGAGCTCAAGCTTCGAATTCTGCAGTCGACGGTACCGCGGGCCCGGGATCTGGCCTCGGCGGC
CAAGCTTGGCAATCCGGTACTGTTGGTAAAGCCACCATGGAAGATGCCAAAAACATTAAGAAGGGCCCAGCG
CCATTCTACCCACTCGAAGACGGGACCGCCGGCGAGCAGCTGCACAAAGCCATGAAGCGCTACGCCCTGGTG
CCCGGCACCATCGCCTTTACCGACGCACATATCGAGGTGGACATTACCTACGCCGAGTACTTCGAGATGAGC
GTTCGGCTGGCAGAAGCTATGAAGCGCTATGGGCTGAATACAAACCATCGGATCGTGGTGTGCAGCGAGAAT
AGCTTGCAGTTCTTCATGCCCGTGTTGGGTGCCCTGTTCATCGGTGTGGCTGTGGCCCCAGCTAACGACATC
TACAACGAGCGCGAGCTGCTGAACAGCATGGGCATCAGCCAGCCCACCGTCGTATTCGTGAGCAAGAAAGGG

CTGCAAAAGATCCTCAACGTGCAAAAGAAGCTACCGATCATACAAAAGATCATCATCATGGATAGCAAGACC
GACTACCAGGGCTTCCAAAGCATGTACACCTTCGTGACTTCCCATTTGCCACCCGGCTTCAACGAGTACGAC
TTCGTGCCCGAGAGCTTCGACCGGGACAAAACCATCGCCCTGATCATGAACAGTAGTGGCAGTACCGGATTG
CCCAAGGGCGTAGCCCTACCGCACCGCACCGCTTGTGTCCGATTCAGTCATGCCCGCGACCCCATCTTCGGC
AACCAGATCATCCCCGACACCGCTATCCTCAGCGTGGTGCCATTTCACCACGGCTTCGGCATGTTCACCACG
CTGGGCTACTTGATCTGCGGCTTTCGGGTCGTGCTCATGTACCGCTTCGAGGAGGAGCTATTCTTGCGCAGC
TTGCAAGACTATAAGATTCAATCTGCCCTGCTGGTGCCCACACTATTTAGCTTCTTCGCTAAGAGCACTCTC
ATCGACAAGTACGACCTAAGCAACTTGCACGAGATCGCCAGCGGCGGGGCGCCGCTCAGCAAGGAGGTAGGT
GAGGCCGTGGCCAAACGCTTCCACCTACCAGGCATCCGCCAGGGCTACGGCCTGACAGAAACAACCAGCGCC
ATTCTGATCACCCCCGAAGGGGACGACAAGCCTGGCGCAGTAGGCAAGGTGGTGCCCTTCTTCGAGGCTAAG
GTGGTGGACTTGGACACCGGTAAGACACTGGGTGTGAACCAGCGCGGCGAGCTGTGCGTCCGTGGCCCCATG
ATCATGAGCGGCTACGTTAACAACCCCGAGGCTACAAACGCTCTCATCGACAAGGACGGCTGGCTGCACAGC
GGCGACATCGCCTACTGGGACGAGGACGAGCACTTCTTCATCGTGGACCGGCTGAAGAGCCTGATCAAATAC
AAGGGCTACCAGGTAGCCCCAGCCGAACTGGAGAGCATCCTGCTGCAACACCCCAACATCTTCGACGCCGGG
GTCGCCGGCCTGCCCGACGACGATGCCGGCGAGCTGCCCGCCGCAGTCGTCGTGCTGGAACACGGTAAAACC
ATGACCGAGAAGGAGATCGTGGACTATGTGGCCAGCCAGGTTACAACCGCCAAGAAGCTGCGCGGTGGTGTT
GTGTTCGTGGACGAGGTGCCTAAAGGACTGACCGGCAAGTTGGACGCCCGCAAGATCCGCGAGATTCTCATT
AAGGCCAAGAAGGGCGGCAAGATCGCCGTGTAATAATTCTAGATAATTCTACCGGGTAGGGGAGGCGCTTTT
CCCAAGGCAGTCTGGAGCATGCGCTTTAGCAGCCCCGCTGGGCACTTGGCGCTACACAAGTGGCCTCTGGCC
TCGCACACATTCCACATCCACCGGTAGGCGCCAACCGGCTCCGTTCTTTGGTGGCCCCTTCGCGCCACCTTC
TACTCCTCCCCTAGTCAGGAAGTTCCCCCCCGCCCCGCAGCTCGCGTCGTGCAGGACGTGACAAATGGAAGT
AGCACGTCTCACTAGTCTCGTGCAGATGGACAGCACCGCTGAGCAATGGAAGCGGGTAGGCCTTTGGGGCAG
CGGCCAATAGCAGCTTTGCTCCTTCGCTTTCTGGGCTCAGAGGCTGGGAAGGGGTGGGTCCGGGGGCGGGCT
CAGGGGCGGGCTCAGGGGCGGGGCGGGCGCCCGAAGGTCCTCCGGAGGCCCGGCATTCTGCACGCTTCAAAA
GCGCACGTCTGCCGCGCTGTTCTCCTCTTCCTCATCTCCGGGCCTTTCGACCTGCAGCCCAAGCTTACCATG
ACCGAGTACAAGCCCACGGTGCGCCTCGCCACCCGCGACGACGTCCCCAGGGCCGTACGCACCCTCGCCGCC
GCGTTCGCCGACTACCCCGCCACGCGCCACACCGTCGATCCGGACCGCCACATCGAGCGGGTCACCGAGCTG
CAAGAACTCTTCCTCACGCGCGTCGGGCTCGACATCGGCAAGGTGTGGGTCGCGGACGACGGCGCCGCGGTG
GCGGTCTGGACCACGCCGGAGAGCGTCGAAGCGGGGGCGGTGTTCGCCGAGATCGGCCCGCGCATGGCCGAG
TTGAGCGGTTCCCGGCTGGCCGCGCAGCAACAGATGGAAGGCCTCCTGGCGCCGCACCGGCCCAAGGAGCCC
GCGTGGTTCCTGGCCACCGTCGGCGTCTCGCCCGACCACCAGGGCAAGGGTCTGGGCAGCGCCGTCGTGCTC
CCCGGAGTGGAGGCGGCCGAGCGCGCCGGGGTGCCCGCCTTCCTGGAGACCTCCGCGCCCCGCAACCTCCCC
TTCTACGAGCGGCTCGGCTTCACCGTCACCGCCGACGTCGAGGTGCCCGAAGGACCGCGCACCTGGTGCATG
ACCCGCAAGCCCGGTGCCTGACCGCGTCTGGAACAATCAACCTCTGGATTACAAAATTTGTGAAAGATTGAC
TGGTATTCTTAACTATGTTGCTCCTTTTACGCTATGTGGATACGCTGCTTTAATGCCTTTGTATCATGCTAT
TGCTTCCCGTATGGCTTTCATTTTCTCCTCCTTGTATAAATCCTGGTTGCTGTCTCTTTATGAGGAGTTGTG
GCCCGTTGTCAGGCAACGTGGCGTGGTGTGCACTGTGTTTGCTGACGCAACCCCCACTGGTTGGGGCATTGC
CACCACCTGTCAGCTCCTTTCCGGGACTTTCGCTTTCCCCCTCCCTATTGCCACGGCGGAACTCATCGCCGC
CTGCCTTGCCCGCTGCTGGACAGGGGCTCGGCTGTTGGGCACTGACAATTCCGTGGTGTTGTCGGGGAAGCT
GACGTCCTTTCCATGGCTGCTCGCCTGTGTTGCCACCTGGATTCTGCGCGGGACGTCCTTCTGCTACGTCCC
TTCGGCCCTCAATCCAGCGGACCTTCCTTCCCGCGGCCTGCTGCCGGCTCTGCGGCCTCTTCCGCGTCTTCG
CCTTCGCCCTCAGACGAGTCGGATCTCCCTTTGGGCCGCCTCCCCGCCTGGAATTAATTCTGCAGTCGAGAC
CTAGAAAAACATGGAGCAATCACAAGTAGCAATACAGCAGCTACCAATGCTGATTGTGCCTGGCTAGAAGCA
CAAGAGGAGGAGGAGGTGGGTTTTTCCAGTCACACCTCAGGTACCTTTAAGACCAATGACTTACAAGGCAGC
TGTAGATCTTAGCCACTTTTTAAAAGAAAAGAGGGGACTGGAAGGGCTAATTCACTCCCAACGAAGACAAGA
TATCCTTGATCTGTGGATCTACCACACACAAGGCTACTTCCCTGATTAGCAGAACTACACACCAGGGCCAGG
GGTCAGATATCCACTGACCTTTGGATGGTGCTACAAGCTAGTACCAGTTGAGCCAGATAAGGTAGAAGAGGC
CAATAAAGGAGAGAACACCAGCTTGTTACACCCTGTGAGCCTGCATGGGATGGATGACCCGGAGAGAGAAGT
GTTAGAGTGGAGGTTTGACAGCCGCCTAGCATTTCATCACGTGGCCCGAGAGCTGCATCCGGAGTACTTCAA
GAACTGCTGATATCGAGCTTGCTACAAGGGACTTTCCGCTGGGGACTTTCCAGGGAGGCGTGGCCTGGGCGG
GACTGGGGAGTGGCGAGCCCTCAGATCCTGCATATAAGCAGCTGCTTTTTGCCTGTACTGGGTCTCTCTGGT
TAGACCAGATCTGAGCCTGGGAGCTCTCTGGCTAACTAGGGAACCCACTGCTTAAGCCTCAATAAAGCTTGC
CTTGAGTGCTTCAAGTAGTGTGTGCCCGTCTGTTGTGTGACTCTGGTAACTAGAGATCCCTCAGACCCTTTT
AGTCAGTGTGGAAAATCTCTAGCAGTAGTAGTTCATGTCATCTTATTATTCAGTATTTATAACTTGCAAAGA
AATGAATATCAGAGAGTGAGAGGCCTTGACATTGCTAGCGTTTTACCGTCGACCTCTAGCTAGAGCTTGGCG
TAATCATGGTCATAGCTGTTTCCTGTGTGAAATTGTTATCCGCTCACAATTCCACACAACATACGAGCCGGA

AGCATAAAGTGTAAAGCCTGGGGTGCCTAATGAGTGAGCTAACTCACATTAATTGCGTTGCGCTCACTGCCC
GCTTTCCAGTCGGGAAACCTGTCGTGCCAGCTGCATTAATGAATCGGCCAACGCGCGGGGAGAGGCGGTTTG
CGTATTGGGCGCTCTTCCGCTTCCTCGCTCACTGACTCGCTGCGCTCGGTCGTTCGGCTGCGGCGAGCGGTA
TCAGCTCACTCAAAGGCGGTAATACGGTTATCCACAGAATCAGGGGATAACGCAGGAAAGAACATGTGAGCA
AAAGGCCAGCAAAAGGCCAGGAACCGTAAAAAGGCCGCGTTGCTGGCGTTTTTCCATAGGCTCCGCCCCCCT
GACGAGCATCACAAAAATCGACGCTCAAGTCAGAGGTGGCGAAACCCGACAGGACTATAAAGATACCAGGCG
TTTCCCCCTGGAAGCTCCCTCGTGCGCTCTCCTGTTCCGACCCTGCCGCTTACCGGATACCTGTCCGCCTTT
CTCCCTTCGGGAAGCGTGGCGCTTTCTCATAGCTCACGCTGTAGGTATCTCAGTTCGGTGTAGGTCGTTCGC
TCCAAGCTGGGCTGTGTGCACGAACCCCCCGTTCAGCCCGACCGCTGCGCCTTATCCGGTAACTATCGTCTT
GAGTCCAACCCGGTAAGACACGACTTATCGCCACTGGCAGCAGCCACTGGTAACAGGATTAGCAGAGCGAGG
TATGTAGGCGGTGCTACAGAGTTCTTGAAGTGGTGGCCTAACTACGGCTACACTAGAAGAACAGTATTTGGT
ATCTGCGCTCTGCTGAAGCCAGTTACCTTCGGAAAAAGAGTTGGTAGCTCTTGATCCGGCAAACAAACCACC
GCTGGTAGCGGTTTTTTTGTTTGCAAGCAGCAGATTACGCGCAGAAAAAAAGGATCTCAAGAAGATCCTTTG
ATCTTTTCTACGGGGTCTGACGCTCAGTGGAACGAAAACTCACGTTAAGGGATTTTGGTCATGAGATTATCA
AAAAGGATCTTCACCTAGATCCTTTTAAATTAAAAATGAAGTTTTAAATCAATCTAAAGTATATATGAGTAA
ACTTGGTCTGACAGTTACCAATGCTTAATCAGTGAGGCACCTATCTCAGCGATCTGTCTATTTCGTTCATCC
ATAGTTGCCTGACTCCCCGTCGTGTAGATAACTACGATACGGGAGGGCTTACCATCTGGCCCCAGTGCTGCA
ATGATACCGCGAGACCCACGCTCACCGGCTCCAGATTTATCAGCAATAAACCAGCCAGCCGGAAGGGCCGAG
CGCAGAAGTGGTCCTGCAACTTTATCCGCCTCCATCCAGTCTATTAATTGTTGCCGGGAAGCTAGAGTAAGT
AGTTCGCCAGTTAATAGTTTGCGCAACGTTGTTGCCATTGCTACAGGCATCGTGGTGTCACGCTCGTCGTTT
GGTATGGCTTCATTCAGCTCCGGTTCCCAACGATCAAGGCGAGTTACATGATCCCCCATGTTGTGCAAAAAA
GCGGTTAGCTCCTTCGGTCCTCCGATCGTTGTCAGAAGTAAGTTGGCCGCAGTGTTATCACTCATGGTTATG
GCAGCACTGCATAATTCTCTTACTGTCATGCCATCCGTAAGATGCTTTTCTGTGACTGGTGAGTACTCAACC
AAGTCATTCTGAGAATAGTGTATGCGGCGACCGAGTTGCTCTTGCCCGGCGTCAATACGGGATAATACCGCG
CCACATAGCAGAACTTTAAAAGTGCTCATCATTGGAAAACGTTCTTCGGGGCGAAAACTCTCAAGGATCTTA
CCGCTGTTGAGATCCAGTTCGATGTAACCCACTCGTGCACCCAACTGATCTTCAGCATCTTTTACTTTCACC
AGCGTTTCTGGGTGAGCAAAAACAGGAAGGCAAAATGCCGCAAAAAAGGGAATAAGGGCGACACGGAAATGT
TGAATACTCATACTCTTCCTTTTTCAATATTATTGAAGCATTTATCAGGGTTATTGTCTCATGAGCGGATAC
ATATTTGAATGTATTTAGAAAAATAAACAAATAGGGGTTCCGCGCACATTTCCCCGAAAAGTGCCACCTGAC
GTCGACGGATCGGGAGATCAACTTGTTTATTGCAGCTTATAATGGTTACAAATAAAGCAATAGCATCACAAA
TTTCACAAATAAAGCATTTTTTTCACTGCATTCTAGTTGTGGTTTGTCCAAACTCATCAATGTATCTTATCA
TGTCTGGATCAACTGGATAACTCAAGCTAACCAAAATCATCCCAAACTTCCCACCCCATACCCTATTACCAC
TGCCAATTACCTAGTGGTTTCATTTACTCTAAACCTGTGATTCCTCTGAATTATTTTCATTTTAAAGAAATT
GTATTTGTTAAATATGTACTACAAACTTAGTAGTTTTTAAAGAAATTGTATTTGTTAAATATGTACTACAAA
CTTAGTAGT

Plasmid: LVX-Tomato
Made by: Teresa Coughlan
Users: Teresa Coughlan
Richard Argent
Nektaria Papadopoulou
Yin Yinfei
Hanna Mourad-Agha
Anna Grabowska

Description of plasmid: This construct is based on 'pLVX-DD-tdtomato control' from 'Clontech'. Expression of the fruit fluorescent protein tdTomato is constitutive under the CMV promoter. The construct lacks the degradation domain (DD) in the original vector so that fluorescence can be seen without the need to add substrate. It was made by removing the BamHI/NotI 'DD-tdTomato' fragment from the original vector, and replacing it with the BamHI/NotI tdTomato fragment from ptdTomato (Clontech). Clone 1 is the one to use.

Other relevant details: ABI sequencing shows construct is correct in respect of inserted fragment and patent insertion sites.

Sequencing primers: - see sequence.

Restriction map: (showing only unique sites)

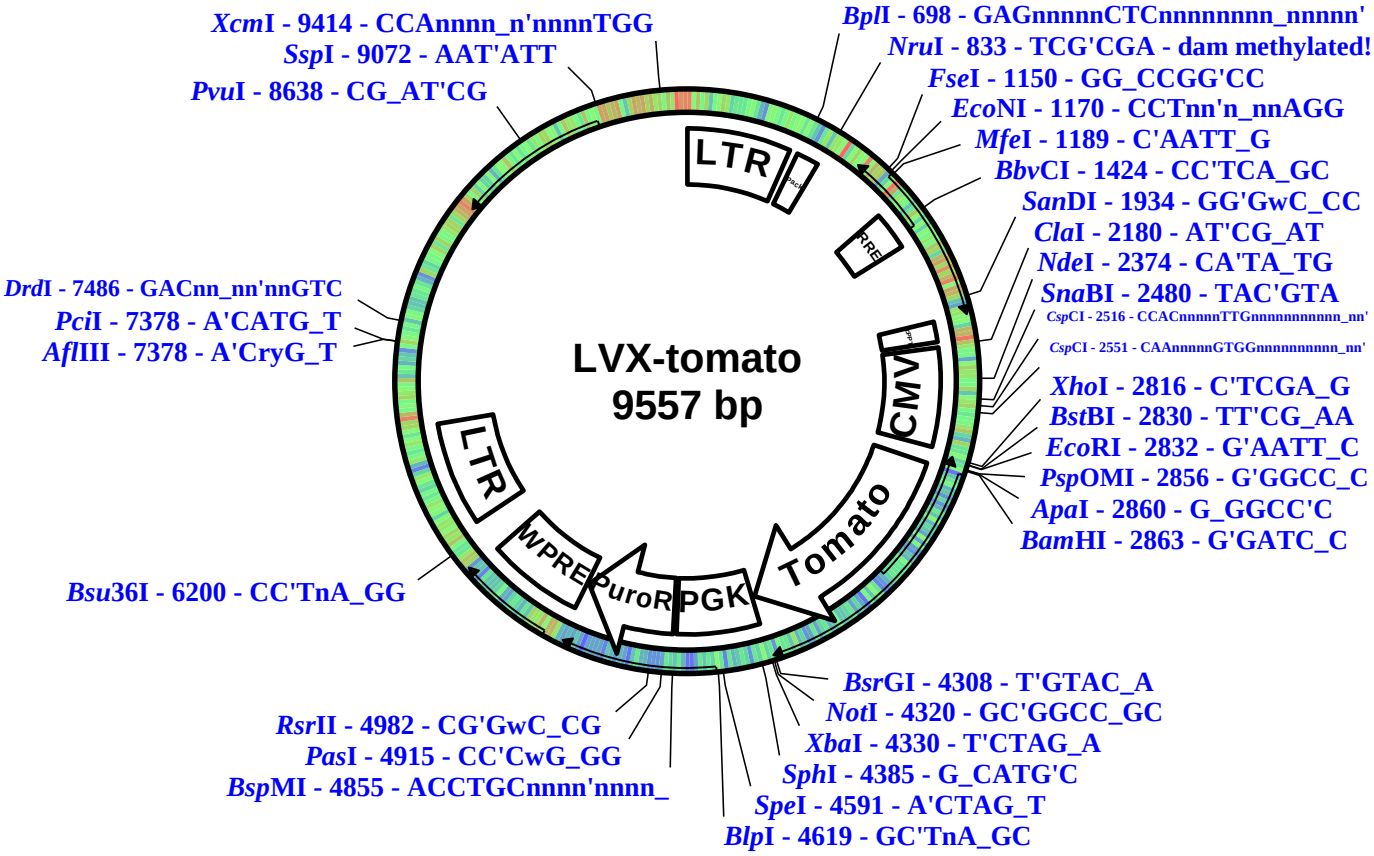

Sequence:

Green(dark)=CMV promoter
Red=tomato ORF
Teal=sequencing primers
Pink=PGKprom
Green(light)=PuroR and WPRE
Blue= packaging signal, RREreg and cPPT elements
Purple=LTRs

TGGAAGGGCTAATTCACTCCCAAAGAAGACAAGATATCCTTGATCTGTGGATCTACCACACACAAGGCTACT
TCCCTGATTAGCAGAACTACACACCAGGGCCAGGGGTCAGATATCCACTGACCTTTGGATGGTGCTACAAGC
TAGTACCAGTTGAGCCAGATAAGGTAGAAGAGGCCAATAAAGGAGAGAACACCAGCTTGTTACACCCTGTGA
GCCTGCATGGGATGGATGACCCGGAGAGAGAAGTGTTAGAGTGGAGGTTTGACAGCCGCCTAGCATTTCATC
ACGTGGCCCGAGAGCTGCATCCGGAGTACTTCAAGAACTGCTGATATCGAGCTTGCTACAAGGGACTTTCCG
CTGGGGACTTTCCAGGGAGGCGTGGCCTGGGCGGGACTGGGGAGTGGCGAGCCCTCAGATCCTGCATATAAG
CAGCTGCTTTTTGCCTGTACTGGGTCTCTCTGGTTAGACCAGATCTGAGCCTGGGAGCTCTCTGGCTAACTA
GGGAACCCACTGCTTAAGCCTCAATAAAGCTTGCCTTGAGTGCTTCAAGTAGTGTGTGCCCGTCTGTTGTGT
GACTCTGGTAACTAGAGATCCCTCAGACCCTTTTAGTCAGTGTGGAAAATCTCTAGCAGTGGCGCCCGAACA
GGGACTTGAAAGCGAAAGGGAAACCAGAGGAGCTCTCTCGACGCAGGACTCGGCTTGCTGAAGCGCGCACGG
CAAGAGGCGAGGGGCGGCGACTGGTGAGTACGCCAAAAATTTTGACTAGCGGAGGCTAGAAGGAGAGAGATG
GGTGCGAGAGCGTCAGTATTAAGCGGGGGAGAATTAGATCGCGATGGGAAAAAATTCGGTTAAGGCCAGGGG
GAAAGAAAAAATATAAATTAAAACATATAGTATGGGCAAGCAGGGAGCTAGAACGATTCGCAGTTAATCCTG
GCCTGTTAGAAACATCAGAAGGCTGTAGACAAATACTGGGACAGCTACAACCATCCCTTCAGACAGGATCAG
AAGAACTTAGATCATTATATAATACAGTAGCAACCCTCTATTGTGTGCATCAAAGGATAGAGATAAAAGACA
CCAAGGAAGCTTTAGACAAGATAGAGGAAGAGCAAAACAAAAGTAAGACCACCGCACAGCAAGCGGCCGGCC
GCTGATCTTCAGACCTGGAGGAGGAGATATGAGGGACAATTGGAGAAGTGAATTATATAAATATAAAGTAGT
AAAAATTGAACCATTAGGAGTAGCACCCACCAAGGCAAAGAGAAGAGTGGTGCAGAGAGAAAAAAGAGCAGT
GGGAATAGGAGCTTTGTTCCTTGGGTTCTTGGGAGCAGCAGGAAGCACTATGGGCGCAGCGTCAATGACGCT
GACGGTACAGGCCAGACAATTATTGTCTGGTATAGTGCAGCAGCAGAACAATTTGCTGAGGGCTATTGAGGC
GCAACAGCATCTGTTGCAACTCACAGTCTGGGGCATCAAGCAGCTCCAGGCAAGAATCCTGGCTGTGGAAAG
ATACCTAAAGGATCAACAGCTCCTGGGGATTTGGGGTTGCTCTGGAAAACTCATTTGCACCACTGCTGTGCC
TTGGAATGCTAGTTGGAGTAATAAATCTCTGGAACAGATTTGGAATCACACGACCTGGATGGAGTGGGACAG
AGAAATTAACAATTACACAAGCTTAATACACTCCTTAATTGAAGAATCGCAAAACCAGCAAGAAAAGAATGA
ACAAGAATTATTGGAATTAGATAAATGGGCAAGTTTGTGGAATTGGTTTAACATAACAAATTGGCTGTGGTA
TATAAAATTATTCATAATGATAGTAGGAGGCTTGGTAGGTTTAAGAATAGTTTTTGCTGTACTTTCTATAGT
GAATAGAGTTAGGCAGGGATATTCACCATTATCGTTTCAGACCCACCTCCCAACCCCGAGGGGACCCGACAG
GCCCGAAGGAATAGAAGAAGAAGGTGGAGAGAGAGACAGAGACAGATCCATTCGATTAGTGAACGGATCTCG
ACGGTATCGCCTTTAAAAGAAAAGGGGGGATTGGGGGGTACAGTGCAGGGGAAAGAATAGTAGACATAATAG
CAACAGACATACAAACTAAAGAACTACAAAAACAAATTACAAAAATTCAAAATTTTCGGGTTTATTACAGGG
ACAGCAGAGATCCAGTTTATCGATAAGCTTGGGAGTTCCGCGTTACATAACTTACGGTAAATGGCCCGCCTG
GCTGACCGCCCAACGACCCCCGCCCATTGACGTCAATAATGACGTATGTTCCCATAGTAACGCCAATAGGGA
CTTTCCATTGACGTCAATGGGTGGAGTATTTACGGTAAACTGCCCACTTGGCAGTACATCAAGTGTATCATA
TGCCAAGTACGCCCCCTATTGACGTCAATGACGGTAAATGGCCCGCCTGGCATTATGCCCAGTACATGACCT
TACGGGACTTTCCTACTTGGCAGTACATCTACGTATTAGTCATCGCTATTACCATGGTGATGCGGTTTTGGC
AGTACACCAATGGGCGTGGATAGCGGTTTGACTCACGGGGATTTCCAAGTCTCCACCCCATTGACGTCAATG
GGAGTTTGTTTTGGCACCAAAATCAACGGGACTTTCCAAAATGTCGTAACAACTCCGCCCCATTGACGCAAA
TGGGCGGTAGGCGTGTACGGTGGGAGGTCTATATAAGCAGAGCTCGTTTAGTGAACCGTCAGATCGCCTGGA
GACGCCATCCACGCTGTTTTGACCTCCATAGAAGACACCGACTCTAGCTAGAGGATCGCTAGCGCTACCGGA
CTCAGATCTCGAGCTCAAGCTTCGAATTCTGCAGTCGACGGTACCGCGGGCCCGGGATCCCCGGGTACCGGT
CGCCACCATGGTGAGCAAGGGCGAGGAGGTCATCAAAGAGTTCATGCGCTTCAAGGTGCGCATGGAGGGCTC
CATGAACGGCCACGAGTTCGAGATCGAGGGCGAGGGCGAGGGCCGCCCCTACGAGGGCACCCAGACCGCCAA

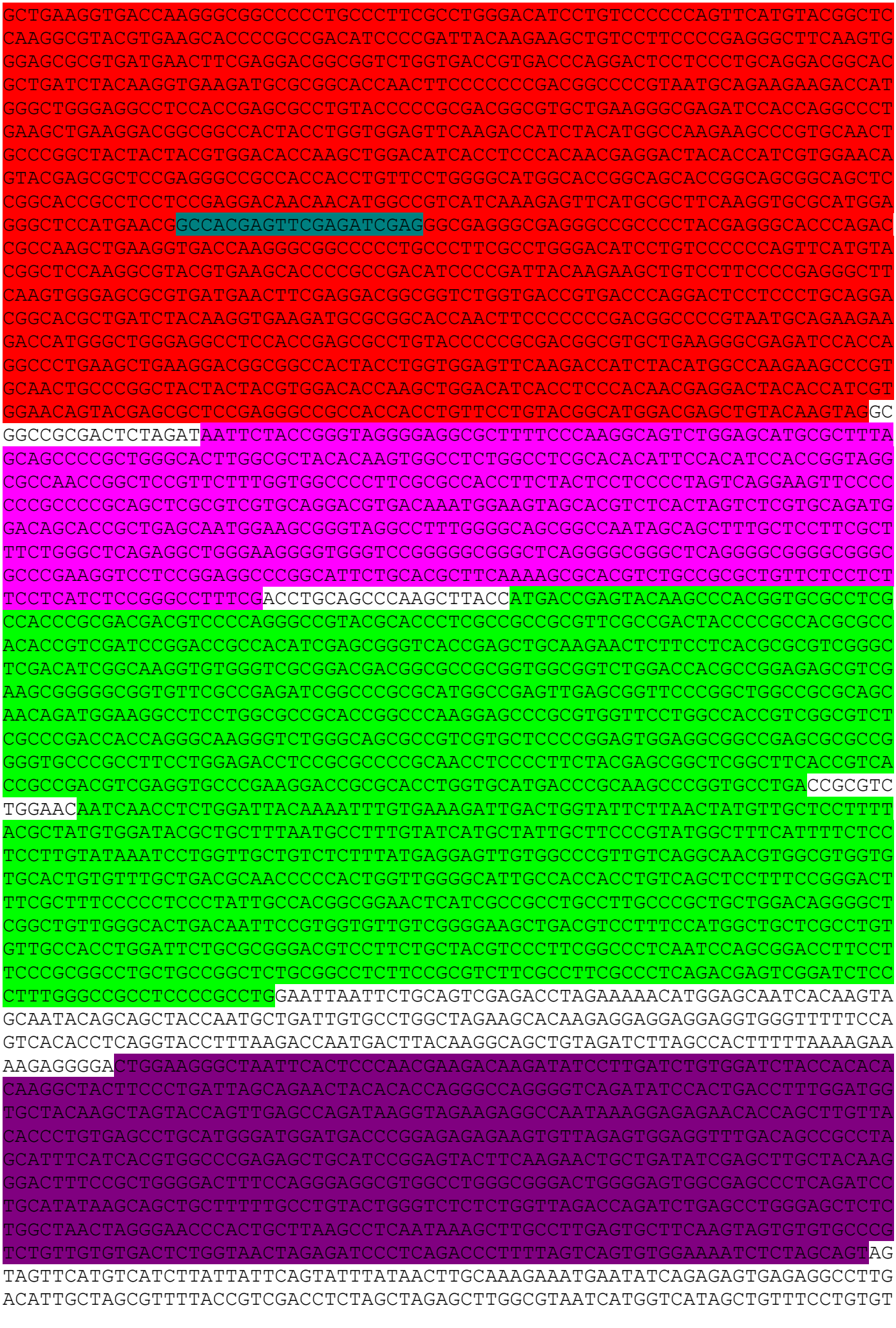

GAAATTGTTATCCGCTCACAATTCCACACAACATACGAGCCGGAAGCATAAAGTGTAAAGCCTGGGGTGCCT
AATGAGTGAGCTAACTCACATTAATTGCGTTGCGCTCACTGCCCGCTTTCCAGTCGGGAAACCTGTCGTGCC
AGCTGCATTAATGAATCGGCCAACGCGCGGGGAGAGGCGGTTTGCGTATTGGGCGCTCTTCCGCTTCCTCGC
TCACTGACTCGCTGCGCTCGGTCGTTCGGCTGCGGCGAGCGGTATCAGCTCACTCAAAGGCGGTAATACGGT
TATCCACAGAATCAGGGGATAACGCAGGAAAGAACATGTGAGCAAAAGGCCAGCAAAAGGCCAGGAACCGTA
AAAAGGCCGCGTTGCTGGCGTTTTTCCATAGGCTCCGCCCCCCTGACGAGCATCACAAAAATCGACGCTCAA
GTCAGAGGTGGCGAAACCCGACAGGACTATAAAGATACCAGGCGTTTCCCCCTGGAAGCTCCCTCGTGCGCT
CTCCTGTTCCGACCCTGCCGCTTACCGGATACCTGTCCGCCTTTCTCCCTTCGGGAAGCGTGGCGCTTTCTC
ATAGCTCACGCTGTAGGTATCTCAGTTCGGTGTAGGTCGTTCGCTCCAAGCTGGGCTGTGTGCACGAACCCC
CCGTTCAGCCCGACCGCTGCGCCTTATCCGGTAACTATCGTCTTGAGTCCAACCCGGTAAGACACGACTTAT
CGCCACTGGCAGCAGCCACTGGTAACAGGATTAGCAGAGCGAGGTATGTAGGCGGTGCTACAGAGTTCTTGA
AGTGGTGGCCTAACTACGGCTACACTAGAAGAACAGTATTTGGTATCTGCGCTCTGCTGAAGCCAGTTACCT
TCGGAAAAAGAGTTGGTAGCTCTTGATCCGGCAAACAAACCACCGCTGGTAGCGGTTTTTTTGTTTGCAAGC
AGCAGATTACGCGCAGAAAAAAAGGATCTCAAGAAGATCCTTTGATCTTTTCTACGGGGTCTGACGCTCAGT
GGAACGAAAACTCACGTTAAGGGATTTTGGTCATGAGATTATCAAAAAGGATCTTCACCTAGATCCTTTTAA
ATTAAAAATGAAGTTTTAAATCAATCTAAAGTATATATGAGTAAACTTGGTCTGACAGTTACCAATGCTTAA
TCAGTGAGGCACCTATCTCAGCGATCTGTCTATTTCGTTCATCCATAGTTGCCTGACTCCCCGTCGTGTAGA
TAACTACGATACGGGAGGGCTTACCATCTGGCCCCAGTGCTGCAATGATACCGCGAGACCCACGCTCACCGG
CTCCAGATTTATCAGCAATAAACCAGCCAGCCGGAAGGGCCGAGCGCAGAAGTGGTCCTGCAACTTTATCCG
CCTCCATCCAGTCTATTAATTGTTGCCGGGAAGCTAGAGTAAGTAGTTCGCCAGTTAATAGTTTGCGCAACG
TTGTTGCCATTGCTACAGGCATCGTGGTGTCACGCTCGTCGTTTGGTATGGCTTCATTCAGCTCCGGTTCCC
AACGATCAAGGCGAGTTACATGATCCCCCATGTTGTGCAAAAAAGCGGTTAGCTCCTTCGGTCCTCCGATCG
TTGTCAGAAGTAAGTTGGCCGCAGTGTTATCACTCATGGTTATGGCAGCACTGCATAATTCTCTTACTGTCA
TGCCATCCGTAAGATGCTTTTCTGTGACTGGTGAGTACTCAACCAAGTCATTCTGAGAATAGTGTATGCGGC
GACCGAGTTGCTCTTGCCCGGCGTCAATACGGGATAATACCGCGCCACATAGCAGAACTTTAAAAGTGCTCA
TCATTGGAAAACGTTCTTCGGGGCGAAAACTCTCAAGGATCTTACCGCTGTTGAGATCCAGTTCGATGTAAC
CCACTCGTGCACCCAACTGATCTTCAGCATCTTTTACTTTCACCAGCGTTTCTGGGTGAGCAAAAACAGGAA
GGCAAAATGCCGCAAAAAAGGGAATAAGGGCGACACGGAAATGTTGAATACTCATACTCTTCCTTTTTCAAT
ATTATTGAAGCATTTATCAGGGTTATTGTCTCATGAGCGGATACATATTTGAATGTATTTAGAAAAATAAAC
AAATAGGGGTTCCGCGCACATTTCCCCGAAAAGTGCCACCTGACGTCGACGGATCGGGAGATCAACTTGTTT
ATTGCAGCTTATAATGGTTACAAATAAAGCAATAGCATCACAAATTTCACAAATAAAGCATTTTTTTCACTG
CATTCTAGTTGTGGTTTGTCCAAACTCATCAATGTATCTTATCATGTCTGGATCAACTGGATAACTCAAGCT
AACCAAAATCATCCCAAACTTCCCACCCCATACCCTATTACCACTGCCAATTACCTAGTGGTTTCATTTACT
CTAAACCTGTGATTCCTCTGAATTATTTTCATTTTAAAGAAATTGTATTTGTTAAATATGTACTACAAACTT
AGTAGTTTTTAAAGAAATTGTATTTGTTAAATATGTACTACAAACTTAGTAGT